UNCLASSIFIED

AD NUMBER

AD846243

LIMITATION CHANGES

TO:

Approved for public release; distribution is unlimited.

FROM:

Distribution authorized to U.S. Gov't. agencies and their contractors; Critical Technology; NOV 1968. Other requests shall be referred to Rome Air Development Center (RADC), Attn: EMCVI, Griffiss AFB, NY 13441-5700. This document contains export-controlled technical data.

AUTHORITY

RADC/USAF ltr dtd 17 Sep 1971

THIS PAGE IS UNCLASSIFIED

[illegible] TRANSMISSION LINE SITING CRITERIA

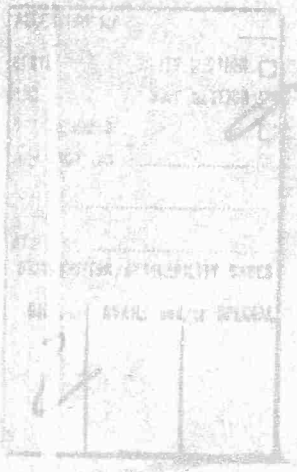
[illegible] E. Palmer
[illegible] L. Chartier
[illegible] T. Hanson
[illegible] Electronic Corporation

TECHNICAL REPORT NO. RADC-TR-68-316
[illegible] 1968

This document is subject to special export controls and each transmittal to foreign governments, foreign nationals or representatives thereto may be made only with prior approval of RADC (EMCVH), GAFB, N.Y.

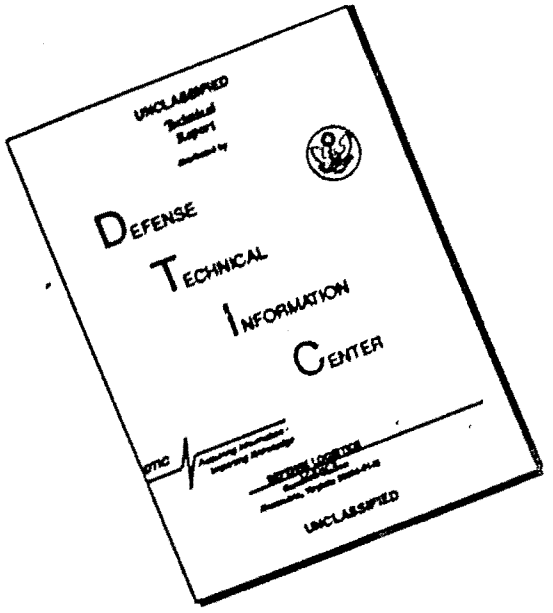
DDC
RECEIVED
JAN 21 1969
[illegible]
A

Rome Air Development Center
Air Force Systems Command
Griffiss Air Force Base, New York



Do not [illegible] main copy. Retain or destroy.

DISCLAIMER NOTICE



THIS DOCUMENT IS BEST QUALITY AVAILABLE. THE COPY FURNISHED TO DTIC CONTAINED A SIGNIFICANT NUMBER OF PAGES WHICH DO NOT REPRODUCE LEGIBLY.

HIGH VOLTAGE POWER LINE SITING CRITERIA

W. E. Pakala
V. L. Chartier
R. T. Harrold
Westinghouse Electric Corporation

This document is subject to special export controls and each transmittal to foreign governments, foreign nationals or representatives thereto may be made only with prior approval of RADC (EMCVI), GAFB, N.Y. 13440.

AFLC, GAFB, N.Y., 20 Dec 68-146

FOREWORD

This final report was prepared by W. E. Pakala, R. T. Harrold, and V. L. Chartier of Westinghouse Electric Corporation, Electric Utility Headquarters Department, Pittsburgh, Pennsylvania, under Contract F30602-67-C-0171, Project 4540, Task 454002. Secondary report number is 68-69%. RADC project engineer is Jacob Scherer (EMCVI).

The distribution of this document is limited under the U.S. Mutual Security Acts of 1949.

This technical report has been reviewed and is approved.

Approved: JACOB SCHERER
Interf Anal & Control Sec
Vulnerability Reduction Branch

Approved: RICHARD M. COSEL
Colonel, USAF
Chief, Communications Division

FOR THE COMMANDER:
IRVING J. GABELMAN
Chief, Advanced Studies Group

ABSTRACT

This Technical Report describes the work performed under Contract F30602-67-C-0171. The objective was to develop a High Voltage Power Line Siting Criteria so that communication sites can be selected which will not be seriously affected by radio interference from existing power lines, or proposed lines in the vicinity of the communication site.

Under a previous Contract AF30(602)-3822, a High Voltage Power Line Siting Criteria was developed and reported in Technical Report No. RADC-TR-66-606, March 1967, Vols. I, II, III (AD 812 266, AD 812 267, AD 812 268) for power lines rated 2.4 kV through 345 kV, and covering the frequency spectrum of 60 Hertz through one Gigahertz.

This Technical Report extends the Siting Criteria to power lines operating at 525 kV ac, 735 kV ac and 800 kV dc, covering the frequency range from 60 Hz to 10 GHz. Also the investigation of the radio noise and frequency spectrum of the 345-kV lines studied in the previous contract has been extended to 10 GHz.

The following information is included in this report:

1. A systematic procedure to determine the radio noise generated by 525-kV ac, 735-kV ac and 800-kV dc lines covering the frequency spectrum of 60 Hz to 10 GHz, and lines from 2.4-kV ac to 345-kV ac covering the frequency spectrum of 1 GHz to 10 Ghz.

2. Description and comparison of test methods using radio noise meters both manually and with X-Y recorder and Spectrum analyzer.

3. Measured data and data analysis.

4. Methods to determine the propagation loss of the noise generated by power lines.

5. Literature Survey.

CONTENTS

	Page No.
Scope	1
1. Introduction	2
2. Generation of Radio Noise by Power Lines	3
2.1 Electrical Characteristics of Gap Type Discharges	3
2.2 Electrical Characteristics of the Corona Discharge	3
3. Instrumentation	5
3.1 Principal Instruments Used	5
3.2 Antennas Used	7
3.3 Calibration of Instruments	7
4. Methods of Measurement	7
4.1 The Artificial Gap-Type Radio Noise Generator	8
4.2 Power Lines Measured for Radio Noise	8
4.3 Laboratory Measurement	9
4.3.1 Conducted and Radiated Measurements	9
4.3.2 Artificial Gap Spectra	9
4.3.3 Gap-Discharge Between Two Suspension Insulators	10
4.3.4 Corona Source Spectrum	10
5. Discussion of Measurements on Power Lines	11
5.1 Frequency Spectrum for 7.2-kV Low Voltage Line	11
5.2 345-kV Vertical Configuration Double Circuit Line	11
5.2.1 Line Normal	11
5.2.2 With 5/16-Inch Artificial Gap on 345-kV ac Line	11

		Page No.
5.3	345-kV Horizontal Configuration Wood Pole Line	12
5.4	525-kV Horizontal Configuration Steel Tower Line	12
5.4.1	Measurements with Line Normal	12
5.4.2	Measurements with 5/16-inch Gap at Tower	12
5.5	735-kV Horizontal Configuration Steel Tower Lines	13
5.5.1	Frequency Spectra 0.015 MHz to 7.4 GHz	13
5.5.2	Lateral Profile	13
5.5.3	Frequency Spectra in the 0.15 - 25 MHz Range	14
5.6	765-kV Apple Grove Test Line	14
5.6.1	Measurements in the 1 - 10 GHz Range	15
5.6.2	Effect of Gap Discharge at Fence	15
5.7	800-kV Direct Current Test Line	15
5.7.1	Frequency Spectra with 800-kV Direct Current Line Normal	16
5.7.1.1	Bipolar Operation	16
5.7.1.2	Monopolar Operation	16
5.7.1.3	Lateral Profile at Mid-span	17
5.7.1.4	Comparison of 800-kV dc Line with 345-kV ac Line	17
5.7.2	Measurements with 5/16-inch Gap	17
5.7.2.1	Frequency Spectra with Bipolar Operation at 800 kV	17
5.8	Low Frequency Electric Field Measurements - 60 Hz to 15 KHz	18
6.	Discussion of Results for Lines Normal	20
6.1	12-kV Line in the 1 - 10 GHz Range	20
6.2	345-kV Line in the 1 - 10 GHz Range	20

		Page No.
6.3	525-kV Line in the 60 Hz to 10 GHz Range	20
6.4	735-kV Line in the 60 Hz to 10 GHz Range	20
6.5	Apple Grove 765-kV Test Project	20
6.5.1	1 - 10 GHz Range	20
6.5.2	Gap Discharge on Fence Beneath Test Line in the 0.015 MHz to 10 GHz Range	21
6.6	800-kV dc Test Line in the 60 Hz - 10 GHz Range	21
7.	Discussion of Results of Laboratory Tests	21
8.	Application of Results	21
8.1	Prediction for the 525-, 735-kV ac and 800-kV dc Lines for Conductor-Corona Radio Noise	22
8.2	Prediction for 7.2-kV Lines in the 1 - 10 GHz Range	23
8.3	Prediction Method with Gap-Type Sources for the 735-kV Line in the 1 - 10 GHz Range	24
8.4	Prediction for the Fence Near 765-kV Line for the 1 - 10 GHz Range	25
Appendix I	New Instrumentation and Measurement Techniques	91
Appendix II	Application of Antenna Theory to Radiation from Transmission Lines (1.25 - 10.0 GHz)	150
Appendix III	Bibliography	184

LIST OF FIGURES

		Page No.
Fig. 1	Artificial Gap Type Radio Noise Generator, 18 kV rms B.D. Voltage (floating) Approx. to 1/4 Scale.	26
Fig. 2	Frequency Spectrum for 5/16-inch Gap, and for Suspension Insulator Gap.	27
Fig. 3	Photographs of Artificial Gap Type Radio Noise Generator, 12-kV Line, Test Set-up for Measuring Corona Noise in Laboratory, and Corona at the Ends of Dipole Antenna.	28
Fig. 4	345-kV Vertical Line Configuration and Test Locations	29
Fig. 5	345-kV Wood Pole Line Configuration and Test Locations.	30
Fig. 6	525-kV Line Configuration and Test Locations	31
Fig. 7	735-kV Lines Configuration and Test Locations.	32
Fig. 8	750-kV Test Line Configuration and Test Locations and Fence Gap Location.	33
Fig. 9	800-kV dc Line Configuration and Test Locations	34
Fig. 10	345-kV Steel Tower Line Configuration and Test Location.	35
Fig. 11	Photographs of 345-kV Double Circuit Vertical, 345-kV Wood Pole, 525-kV, and 735-kV Lines Measured.	36
Fig. 12	Photographs of 800-kV dc Test Line, 750-kV Test Lines, and Discharge to Wire near 750-kV Line	37
Fig. 13	Trafford Laboratory 650-kV NEMA Test Circuit.	38
Fig. 14	Frequency Spectra from 5/16-inch Gap in Lab.	39
Fig. 15(a)	Frequency Spectrum of Conductor Corona in Lab. Rain	
Fig. 15(b)	Comparison of Radio Noise Levels from 5/16-inch Gap and Rain Type Sources	41
Fig. 16	Frequency Spectra for 12-kV Line with Gap Type Source 100 Feet Away.	42

		Page No.
Fig. 17	345-kV VCDCST Normal Line Frequency Spectra 200 Feet From Tower	43
Fig. 18	Frequency Spectrum from 1 to 10 GHz on 345-kV Line at Tower 473.	44
Fig. 19	Lateral Distance from 5/16-inch Gap at Tower on 345-kV Line.	45
Fig. 20	Lateral Attenuation from 5/16-Inch Gap at Tower on 345-kV Line	46
Fig. 21	Frequency Spectra with 5/16-inch Gap on 345-kV Line at Tower	47
Fig. 22	345-kV Wood Pole Line Frequency Spectra, 200 feet from Tower	48
Fig. 23	Frequency Spectrum 1 - 10 GHz on 345-kV Wood Pole Line.	49
Fig. 24	Frequency Spectrum of 525-kV ac Line	50
Fig. 25	525-kV Lines, Lateral Profile Near Midspan.	51
Fig. 26	Frequency Spectra at Several Distances from 525-kV Line Tower	52
Fig. 27	Frequency Spectra at Several Distances with 5/16-inch Gap at 525-kV Tower.	53
Fig. 28	Frequency Spectra with 5/16-inch Gap on 525-kV Line at Tower	54
Fig. 29	Lateral Attenuation from 5/16-inch Gap on 525-kV Line in 1-2 GHz Range	55
Fig. 30	Frequency Spectrum of 735-kV Line at 50 foot Lateral Distance from Tower.	56
Fig. 31(a)	Frequency Spectrum of 735-kV South Line at 200 foot Lateral Distance from Tower.	57
Fig. 31(b)	Frequency Spectrum of 735-kV North Line at 200 Feet from Tower.	58
Fig. 32	Lateral Profile Near Center Span of 735-kV Line.	59
Fig. 33	Frequency Spectrum for 735-kV North and South Lines 150 Feet from Conductor	60

		Page No.
Fig. 34	Frequency Spectra for 735-kV Line with Corona and with Natural Gap.	61
Fig. 35	Comparison of Frequency Spectra on Opposite Sides of 735-kV Line Tower.	62
Fig. 36	Frequency Spectrum Near 765-kV Substation.	63
Fig. 37	Frequency Spectrum of Discharge Gap on Fence Near 765-kV Line.	64
Fig. 38	Frequency Spectrum of 800-kV dc Test Line 50 Feet Opposite Tower.	65
Fig. 39	Frequency Spectra of 500-kV dc Test Line in Fair Weather and Rain.	66
Fig. 40	Lateral Profiles at Mid-Span, 800-kV Direct Current Test Line.	67
Fig. 41	Frequency Spectra from Monopolar Operation of ±400-kV dc Test Line.	68
Fig. 42	Frequency Spectrum with 5/16-inch Gap on 800-kV dc Test Line	69
Fig. 43	Frequency Spectra with 5/16-Inch Gap on Positive and Negative Conductor of 800-kV dc Test Line	70
Fig. 44	Lateral Attenuation from 800-kV Line 0.01 - 0.154 MHz with Gap at Tower.	71
Fig. 45	Lateral Attenuation from 800-kV dc Line 0.154 - 25 MHz with Gap at Tower.	72
Fig. 46	Lateral Attenuation from 800-kV dc Line 30 - 400 MHz with Gap at Tower.	73
Fig. 47	Frequency Spectrum for 5/32-inch Gap on + and -, dc Voltage.	74
Fig. 48	Comparison of 800-kV dc Line with 345-kV ac Line in Fair Weather at 50 Feet.	75
Fig. 49	Photograph of dc Test Line Showing Positive Conductor with the Most Corona.	76
Fig. 50	525-kV Line, 60 Hz and Harmonics.	77

		Page No.
Fig. 51	735-kV Line, 60 Hz and Harmonics at 200 Feet from Outside Phase.	78
Fig. 52	800-kV dc Line, 60 Hz and Harmonics, Antenna Located Midway Between Positive and Negative Pole.	79
Fig. 53	Audio Frequency Receiver Residual with Different Engine Power Supplies.	80
Fig. 54	Lateral Attenuation of 60 Hz and Harmonics for 525-kV Line	81
Fig. 55	Prediction Curves for Conductor Corona Radio Noise 525-, 735-, and 800-kV Lines.	82
Fig. 56	Predicted 525-kV Line Conductor Corona Radio Noise for Heavy Rain	83
Fig. 57	Predicted Line Conductor Corona Radio Noise in Heavy Rain.	84
Fig. 58	Lateral Attenuation in the 30 - 1000 MHZ Range for Vertical Polarization	85
Fig. 59	Lateral Attenuation in the 1 - 10 GHz Range for Vertical Polarization	86
Fig. 60	Measured Radio Noise in the 1 - 10 Ghz Range.	87
Fig. 61	Lateral Attenuation in the 1 - 10 GHz Range.	88
Fig. 62	Predicted Power Line Radio Noise in the 1 - 10 GHz Range.	89
Fig. 63	Predicted Radio Noise from Gap Source on Fence Near 765-kV Line	90

High Voltage Power Line Siting Criteria

This effort has developed simplified procedures which can be used to determine the field strength of noise generated by high voltage transmission and distribution lines. These procedures are applicable to 525 kV and 735 kV ac and 800 kV dc lines covering the frequency range of 60 hertz to 10 GHz, and to 2.4 kV to 345 kV ac lines covering a frequency range of 1 GHz to 10 GHz.

These procedures will be used to develop siting criteria for Air Force C&E installations when located in the vicinity of these lines. This effort is a part of an R&D program to develop good engineering standards for siting C&E installations.

Jacob Scherer

JACOB SCHERER
Effort Engineer

SCOPE

This is the complete report including Foreword and Abstract, and three Appendices. The description of lines tested is given with results of field strength measurements on lines and in the laboratory. Predictions of line radio noise magnitude with lateral distance from the line are included for conductor corona-type and gap-type sources of radio noise. The measurements include manual readings, X-Y plotting, and photos of spectra as seen on the spectrum analyzer.

1. Introduction

The purpose of the radio noise measurements and analysis described is to determine the ground wave radio noise levels and factors for ac and dc power transmission lines. These data are for use in the selection of a communication site which will not be seriously affected by radio interference from existing or proposed power transmission lines. The frequency range of measurements was 60 Hz to 10 GHz.

Power line radio noise can be generated by line components such as hardware, insulators, conductors, line apparatus, etc. In many cases the generation is because of faulty components, corrosion between metal parts, discharges between unbonded or floating metal parts and hardware, and between neutral conductors and ground and pole guys and because of conductor corona. Most of the possible generation sources mentioned can be found and, except for conductor corona, can be and have been eliminated on their lines by electric utilities. Radio noise from conductor corona is the principal problem on extra high voltage lines (EHV) (345-1000 kV) and to a lesser extent on lines below 100 kV.

With respect to radio noise power lines should be considered in two classes, (1) lines below 70 kV and (2) lines from 110 - 1000 kV. These classes are based on the fact that all lines below 70 kV can be made free of conductor corona generation, and that higher voltage lines, especially EHV lines, cannot be constructed free of conductor corona radio noise for economic reasons. For EHV lines a prediction technique is developed which is based on laboratory measurements on conductors, and on the comparison of radio noise field measurements on lines in service.

The radio noise field strengths in the vicinity of lines were measured under three conditions. These were (1) under normal conditions, (2) with natural gap in line, and (3) with artificial gap connected to one phase conductor. The artificial gap was used as a measurement tool to increase the radio noise level from a line so that the field strength could be measured farther away and at the higher frequencies with the radio noise meters and amplifiers available. Measurements were made manually and with X-Y recorder and with spectrum analyzers. Very good agreement was found between the semi-automatic and manual methods of measurement.

It was found that the measured field strength decreases laterally from the line approximately inversely as the first second, or third power of the distance from the line depending on the frequency. Calculations of the lateral attenuation were made for the 1.25 - 10 GHz range. The field strength is not the same on both sides of line or tower when the antenna is not too far from a local source, such as a natural gap or the artificial gap. As the antenna is moved along the line the field strength on the two sides of the line becomes more symmetrical, as would be expected. Radio noise was detected in the 1 to 10 GHz range from the 7.2 kV line and from the 345, 525, and 725-kV lines and in the laboratory from conductors in artificial rain.

This report includes additional bibliography*, laboratory tests,

* Refer to Report No. RADC-TR-66-606, Vol. II in order to have the complete Bibliography.

nalysis, calculation of field strength near lines and far away, line conductor gradients, field strength measurements; near power lines by manual means; X-Y plotting and with a spectrum analyzer.

2. Generation of Radio Noise by Power Lines

Radio noise on power lines is caused by partial electrical discharges, such as corona, by electrical discharges at small gaps in insulators, at tie wires, between hardware parts, by excessive electric stress across wood or due to corrosion between metal parts, at small gaps between neutral wire and ground wires and hardware, and ground wires and hardware, and by many types of corona or gap sources in electrical apparatus if defective or damaged, or if improperly designed or installed.

Interference was discovered in the early days of radio and measures were taken by electric utilities and electrical manufacturers to reduce or eliminate radio noise from lines and apparatus. Radio-free pintype insulators were developed and lines with these insulators were found to be quite free of radio noise whereas lines with comparable size plain pintype insulators were not as good. Laboratory and shop test methods for radio noise were developed and adopted as standard for high voltage apparatus as early as 1938. Radio influence voltage (RIV) limits were later established for high voltage apparatus by the National Electrical Manufacturers Association (NEMA).

With the advent of extra high voltage lines (EHV) it was soon found that conductor corona formed at conductor gradients well below the theoretical critical gradient because of conductor surface burrs, contamination, rain, and that EHV line design would require consideration of radio noise generation by conductor corona.

2.1 Electrical Characteristics of Gap Type Discharges

The gap-type radio noise source is a more or less complete electrical discharge mainly in air between two metal parts. The type of discharge permits very low 60 Hz currents since one or both of the electrodes concerned have a high 60 Hz impedance to line conductors or to ground. These gap-type discharges may be localized or they may be distributed along the line. They are the principal cause of radio noise occurring on low voltage lines, below 70 kV. The artificial gap-type radio noise generator, Fig. 1, had an electrode spacing of 5/16 inches and was used on some of the lines tested. It was used with one electrode connected to the line conductor and the other electrode was left floating. This gap-type radio noise generator will produce broadband radio noise which can be measured beyond 1 GHz with dipole antenna 50 feet from line. The frequency spectra of this gap and of a gap between two suspension insulators as measured in the laboratory are shown on Fig. 2.

2.2 Electrical Characteristics of the Corona Discharge

The generation of radio noise by conductor corona is by means of the electrical discharge, usually called corona, occurring at or near the conductor surface. Corona is defined as "a luminous discharge due to ionization of the air surrounding a conductor around which exists a voltage gradient exceeding

a certain critical value." Many aspects on lines are unknown, undefined, and a calculation of radio noise generation, at least for the conductor diameters used for EHV lines, is not possible with the present state of knowledge. A short resume of the known corona processes for the case of a conductor will be given.

The basic physical process is that of electron multiplication or avalanche formation. The electric gradient in the vicinity of the line conductor is the highest gradient, and if this gradient or electric stress is sufficiently high, any electrons in the air around the conductor will ionize the gas molecules, and electrons produced by this ionization will produce an avalanche. If an additional electron is formed in this gradient by some process from the original electron avalanche, a new avalanche is formed by this secondary process and a self-maintaining discharge is developed.

In the case of the transmission line conductor, it is believed that the important secondary process is the ejection of electrons from gas molecules by high energy ultraviolet light (photoionization) generated by the original avalanche. It has been found by several investigators that the radio noise generated when the conductor is at positive potential is signifi tly greater, at the gradients generally used for line conductors, than it is with the conductor at negative potential. In the case of a positive line conductor, the cathode is so far away that cathode emission is of no consequence, and the secondary process existing in this case is photoionization of the gas.

The positive corona which is the principal cause of radio interference is of the streamer type; that is, a compact and bright filament starting from the conductor and extending out and ending in a tree-like discharge array. This type of discharge can be heard by ear directly and readily photographed at night. Sharp current pulses occur and radio noise is produced. Some aspects of this streamer corona are known. These streamers propagate at very high velocities 2×10^7 to over 10^8 cm per sec. Also because of the electric field intensification by the streamer itself, it propagates into fields which are below the critical breakdown as based on the non-uniform field around the conductor with no ionization. Near the conductor surface, however, an opposite effect occurs in that the field is reduced which tends to inhibit the streamer. The current pulse formed is of the form $i = te^{-at}$. The positive corona pulse for a 5 cm advance of streamer at a velocity of 5×10^7 cm/sec. gives a rise time of 10^{-7} seconds.

When the conductor is at sufficiently high negative potential ionization occurs. In this case, the cathode emission process prevails and since this process is more efficient than the gas photoemission process with conductor positive, it is expected that negative corona starts at lower conductor gradients than does positive corona. The current pulses have longer rise time and their peak values will not reach the magnitude of the positive pulses. The negative corona pulses will give considerably lower readings as has been found by measurement using an oscilloscope in the radio noise meter peak detector output.

When streamer corona forms at a "point" on the conductor two pulse fields will exist. Near the streamer a localized or direct field is formed,

and along the line the indirect field is developed due to the pulses traveling down the line. For design of EHV lines only the indirect field is considered and the most significant measurements are made at some distance from the streamer locations and their direct field.

Gap-type sources can and do occur on EHV lines, however, they occur rarely and the cause can usually be eliminated when necessary. The principal radio noise source on EHV lines is the corona-type discharges which may form at hardware, insulators, at burrs and scratches on the conductor surface and by discharges of various kinds at towers. Since radio noise may be caused by particles, such as raindrops, snow, aerosols, dirt, vegetation and insects, that may pass within the near electric field of the conductor or be on the surface of the conductor, radio noise generation becomes variable and determination of the average radio noise level of a line is usually made by comparison methods based on long term recordings or several fair weather readings and on measurements made in rain. With respect to communication sites near lines the radio noise levels in rain are highest and therefore most important.

3. Instrumentation

3.1 The principal instruments used for the field strength measurements were:

Frequency Range	Name	Manufacturer
30-15,000 Hz	NM-40 Field Intensity Meter	Stoddart Electro-Systems
0.014-0.25 MHz	NM-10 Field Intensity Meter	Stoddart Electro-Systems
0.010-0.16 MHz	NM-12T Field Intensity Meter	Stoddart Electro-Systems
0.15-25 MHz	NM-20B Field Intensity Meter	Stoddart Electro-Systems
20-400 MHz	NM-30A Field Intensity Meter	Stoddart Electro-Systems
375-1000 MHz	NM-52A Field Intensity Meter	Stoddart Electro-Systems
30-300 MHz	AP-501R Low Noise Tunable Amp.	Electro-International Inc.
300-1000 MHz	AP-502R Low Noise Tunable Amp.	Electro International Inc.

Frequency Range	Name	Manufacturer
1-10 GHz	Polarad FIM-B2 with Tuning Heads FIM-L, FIM-S2, FIM-M2.	
1-10 GHz	Polarad Microwave Receiver Model TR with Tuning Units CFI-L, CFI-S, CFI-M, CFI-X	
1-10 GHz	Watkins-Johnson Traveling Wave Tubes Models WJ-268, WJ-269, WJ-271, WJ-276.	
10 MHz-10 GHz	Hewlett-Packard Model 8551A/ 851A Spectrum Analyzer	
0.010 MHz-10 MHz	Hewlett-Packard Model K15-8551B Spectrum Analyzer UP Converter	
50 Hz - 1 MHz	Tektronix Type 1L5 Spectrum Analyzer Unit	
-	Tektronix Type 549 Storage Oscilloscope	
0.01 MHz-10 GHz	Empire Devices Inc. Model 1G118B Microwave Impulse Generator	
0.01 MHz-1 GHz	Empire Devices Inc. Model 1G-115 Impulse Generator	
300-1000 MHz	Measurement Corp. Standard SG Model 84 TV	
2-400 MHz	Measurement Corp. Standard SG Model 80	
5 KHz-50 MHz	General Radio SG Model 1001A	
0.55-720 MHz	Sprague Interference Locator M-500	
	Mosely X-Y Recorder Model No. 3	
	Polaroid Scope Camera with UV Light	

These instruments and accessories were carried in a 7-1/2 ton van, equipped with antenna supports, shelves and straps for tying down the instruments.

3.2 Antennas Used

Frequency Range	Name	Manufacturer
30-15,000 Hz	Electric Probe	Stoddart Electro-Systems
0.15-0.25 MHz	1 and 2 Meter Vertical	Stoddart Electro-Systems
0.15-25 MHz	1 Meter Vertical	Stoddart Electro-Systems
20-80 MHz	Dipole	Stoddart Electro-Systems
90-350 MHz	BCA-902 Bi-Conical	Electro-International Inc.
275-1000 MHz	BCA-901 Bi-Triangle	Electro-International Inc.
1-10 GHz	Polarad Horn Antennas Model CA-L, CA-S, CA-M, CA-X and Reflector Model CA-R.	

3.3 Calibration of Instruments

The instruments were calibrated with signal generators and impulse generators. In this report practically all the data is in dB peak above 1 μV/m/MHz bandwidth and all calibrations are referred to rms value of sine wave. The overall general accuracy of measurements is estimated to be $\pm$2 dB up to 25 MHz and $\pm$3 dB from 25-10,000 MHz.

4. Methods of Measurement

In the frequency range up to 24 MHz measurements of the field strength were made with receivers on the ground and antenna on the receiver or on a ground plane. Above 24 MHz up to 1000 MHz practically all field strength measurements were made with receivers inside the van and the antenna on the van roof bringing the antenna 20.5 feet above ground level. For the 1-10 GHz range the horn antennas were 15 feet above ground level. As many as three receivers were used at the same time at different distances from the line under test. All receivers were monitored by headphones and readings were taken even if only the meter residual was present. This was done in order to make sure that at the specific test location radio noise from the line could not be measured or heard in the headphones.

All directional antennas were rotated for maximum signal with the aid of the remote indicating meter available with instruments. Dipole antennas

were set true vertical and horizontal with the horizontal dipole rotated for maximum and the horn antennas (1-10 GHz) were tilted for maximum. The FI (Field Intensity), QP (Quasi-Peak), and Peak detector readings were taken on all meters at practically all test locations.

The antennas were set up on all lines at standard distances of 50 and or 200 feet laterally from nearest phase conductor. Other distances used were 300, 400, 500, 800, 1200 and 1600 feet. Locations farther away were in sight of the line and were chosen depending on accessibility, trees, cultivation, other lines, auto and truck traffic, and on permission of the land owner. For the investigations of the field strength lateral profiles were usually taken at distances 20 feet apart and to 200 feet on both sides of center line. In the laboratory the antennas were 20 feet from the test conductor.

The X-Y recorder or the spectrum analyzer were used with 41-inch vertical antenna from .014 to 30 MHz, with dipole tuned to 60 MHz (calibrated for the other frequencies used with this dipole antenna) from 30 to 100 MHz and with the broadband antennas above 100 MHz. The correlation of manual readings with spectrum analyzer photographs is discussed in Appendix I of this report.

4.1 The Artificial Gap-Type Radio Noise Generator

The artificial gap-type radio noise generator simulates natural gaps on lines and it was used as an aid in the investigation of the radiation from lines and of the longitudinal and lateral propagation characteristics. A gap in air can be made to generate noise above the normal noise level of a line and it also extends the normal line frequency spectrum to much higher frequencies.

The artificial gap can be placed on a line at least nine miles from end of the line and at a place with suitable terrain and low ambient for investigations and for measurements. A natural gap on a line may generate just as much radio noise but it may be at a location unsuitable for the measurements required.

A drawing of the gap is shown on Fig. 1 and a photograph on Fig. 3a. The frequency spectrum of radio noise voltage of this gap is given by Fig. 2.

4.2 Power Lines Measured for Radio Noise

The following list of lines includes figure numbers for the test location plan, figure numbers of photograph of nearest tower or pole, conductor heights, conductor gradient and figure numbers of normal line frequency spectrum. Conductor gradients are for center phase and outside phase for vertical and horizontal conductor configuration respectively. For the 800-kV dc line the conductor gradients are given for the positive and negative conductor for both bipolar and monopolar operation.

Line kV and Type*	Test Loc. Fig. No.	Photo Fig. no.	Phase Cond. Heights Feet	Cond. Gradient kV_{rms}/cm	RI Freq. Spectrum Fig. No.
12 HCWP	-	3	38	-	16
345 VCDC	4	11a	108,129.5,153	17	17,18
345 HCWP	5	11b	46	15.7	22,23
525 HCST	6	11c	55 116	15.6	24,26
735 HCST	7	11d	90	16	30,31,33,34,35
765 HCST	8	12b,d	90	17.1-A Line 22.32-C Line	
**800 HCST	9	12a	67	-22.57,+22.57	38,39,48
+400,-400 HCST	-	-	-	+19.4,-19.4	41
345 HCST	10	-	55	15.4	48

* = In the above tabulation the abbreviations for the lines are:

VCDC = Vertical Configuration Double Circuit
HCWP = Horizontal Configuration Wood Pole
HCST = Horizontal Configuration Steel Tower
** = This is direct current test line bipolar.
+400 and -400 are for direct current line monopolar.

The original photographs of line towers etc., were obtained with Polaroid black and white or on 35 mm film. The conductor heights were measured at the test location by means of a "Telehite" and tape measure and the conductor gradients were obtained by computer.

4.3 Laboratory Measurement

4.3.1 Conducted and radiated measurements were made in the Trafford EHV Laboratory with the 650-kV NEMA-107-1964 High voltage test circuit as shown by schematic on Fig. 13. Conducted measurements were made in the 5L38 shielded room, which has a 60-kV NEMA high voltage test circuit. These laboratory measurements were made with (1) artificial rain falling on a conductor (see Fig. 3c), (2) with the 5/16-inch artificial gap connected to conductor and (3) with two suspension insulators with a gap type discharge between them.

The measurements were made to obtain data as to what correlation, if any, exists between laboratory and field measurements and to determine if radio noise is generated by conductor corona and gap discharges in the 1 to 10 GHz frequency range.

4.3.2 Artificial Gap Spectra

The conducted frequency spectrum of the 5/16-inch artificial gap was measured in both the 60-kV and the 650-kV laboratory test circuit from 0.015 to 10,000 MHz. The frequency spectrum and the circuit used in the 60-kV lab-

oratory are shown on Fig. 2. The test circuit is the same as Fig. 1 of Technical Report No. RADC-TR-66-606, March 1967. The spectrum obtained from 1 - 10 GHz has been added. Several check measurements were made at lower frequencies to make sure the test conditions and circuit were essentially the same. The output of the gap with the 150 ohm loading is 150 ±2 dB above 1 μV/MHz bandwidth up to 30 MHz. Beyond this frequency the output drops and with marked fluctuations above 200 MHz. It can be seen from Fig. 2 that radio noise can be measured from a gap discharge up to the maximum test frequency of 10 GHz.

The conducted and radiated measurements made with the 5/16-inch gap on the 650-kV NEMA test circuit, Fig. 13, in Trafford High Voltage Laboratory, are shown in Fig. 14. The conducted spectrum obtained with the ultra high voltage test circuit has lower values than the 60-kV test circuit and readings start to decrease rapidly at much lower frequency (about 5 MHz). Also, because of circuit losses, this 650-kV test circuit cannot measure conducted above 250 MHz whereas the 60-kV test circuit in 5L38 Laboratory will measure up to 3 GHz, since this test circuit is physically much smaller, and is considered to have lower losses.

The laboratory radiated measurements gave a spectrum which corresponds much better than laboratory conducted measurements to the spectra obtained on power lines with the 5/16-inch artificial gap, see for instance, Fig. 42 obtained on power lines. Where radiation measurements were made with dipole or vertical antennas it was necessary to use small metal shields at tips of antennas to prevent tip corona. Figure 3d is a photograph of corona on ends of a dipole which is 20 feet from conductor energized at 255 kV to ground.

4.3.3 Gap-Discharge Between Two Suspension Insulators

Two suspension insulators of the type used on high voltage lines were insulated from each other with two thicknesses of 7 mil tape at the ball and socket joint. The two insulators were then suspended from the center of the test conductor in the 5L38 Laboratory and energized at 22 kV ac to ground. Conducted radio noise measurements were made in the 0.15 MHz to 10 GHz range. Figure 2 gives the frequency spectrum in the 0.15 MHz to 10 GHz range for the suspension insulator gap discharge. Radio noise could be measured up to 4 GHz. The spectra for the 5/16-inch gap is included in this figure for easy comparison. These spectra are attenuated rapidly with frequency above 50 MHz by the 650-kV NEMA test circuit. It can be seen that the shorter gap, about 0.014", in the suspension insulators, has about 30 dB less output than the 5/16-inch gap at frequencies below 20 MHz. However, the difference in magnitude from the two gaps decreases with increasing frequency and is only a few dB above 100 MHz.

4.3.4 Corona Source Spectrum

The radiated spectrum of conductor corona was also obtained in the Trafford Laboratory with artificial rain to the test conductor, which was a two-conductor bundle of two 1.65 inch diameter 5005 all-aluminum alloy conductors. Figure 3c is a photograph of a conductor in laboratory rain.

Figure 15 is the spectrum obtained in heavy rain amounting to 0.03 inches per minute. The corona spectrum for a conductor in rain is of lower magnitude and of different form than the spectrum obtained with the 5/16-inch gap. Radio noise was low at 5 GHz but it could be measured with the instruments available.

5. Discussion of Measurements on Power Lines

This Section 5 discusses data and curves of frequency spectra for power lines as found and tests on lines where the 5/16-inch artificial gap was connected to one of the line conductors.

5.1 Frequency Spectrum for 7.2-kV Low Voltage Line

Measurements were made on a low voltage line with a gap-type radio noise source. The pole which has this source is shown on photograph of Fig. 3b and was found originally with the Sprague Interference Locator M-500. The frequency spectrum shown on Fig. 16 was measured at 100 feet in the 0.15 to 25 MHz range and in the 1 to 10 GHz range. Radio noise was detected in the 1 - 10 GHz range from 1 to 2 GHz. In the 0.15 - 25 MHz range the spectrum is quite flat with maximum and minimum values 20 dB apart.

5.2 345-kV Vertical Configuration Double Circuit Line

5.2.1 Line Normal

This line, see Fig. 11a and Fig. 4, was tested in the 0.15 to 25 MHz and in the 1 - 10 GHz range. The measurements in the 0.15 - 25 MHz range were made for reference purposes at 100 feet laterally and east of tower 473. (This is the same test location used for tests reported in RADC-TR-66-606, March 1967.) The frequency spectra for the 0.15 - 25 MHz range are shown in Fig. 17 for October 6 1967 and for previous tests made on November 19, 1965. The frequency spectrum obtained in the 1 - 10 GHz range was obtained at 50 feet laterally on October 6, 1967. The spectrum obtained is on Fig. 18. This figure also shows the location of antenna and height of line conductors. Radio noise could be measured above instrument residual up to 2 GHz. See Figures 46 and 47 in previous report RADC-TR-66-606 March 1967, for radio noise data on this line in the 0.015 to 1000 MHz range.

5.2.2 With 5/16-Inch Artificial Gap on 345-kV ac Line

The 5/16-inch gap was connected to the bottom phase and measurements were made in the 1 - 10 GHz range on the test location shown by Fig. 4. With the gap at tower it was possible to obtain data which indicates lateral attenuation near ground level in the giga-hertz range.

The measured lateral attenuation for 1, 1.25, 2, 2.5, 3 and 3.5 GHz is shown in Fig. 19 for vertical polarization and on Fig. 20 for horizontal polarization. The curves shown approximate the radiation attenuation of 1/distance for both vertical and horizontal polarizations. The frequency spectra obtained at the various distances from the gap are shown on Fig. 21. The radio noise from this gap could be measured up to 8 GHz at 109 feet and up to 3.7 GHz at 900 feet.

5.3 345-kV Horizontal Configuration Wood Pole Line

5.3.1 This line uses wood towers as shown on Fig. 11b. The test locations for this line are on Fig. 5. Measurements were made in the 1 - 10 GHz range for the first time and in the 0.15 - 25 MHz range for reference purposes and comparison with previous measurements reported in RADC-TR-66-606, March 1967. Figure 22 is a plot of the data obtained in 1966 and of the data obtained in 1968 when the measurements in the 1 - 10 GHz range were made. The "flatness" of these spectra indicate that gap type source or sources were present on this line during both test times.

The measurements obtained in the 1 - 10 GHz range 50 feet laterally (60 feet from nearest conductor) are plotted on Fig. 23. In this case radio noise could be measured up to 2.5 GHz with antenna 15 feet above the ground plane (earth).

5.4 525-kV Horizontal Configuration Steel Tower Line

A photograph of the two 525-kV lines is shown on Fig. 11c and the test locations are shown on Fig. 6. Only one of the 525-kV lines shown on Fig. 11c was energized during the test period in January 1968.

5.4.1 Measurements with Line Normal

The radio noise spectrum was measured from 0.01 MHz to 10 GHz and is shown on Fig. 24. The spectrum was measured 50 feet laterally from a point on the ground directly under the outside phase conductor. Radio noise was detected from 0.010 MHz to 1.75 GHz. A lateral profile as on Fig. 25 was obtained for this line near midspan. It will be noted that the profile is unsymmetrical and that the radio noise is higher going west and under the unenergized West line conductors. A calculated curve is shown for the East side of the line. This calculated curve is based on the method described in Appendix II - Calculation of Electric Field Near a Transmission Line found in previous report RADC-66-606 March 1967. Readings were taken at five distances up to 3500 feet from line tower in the 0.01 - 25 MHz range. The frequency spectra for each distance are shown on Fig. 26. The form of spectra changes with distance, as would be expected.

5.4.2 Measurements with 5/16-Inch Gap at Tower

The 5/16-inch gap was connected to the outside phase (East phase of the East line) at the tower. Measurements were then made in the 0.15 - 25 MHz and 1 - 10 GHz ranges at several lateral distances from the gap. Measurements were made in the 0.15 - 25 MHz range to determine if the guyed steel towers used on this line had radiation characteristics similar to the radiation characteristics of the self-supporting steel towers used on the other lines. These frequency spectrum measurements are plotted in Fig. 27 for the 0.15 - 25 MHz range and on Fig. 28 for the 1 - 10 GHz range for vertical polarization. The values were on the average lower with horizontal polarization.

Large variations in magnitude, 10 - 15 dB, occurred with small frequency changes in the frequency range from 2 MHz to 10 MHz. This type of variation in magnitude was found for all lines tested which had a natural

gap source or were tested with the 5/16-inch artificial gap. See Figure numbers 86,87, 92, 98 in Vol. I of RADC-TR-66-606, March 1967 report on High Voltage Power Line Siting Criteria.

This oscillation in the spectrum shows up at other towers on the line as shown by part of data on Fig. 92 of above report taken 2.75 miles from the tower with the gap type source. This 525-kV line under normal conditions with conductor corona, gives a smooth spectrum as can be seen from Fig. 26. It is expected that with gap type sources the radiation is more efficient and the towers on the line for several miles act as relatively efficient radiators. The direction and magnitude of the radiation changes with frequency in a most complex manner because of the many possible radiating elements composing a steel tower.

A comparison of Figures 26 and 27 shows that this line had about the same radio noise level under normal conditions up to 3 MHz as was obtained with the 5/16-inch artificial gap on the East phase conductor. It is expected based on past experience that this noise level will decrease with aging of the conductors. The data should not be used to determine the noise level with rain. For noise level with rain compare with other similar lines on the basis of gradient, conductor diameter and conductor height.

The lateral attenuation from the gap in the 1 - 2 GHz range for both vertical and horizontal polarization is shown on Fig. 29. The inverse distance relationship is not as evident, especially at 2 GHz on horizontal polarizations, as was found on the 345-kV line, Fig. 19.

5.5 735-kV Horizontal Configuration Steel Tower Lines

The tests for 735-kV ac lines were made on the essentially identical North and South lines shown in photograph Fig. 11d. The configurations for these two lines and the test locations are given on Fig. 7.

5.5.1 Frequency Spectra 0.015 MHz to 7.4 GHz

Measurements were made from 60 Hz to 7.4 GHz. The frequency spectrum measurements at 50 and 200 feet from tower 0.015 MHz to 7.4 GHz are given on Figs. 30 and 31. Data for frequencies below 0.015 MHz are reported in Section 5.8. At 50 feet laterally from line tower radio noise was detected up to 1.5 GHz. In the 1 - 1.5 GHz range the antenna pointed toward the line insulators except at 1.12 GHz the antenna pointed toward nearest bundle conductor's spacer. At 200 feet laterally from the tower, radio noise was detected up to 400 MHz.

5.5.2 Lateral Profile

The lateral profile for these lines was obtained for the South line when the North line was de-energized. The lateral profiles are shown on Fig. 32 for 0.154, 0.5, 1.035 3.05 10.05 and 22.3 MHz. The effect of the de-energized North line can be seen as the appreciable increase in magnitude shown under the North line conductor, Fig. 32. In order to obtain a calculated field strength profile at 1.035 MHz of a magnitude about the same as the measured profile, a generation of 83.2 dB above 1 μV is required by the outside phase conductor and 87 dB by the center phase conductor.

5.5.3 Frequency Spectra in the 0.15 - 25 MHz Range

Several tests were made in the 0.15 - 25 MHz range on both the North and South lines. These tests were made because of the difference found in the noise level of the two lines in the beginning of tests and because a gap-type source appeared later in the tests resulting in modications of the frequency spectrum and an increase in the noise level.

The two lines are compared on Fig. 33. These curves were obtained from data taken 200 feet laterally from the center-line of the line. This location is 150 feet laterally from the outside phase. There is a considerable difference between these lines, varying from 19 dB to about 1.5 dB from 0.15 to 8 MHz respectively. This difference may be due to aging of the North line conductors. The North line was first energized on September 21, 1965 and was in service an average of 21 days per month; whereas, the South line was first energized on November 20, 1966 and was in service an average of 9 days per month. Obviously, the South line did not have a long continuous aging period as the North line. Also, the South line had been de-energized for exactly a month previous to the day these data were obtained. During this period, bugs dirt, etc. probably settled on the de-energized conductors.

During the tests a gap type source was first detected in headphones by its characteristic buzz on August 28th soon after the North line was re-energized after being de-energized on August 23, 24, 25, 26 and 27th. The radio noise level near the North line increased from 10 to 20 dB depending on the frequency as shown by curves on Fig. 34. The change with frequency was about 1/f before the gap source was detected and about $(1/f)^{1/2}$ after it was detected.

Measurements were made on both sides of towers at 14.1 and 22 MHz near the test site and at six locations from approximately 4.8 miles west to and approximately 6 miles east of the test site. The highest readings were obtained on the south side of tower 808 which is adjacent to the test site. See Fig. 7. The frequency spectrum was then obtained on both sides of tower 808 at a distance of 100 feet laterally from the center-line of the tower. The frequency spectra are on Fig. 35. At the higher frequencies the radio noise level becomes unsymmetrical indicating that the source is at this tower 808 or not too far away. The same type of measurements were then made on tower 809. At this tower the radio noise level was symmetrical again supporting the view that the source is on the South phase of tower 808. Visual inspection and photographs were then made at night at tower 808. No sources were found other than those normally seen on the lower insulators on all phase conductors on this line.

5.6 765-kV Apple Grove Test Lines

This test line was used to obtain 765-kV data in the 1 - 10 GHz range because the data on the 735-kV lines described in Sec. 5.5 was not complete, in that it did not include measurements from 7.5 to 10 GHz because instrumentation was not then available.

The Apple Grove 765-kV C-line configuration and relative location of the three 2400-ft. test lines are shown on Fig. 8. Photographs of the A-line and C-line towers are shown by Figs. 12b and 12d. These test lines differ in that grading rings are used on the bottom of the insulator strings on the A-line and in that the A-line conductors are a bundle of four 1.38-inch diameter, 18-inch subconductor spacing, and the C-line conductors are a bundle of four 1-inch diameter, 18-inch subconductor spacing.

5.6.1 Measurements in the 1 - 10 GHz Range

Radio noise could not be detected in the 1 - 10 GHz range opposite A-line and C-line towers 90 feet from the nearest conductor and insulator string and hardware. Radio noise was, however detected in the 1 - 10 GHz range at approximately 60 feet from the nearest 765-kV substation apparatus. The spectrum for this substation source is on Fig. 36. Radio noise could be detected from 1 to 6 GHz. Time was not available for finding this source. Tests could only be made from outside the substation fence.

5.6.2 Effect of Gap Discharge at Fence

Metal objects even near ground level and in the electric field of extra high voltage lines may discharge to each other and cause radio noise. Fences parallel to and near the conductors may have these discharges.

A 200 foot long steel wire was placed four feet above ground level and insulated from the steel fence posts used for this experiment. A gap about 5/32 inch long was then formed between the fence wire and one of the posts. This gap and fence are shown on Fig. 12c.

Measurements were made on this fence discharge in the frequency range from 0.015 MHz to 10 GHz at a distance of 200 feet laterally from the fence. Figure 37 gives the frequency spectrum obtained.

This spectrum for discharge at the fence is characteristic of gap-type discharges and radio noise is higher than for normal high voltage lines in corona with the conductors dry. Higher and lower noise levels can be obtained depending on the radiation characteristics of the metal objects forming these gap discharges in the electric field. Also the number of pulse groups from a three phase line will be twice as many as for conductor corona because these air gaps generate noise on positive and negative half cycles of the 60 Hz wave. In fact, an oscilloscope connected to output of radio noise meter will indicate if a line has gap-type sources energized from all three phases or if the line has corona-type sources.

5.7 800-kV Direct Current Test Line

Radio noise measurements were made on a 4.9 mile long direct current test line which could be operated ±400-kV bipolar, or negative or positive monopolar. This test line has two conductors and one ground wire. It has 1.26 miles of two-conductor bundle of 1.82 inch diameter ACSR and 2.96 miles of a single 2.4 inch diameter ACSR conductor. All the tests were made near

the center of the line and adjacent to the 2.4 inch diameter conductor. A photograph of steel tower at the test site is shown by Fig. 12a and the dc line conductor configuration and the radio noise measurement locations are shown by Fig. 9.

A photograph of this line in bipolar operation is shown by Fig. 49. The positive conductor has numerous corona plumes whereas the negative conductor is practically dark. This photograph was made by the Bonneville Power Administration and it is included in this report with their kind permission.

Besides the tests made with line normal, tests were also made with the 5/16-inch gap connected to the positive conductor and to the negative conductor. It was necessary to modify the gap for direct current operation by removing the 6-inch hemisphere and replacing it with a 6-inch diameter barbed ring. In this way some corona is produced at the ring and repetitive discharges are formed at the gap.

5.7.1 Frequency Spectra with 800-kV Direct Current Line Normal

5.7.1.1 Bipolar Operation

The frequency spectrum in fair weather obtained at 50 feet laterally from tower (76 feet from the nearest conductor for 0.015 - 25 MHz range and 70 and 72 feet in the 30 MHz to 10 GHz range) is shown on Fig. 38. Radio noise was detected up to 350 MHz. No noise could be measured in the 1 - 10 GHz range - fair weather or in light rain. The magnitude of noise in the 0.015 to 30 MHz range is about the same in fair weather as for ac lines with the same conductor gradients. Manual data in rain was obtained only in the 0.15 - 25 MHz range and in the 1 - 10 GHz range. Rain data was obtained with the spectrum analyzer at other frequencies. Intermittent high noise levels were noted during rain at 50 feet from tower especially on dipole antennas. This is believed to be due to static on the antenna. These results are discussed in Appendix I.

The effect of rain was obtained in the 0.15 to 25 MHz range. In this range the frequency spectra shown on Fig. 39 were obtained 200 feet laterally at mid-span with and without rain. These spectra are not as smooth as found on long lines but vary considerably because of reflections from the open end of the test line and partial reflections at the station end. The noise level in rain is, however, consistently lower than in fair weather. This characteristic for dc lines is just the opposite to ac lines where heavy rain produces an increase in the radio noise level of 24 dB. With respect to radio noise due to conductor corona in rain dc lines are not as important as ac lines. Measurements by other investigators on 800-kV dc lines confirm this effect of rain for dc lines.

5.7.1.2 Monopolar Operation

Measurements were made in the 0.15 - 25 MHz range with positive monopolar operation (+400 kV on positive conductor to ground, negative con-

ductor grounded) and negative monopolar operation (positive conductor grounded). These measurements were made to obtain a comparison between conductor negative and conductor positive. The frequency spectra were obtained in the 0.15 to 25 MHz range and they are shown in Fig. 41. The radio noise was about the same for positive and negative conductor polarity between 0.5 MHz and 1.6 MHz. Below 0.5 MHz it was considerably higher on monopolar negative, 25 dB at 0.154 MHz, and it was 25 dB higher from 3 to 4 MHz on monopolar positive. It will be shown later that for tests with the 5/16-inch gap on positive and on negative monopolar operation, monopolar negative has the higher radio noise above 0.6 MHz.

5.7.1.3 Lateral Profile at Mid-span

The lateral profile for this dc test line at mid-span under bipolar operation is shown on Fig. 40. The lateral profile is considerably different than for ac lines, see Fig. 32, in that only one crest occurs and that the crests are shifted to be under the conductors. This is because the positive and negative polarity generators are not of the same magnitude and these relative magnitudes change with frequency. The calculated lateral profile for the same generation on both positive and negative conductors is shown by the dashed line on Fig. 40 for 1 MHz. This profile was obtained assuming a generation of 100 dB above 1 μV on the positive conductor.

5.7.1.4 Comparison of 800-kV dc Line with 345-kV ac Line

A 345-kV ac line which has been in service for several years was tested in fair weather at the same time as the 800-kV dc line. Both lines were measured at 50 feet laterally from the outside conductor. This ac line is approximately four miles from the dc line. The comparison tests started at 1445 hours and finished near 1520 hours on January 8, 1968. The frequency spectra obtained are on Fig. 48. The radio noise level on the 345-kV ac line is lower than on the dc line. This is expected for this ac line, based on the conductor diameters and their gradients as shown by the calculated curves for the 2.4 inch conductor at 800 kV dc and the 345-kV ac line on Fig. 48 for the lateral distance of 50 feet.

5.7.2 Measurements with 5/16-Inch Gap

Radio noise measurements were made in the 0.015 MHz to 10 GHz range with bipolar operation at 800-kV dc on the test line and with the 5/16-inch artificial gap connected to the negative conductor at tower. Measurements were also made in the 0.15 to 25 MHz range with bipolar operation $\pm$400 kV with the 5/16-inch gap connected to the positive conductor.

5.7.2.1 Frequency Spectra with Bipolar Operation at 800 kV

The frequency spectrum obtained at 200 feet with the gap connected to the negative conductor is shown on Fig. 42. It was possible to measure radio noise at this distance over the range of 0.015 MHz to 7 GHz. The noise level fluctuates at the low frequencies, below 1.5 MHz, because of the

test line characteristics and it fluctuates rapidly because of tower radiation characteristics in the 1.8 to 5 MHz range as has been found and discussed previously for gap type sources. The 5/16-inch gap was connected to the positive conductor and measurements made in the 0.15 - 25 MHz range. These measurements are compared on Fig. 13 to those obtained with the gap connected to the negative conductor. At the higher frequencies, above 4 MHz, there is as much as 30 dB difference in gap output. This was unexpected since the gap is symmetrical in that both of the gap electrodes are exactly alike. Later on, measurements were made in the 2-L Laboratory with a $\pm$250-kV high potential tester. The 5/16-inch artificial gap was set at 5/32 inch for insulation reasons and measurements were made in the 0.15 - 25 MHz range on both positive and negative polarity. The test circuit was the same as shown on Fig. 2 and used for ac tests on gaps. Measurements were also made of the peak output on positive and negative half-cycles of the 60 hertz wave. This was done by means of a scope in the output of the NM-20 receiver and the peak measuring slide back circuit on this receiver. It was found for dc that the output is essentially the same on positive and negative polarity. For ac the peak values were essentially the same for both half cycles and of the same magnitudes as for the plus or minus dc measurements.

From these laboratory tests it appears that gaps give the same peak output on ac and dc. The reason for the decreased output for positive polarity on the 800-kV test line as shown on Fig. 43 is not known. At the test line there is a movement of ions from one conductor toward the other and these ions may have reached the gap and changed the breakdown characteristics of the gap when it was connected to the positive conductor. This effect did not exist during the laboratory tests. Comparison of Figures 27 and 42 for 200 feet distance shows that the radio noise from the gap was about the same from the 800-kV dc line as it was from the 525-kV ac line. This is expected based on the laboratory tests described above.

With the 5/16-inch gap on the negative conductor and the test line energized at 800 kV it was possible to make measurements from 0.015 to 400 MHz at 200, 400, 800 and 1300 feet from the tower with the 5/16-inch gap type source. The results are plotted on Figures 44, 45, and 46 for three frequency ranges. In the lowest frequency range of 0.01 to 0.154 MHz the attenuation is about $1/d^3$ or $1/d^2$ (see Fig. 44) and about $1/d$ in the other two frequency ranges, Figures 45,46.

At 1300 feet there was a fence 50 feet away and the antenna was between this fence and the line. This may be why Figures 45 and 46 show that readings at 1300 feet average somewhat higher than they do at 800 feet. At 400 feet on Fig. 46 there are two groups of readings. The lower group is at frequencies above 150 MHz. No explanation is available for this abrupt change in level above 150 MHz. These lateral attenuation curves for dc lines are similar to those obtained on ac lines and reported in RADC-TR-66-606 Vol. I, March 1967.

5.8 Low Frequency Electric Field Measurements - 60 Hz to 15 KHz

All measurements were made with the electric antenna mounted on a tripod at a height approximately six feet above ground and oriented for maximum indication on the field strength meter. See Section 3.1 for a

description of the instrument used. All measurements were made with the instrument bandwidth adjustment set to the measurement bandwidth of 8 Hz. The results of these measurements at 200 feet from the outside phase can be seen in Figures 50 through 52. Figure 53 shows the Audio Frequency Receiver residual for the different gasoline engine power supplies.

A lateral profile for the 525-kV line for 60, 180, 240, 300 and 360 Hz is shown plotted on Fig. 54. Figure 54 shows that as the frequency was increased the point at which the field strength started attenuating as the inverse distance cubed occurred closer to the 525-kV line. The electric field strength for 60 Hz between 50 and 400 feet cannot be compared directly with the other levels since the 60 Hz field strength in this distance range was above the instrument's measurement range. At some frequencies, the attenuation was greater than the inverse distance cubed relationship, but this could be due to the uneven terrain.

In Technical Report No. RADC-TR-66-606, March 1967, even order harmonics were measured on some lines 345 kV and below. Even order harmonics were detected on both the 525-kV ac and the 800-kV dc lines. On Fig. 50 all the harmonics for 525-kV line are plotted. The even harmonics were plotted up to and including 1200 Hz; but beyond this, for sake of clarity, only the odd harmonics were plotted. Figure 50 shows that the even and odd harmonics are about equal magnitude and this was also true above 1200 Hz.

The harmonics for the 800-kV dc test line (Fig. 52) were measured half-way between the positive and negative conductors. At locations 100 and 200 feet from the positive conductor, the electric field levels were quite low, mostly below ambient. This data indicates that a small amount of harmonics come through the rectifier equipment and without a definite pattern for either the even or odd harmonics.

The consistent presence of even harmonics during these tests led to laboratory measurements in an attempt to find an explanation. It was found that the 5/16-inch gap produces even harmonics when it is connected to a single phase line. This is similar to a single phase full-wave rectifier in that alternate periods of conduction and non-conduction will produce harmonics with an order of $k = 2n$, n is any integer. This analysis suggests that if similar gaps were hung on each phase of a three-phase line, harmonics of the order of

$$k = 6r \quad ,$$

would be generated which is what a six phase rectifier produces. A scope independent of the Stoddart NM40 was also used to observe the even harmonics generated by the 5/16-inch gap.

A General Radio pulse generator with a variable repetition rate was used to verify that noise could produce harmonics. The utput of the pulse generator was fed directly into the NM40. Repetition rates which produced frequencies of 50, 60 and 100 Hz were used and harmonics of the order of $k = 2n$ were detected.

The harmonics measured on the 525 and 735-kV line were made without the 5/16-inch gap hanging on one of the outside phases. If only corona is present on the line, the above analysis suggests that the positive corona (since it is much larger than the negative corona) would generate harmonics of the order

$$k = 3n \quad ,$$

or similar to a three-phase rectifier. Since the generated corona is larger for the center phase than for the outside phase for horizontal line configurations, it seems logical that the generated harmonics from the center phase would predominate. The harmonics generated would be of the order

$$k = n$$

or similar to a single phase half-wave rectifier.

This reasoning has not been verified experimentally.

6. Discussion of Results for Lines Normal

6.1 12-kV Line in the 1 - 10 GHz Range

Radio noise was detected from 1 to 2 GHz at 100 feet from the line conductors.

6.2 345-kV Line in the 1 - 10 GHz Range

Radio noise was detected on the vertical configuration 345-kV line up to 2 GHz at 105 feet from the nearest conductor and was detected up to 2.5 GHz on the 345-kV horizontal configuration wood-pole line at 60 feet from the nearest conductor.

6.3 525-kV Line in the 60 Hz to 10 GHz Range

In the 60 Hz to 0.01 MHz frequency range both even and odd harmonics of 60 Hz of approximately the same magnitude were detected. These harmonics varied as $1/d^3$ with lateral distance beyond 200 to 400 feet depending on the frequency. Radio noise was detected from 0.10 MHz to 1.75 GHz at 112 feet from the nearest conductor.

6.4 735-kV Line in the 60 Hz to 10 GHz Range

In the 60 Hz to 0.01 MHz frequency range the 120 Hz component and the odd harmonics of 60 Hz were detected. Radio noise was detected from 0.010 MHz to 1.5 GHz at 90 feet from the nearest conductor.

6.5 Apple Grove 765-kV West Project

6.5.1 1 - 10 GHz Range

Radio noise was not detected at 90 feet from the nearest conductor on the A or C test lines; however radio noise was detected from 1 to 6 GHz from the nearest 765-kV substation apparatus.

6.5.2 Gap Discharge on Fence Beneath Test Line in the 0.015 MHz to 10 GHz Range

Radio noise was detected from 0.015 MHz to 7.5 GHz at 200 feet laterally from the fence.

6.6 800-kV dc Test Line in the 60 Hz - 10 GHz Range

In the 60 Hz to 0.010 MHz frequency range a pattern of even and odd harmonics of about the same magnitude were detected, but some were not detected. These measurements were performed midway between the positive and negative conductors at ground level.

Radio noise was detected from 0.10 MHz to 350 MHz at 72 feet from the nearest conductor. This 800-kV dc line radio noise is lower in rain than in fair weather. In fair weather the dc line, based on measurements, has essentially the same radio noise level as ac lines and the prediction method for dry conductor corona for ac lines based on conductor gradients and diameter may be used for dc lines.

7. Discussion of Results of Laboratory Tests

7.1 In the 60 Hz to 0.01 MHz frequency range even harmonics could be detected from the 5/16-inch gap.

7.2 With artificial rain of 0.03 inches per minute applied to a conductor, radio noise was detected from 0.15 to 5 GHz with antenna 20 feet from the conductor.

7.3 Conducted and radiated measurements were compared with the 650-kV NEMA test circuit. It was found that radiated radio noise could be detected up to 10 GHz; whereas conducted radio noise could be detected only to 250 MHz.

7.4 Conducted radio noise was detected from 0.15 to 4 GHz on the 60-kV NEMA test circuit from a gap discharge between two suspension insulators.

8. Application of Results

This section gives methods of prediction for conductor corona type radio noise and for gap-type radio noise. In the predict on methods for power lines it is necessary to consider power lines below 70 kV separately from power lines above 70 kV. This separation is based on the fact that lines below 70 kV may have gap-type local sources and generally are free of conductor corona type radio noise, and that power lines above 70 kV, especially extra high voltage lines (345 kV and above), operate with conductors in corona. These higher voltage lines may also have gap-type local sources which, however, can be located and usually eliminated. Nevertheless, one should be aware of these possible sources. Based on the radio noise measurements made it can be said that there is no line voltage discrimination with respect to radio noise from power lines.

8.1 Prediction for the 525, 735 kV ac and 800 kV dc Lines for Conductor Corona Radio Noise

The measurements and analysis as reported apply to the ground wave propagation as affected by the presence of ground and as defined by Norton (see Appendix II). Sky-waves and tropospheric waves are not considered.

The prediction method for conductor generated radio noise from the 525 and 735 kV ac lines is similar to the method described for lines up to and including 345 kV, and reported in RADC-TR-66-606, Vol. II, March 1967. For dc lines the prediction method is the same except that the magnitude of conductor generated radio noise in fair weather is used because radio noise decreased with rain on the 800 kV dc line. For ac lines radio noise increased with rain and for heavy rain the increase is taken as 24 dB above the average fair weather value for ac lines and the rain value is used for prediction.

In the prediction of radio noise due to conductor corona the magnitude is based on a comparison method as shown by the following empirical equation. A comparison method is necessary because it is not possible to calculate corona noise generation from the presently known physical processes. The reference line is taken as a typical line with a one-inch diameter conductor with a gradient of 18 kV_{rms}/cm. For bundle conductors the maximum gradient on the subconductors is used in this report.

The empirical equation for comparing ac lines with radio noise due to conductor corona in fair weather or in rain is as follows:

$$E = E_o + 3.5\ (g - g_o) + 30 \log_{10} \frac{r}{r_o} + 20 \log_{10} \frac{h}{h_o} \frac{d_o^2}{d^2} \quad \ldots \quad 8.1$$

where E and E_o are in dB above 1 uV/m

g and g_o are the conductor surface gradient in kV_{rms}/cm

r and r_o are the conductor radii

h and h_o are the conductor heights

d and d_o are the distances to the conductor

For dc lines change the constant 3.5 to 2.48 and use the conductor gradient obtained from the dc voltages. The terms with the zero subscript refer to the reference line which has a one-inch diameter conductor with a gradient of 18 kV_{rms}/cm for ac lines and 25.4 kV/cm for dc lines.

The conductor gradients for lines tested are given in section 4.2 and for other lines they can be obtained from the gradient factor curves of Figures 3 and 4 of Appendix II, pp. 174, 175, RADC-TR-66-606, Vol. I, March 1967.

In the prediction method used here the equation is used to establish the radio noise magnitude at 1 MHz. The reference distance is taken as 200 feet because lines can be measured at this distance, data is available from other lines, and at this distance the radio noise magnitude for conductor corona decreases on the average as $\frac{1}{f}$ (20 dB per frequency decade). This can be seen from measured data, Figures 31a, 31b, 42 of this report and Figures 44, 46, 47, in report RADC-TR-66-606, March 1967.

The conductor corona noise magnitude prediction curves of Fig. 55 for the 525- and 735-kV ac lines in rain and for the 800-kV dc line in fair weather were obtained from the above equation with the one-inch diameter conductor in rain as the reference line. The magnitude E_o in equation 8.1 at 1 MHz, for the fair weather curve of Fig. 55 for the reference line is based on the average of published data for radio noise near several 345-kV lines of the Bonneville Power Administration and at the Apple Grove and EHV test projects. The curves for the 525- and 735-kV lines are for rain and are based on rain data on test lines and these curves are for rates of rain where the radio noise level no longer increases with rate of rainfall. For rainfall greater than about 0.25 inches per hour (defined as heavy rain) the increase in radio noise is insignificant.

A prediction for conductor corona type radio noise in heavy rain has been made for the 525-kV line assuming a 90 foot conductor height and 3 foot and 20.5 foot antenna heights and vertical polarization. (For corrections to dipole antenna heights above 20 feet see Fig. II-27, page 39 of report RADC-TR-66-606, Vol. II, March 1967.) The predicted values with lateral distance from the 525-kV line are given by Fig. 56 for the 0.015 - 15.3 MHz range and by Fig. 57 for the 30.72 MHz to 10 GHz range. The values on these figures were obtained by using the predicted magnitude versus frequency curve for 525-kV line from Fig. 55 and the lateral attenuation curves Figures II-8, II-9, II-11, II-12, II-13 in RADC-TR-66-606, Vol. II, pages 20, 21, 23, 24, 25 for the 0.015 - 15.36 MHz range and Figures 58 and 59 of this report for the 30 MHz to 10 GHz range. This prediction assumes plane earth with $\varepsilon = 30$ and $\sigma = 20$ milli-mhos/meter square.

These prediction curves, Figures 56 and 57, may be used for 735-kV line also since all conditions are the same and the magnitude is only 1 dB less (see Fig. 55) than for the 525-kV line. The 525-kV prediction curves may also be used for the 800-kV line given on Fig. 55 for 90 foot conductor height, by subtracting the 20 dB difference shown on Fig. 55 from the predicted values of Figures 56 and 57 for the 525-kV line.

8.2 Prediction for 7.2-kV Line in the 1 - 10 GHz Range

From the measurements made on this line in the 0.15 - 25 MHz range it is found that this line has a 4 - 10 dB higher noise level above 1 MHz than the 4.16-kV low voltage line which had the highest level of the low voltage lines tested and reported in RADC-TR-66-606, Vol. II, March 1967.

This 7.2-kV line is considered a typical low voltage line and the values measured in the 1 - 10 GHz range probably are upper bound values and may be used for all lines below 70 kV. For this range the maximum value of

54 dB was obtained at 1.48 GHz, at 100 feet away, with vertical polarization. For a distance of 200 feet this maximum value will be 6 dB less or 48 dB for test antenna height of 13 feet. For this prediction example a 20.5 foot receiver antenna height is assumed. This results in a correction of +2 dB and the radio noise magnitude is then 50 dB at 1.48 GHz. (For antenna height correction see Fig. II-27, page 39 of Report RADC-TR-66-606, Vol. II, March 1967.)

Figure 60 gives the magnitude for all lines as obtained from measurements in the 1 - 10 GHz range and corrected as in the above example. For some of the lines the highest values were obtained with horizontal polarization and for others with vertical polarization. These curves are for all the lines from which radio noise could be detected in the 1 - 10 GHz range and measured above the instrument residual. The change in magnitude with frequency is shown as $\frac{1}{f}$ or 20 dB per frequency decade. This is based principally on Figs. 21, 37 and 42 for the gap-type sources, where readings were obtained to several giga-hertz. These figures indicate that this is a good approximation for extrapolation of data measured only in the low end of the 1 - 10 GHz range.

By means of Fig. 60 and the lateral attenuation curves of Fig. 61 for antenna height of 20.5 feet and conductor height of 38 feet, the radio noise magnitude with lateral distance was determined and was plotted out to about 80,000 feet from the 7.2 kV line for 1.25, 5 and 10 GHz. This prediction assumes plane earth with $\varepsilon = 30$ and $\sigma = 20$ milli-mhos/meter square.

8.3 Prediction Method with Gap-Type Sources for the 735-kV Line for the 1 - 10 GHz Range

For the 1 - 10 GHz range the prediction will be made for the 735-kV line. The measured values are believed to be from gap-type sources from line parts at the tower. The 1 - 10 GHz antennas pointed at insulator strings for maximum meter reading. It is pointed out here that in the 1 - 10 GHz range no radio noise was detected from the A or C line towers at Apple Grove at 765 kV, see Sec. 5.6. Nevertheless, without a careful investigation of tower components, it is recommended that prediction be based on what was measured in the 1 - 10 GHz range on other lines. In this case the curve on Fig. 60 for the 735-kV line will be used with the lateral attenuation curve of Fig. 59 for conductor height of 90 feet and receiver antenna height of 20.5 feet. This is the same receiver antenna height used for the 7.2-kV line prediction.

The radio noise level to a lateral distance of about 80,000 feet is shown on Fig. 62 for this 735-kV line for the three frequencies of 1.25, 5 and 10 GHz. In this example, the prediction assumes plane earth with dielectric constant $\varepsilon = 30$ and conductivity $\sigma = 20$ milli-mhos/meter square.

The predicted values for most lines below 70 kV in the 1 - 10 GHz range can be approximated for 20.5 foot receiver antenna heights by using Fig. 61 directly because these low voltage lines do not differ much in conductor height.

For the two 345-kV and the 525-kV lines tested the predicted values in the 1 - 10 GHz range can be obtained for any distance out to 10,000 feet

by subtracting from curves of Fig. 62 the difference in magnitude shown on Fig. 60 between the 735-kV line and the 345- and 525-kV lines. Beyond 10,000 feet it is necessary, because of conductor height differences, to also use Figs. 3, 6 and 8 in Appendix II.

8.4 Prediction for the Fence Near 765-kV Line for the 1 - 10 GHz Range

This prediction is included because the conditions during this experiment can exist in practice and because relatively high radio noise was measured. In this case the transmitting antenna is 4 feet high and again a receiver antenna height of 20.5 feet will be assumed. The magnitude of radio noise from the fence gap at 200 feet away is given by Fig. 60. The lateral attenuation curve for prediction out to 60,000 feet is on Fig. 59 of this report. By means of these two curves the predicted radio noise from 200 feet to about 20,000 feet at 1.25, 5 and 10 GHz was determined and plotted on Fig. 63. This fence gap effect will be independent of line voltage as long as the 60 cycle field at fence is sufficient to break down the gap on the fence.

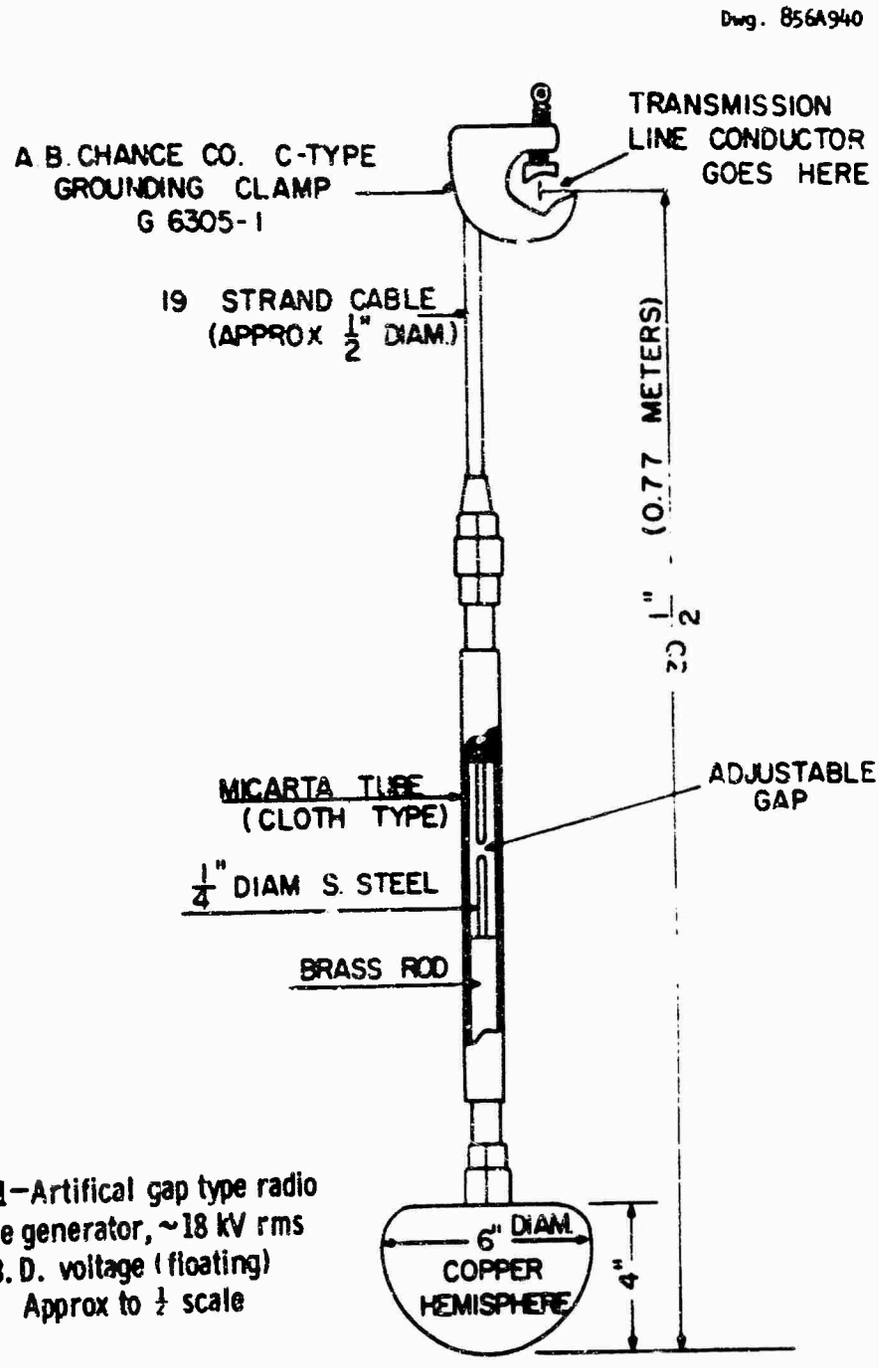


Fig. 1—Artifical gap type radio noise generator, ~18 kV rms B. D. voltage (floating) Approx to ½ scale

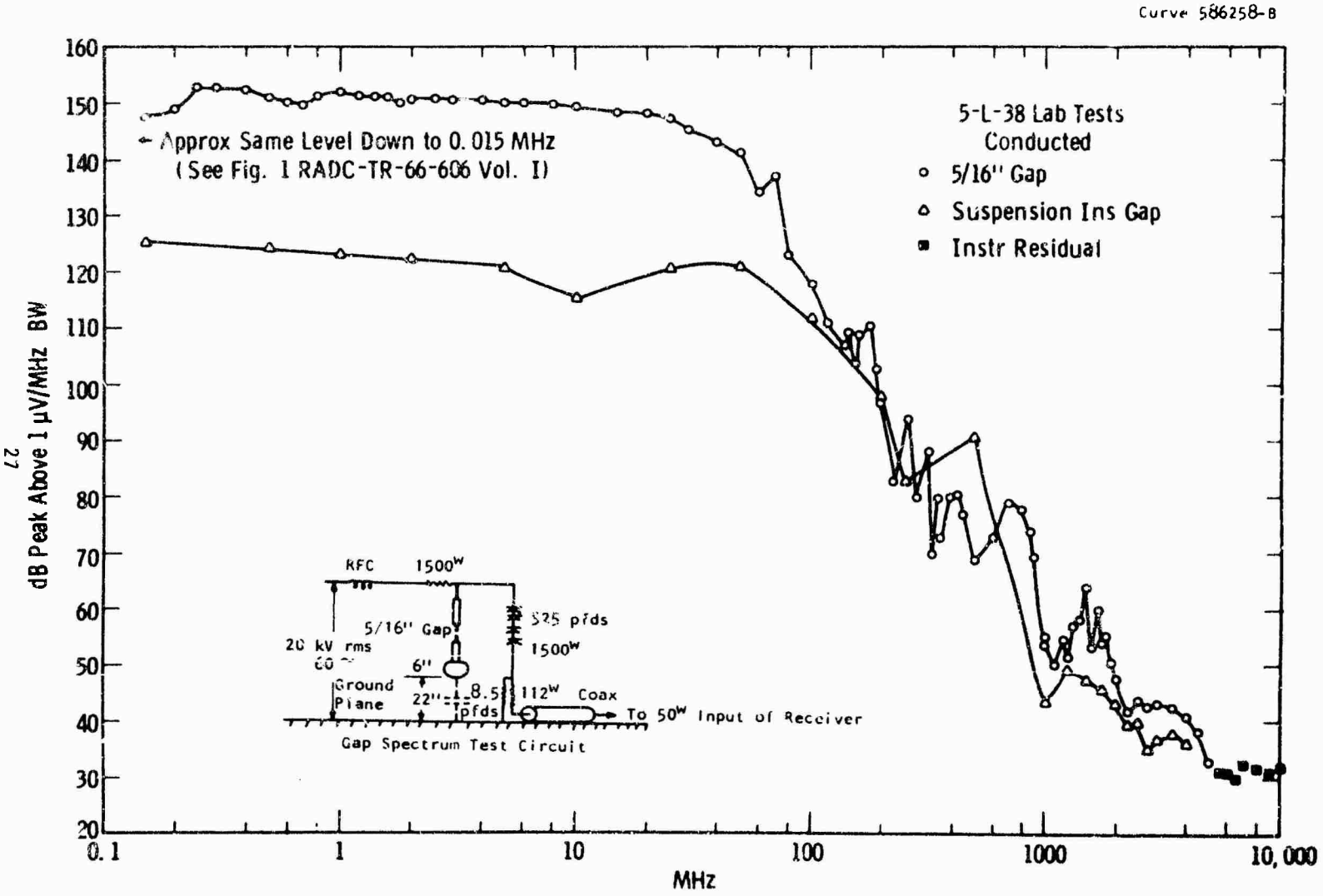
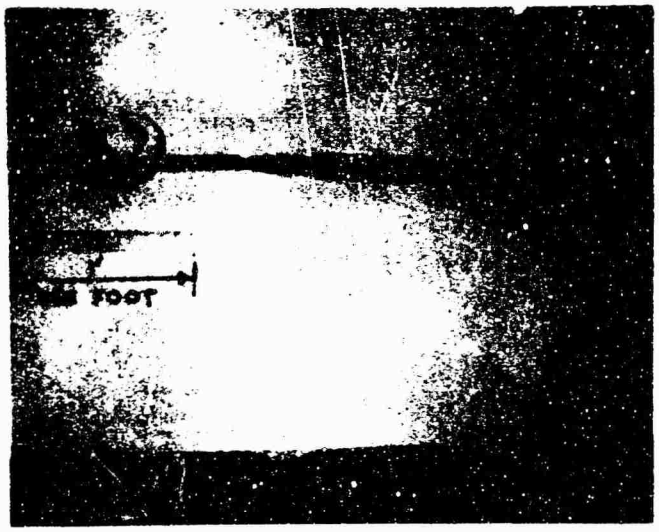


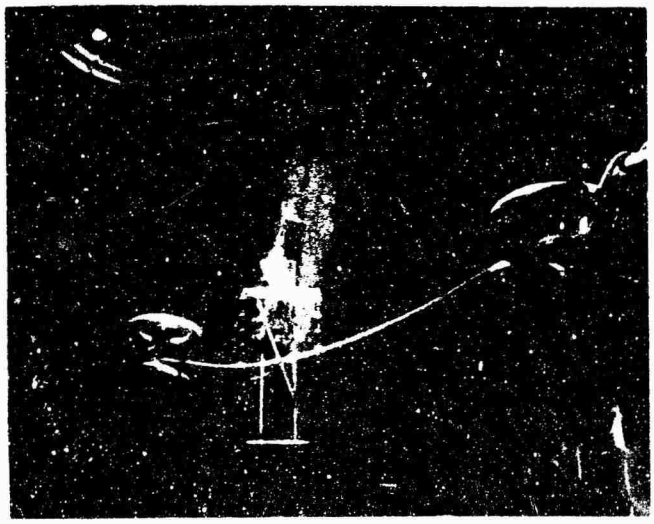
Fig. 2—Frequency spectrum for 5/16" gap and for suspension insulator gap



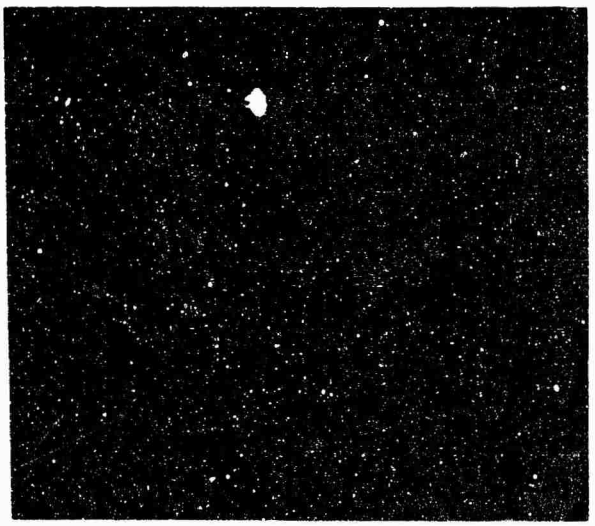
(a) Artificial Gap Type Radio Noise Generator



(b) Low Voltage Line tested in the 1 - 10 GHz Range

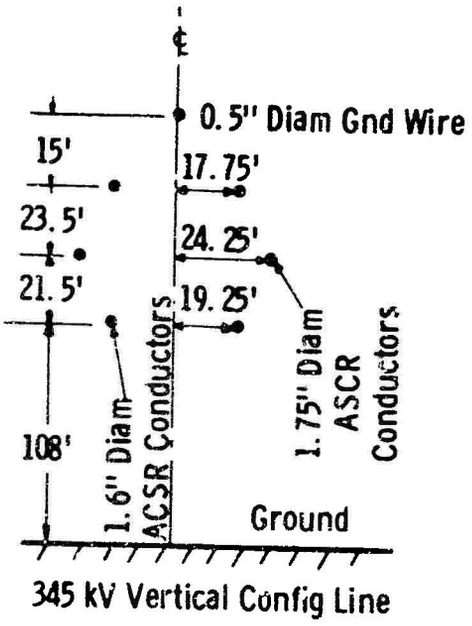


(C) Conductor Radio Noise Test in Laboratory Rain



(d) Corona at ends of dipole antenna

Fig. 3



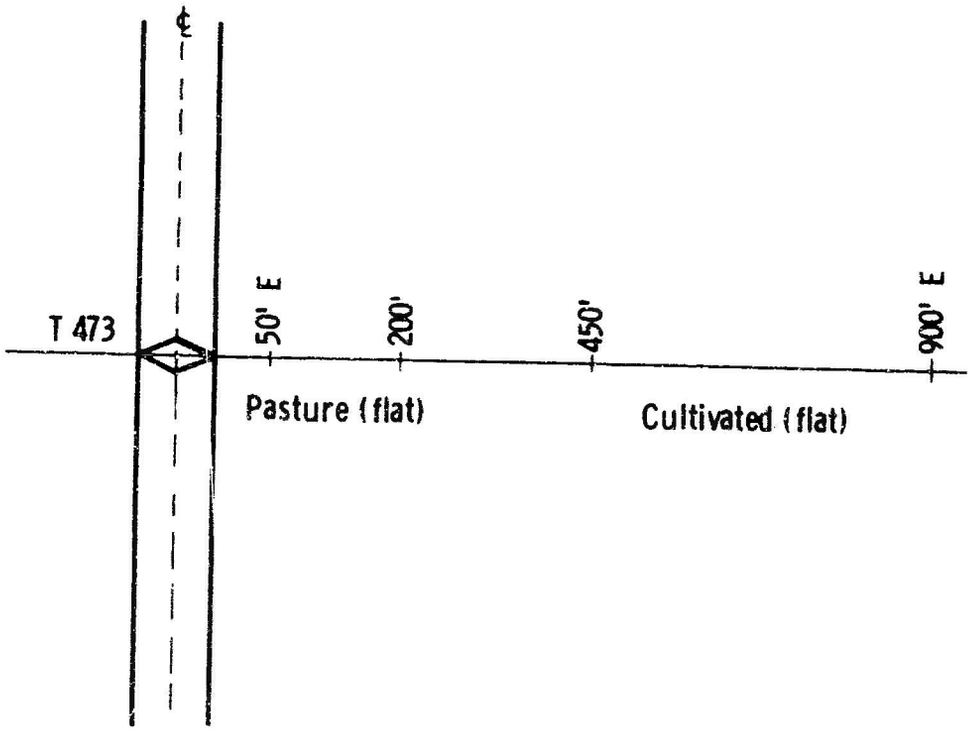


Fig. 4 —345 kV VCST line configuration and test locations

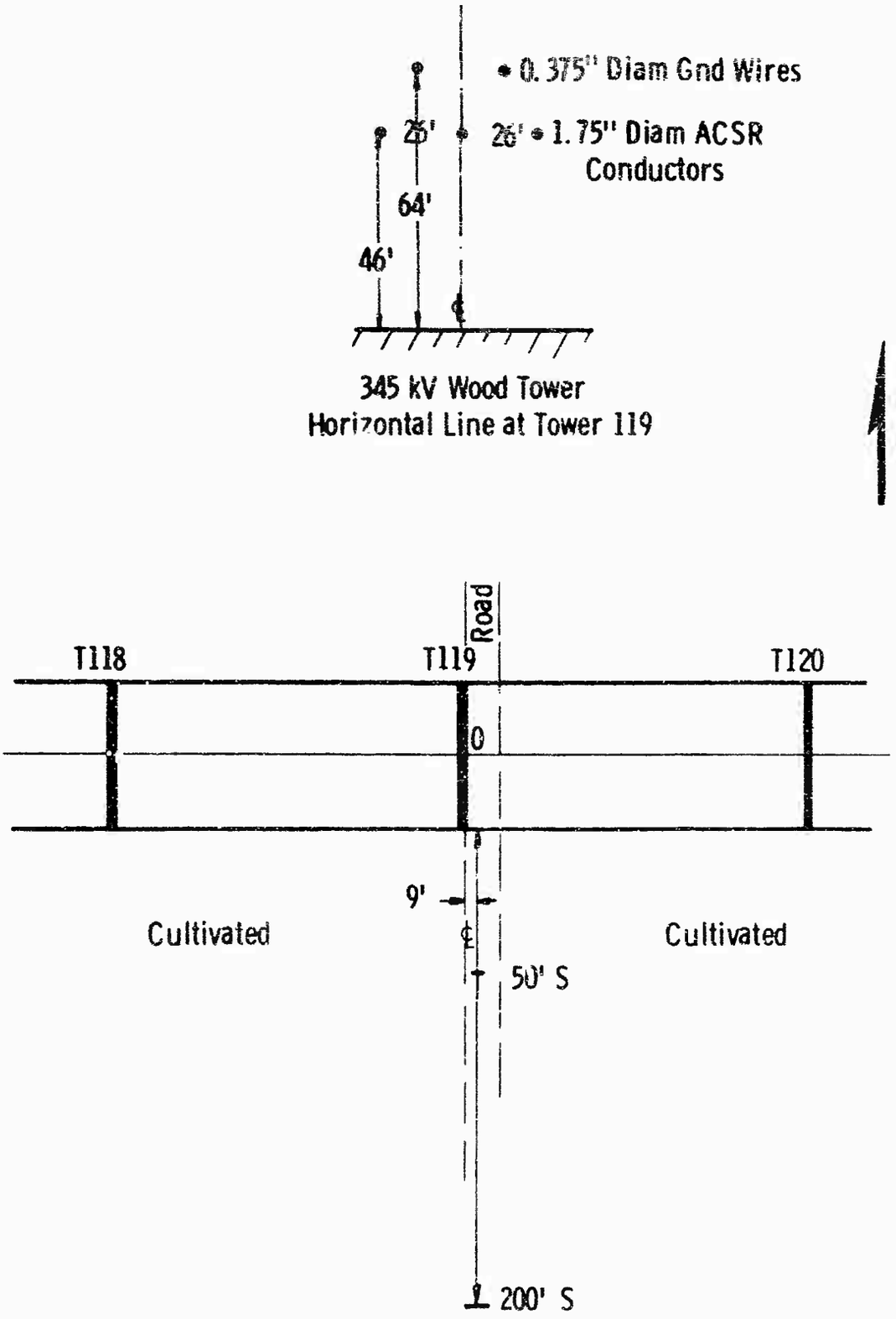


Fig. 5 —345 kV wood pole line configuration and test locations

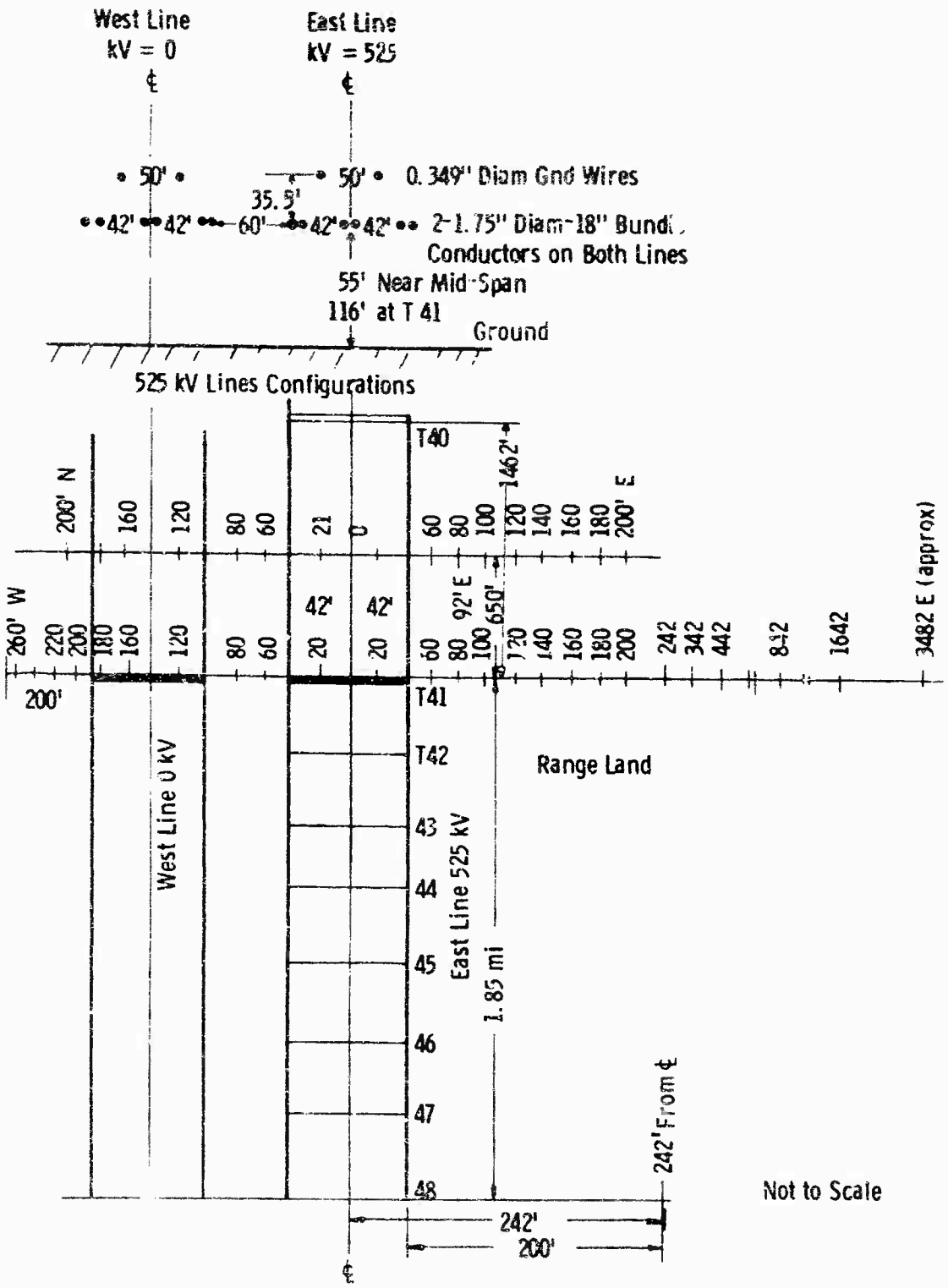
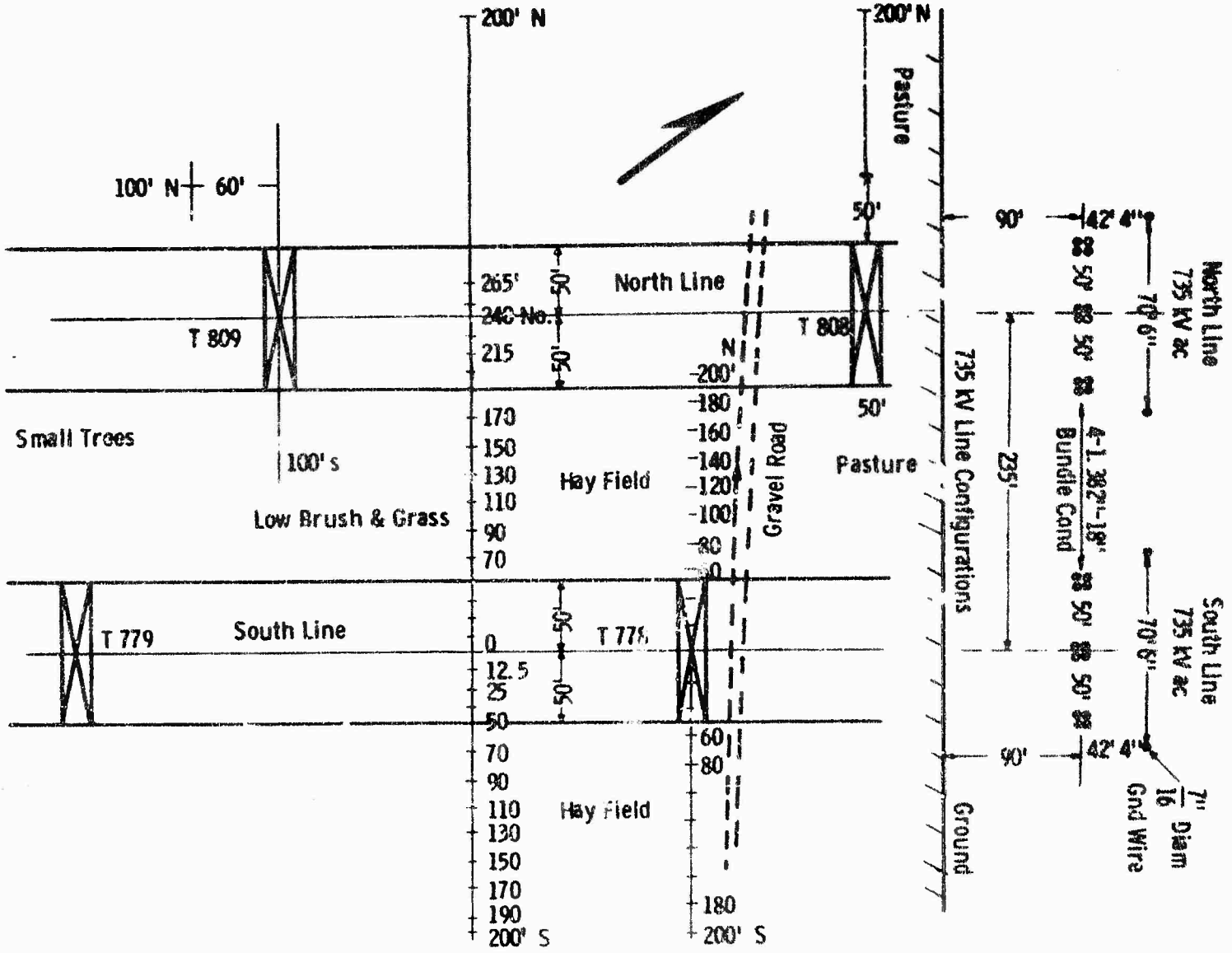
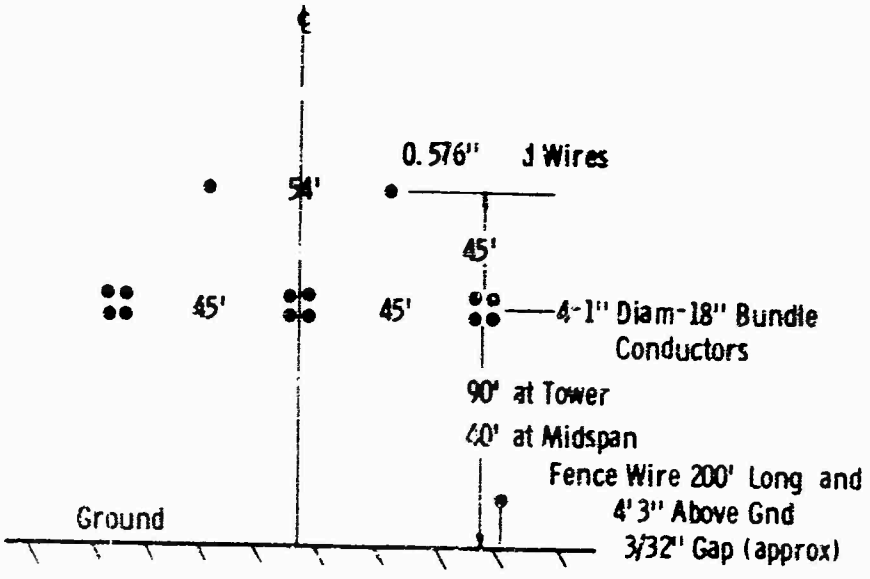


Fig. 6 --525 kV lines configurations and test locations


200' N
200' N
Pasture
100' N
60'
50'
90'
42' 4"
265'
240 No.
215
North Line
T 809
T 808
N
-200'
-180
-160
-140
-120
-100
-80
0
50'
50'
50'



C Line Configuration (Apple Grove)

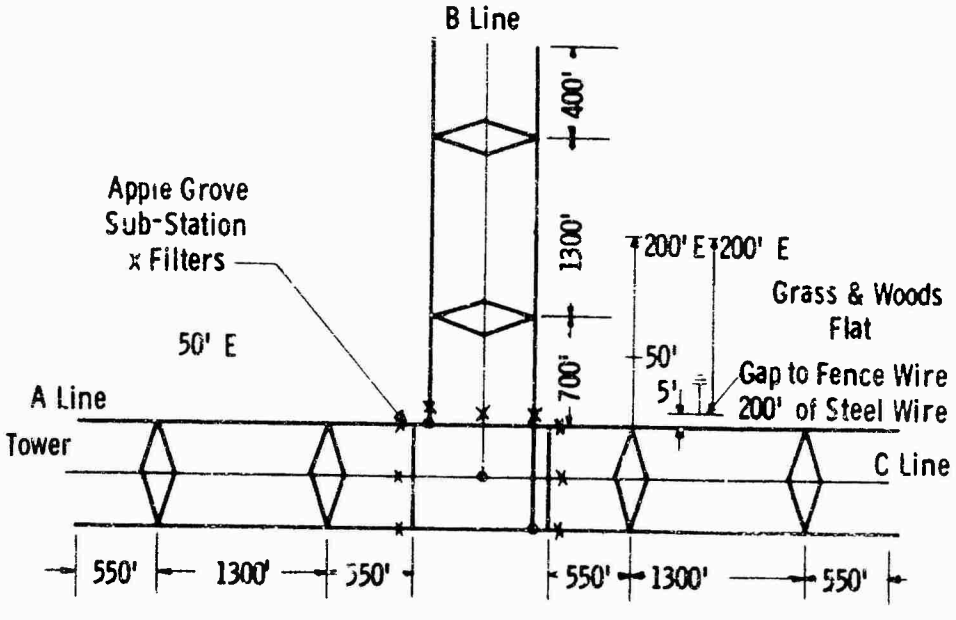
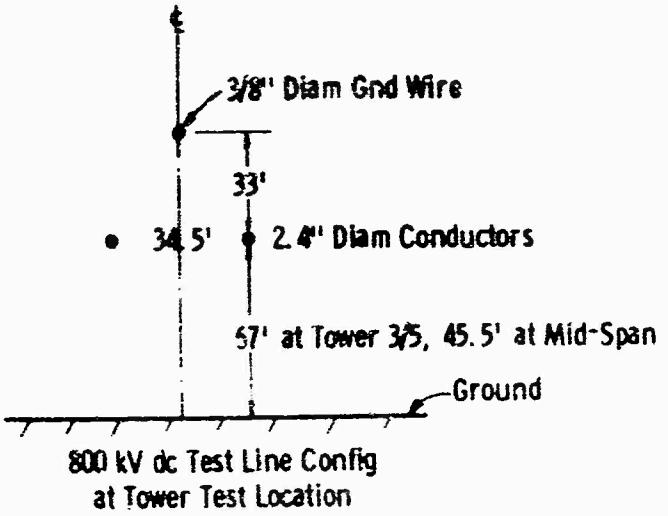


Fig. 8 —750 kV test line configuration and test locations and fence gap location



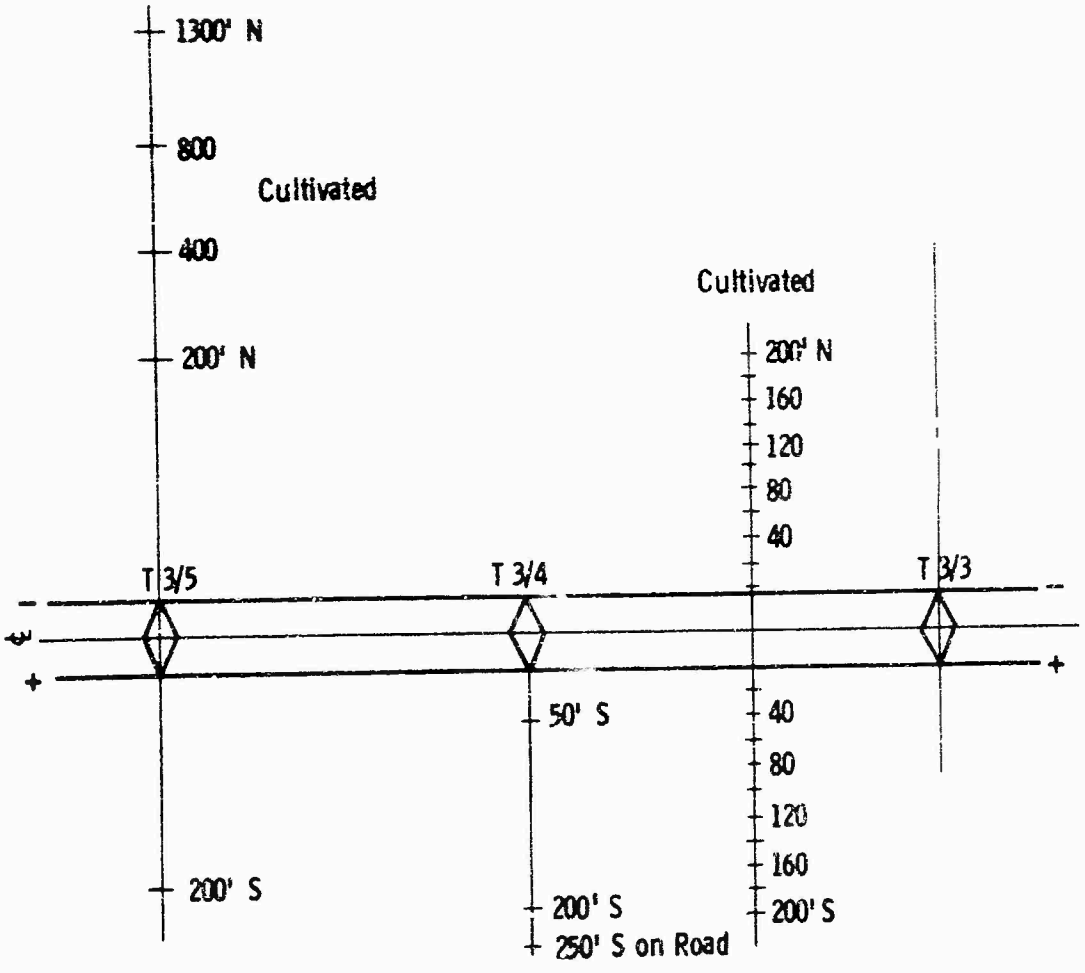


Fig. 9 —800 kV dc line configuration and test locations

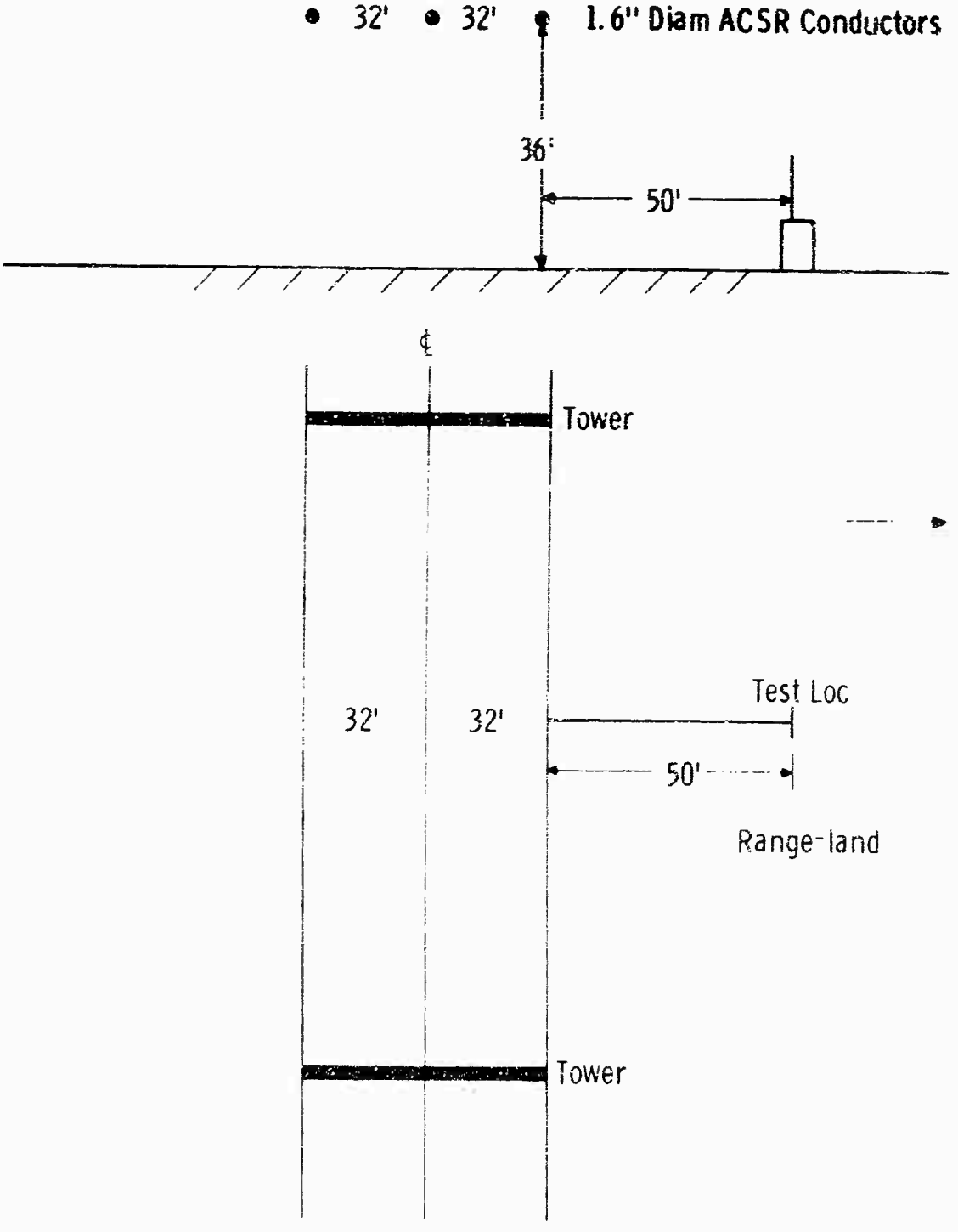
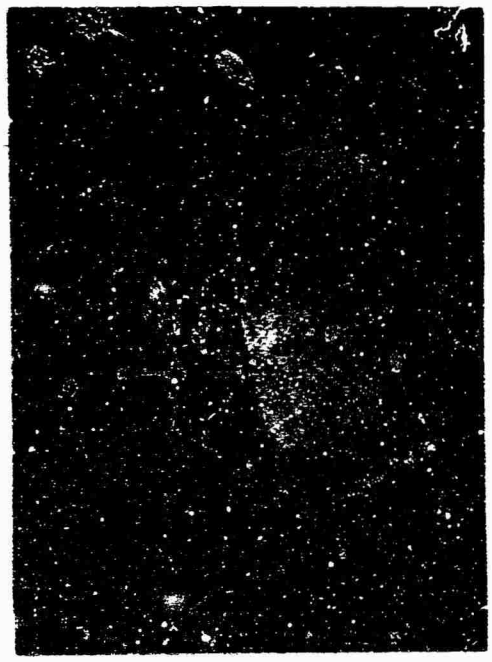


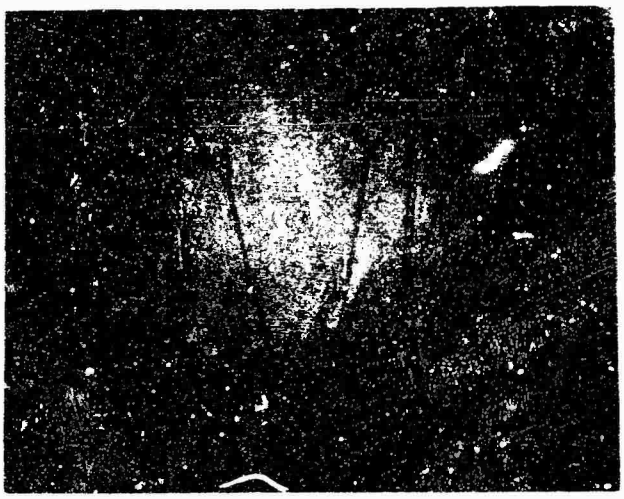
Fig. 10 --345 kV steel tower line configuration and test location



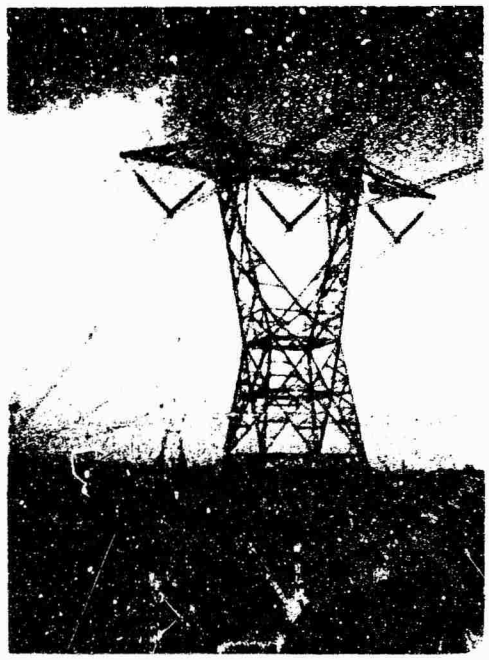
(a) 345 kV Double Circuit Vertical



(b) 345 kV Horizontal (Wood Pole)



(c) 525 kV Horizontal Lines



(d) 735 kV Horizontal Lines

Fig. 11



(a) 800-kV dc Test Line



(b) 750-kV ac Test Line



(c) Discharge to wire near 750-kV Line



(d) 750-kV ac Test Line with Grading Rings

Fig. 12

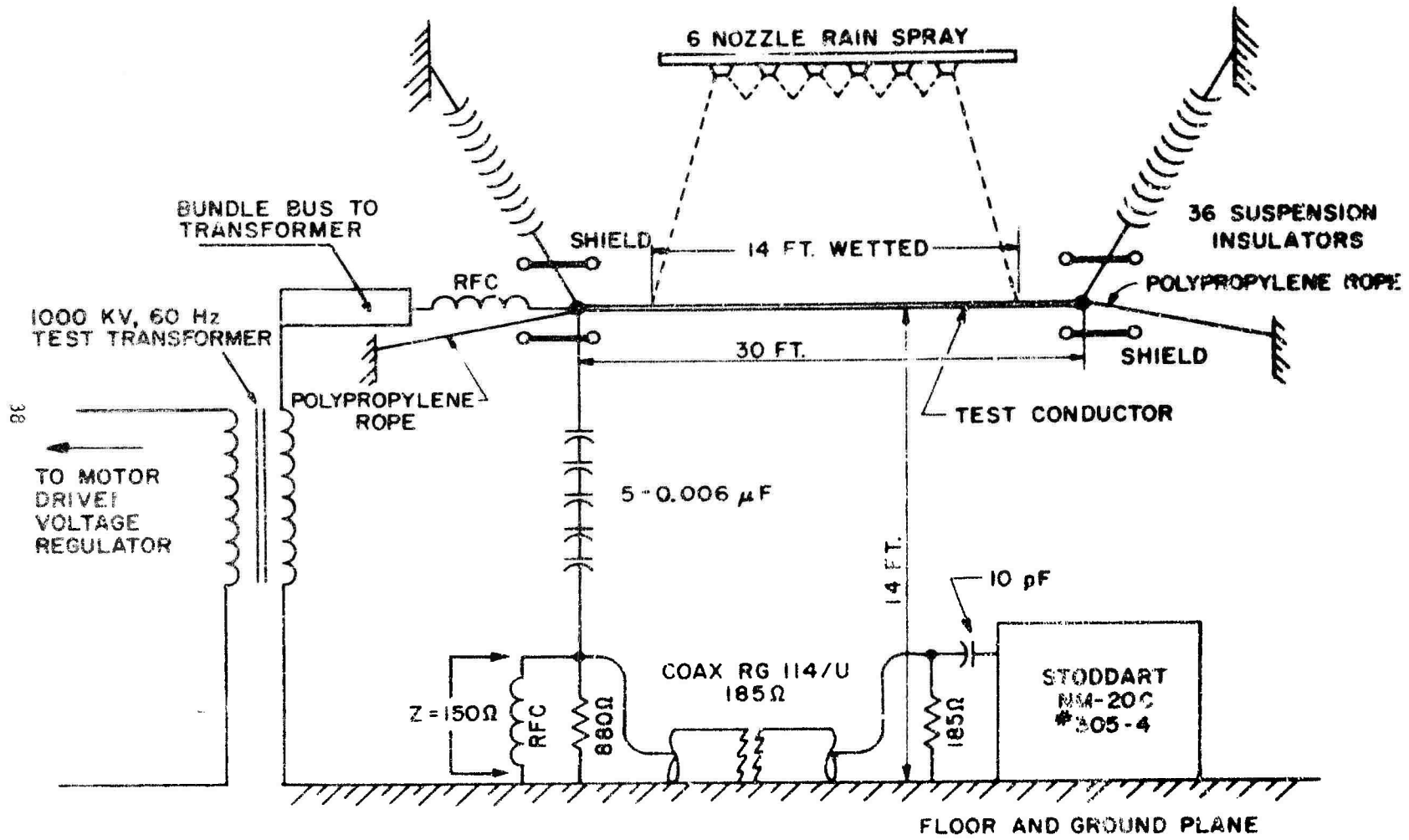


Fig. 13—Trafford laboratory 650 kV Nema test circuit

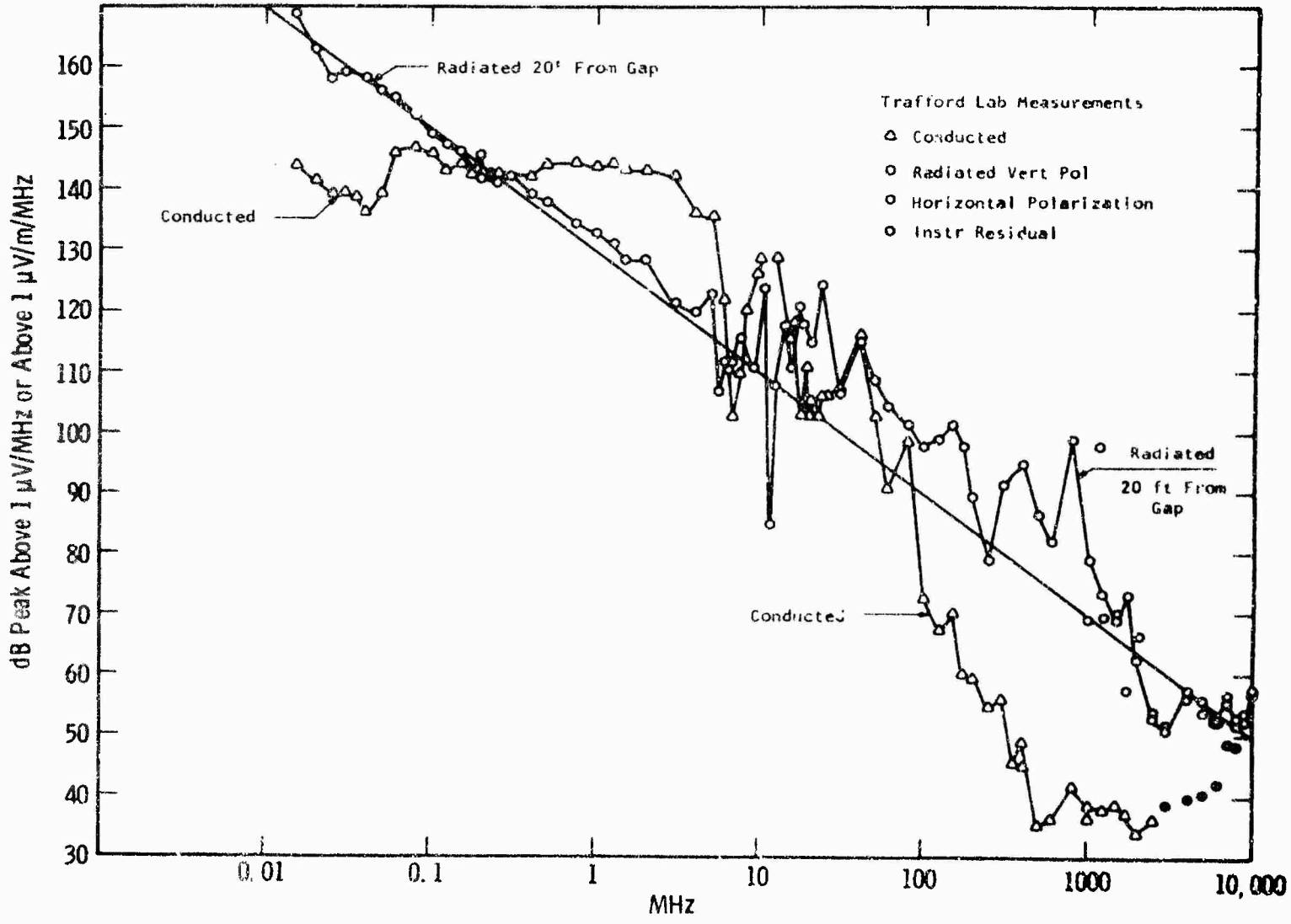


Fig. 14 —Frequency spectra from 5/16" gap in lab - 650 kV Nema 107-1964 circuit

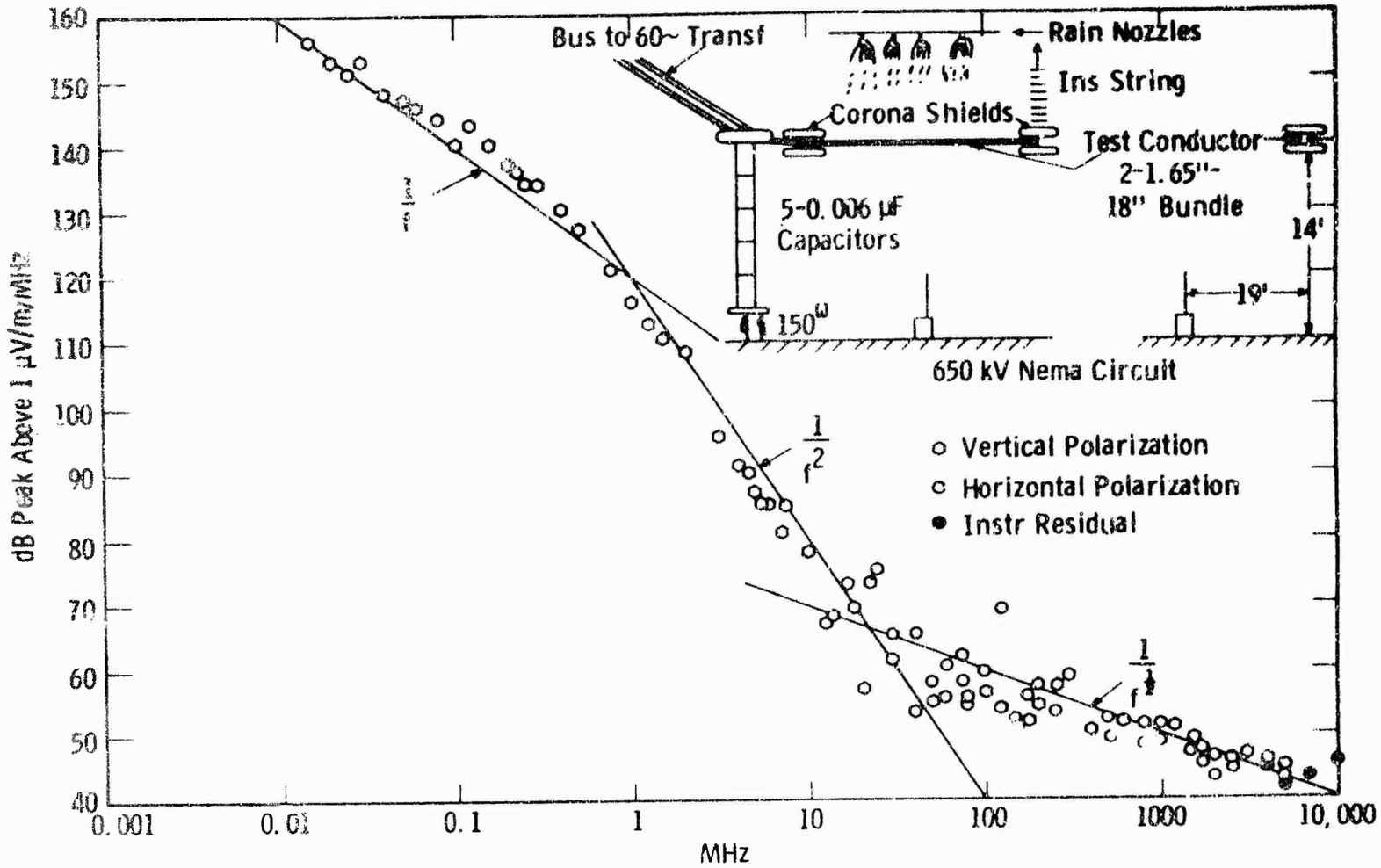


Fig. 15(a)--Frequency spectrum of conductor corona in lab rain

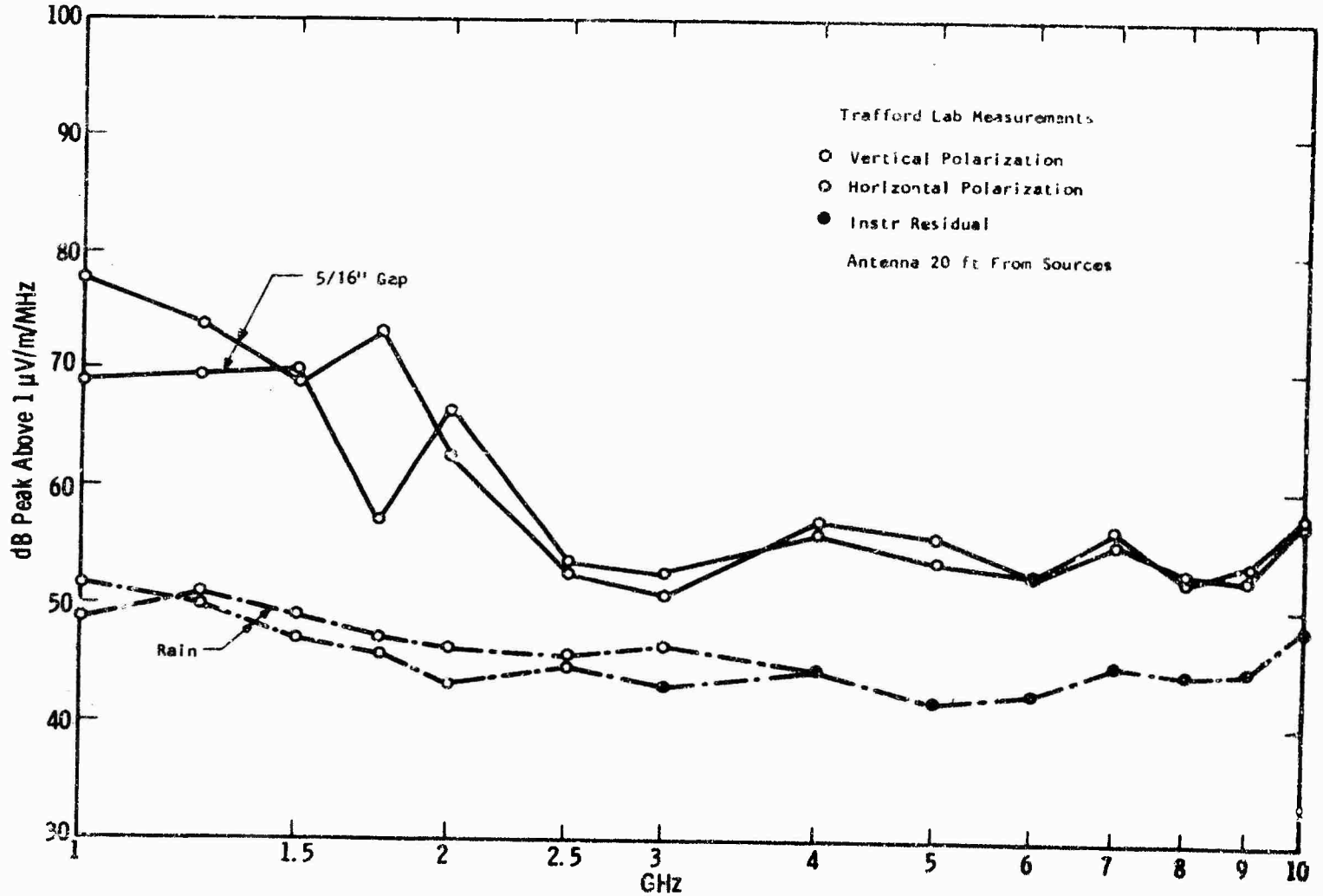


Fig. 15(b) —Comparison of radio noise levels from 5/16" gap and rain type sources

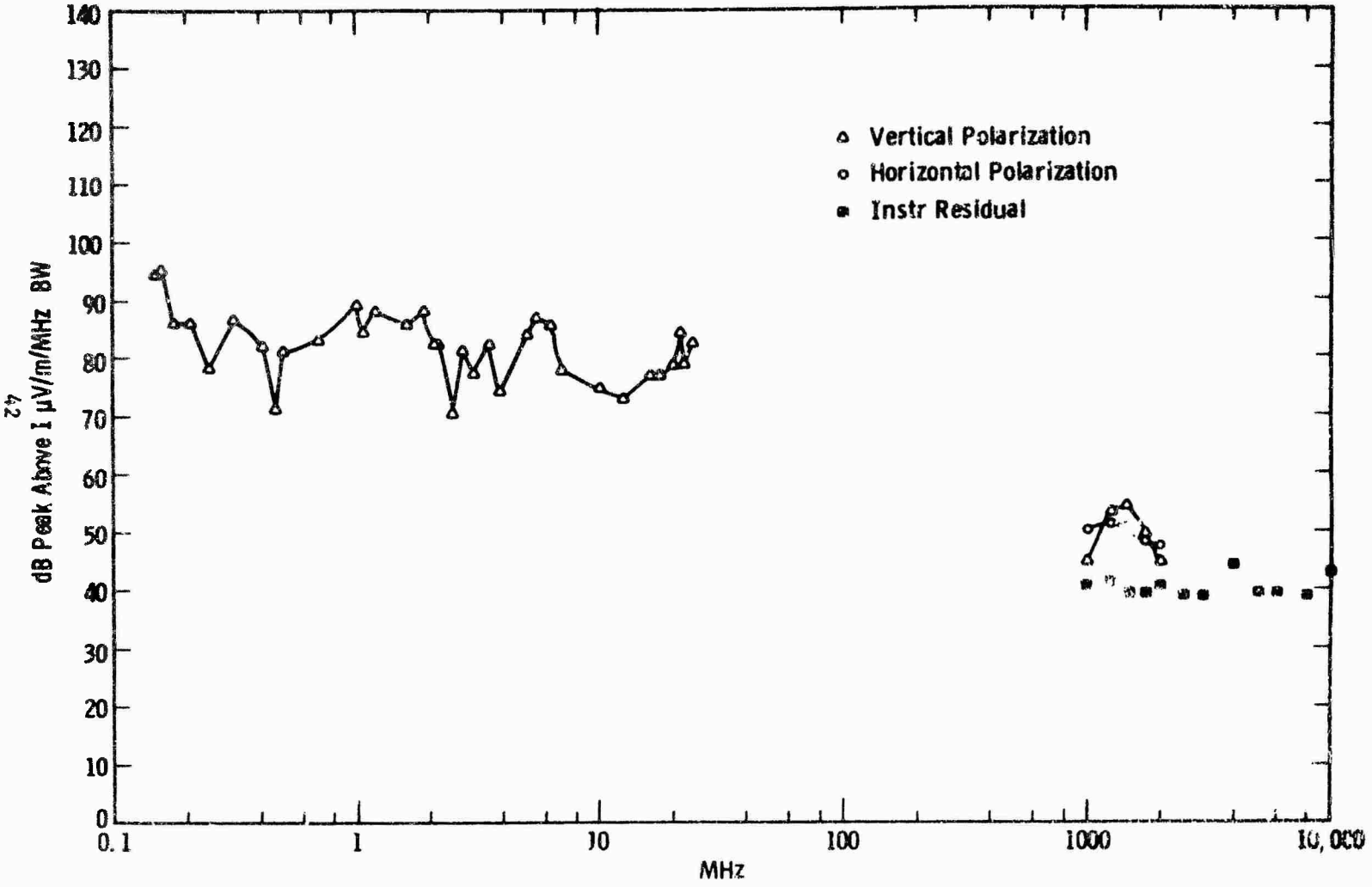


Fig. 16—Frequency spectra for 7.2 kV line with gap-type source 100 ft away

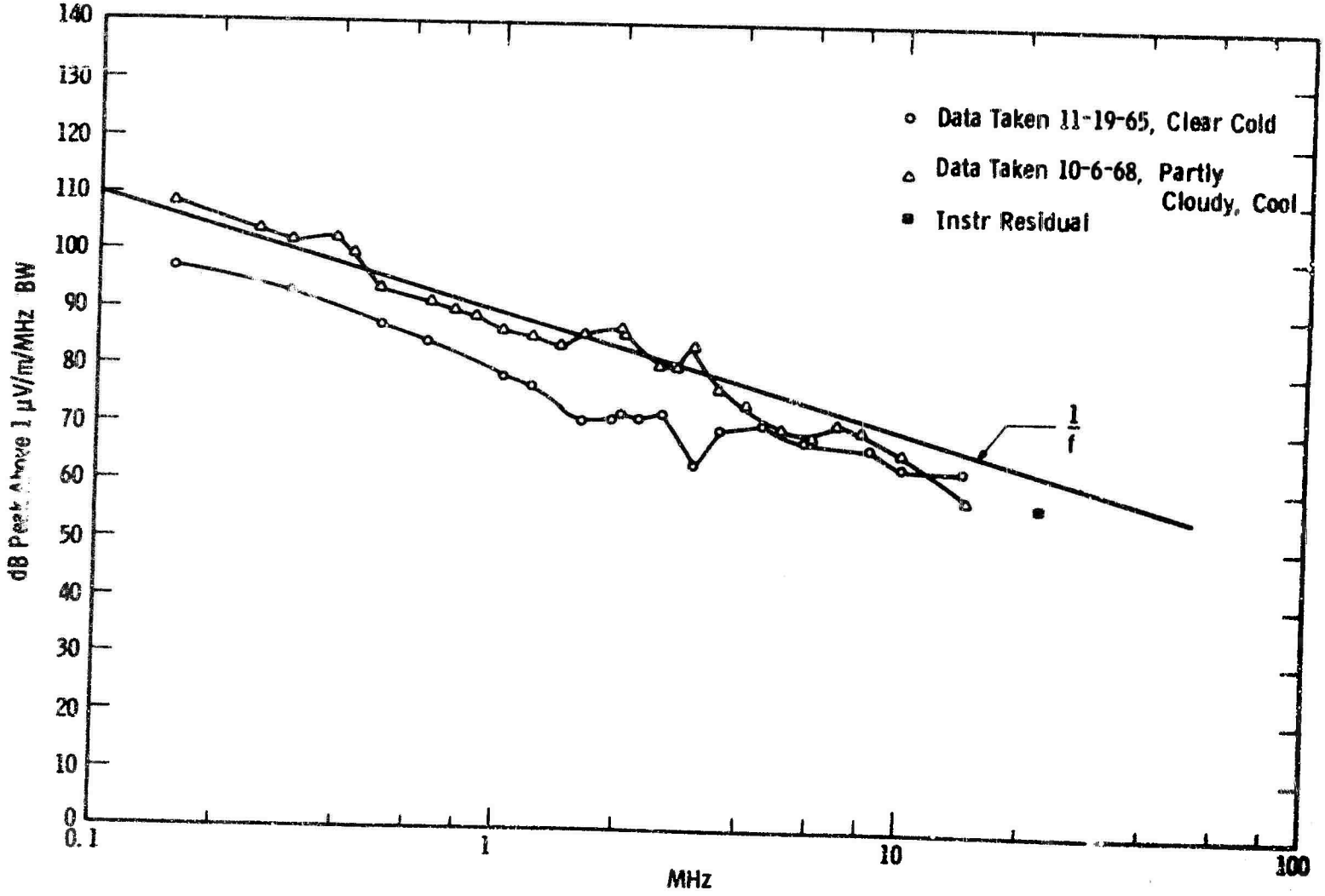


Fig. 17—345 kV VCDCST normal line frequency spectra 200 ft from tower

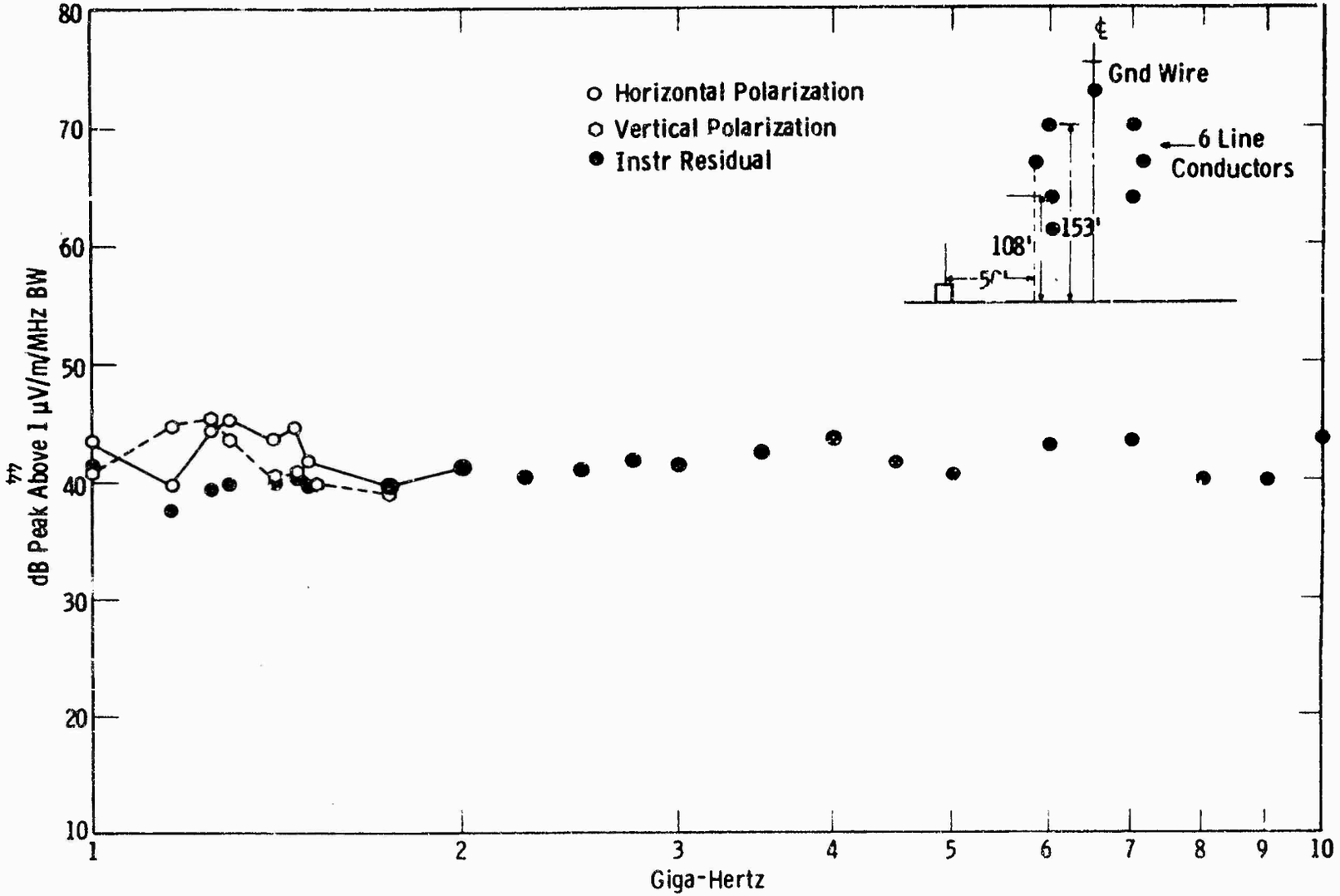


Fig. 18 —Frequency spectrum from 1 to 10 GHz on 345 kV line at tower 473

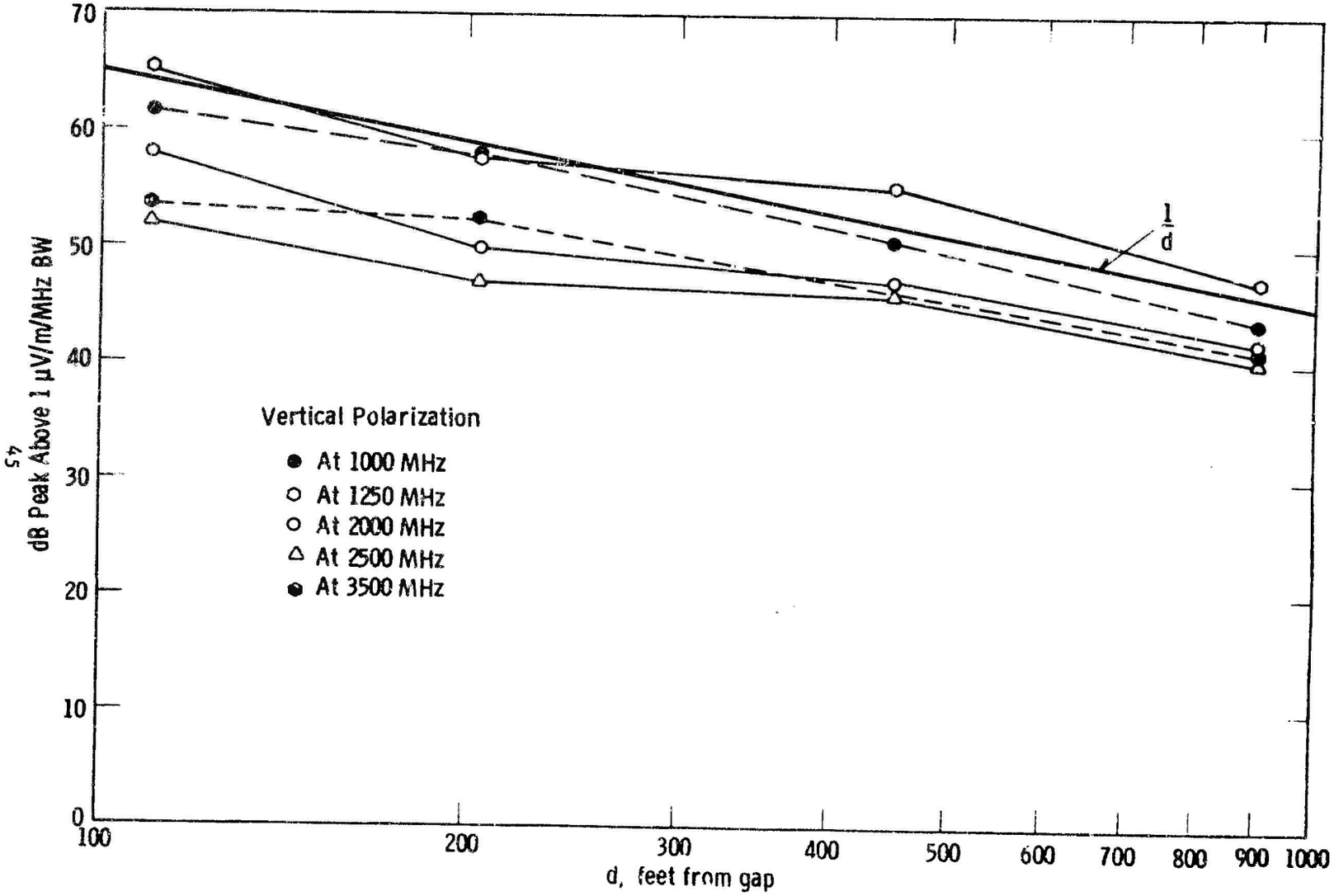


Fig. 19 —Lateral distance from 5/16" gap at tower on 345 kV line

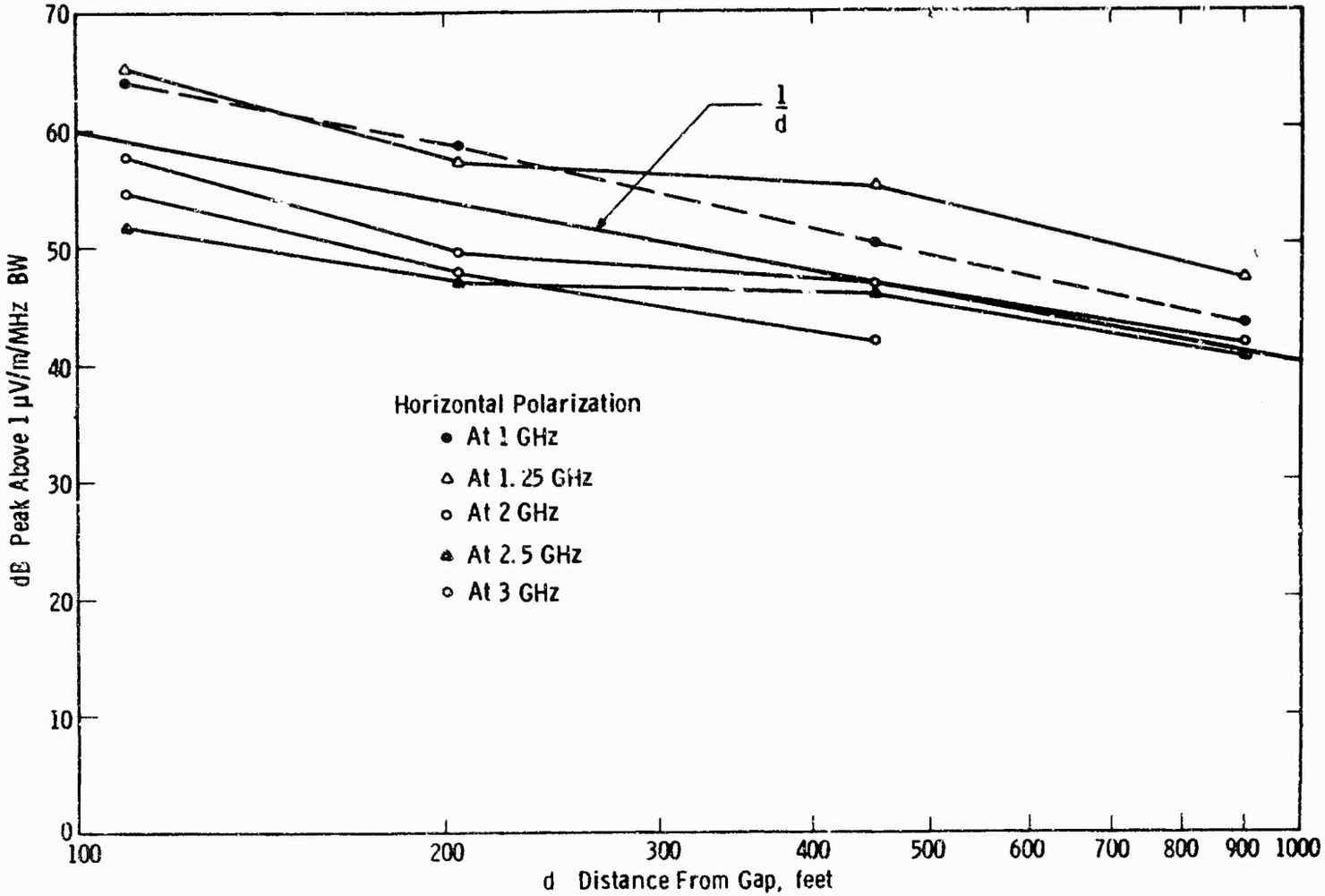


Fig. 20—Lateral attenuation from 5/16" gap at tower on 345 kV line - horizontal polarization

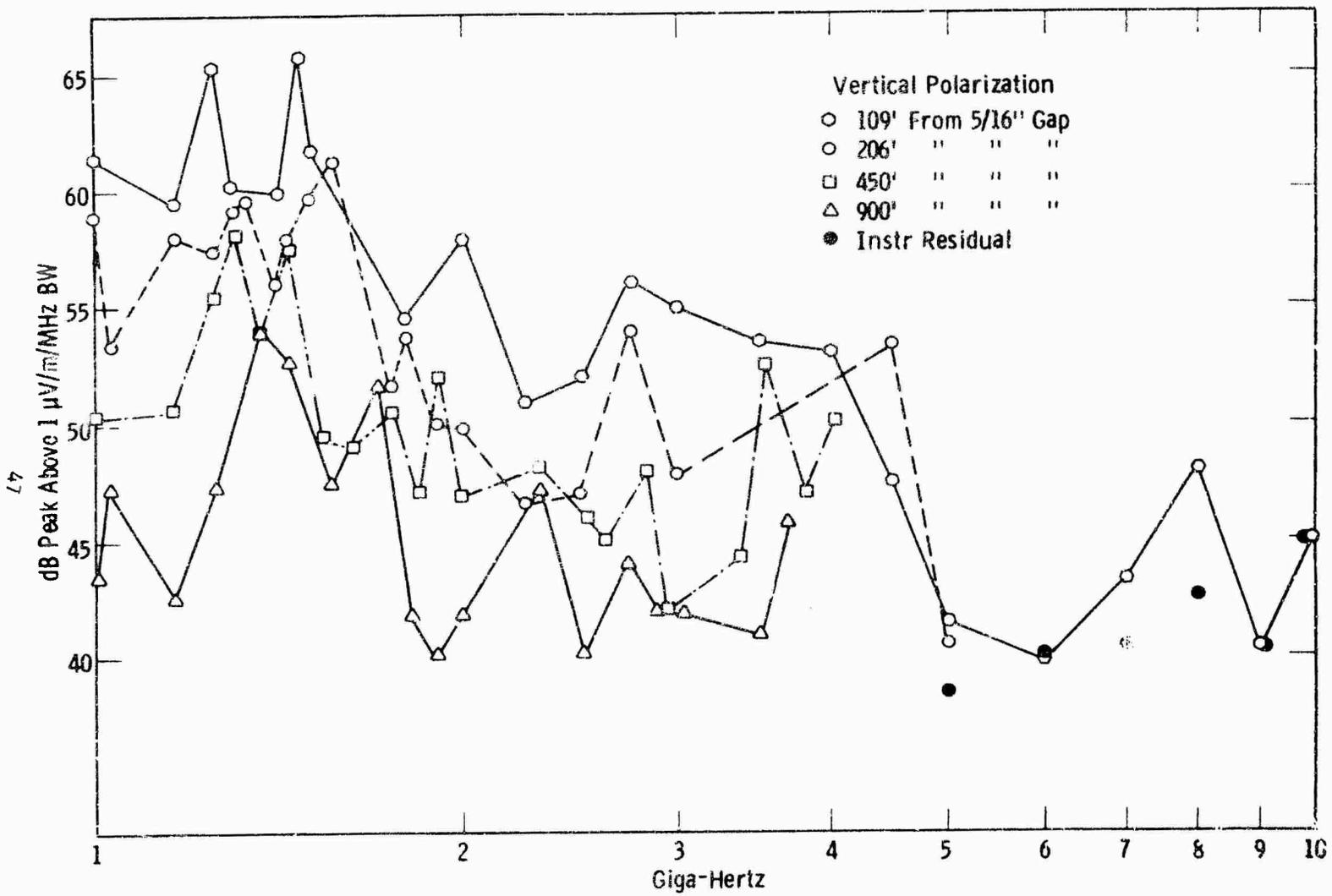


Fig. 21 —Frequency spectra with 5/16" gap on 345 kV line at tower

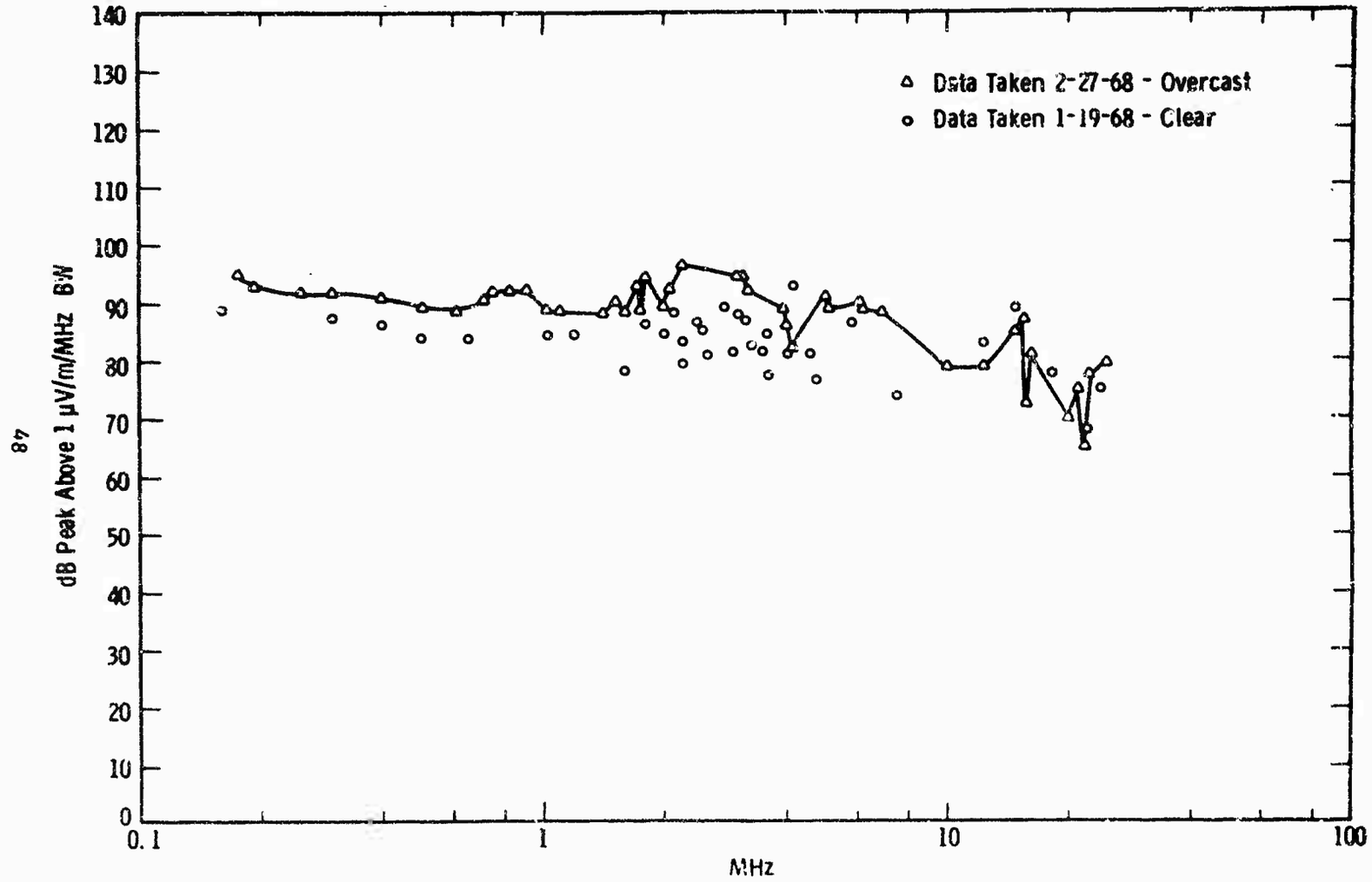


Fig. 22—345 kV wood pole line frequency spectra 200 ft from tower

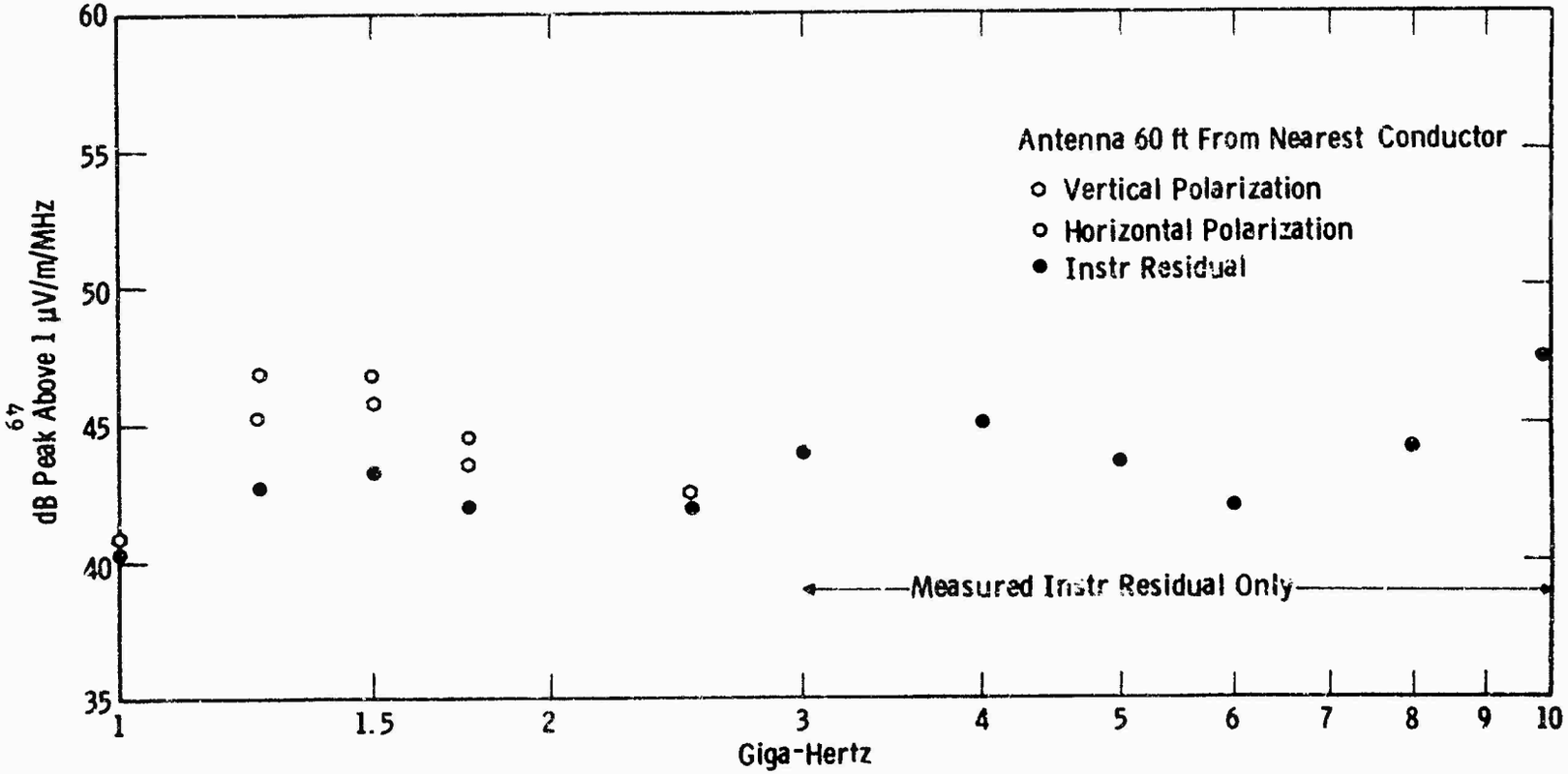


Fig. 23 —Frequency spectrum 1-10 GHz on 345 kV wood pole line

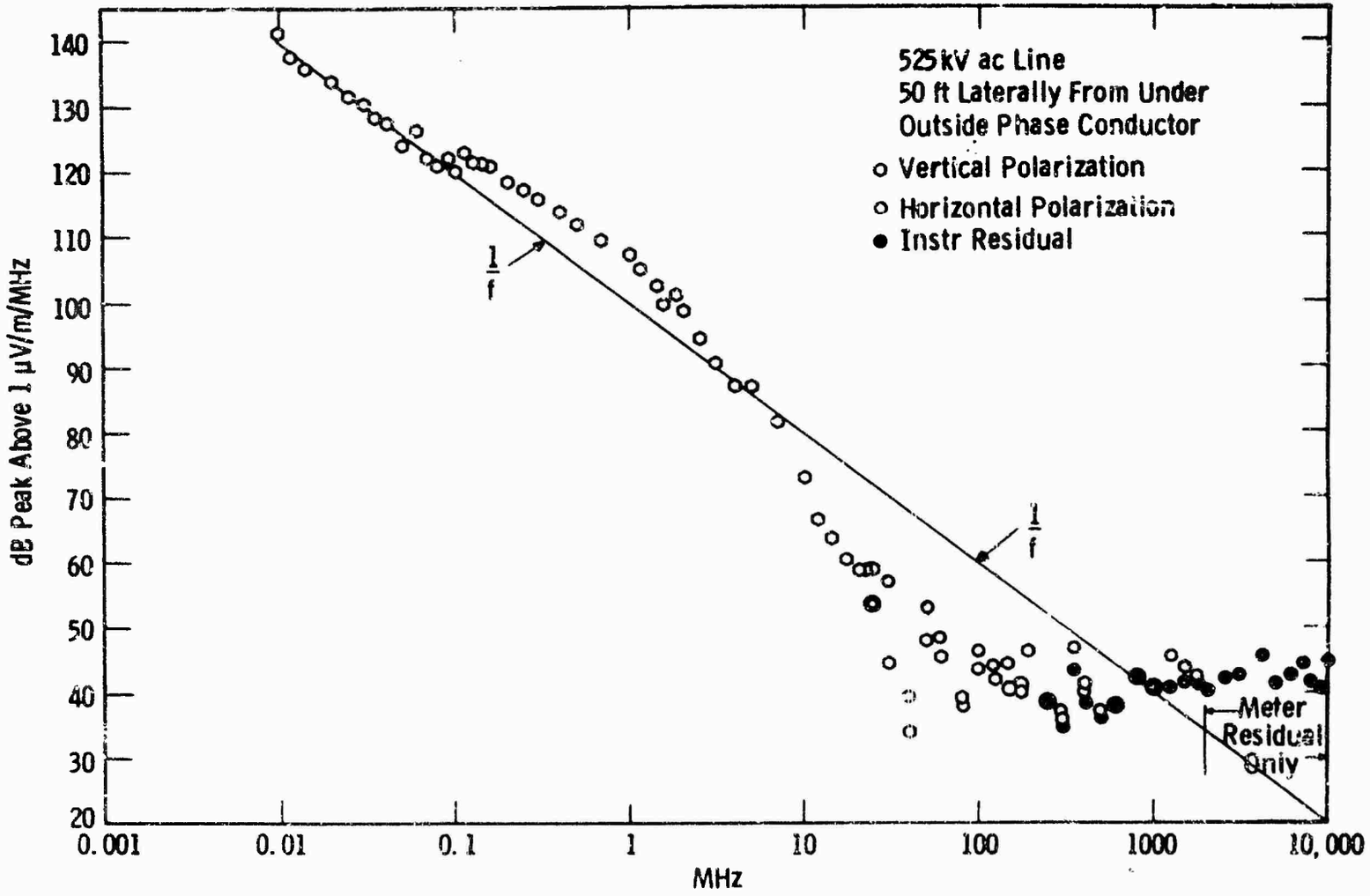


Fig. 24—Frequency spectrum of 525 kV ac line

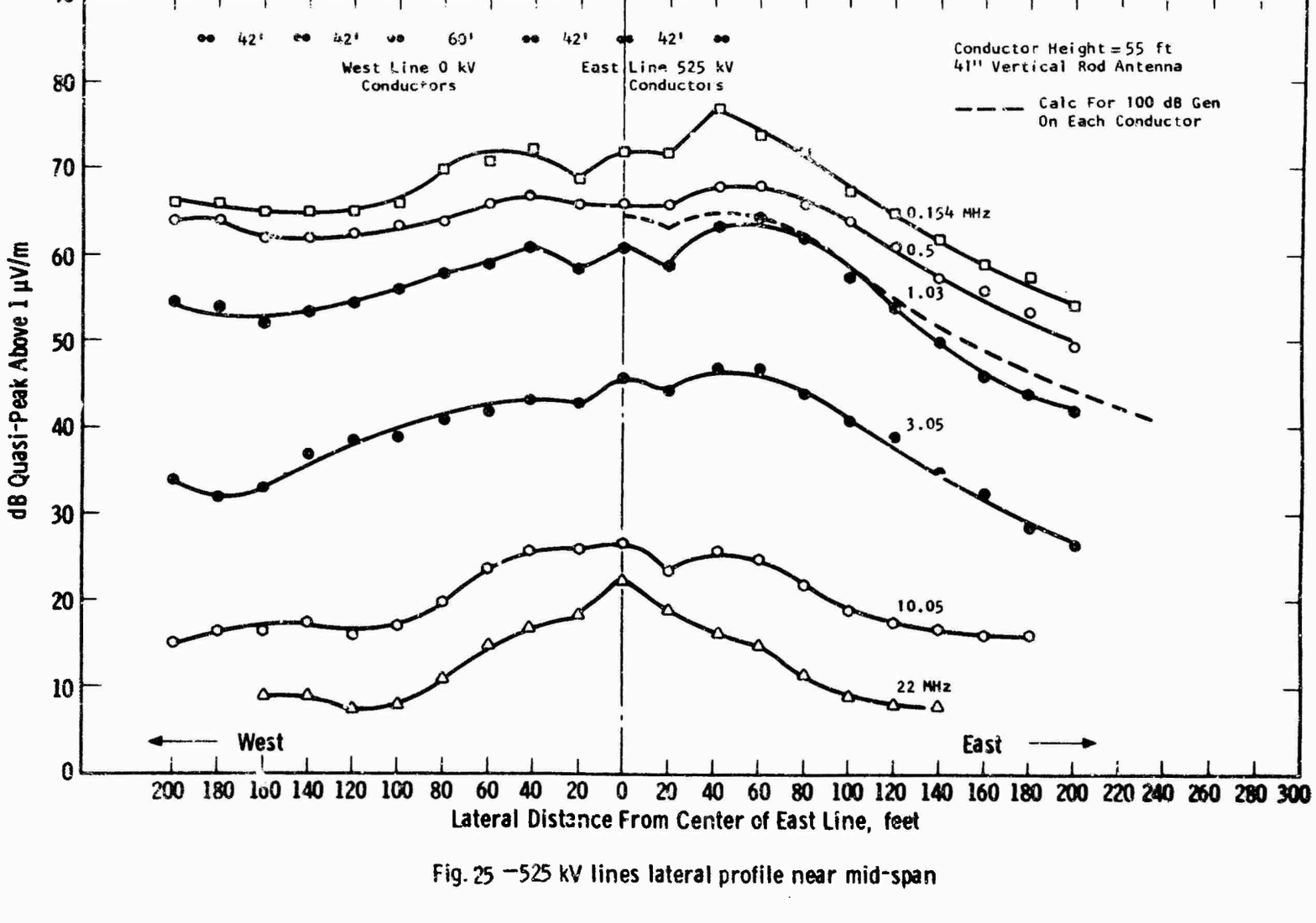


Fig. 25 —525 kV lines lateral profile near mid-span

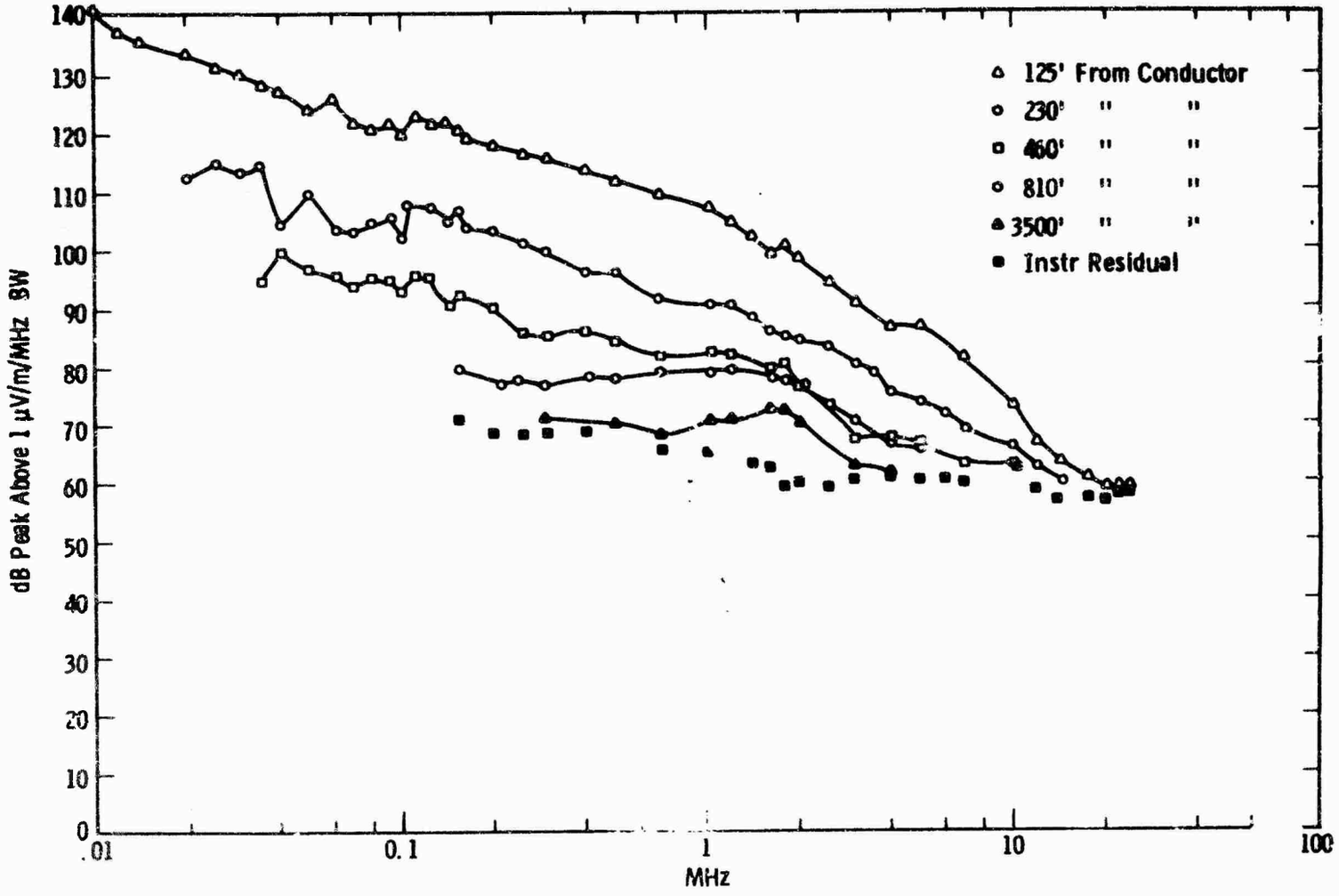


Fig. 26—Frequency spectra at several distances from 525 kV line tower

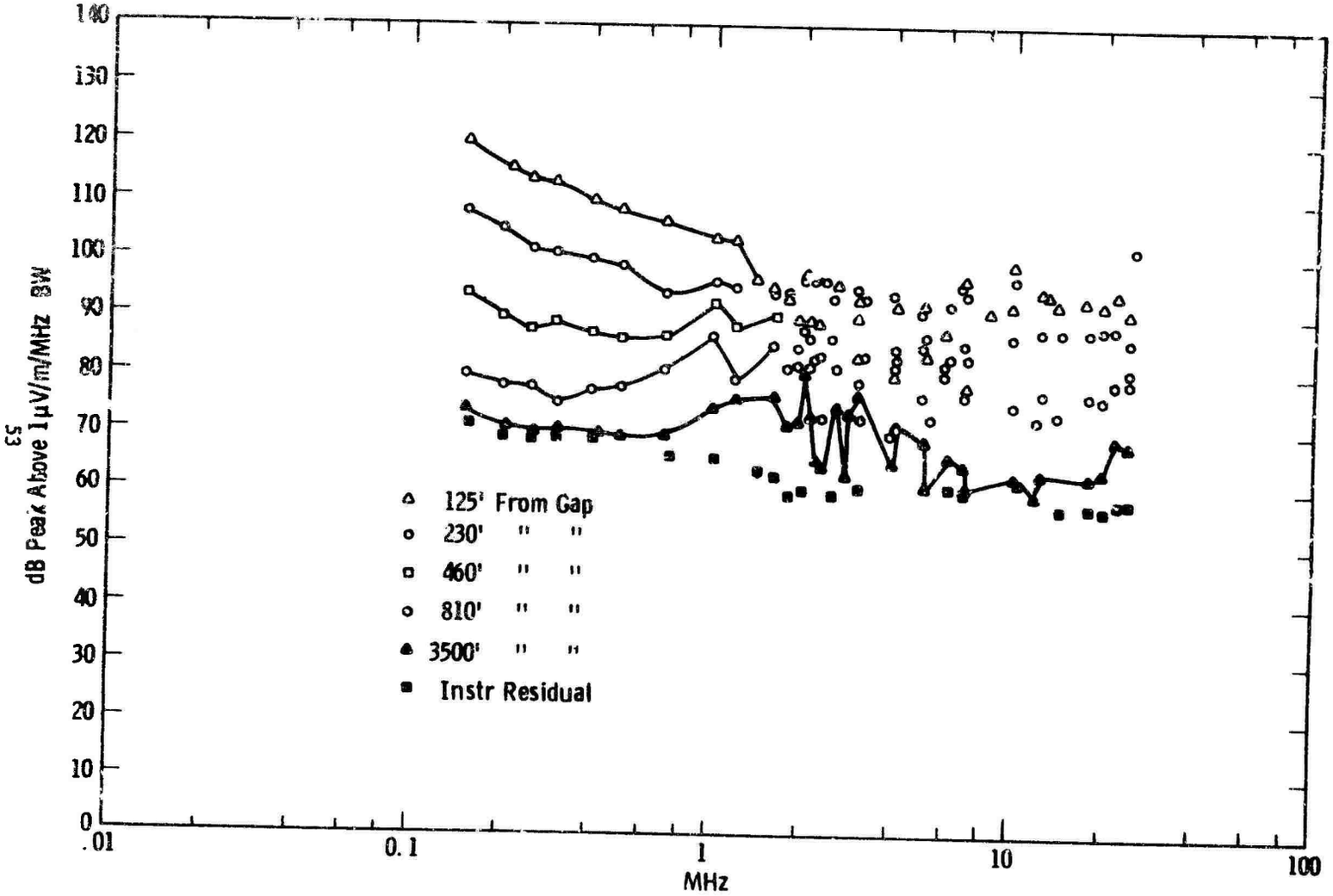


Fig. 27—Frequency spectra at several distances with 5/16" gap at 525 kV tower

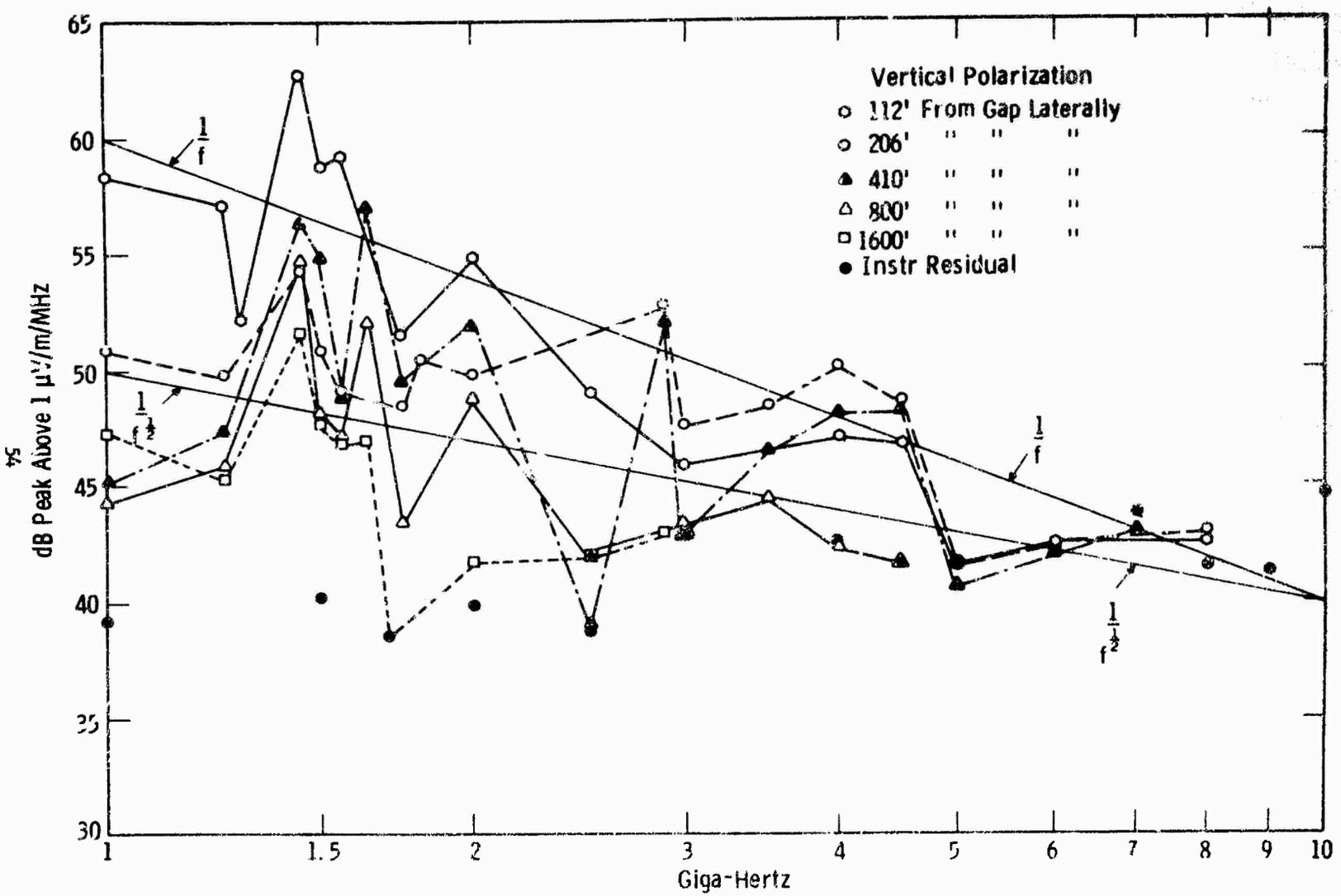


Fig. 28--Frequency spectra with 5/16" gap on 525 kV line at tower

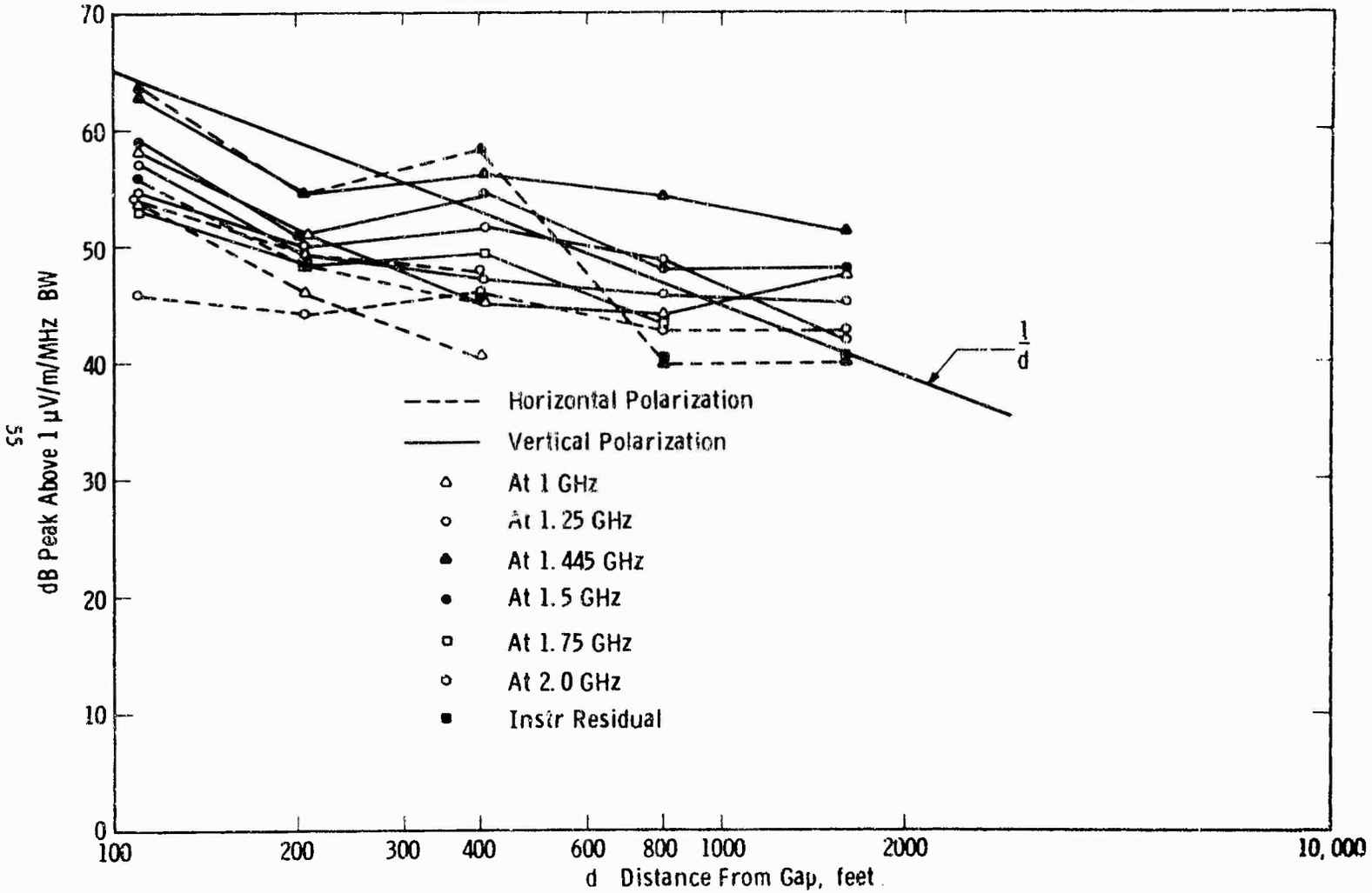


Fig. 29—Lateral attenuation from 5/16" gap on 525 kV line in 1-2 GHz range

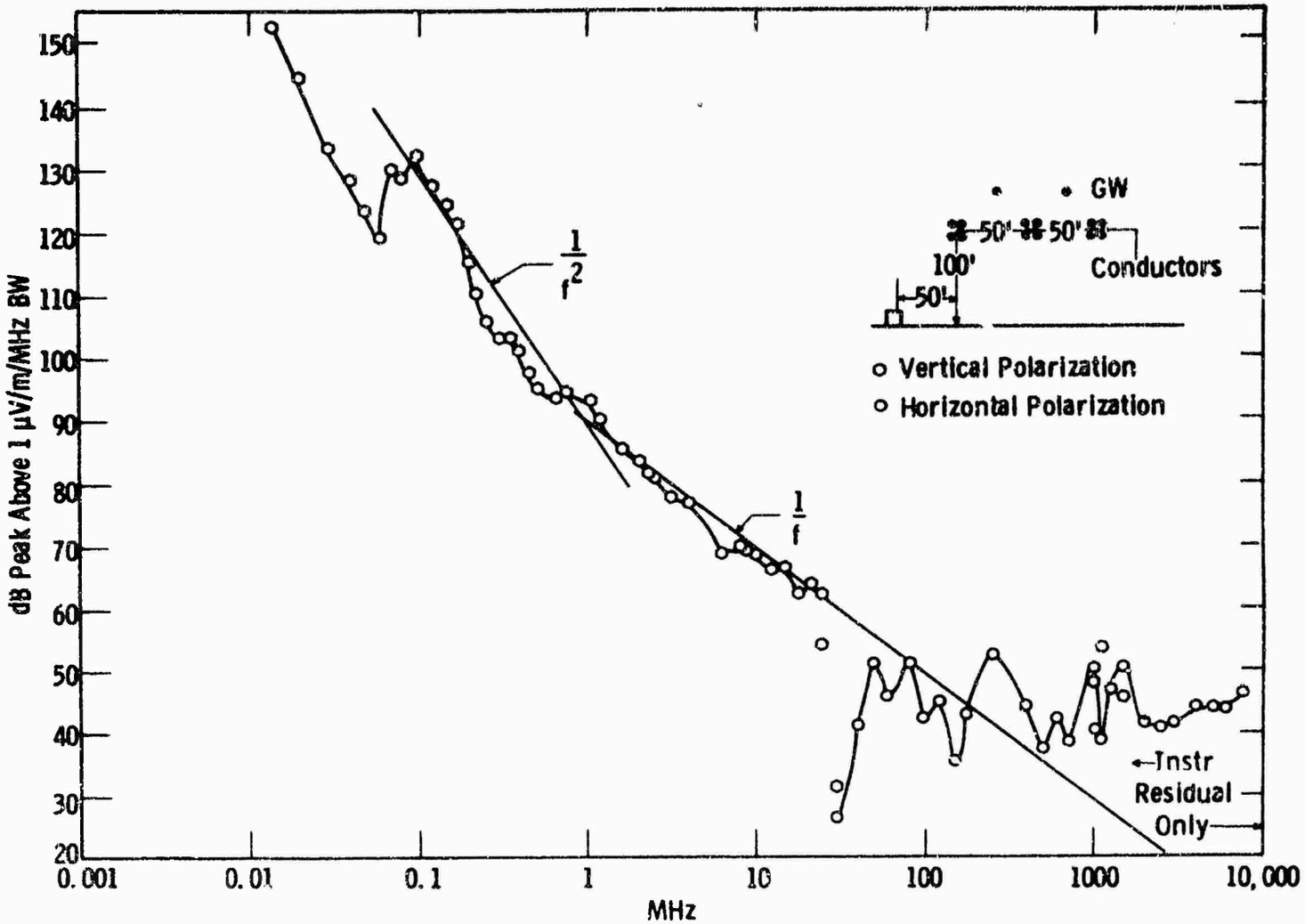


Fig. 30 —Frequency spectrum of 735 kV line at 50 foot lateral distance from tower

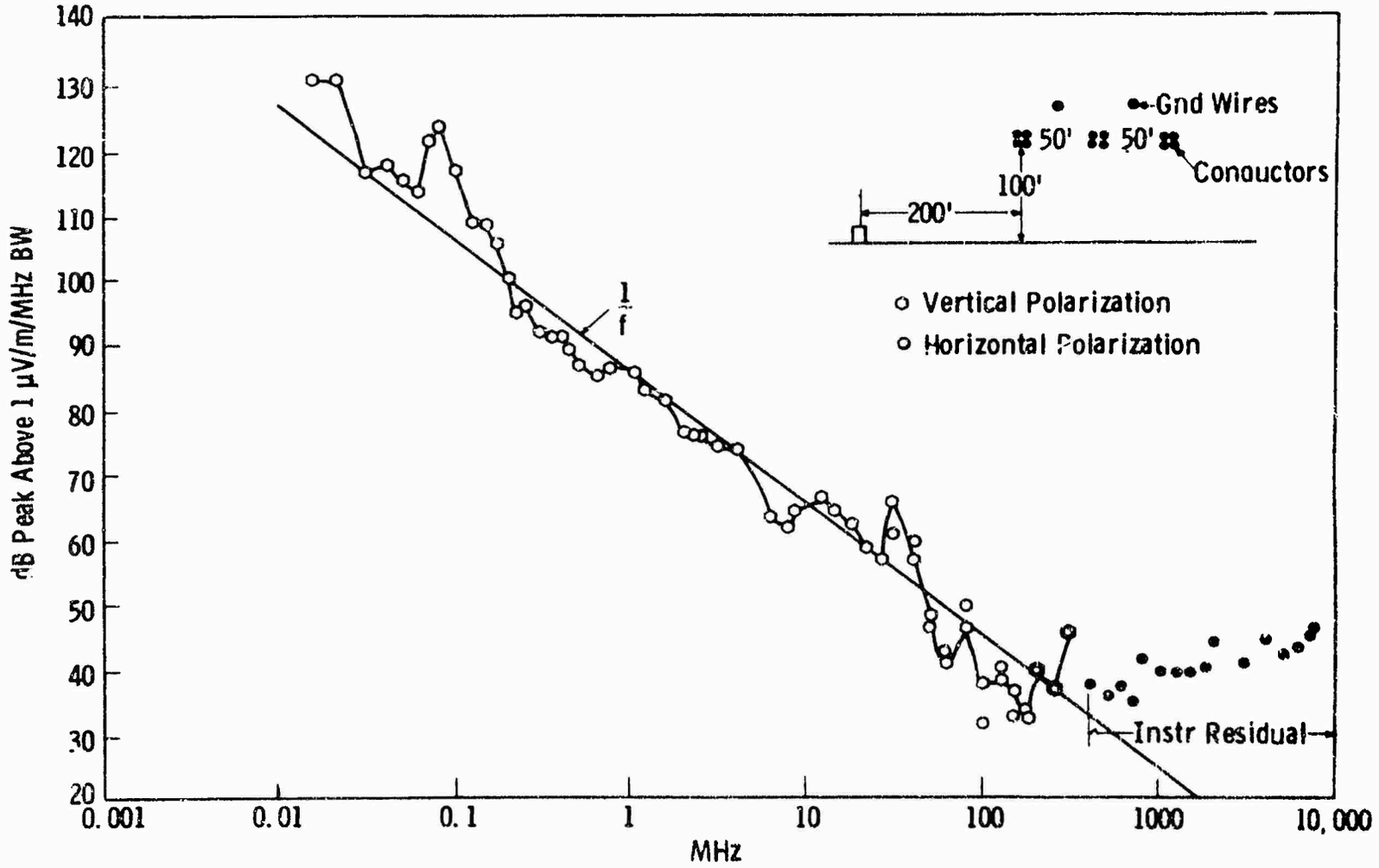


Fig. 31(a)—Frequency spectrum of 735 kV south line at 200 foot lateral distance from tower

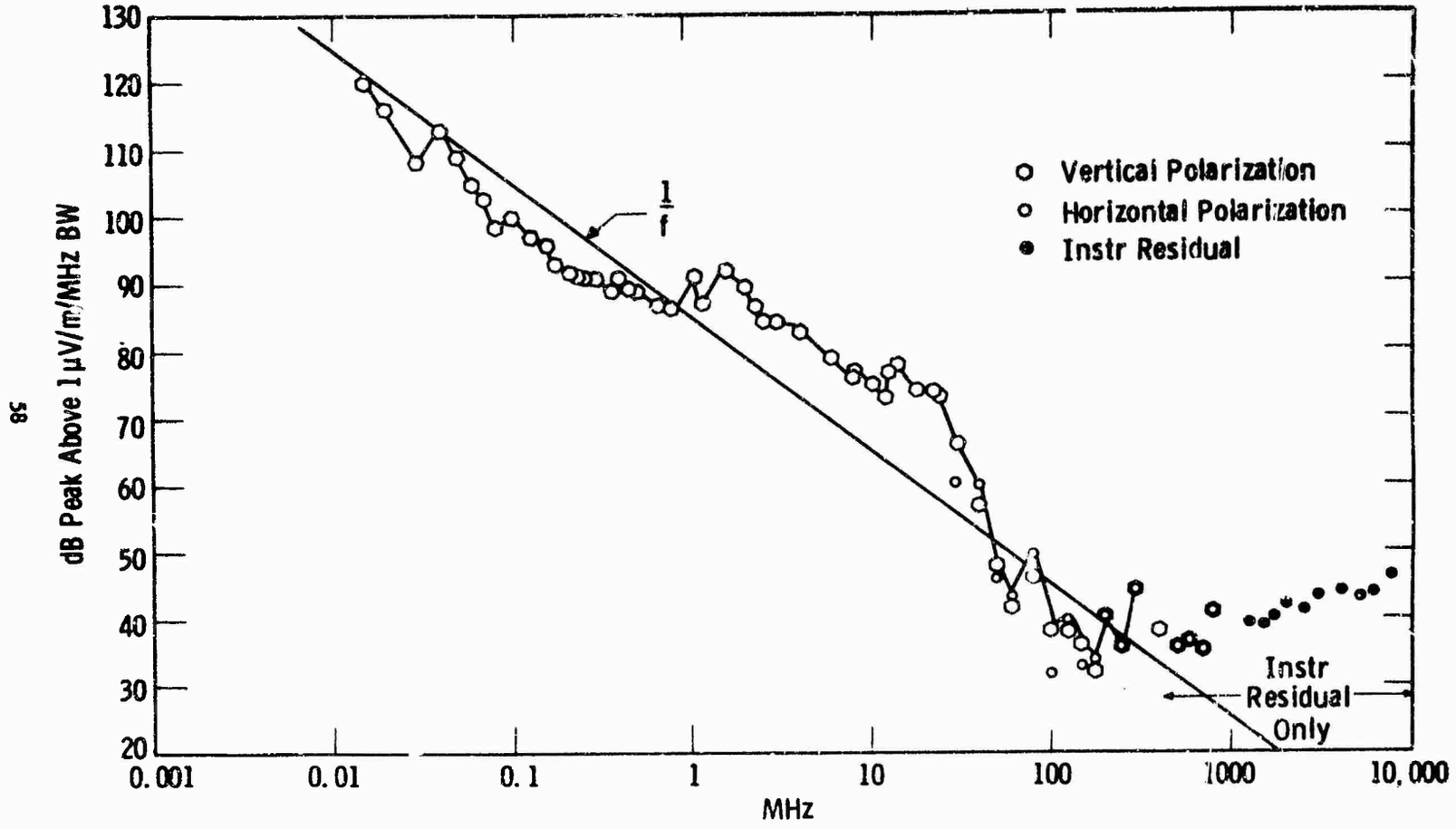


Fig. 31(b)—Frequency spectrum of 735 kV north line at 200 feet from tower

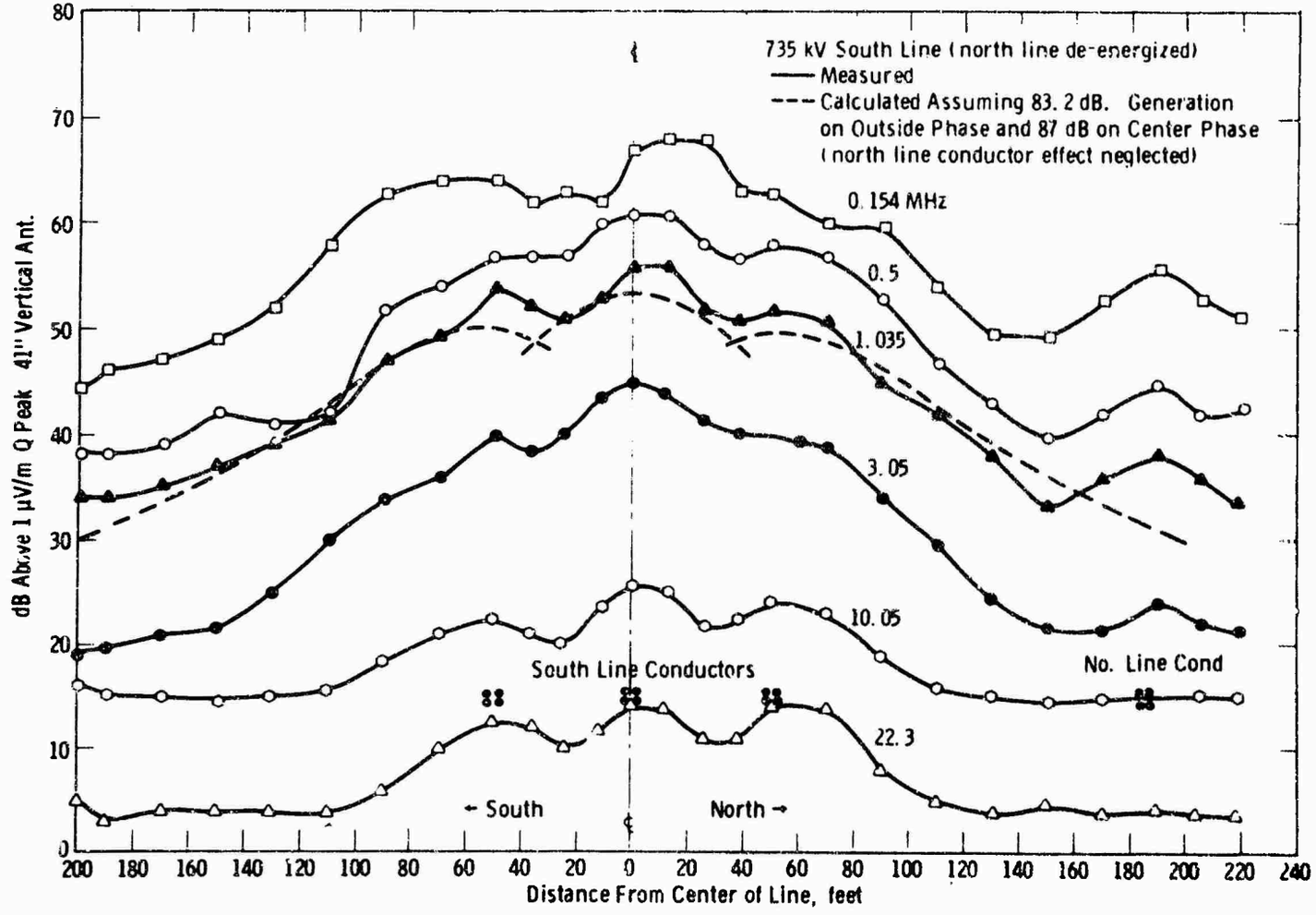


Fig. 32 —Lateral profiles near center of span of 735 kV line

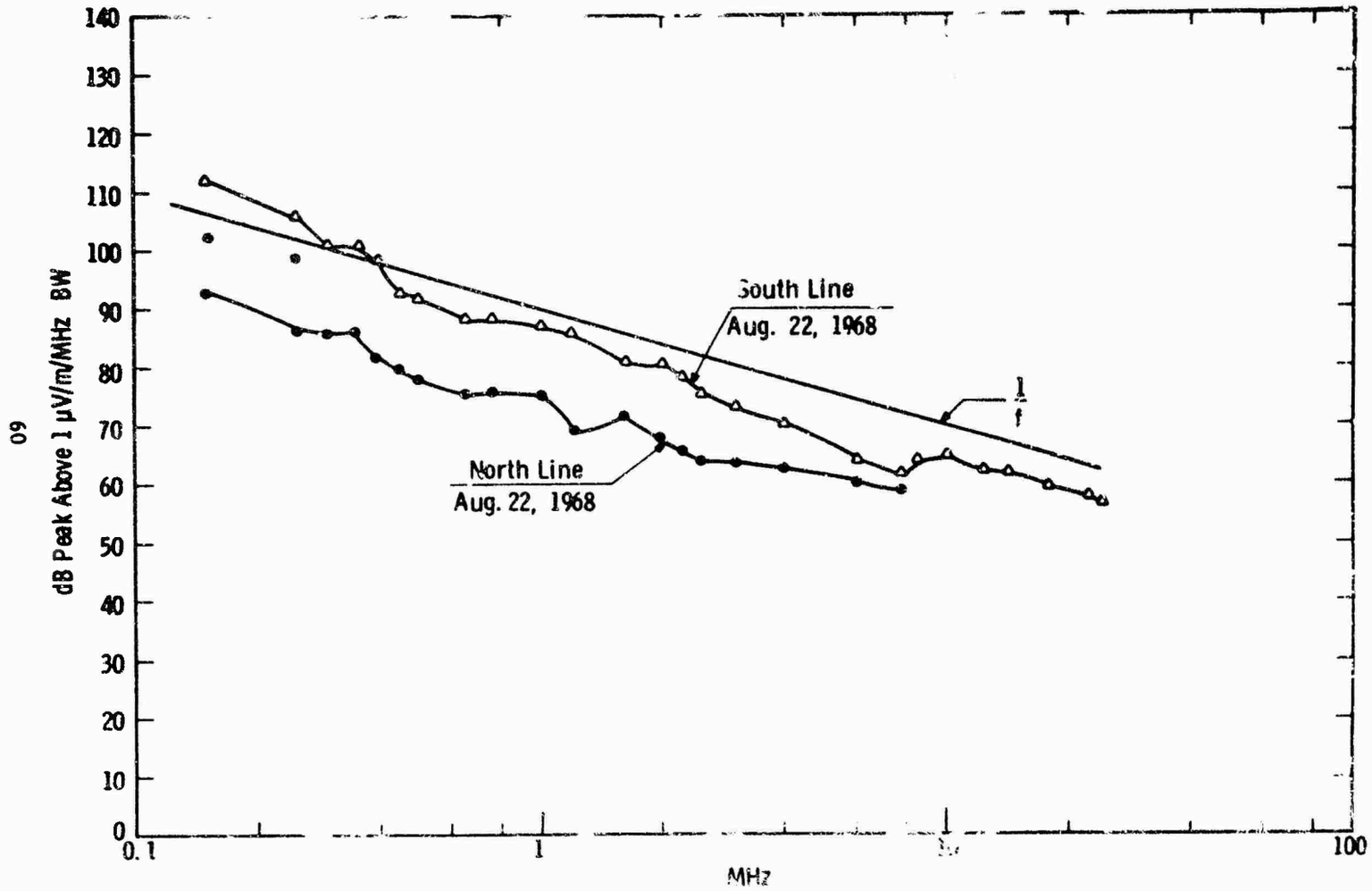


Fig. 33 Frequency spectru... for 73... ...r... ...d south [illegible] 150 ... from conductor

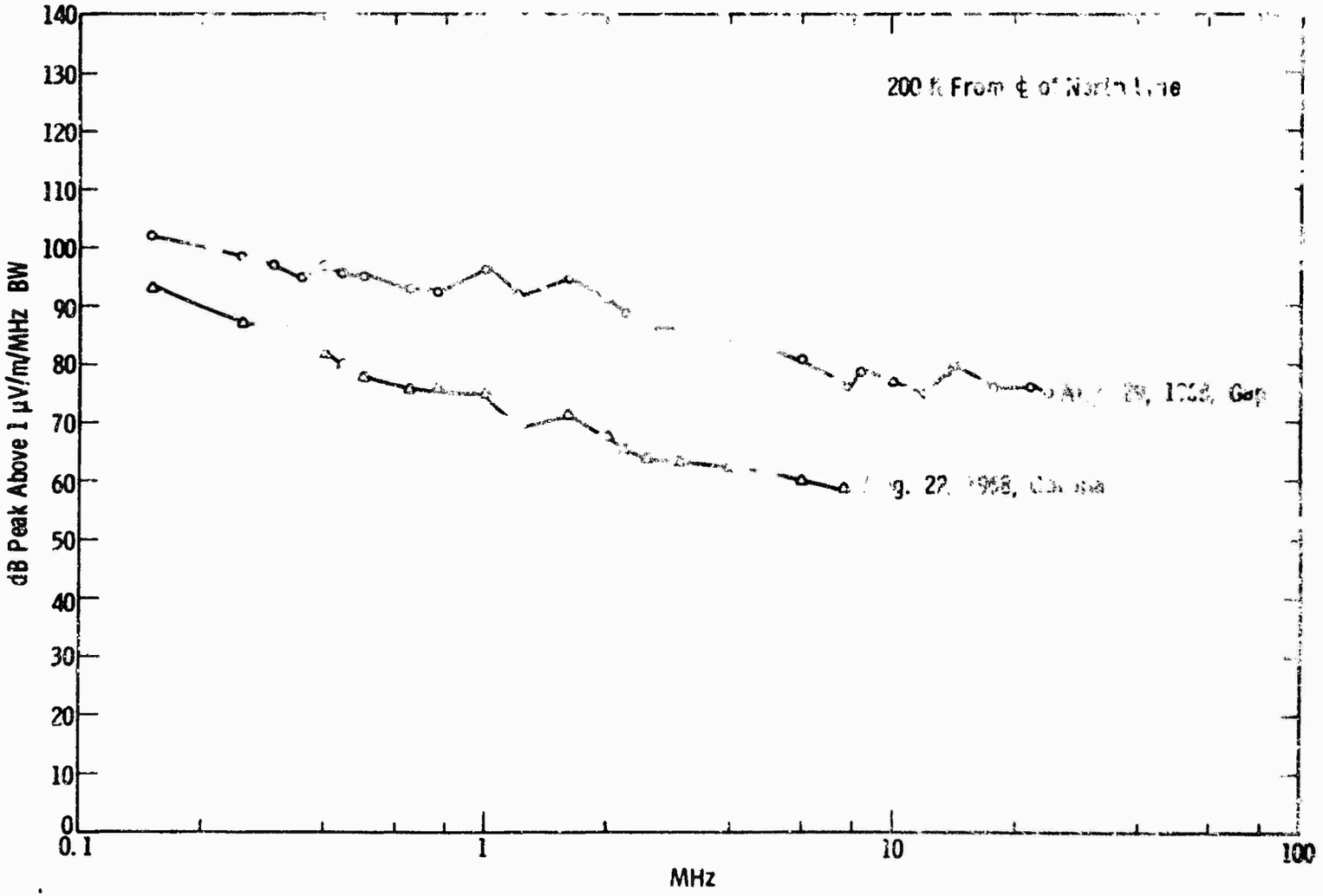


Fig. 34—Frequency spectra for 735 kV line with corona and with natural gap type source

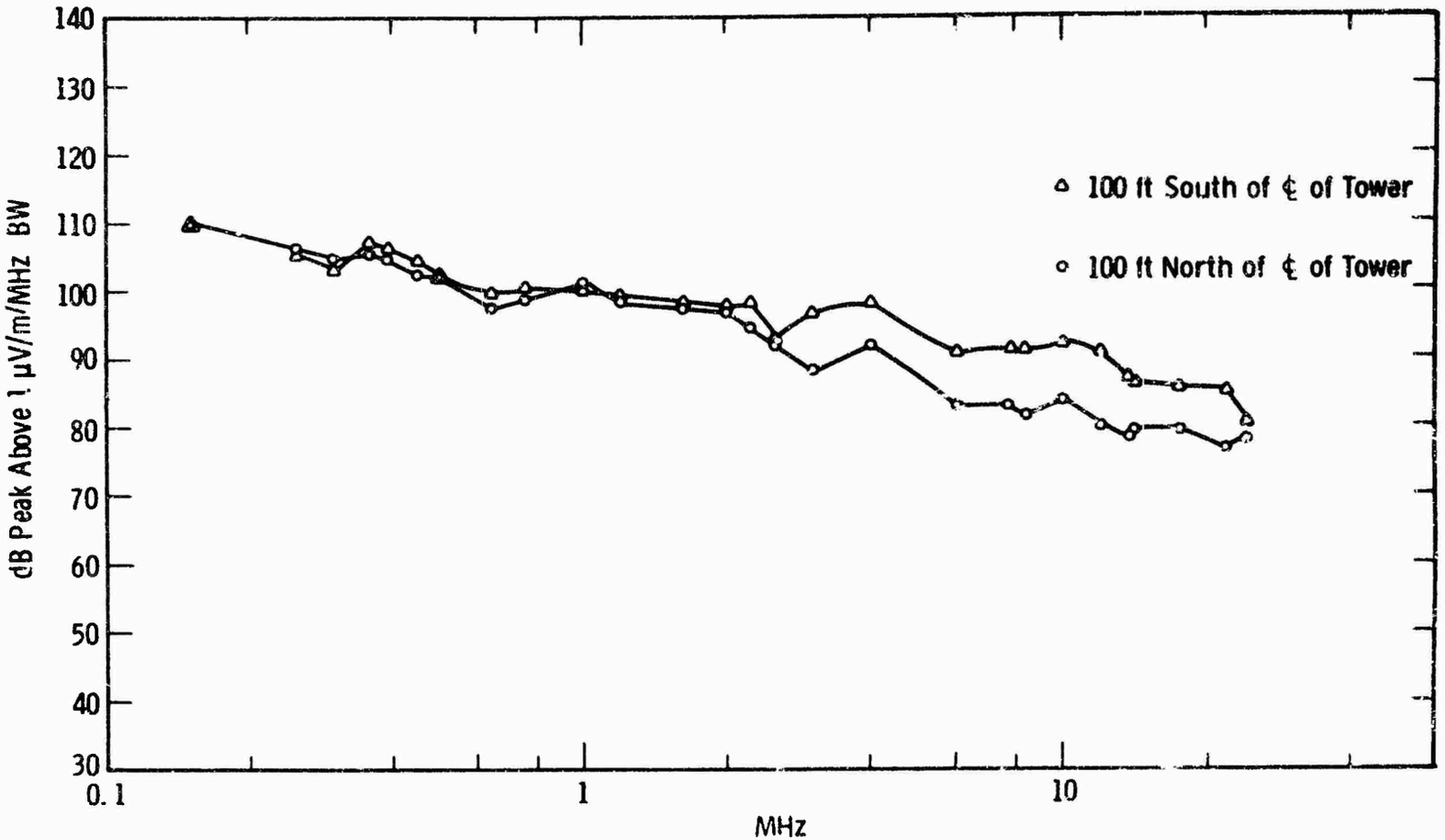


Fig. 35—Comparison of frequency spectra on opposite sides of 735 kV line tower

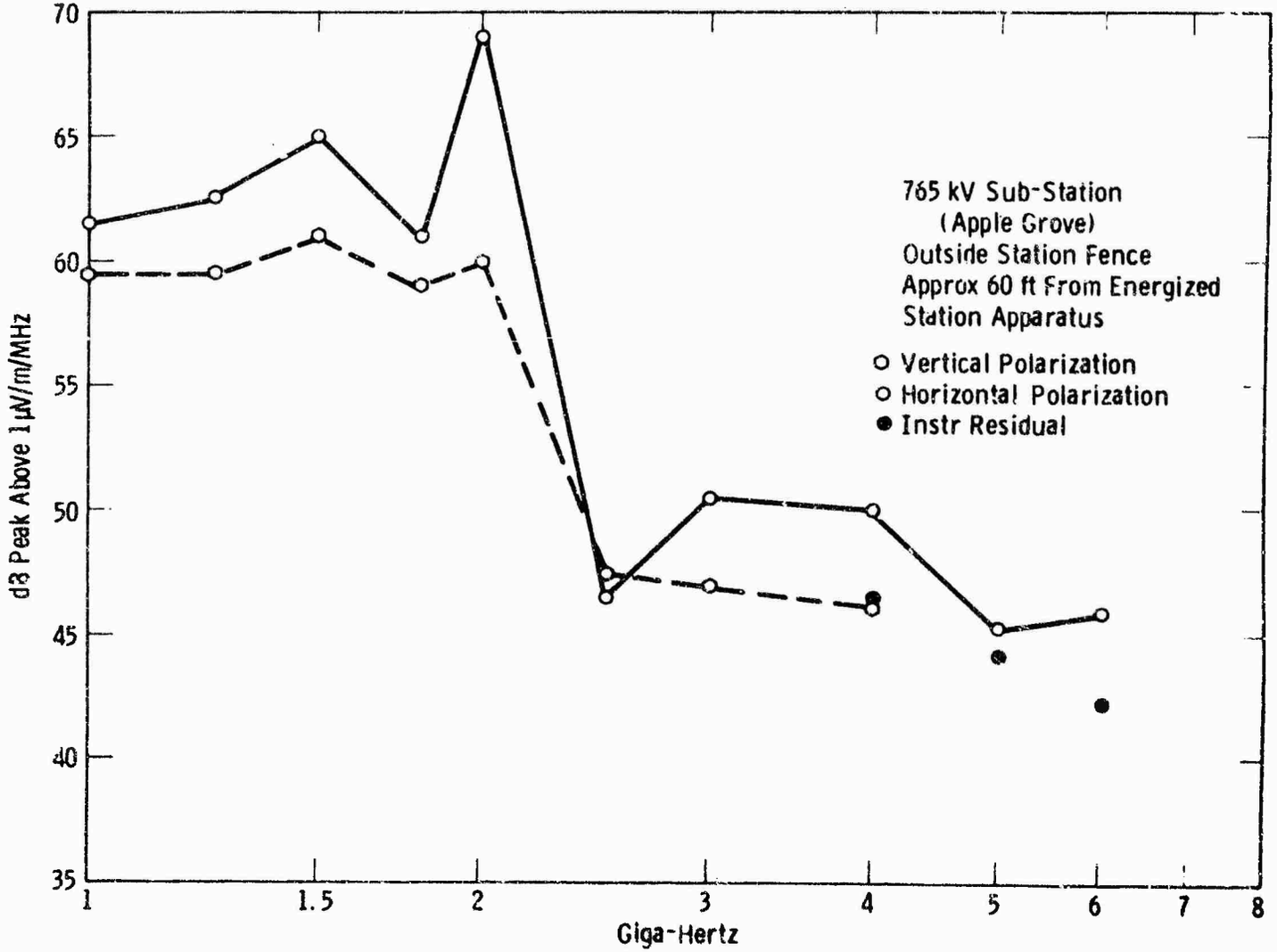


Fig. 36 —Frequency spectrum near 765 kV sub-station

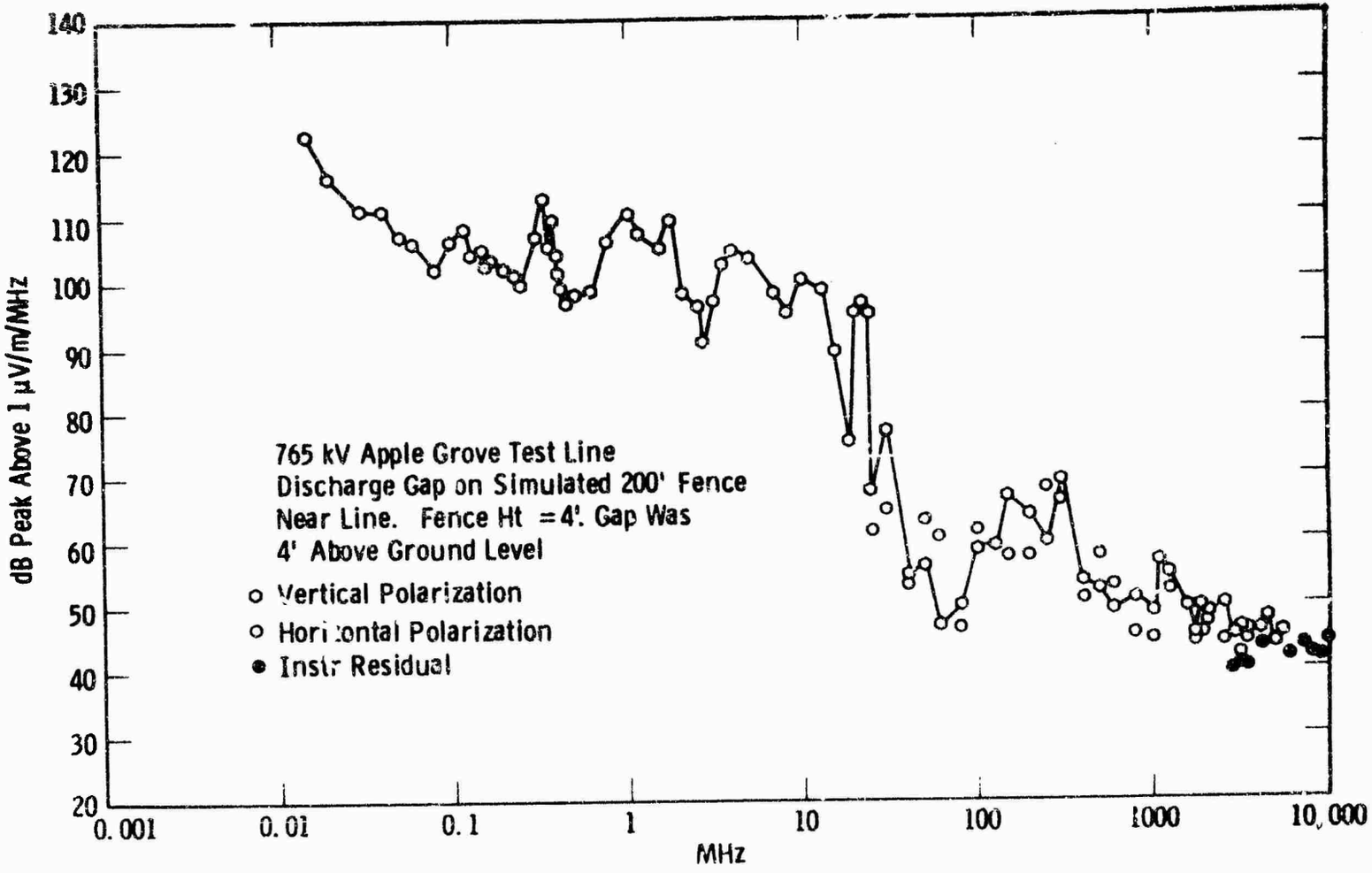


Fig. 37 —Frequency spectrum of discharge gap on "fence" near 765 kV line

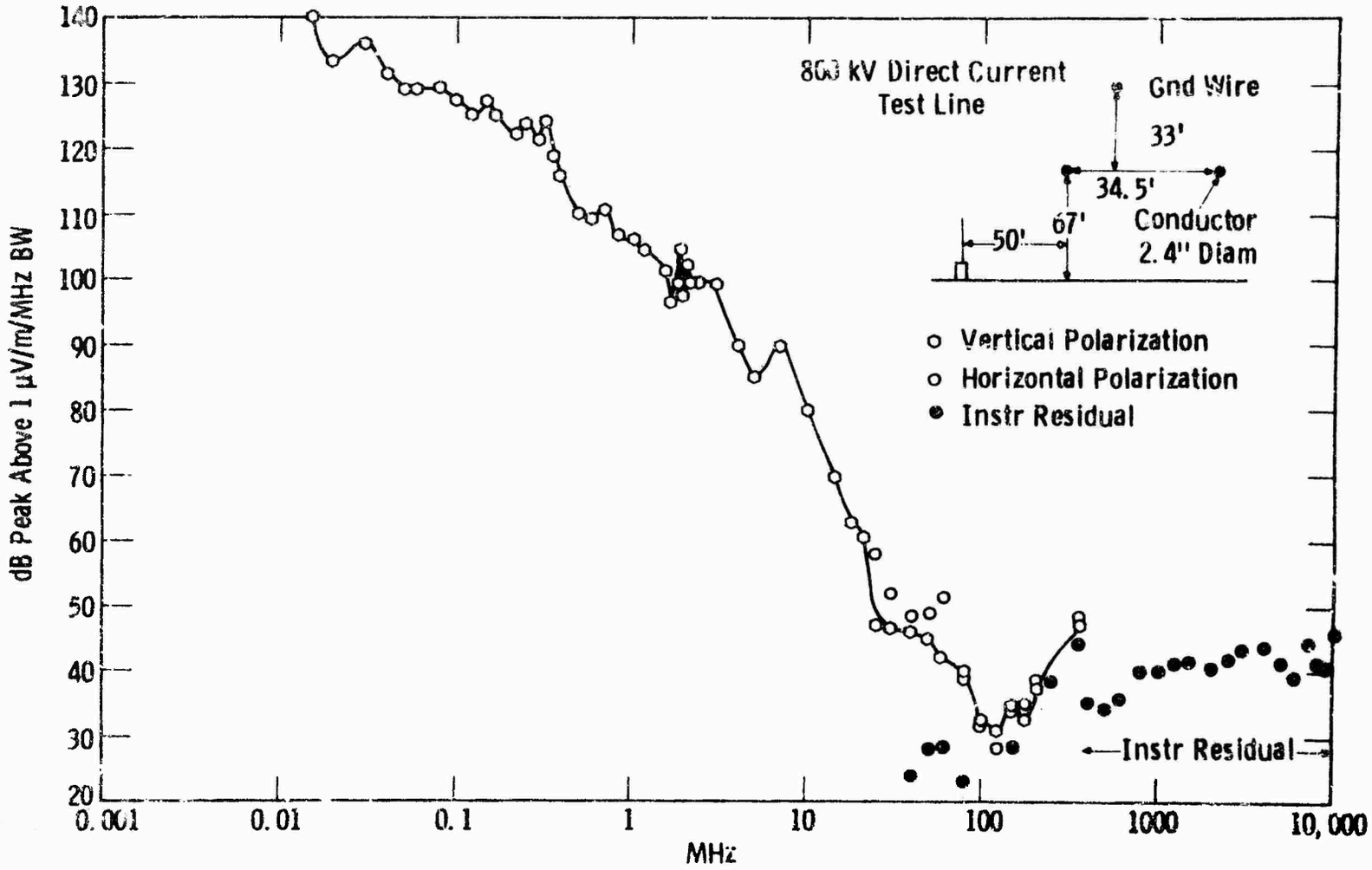


Fig. 38 —Frequency spectrum of 800 kV dc test line 30 ft opposite tower

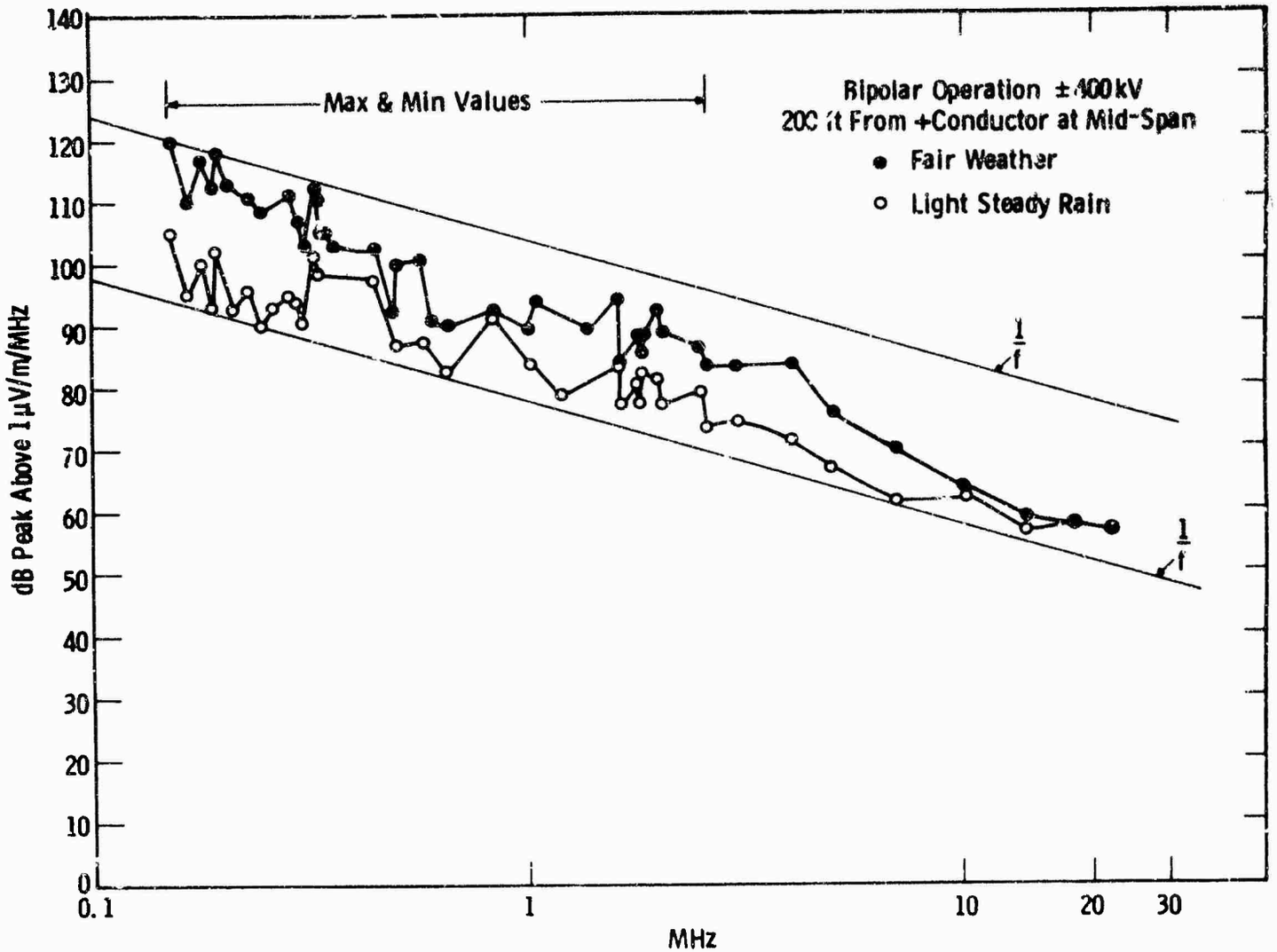


Fig. 39 —Frequency spectra of 800 kV dc test line in fair weather and rain

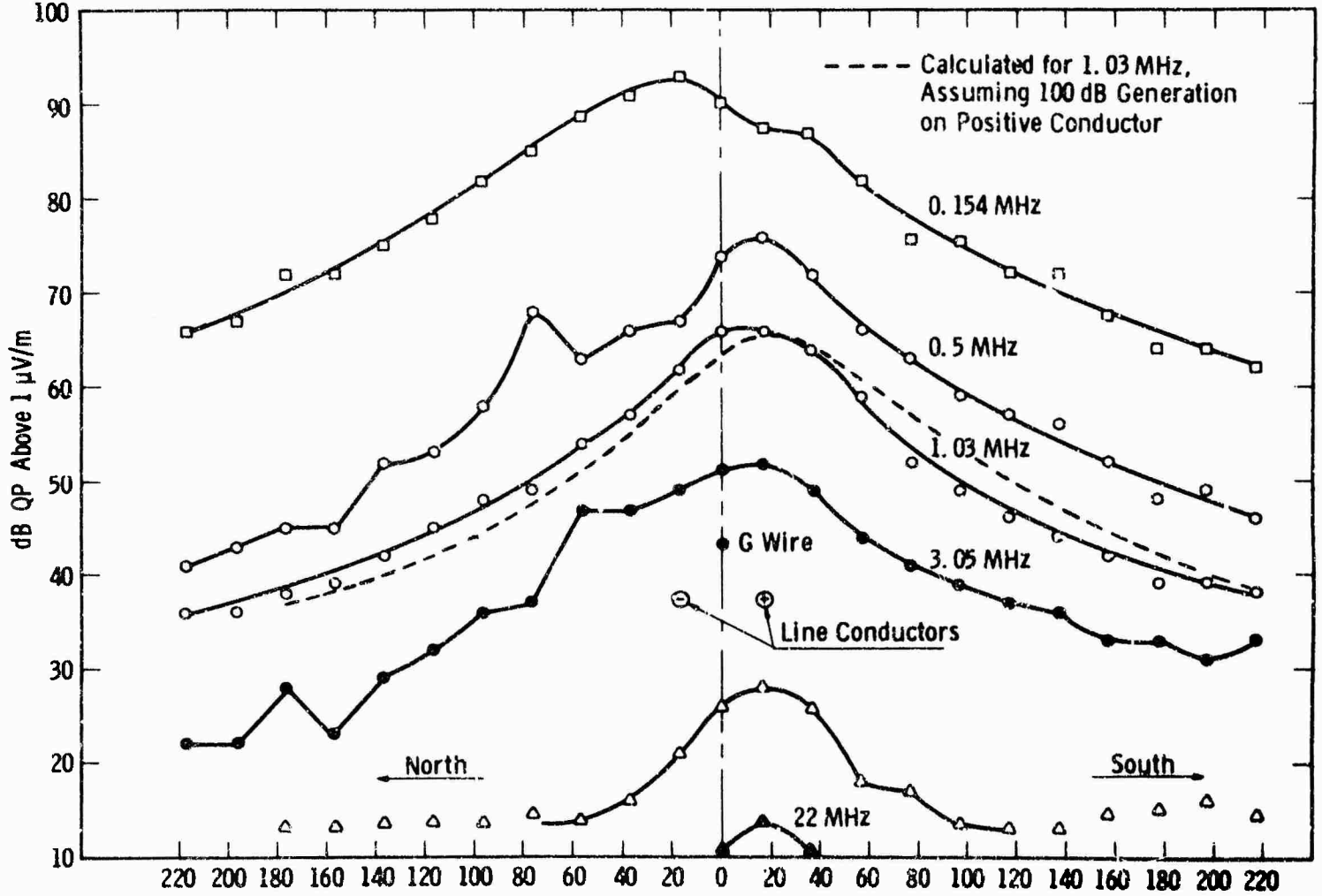


Fig. 40—Lateral profiles at mid-span 800 kV direct current test line

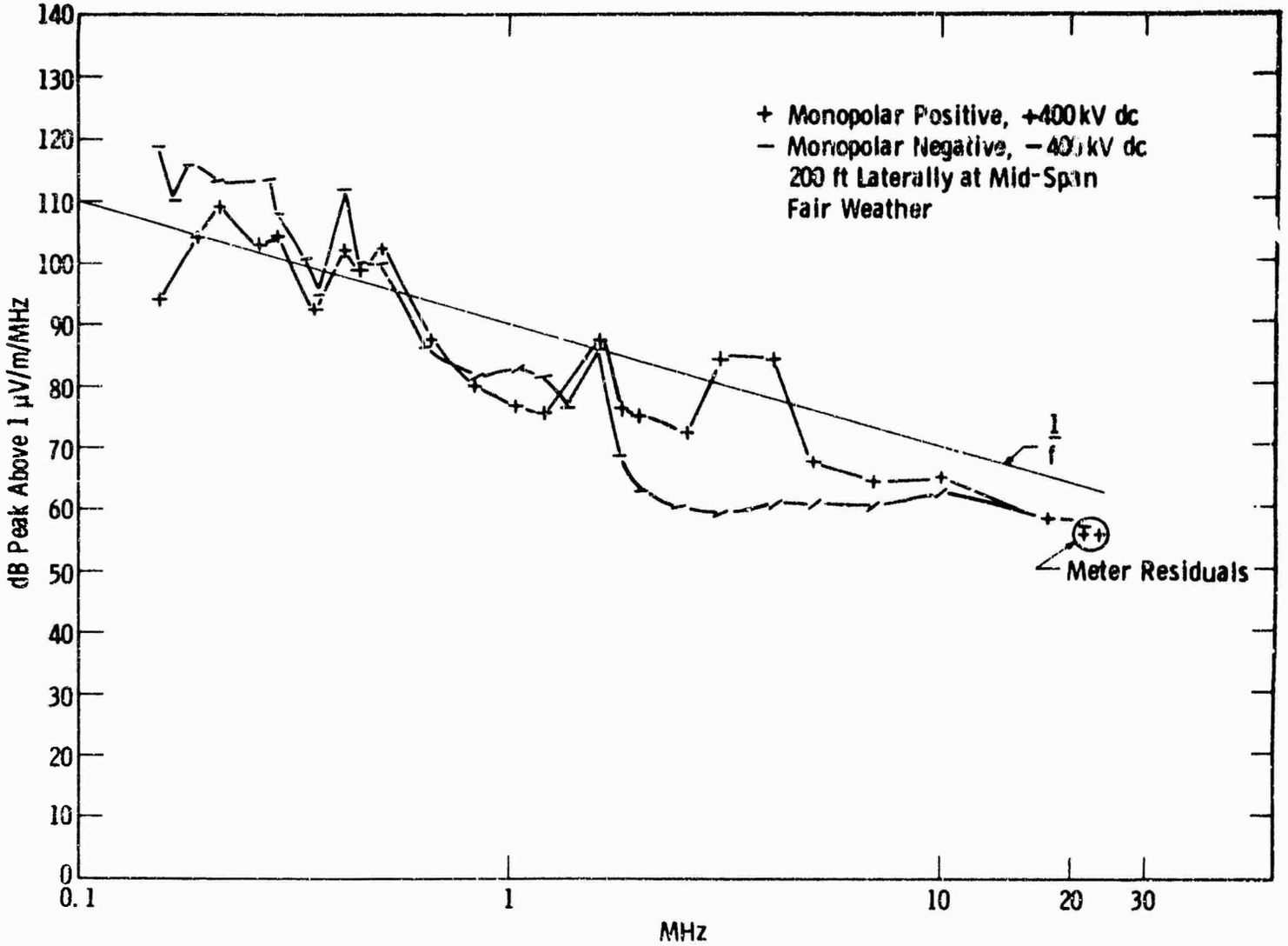


Fig. 41 –Frequency spectra for monopolar operation of ±400 kV dc test line

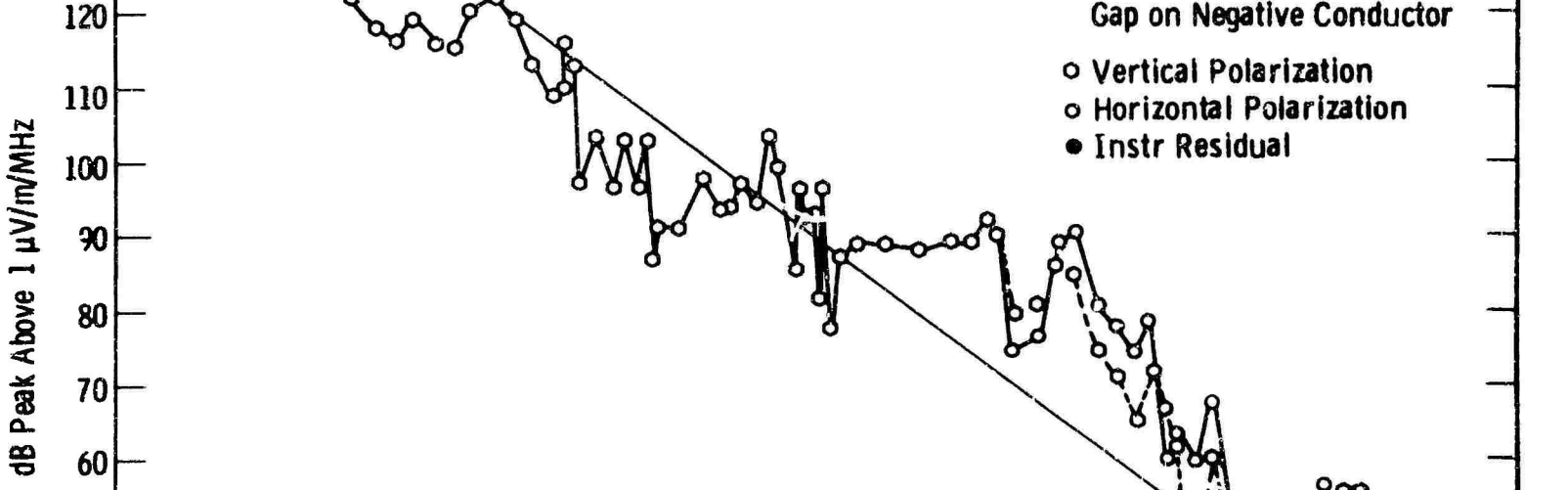


Fig. 42 —Frequency spectrum with 5/16" artificial gap on 800 kV dc test line

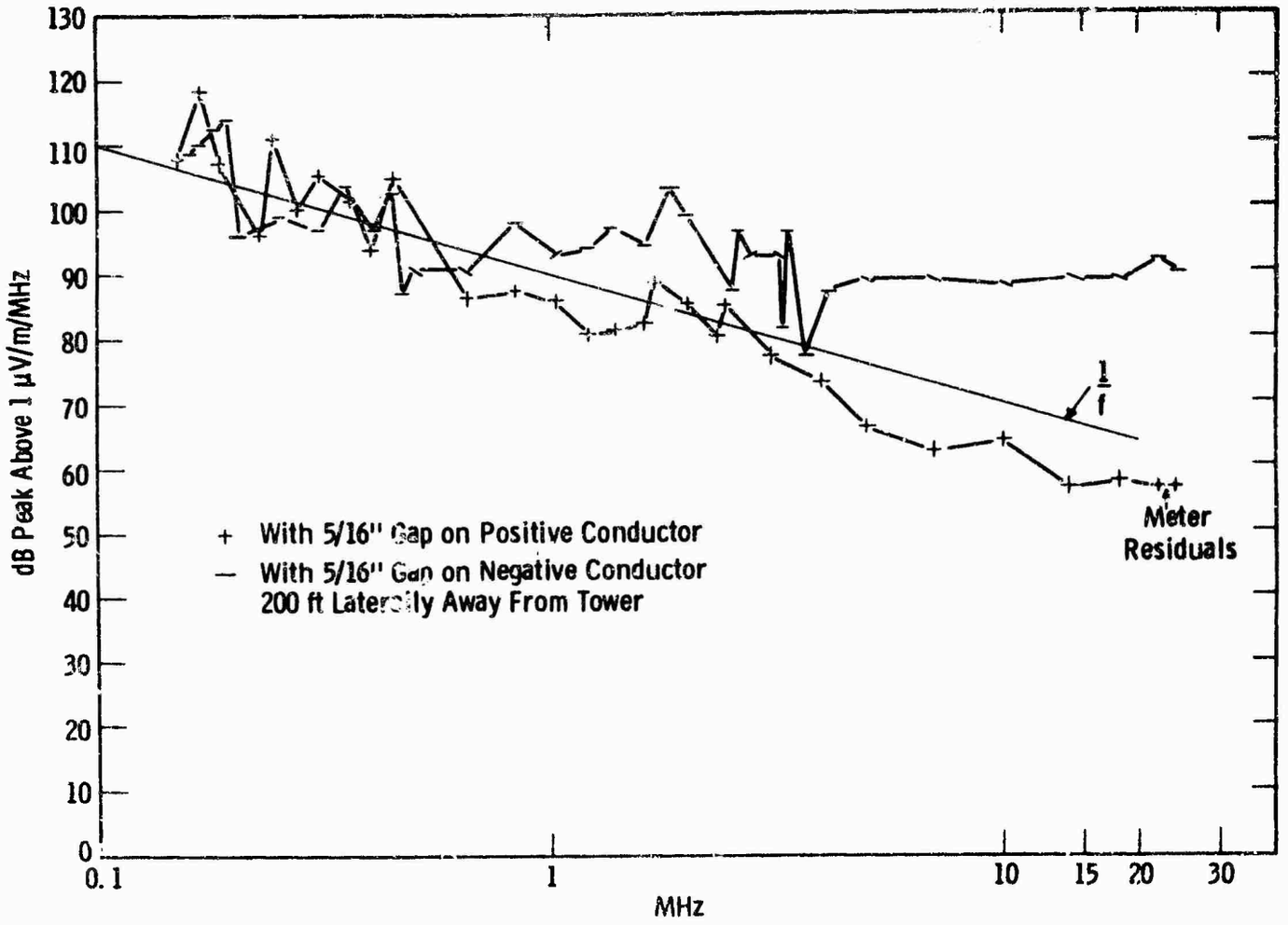


Fig. 43 —Frequency spectra with 5/16" gap on positive and negative conductor

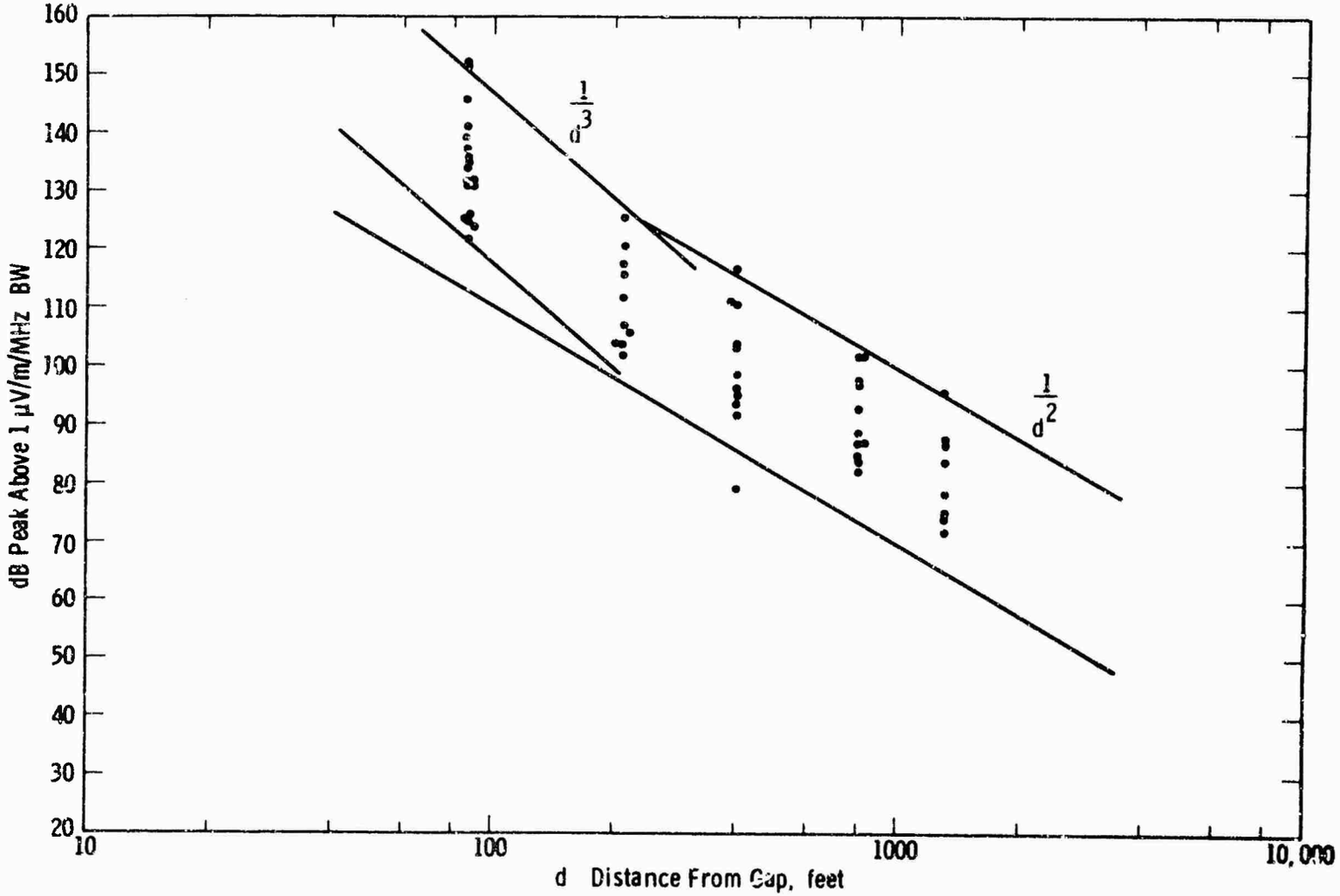


Fig. 44—Lateral attenuation from 800 kV line -0.01-0.154 MHz with gap at tower

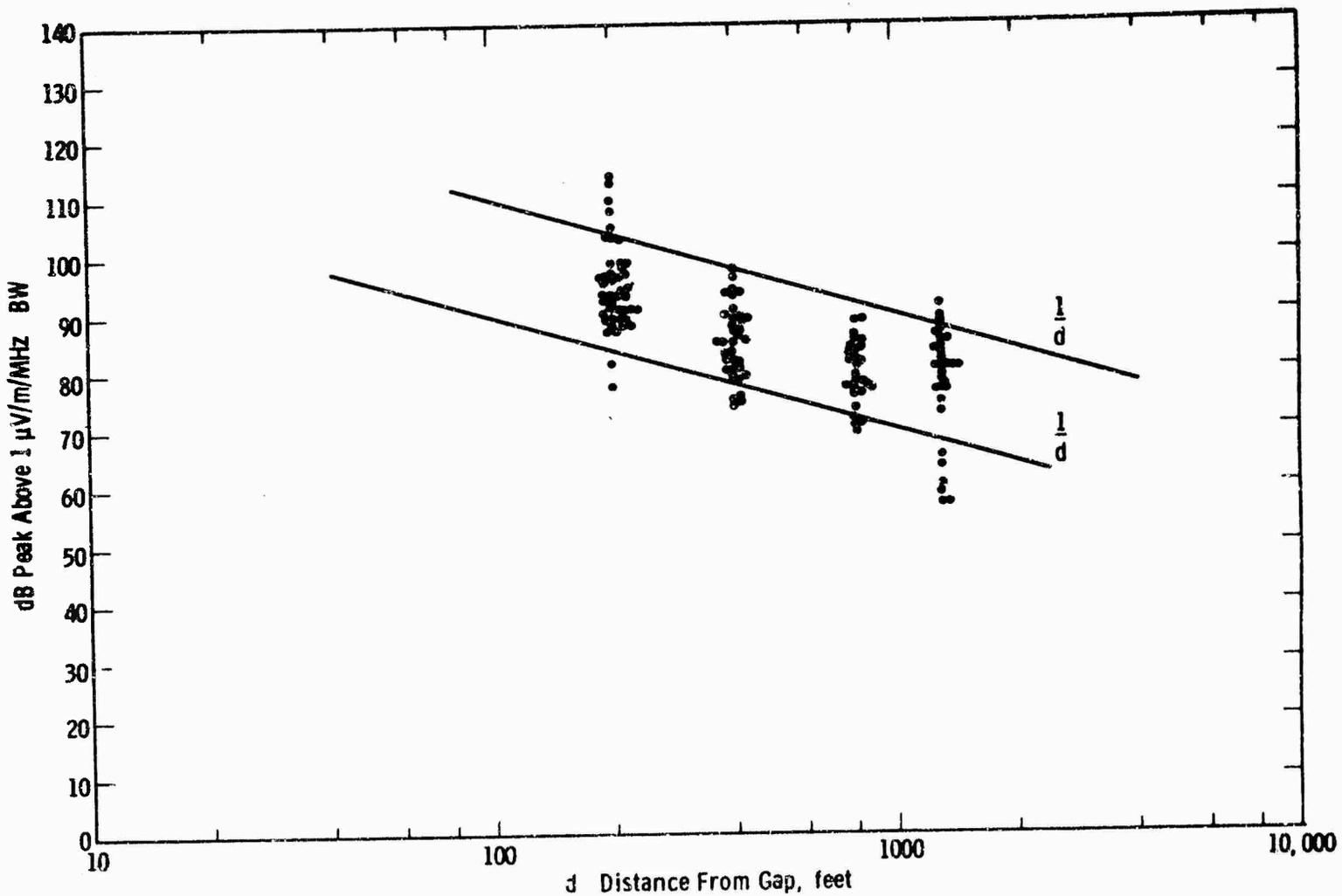


Fig. 45—Lateral attenuation from 800 kV DC line -0.154-25 MHz with gap at tower

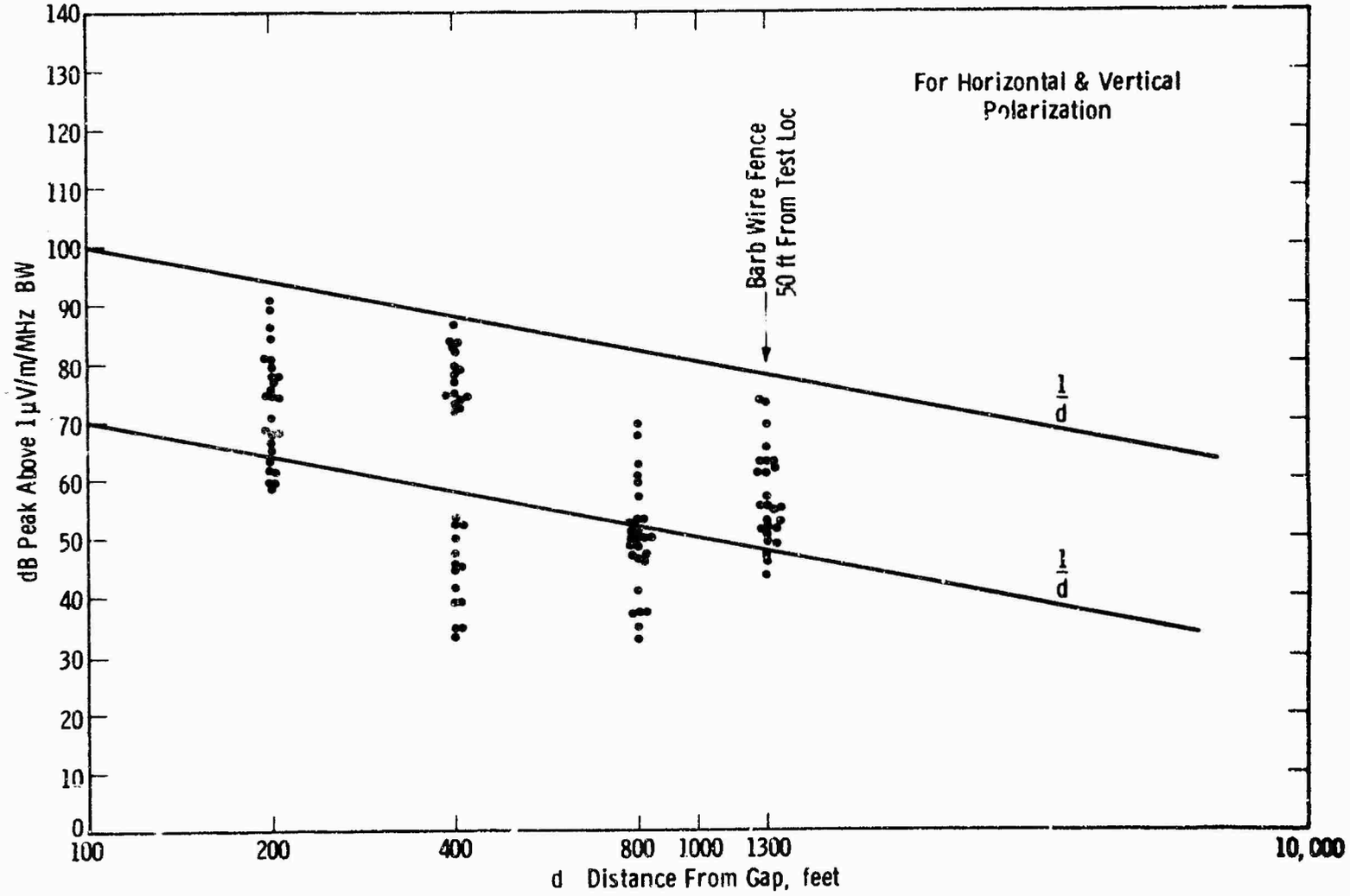


Fig. 46—Lateral attenuation from 800 kV DC line, [illegible]-400 MHz with gap at lower

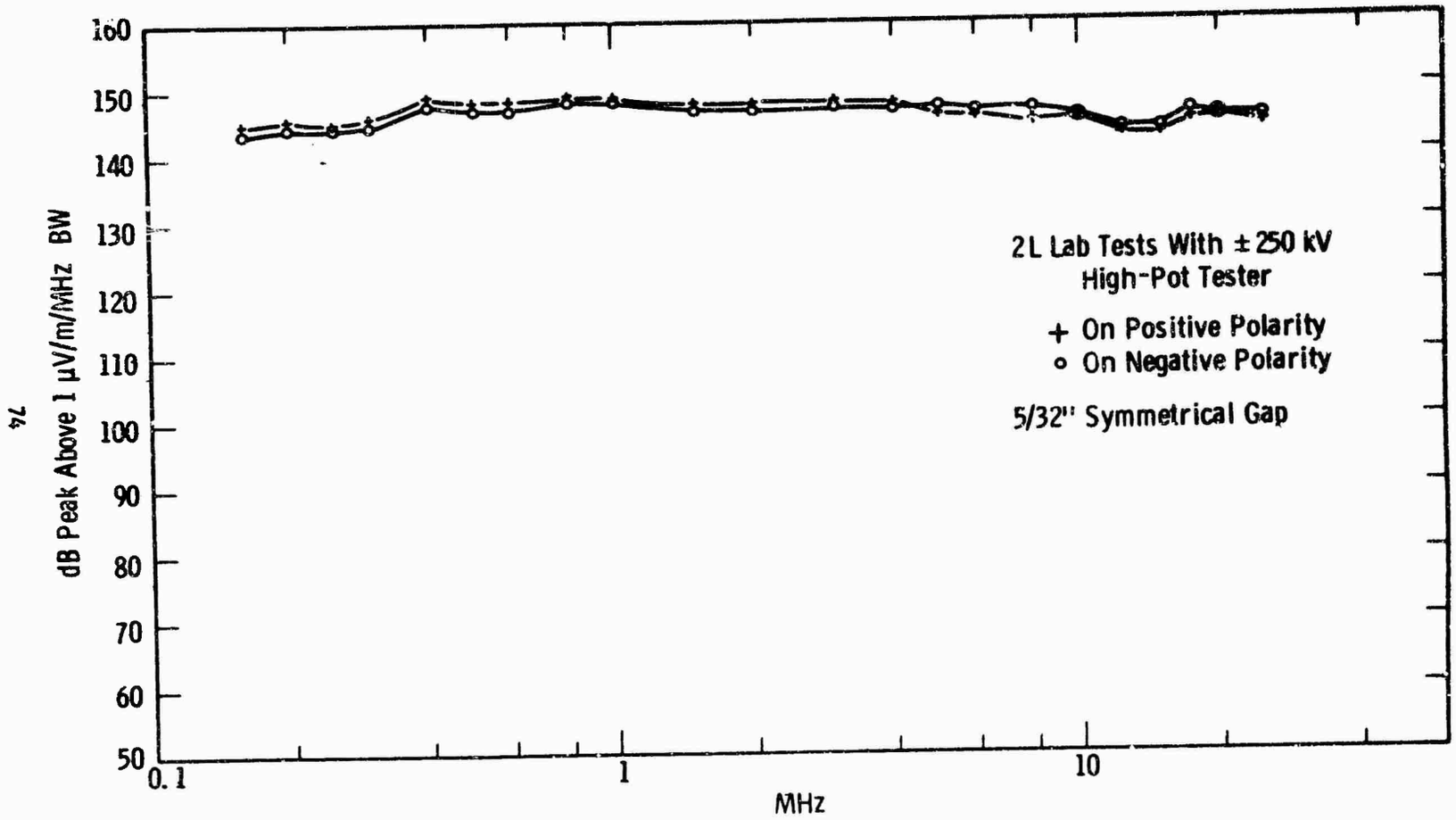


Fig. 47—Frequency spectrum for 5/32" gap on + and − DC voltage

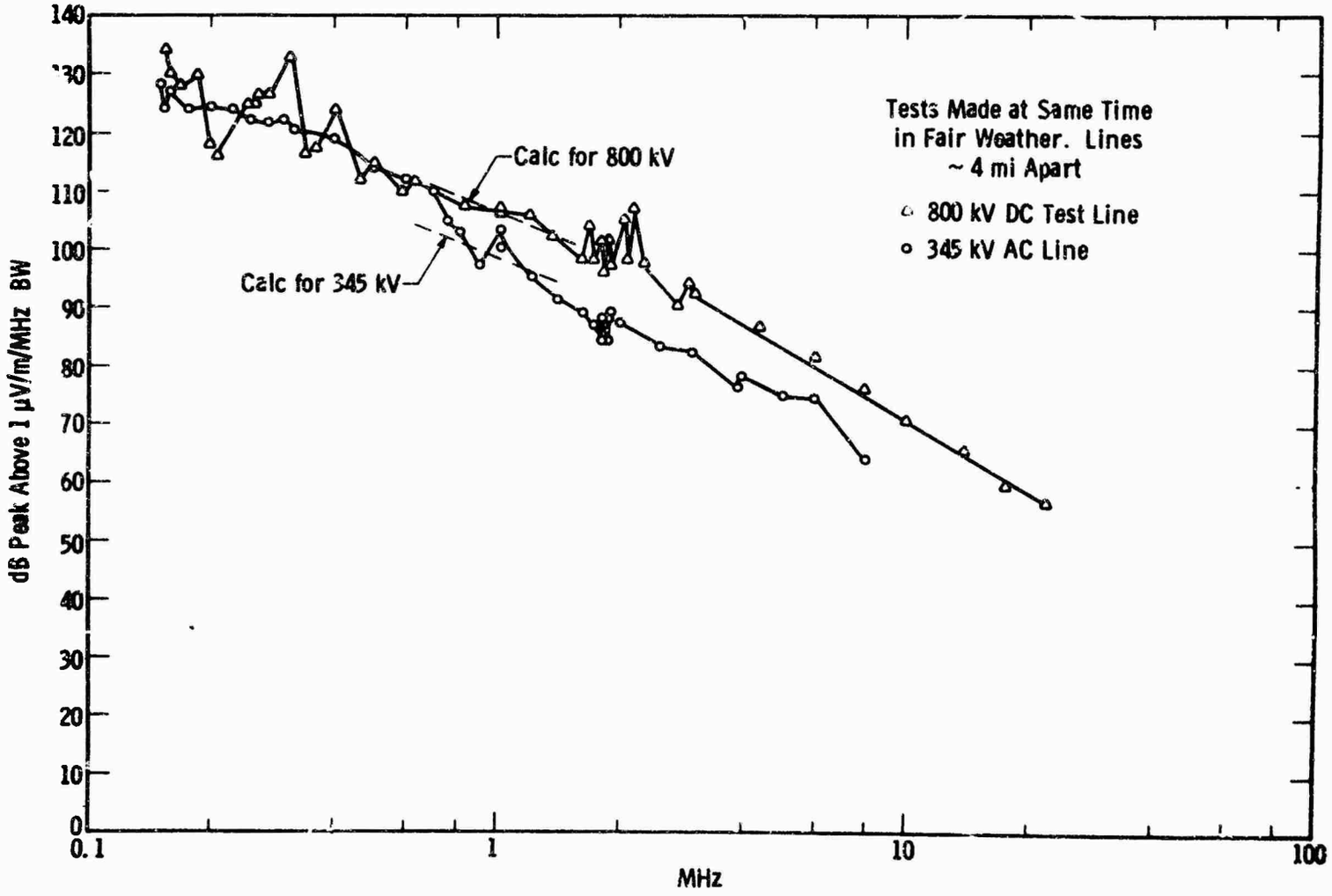


Fig. 48—Comparison of 800 kV DC line with 345 kV AC line in fair weather at 50 ft

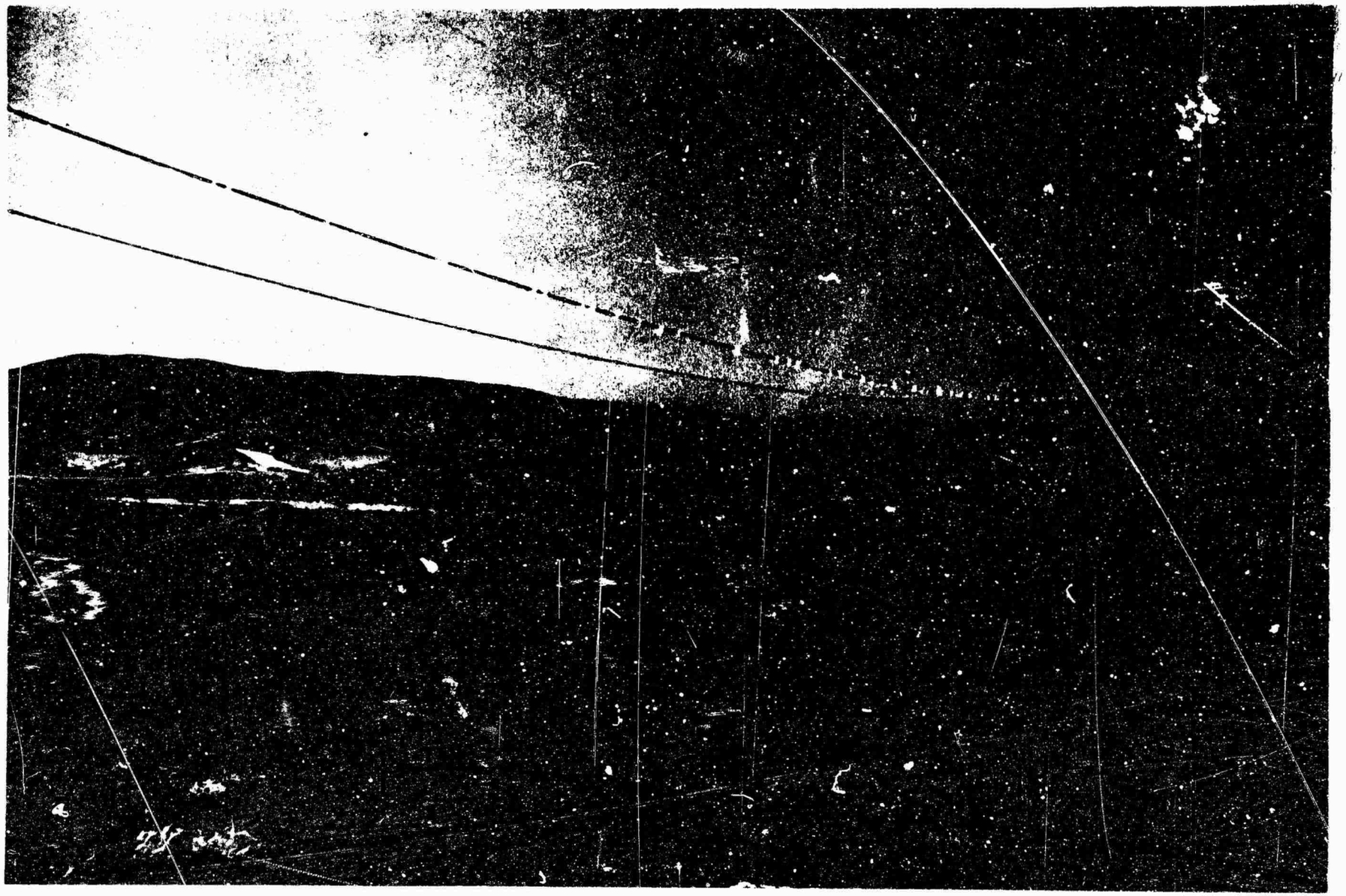
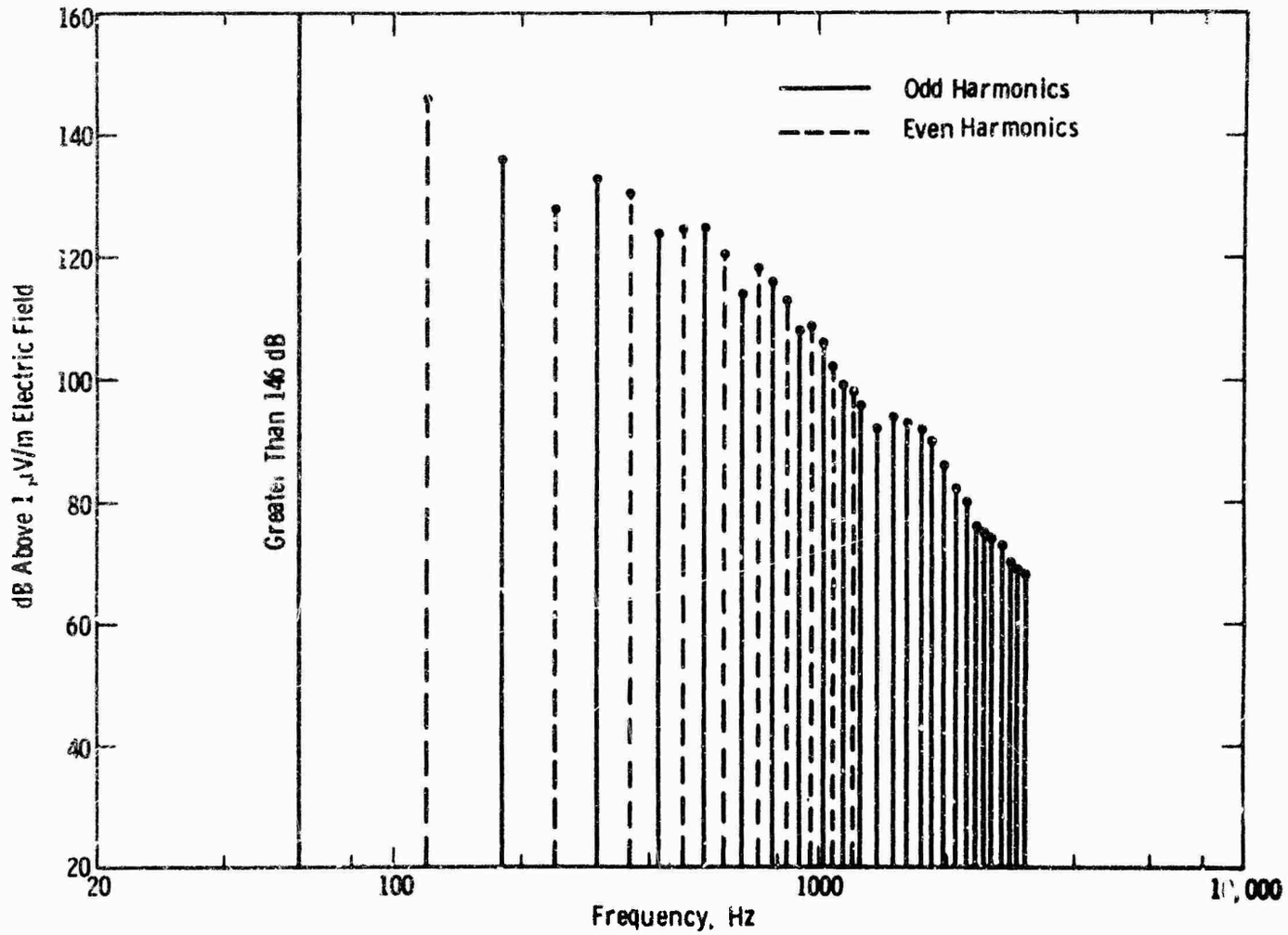


Fig. 49 800 kV dc Line - Positive Conductor has the most corona plumes.



...g. 50-525 kV line 60 Hz and harmonics at 200 ft from outside phase

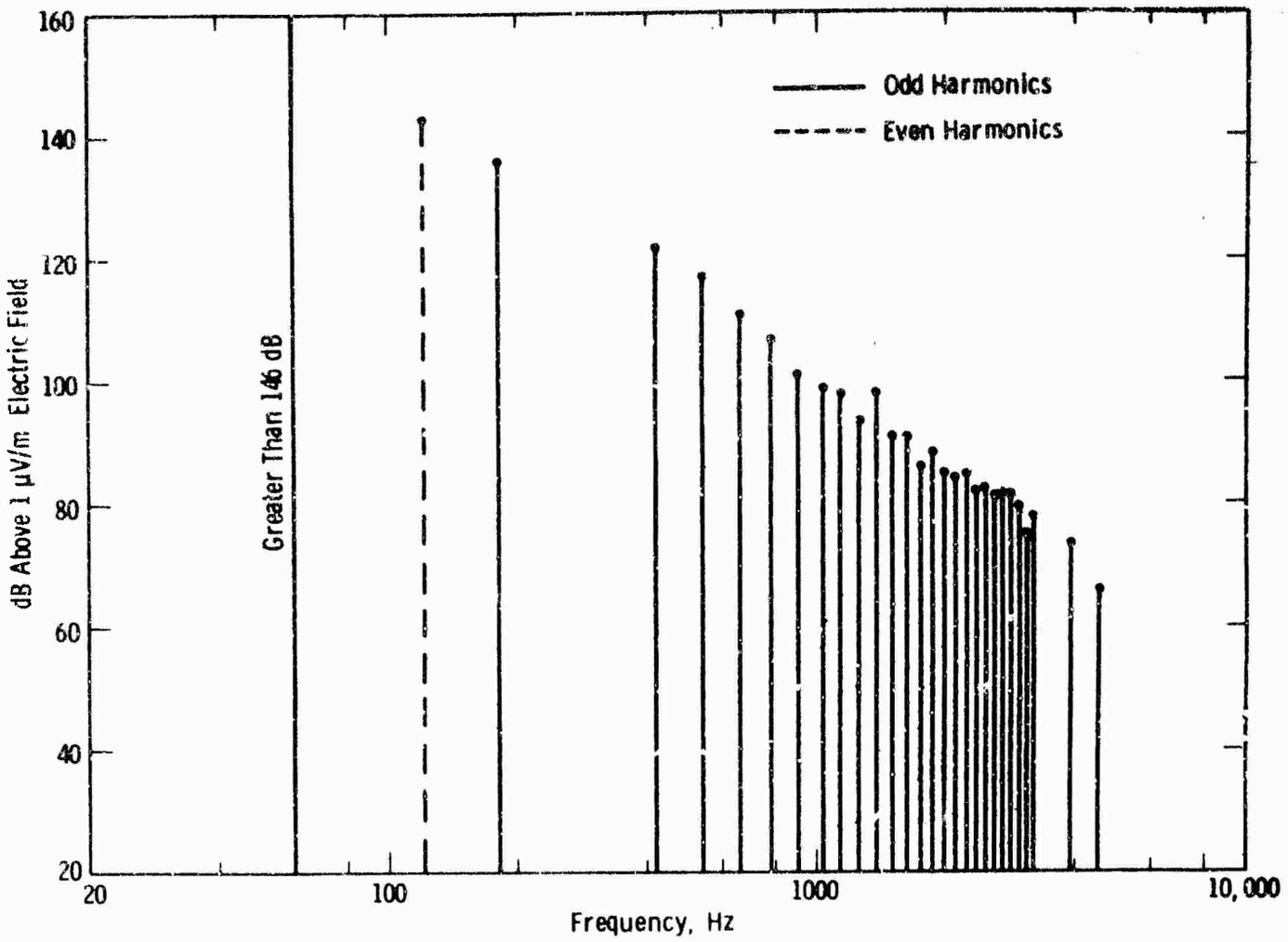


Fig. 51 - 735 kV line 60 Hz and harmonics at 200 ft from outside phase

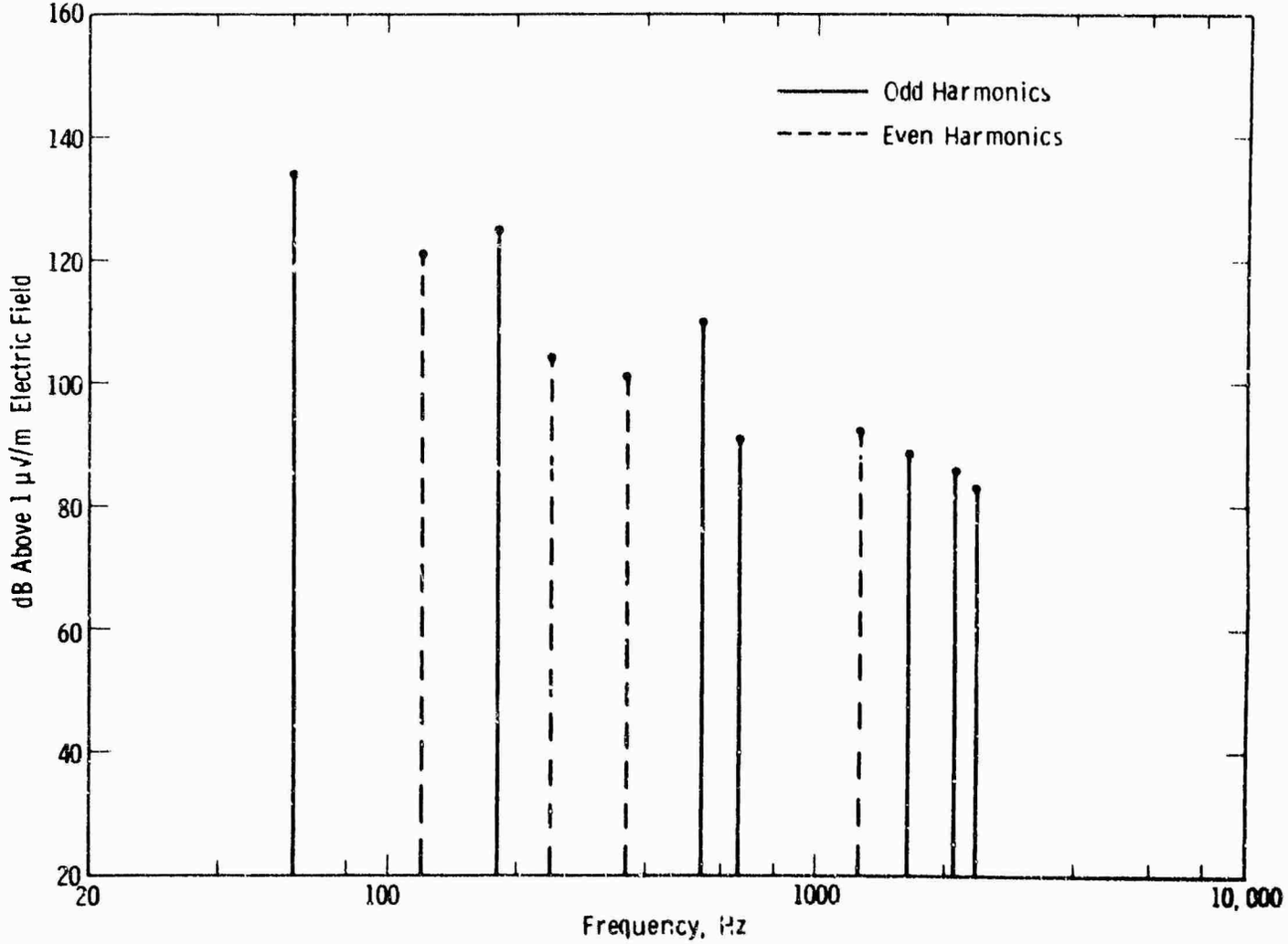


Fig. 52 - 800 kV DC line 60 cycles and harmonics between the positive and negative conductors

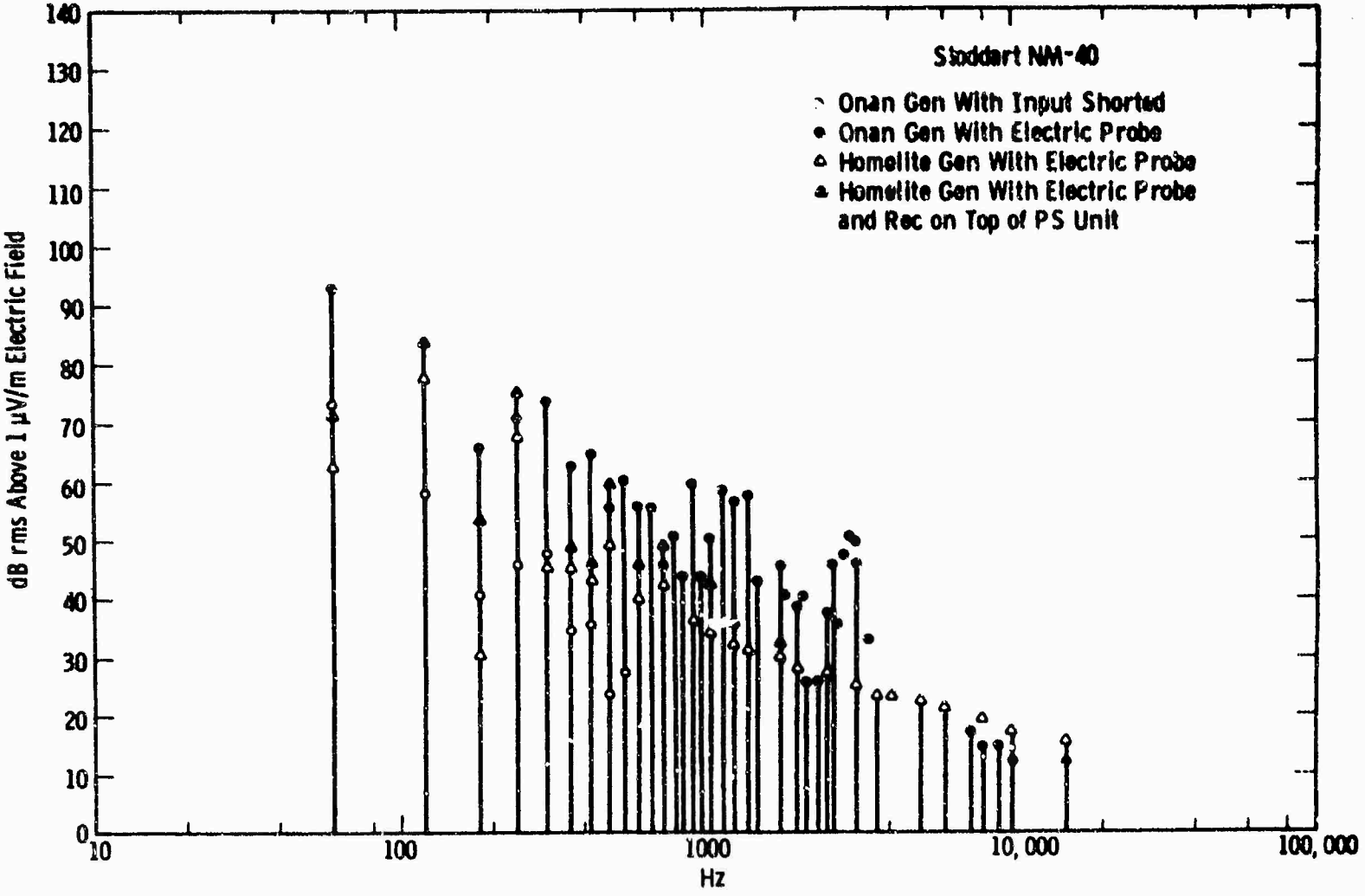


Fig. 53—Audio frequency receiver residual with different engine power supplies

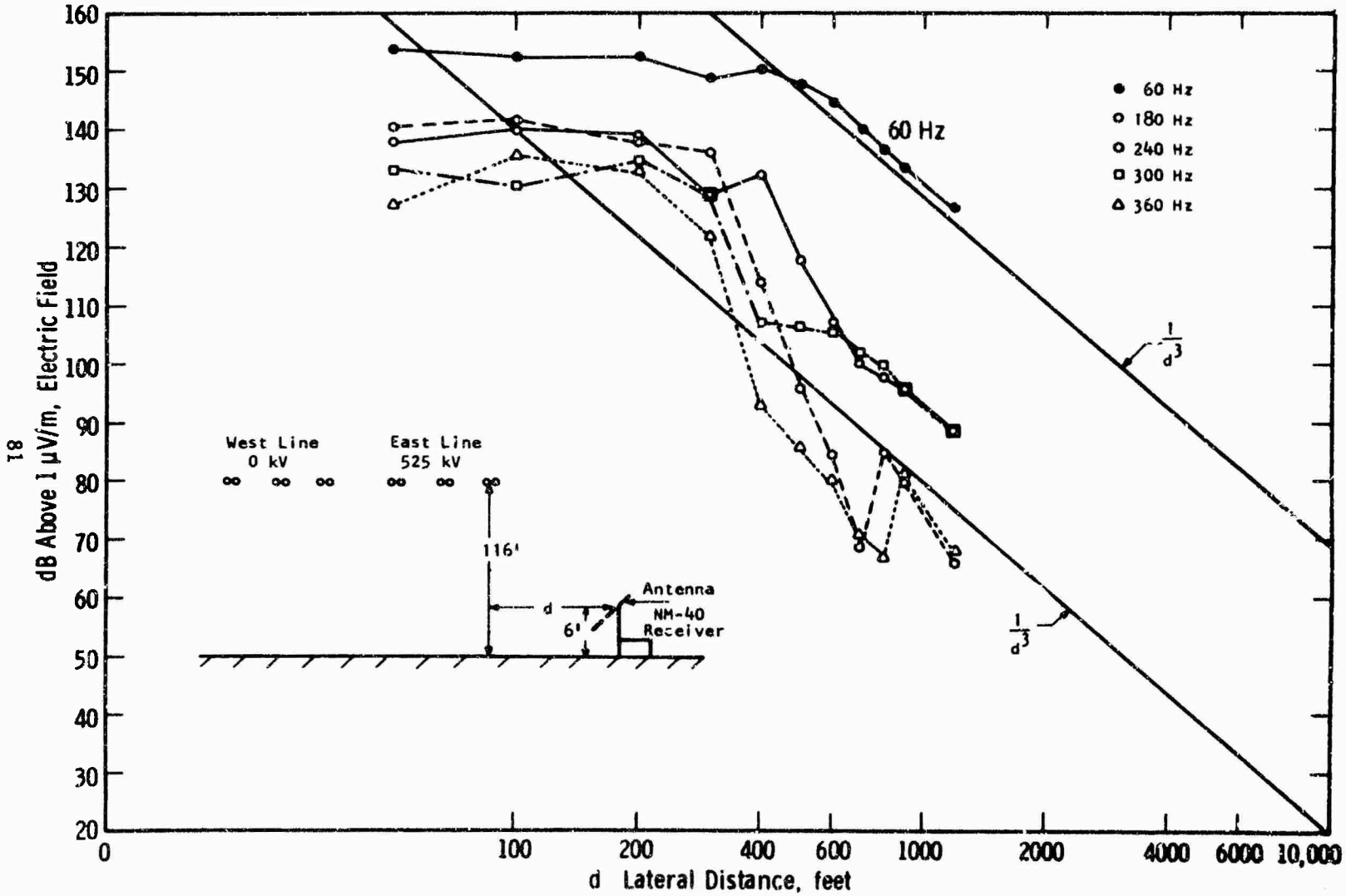


Fig. 54 —Lateral attenuation of 60 Hz and harmonics for 525 kV line

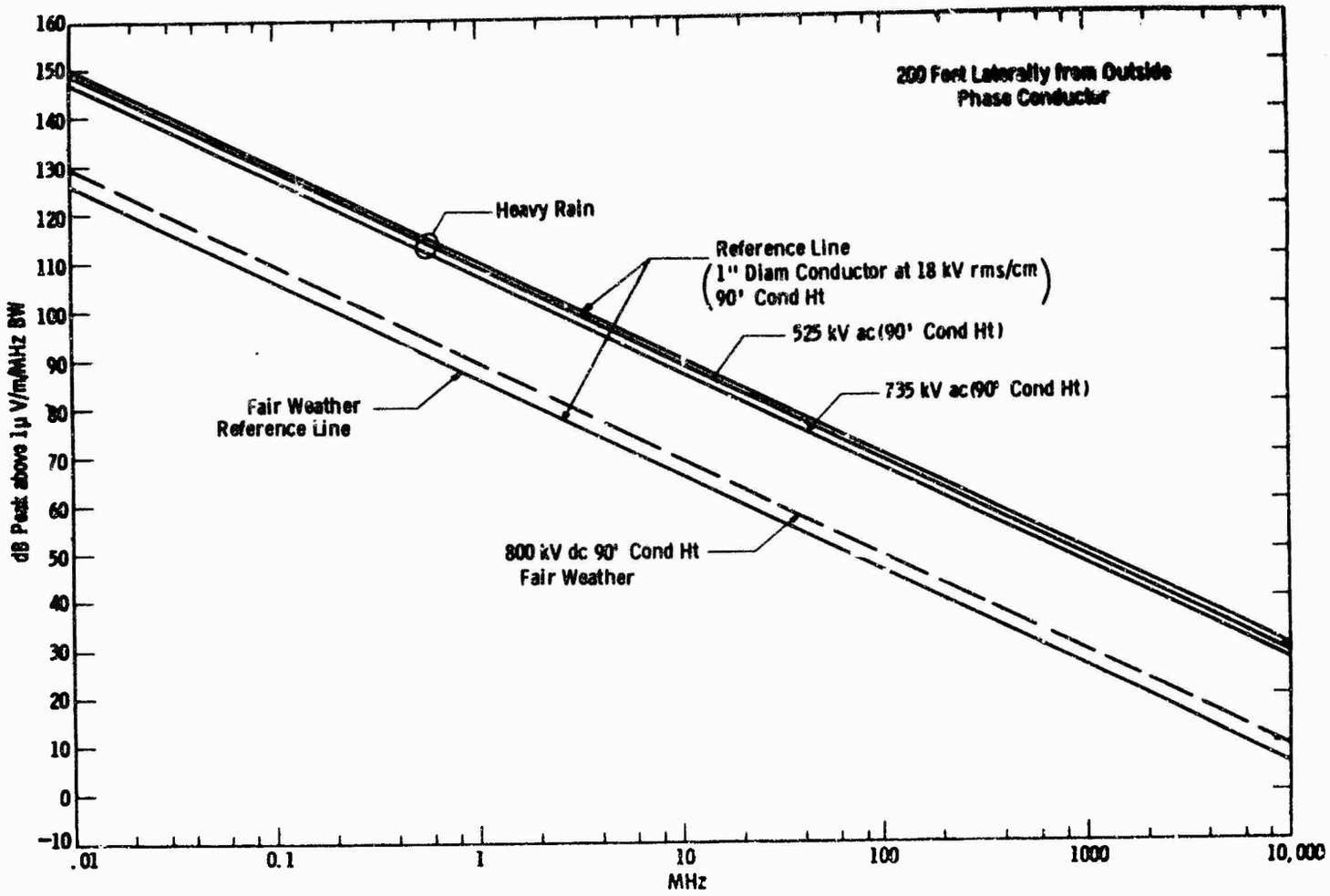


Fig. 55—Prediction curves for conductor corona radio noise 525, 735 and 800 kV lines

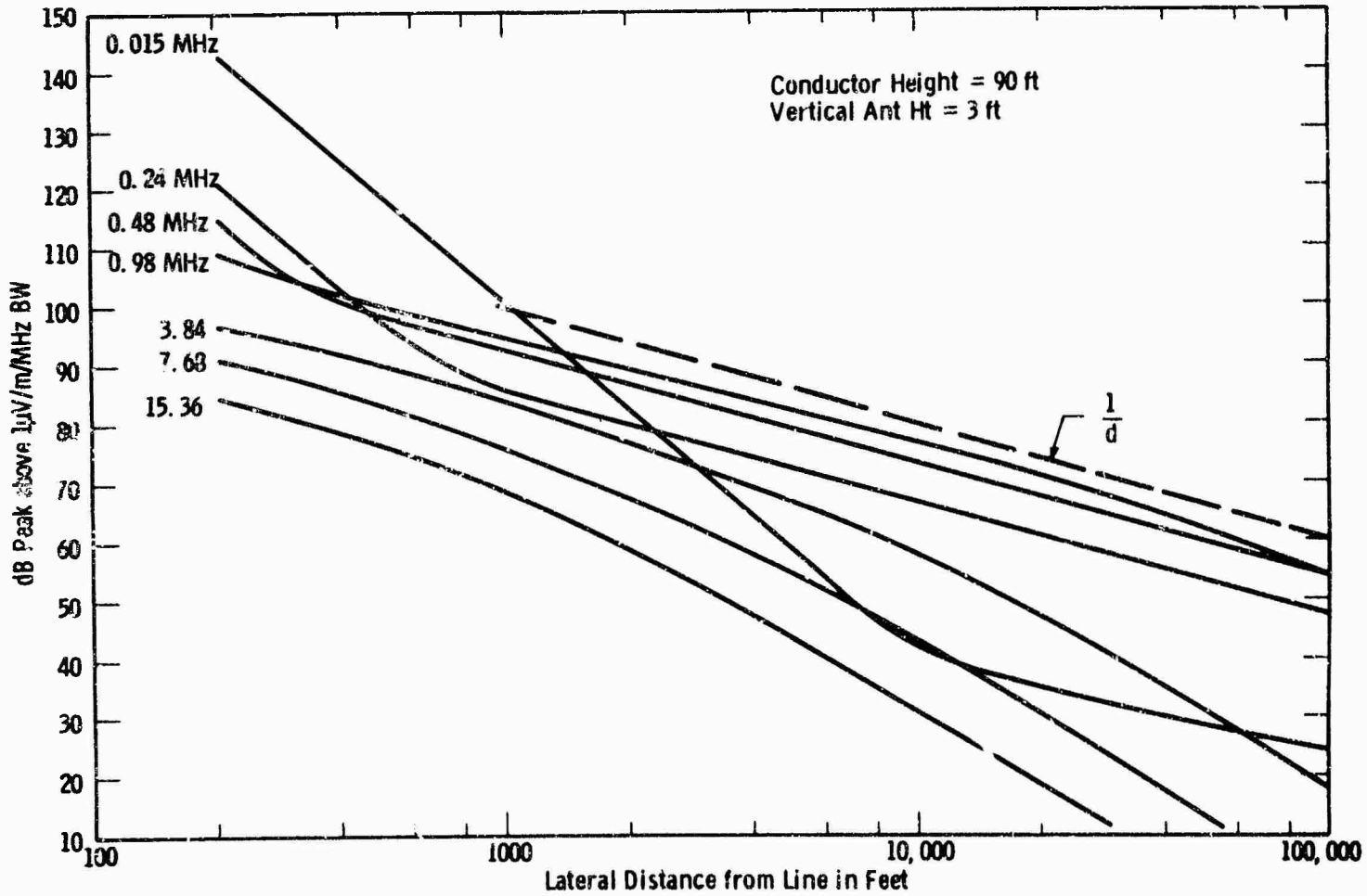


Fig. 56— Predicted 525 kV line conductor corona radio noise for heavy rain

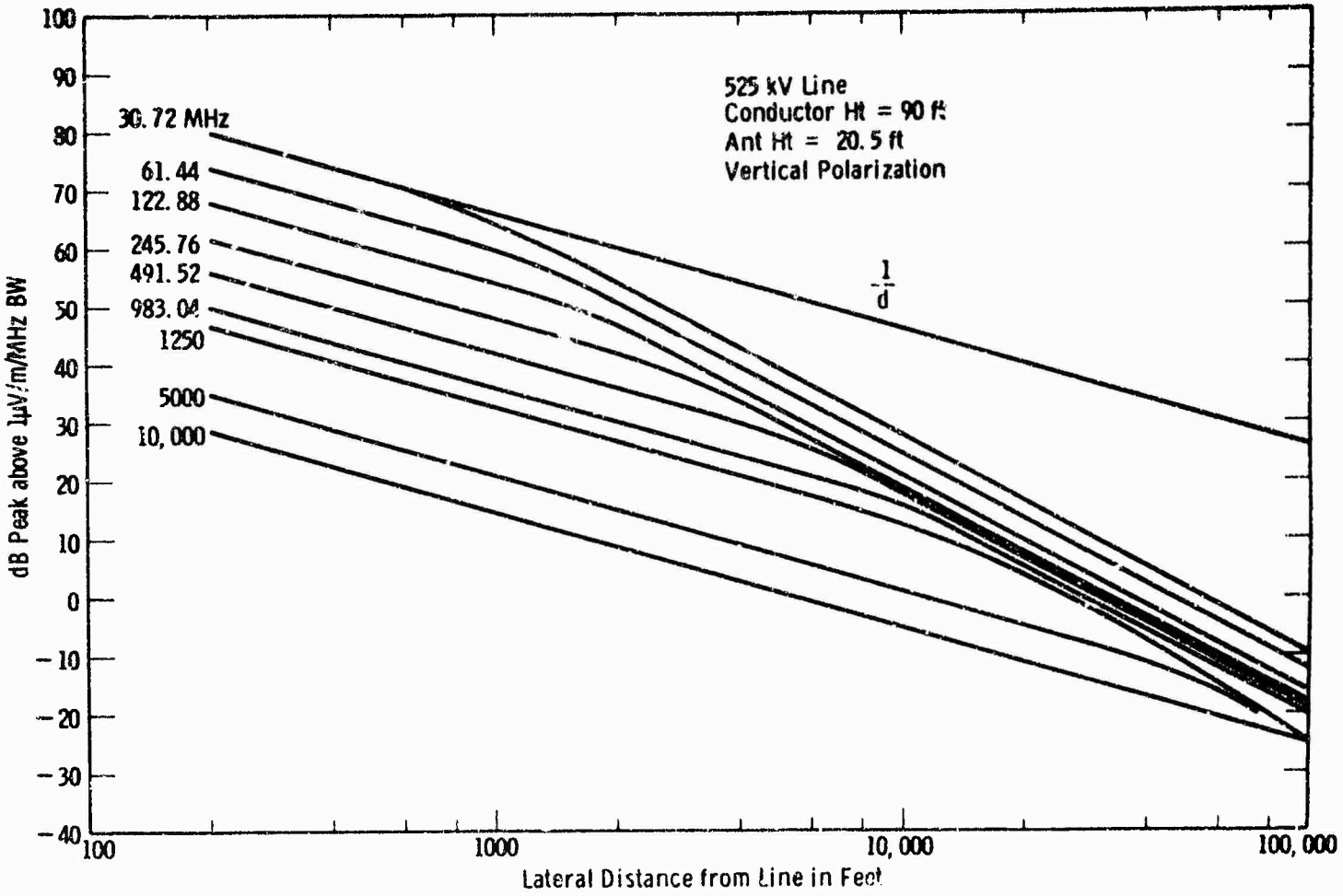


Fig. 57— Predicted line conductor corona radio noise in heavy rain

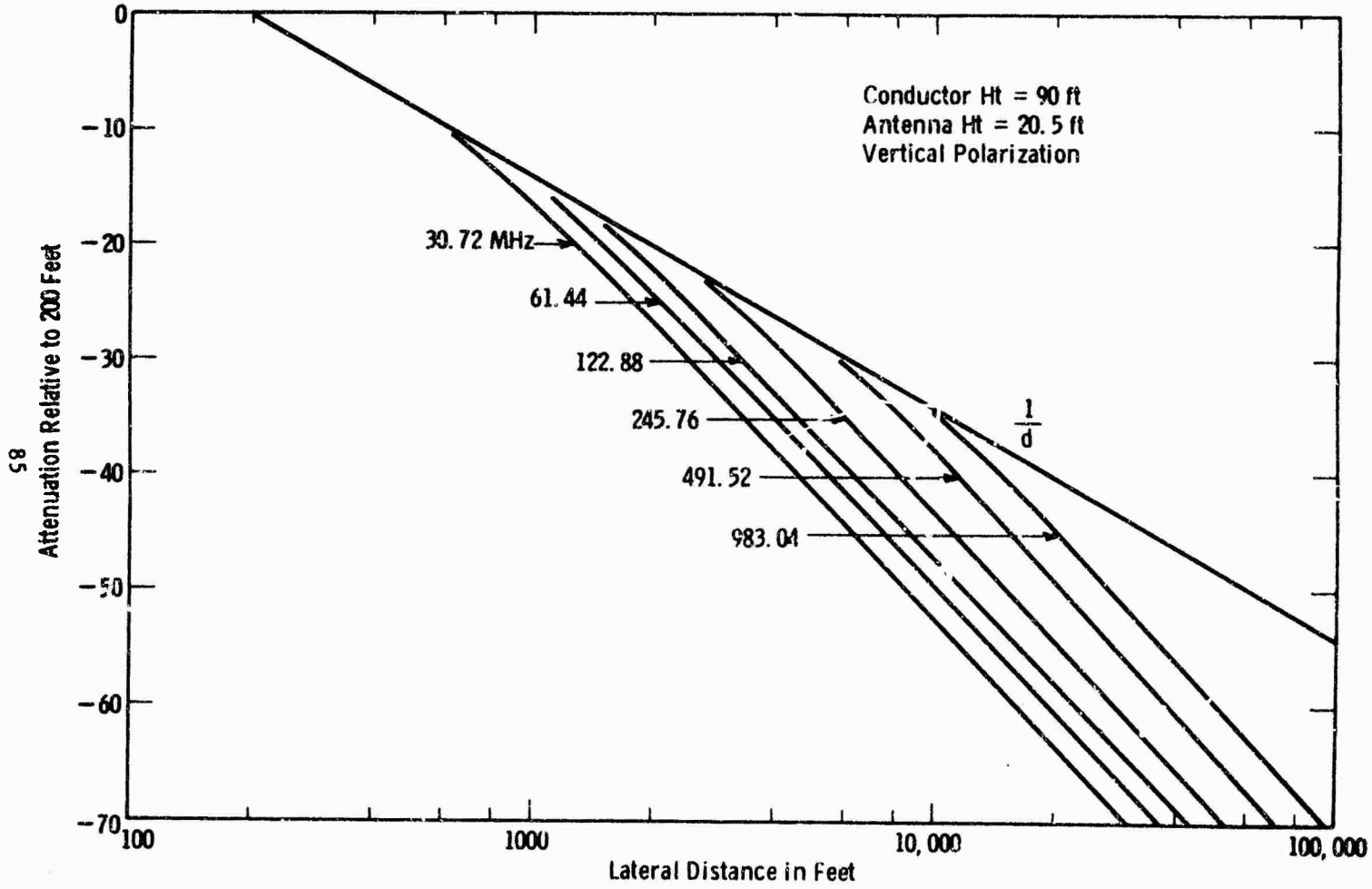


Fig. 58— Lateral attenuation in the 30-1000 MHz range for vertical polarization

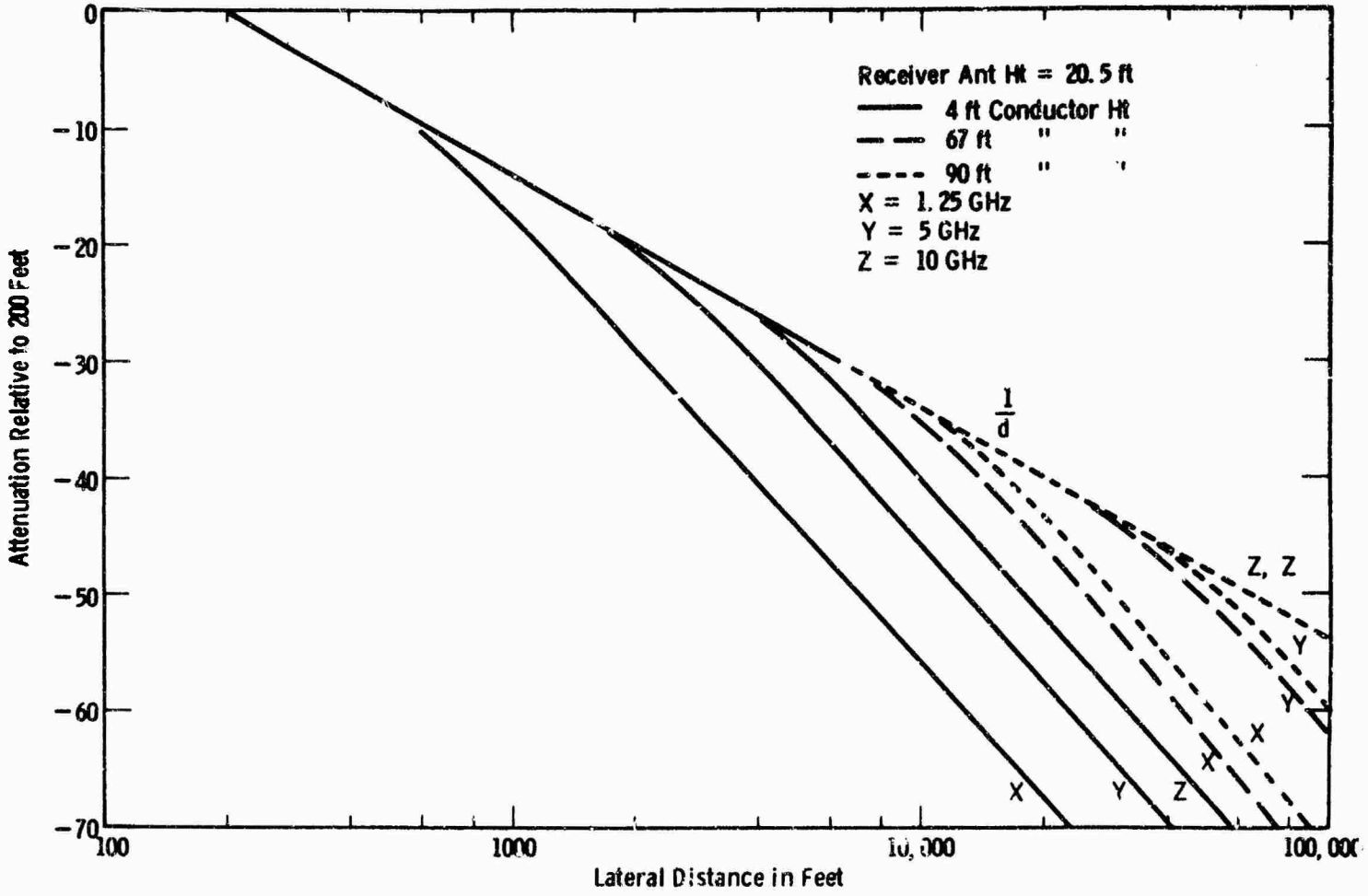


Fig. 59—Lateral attenuation in the 1-10 GHz range for vertical polarization

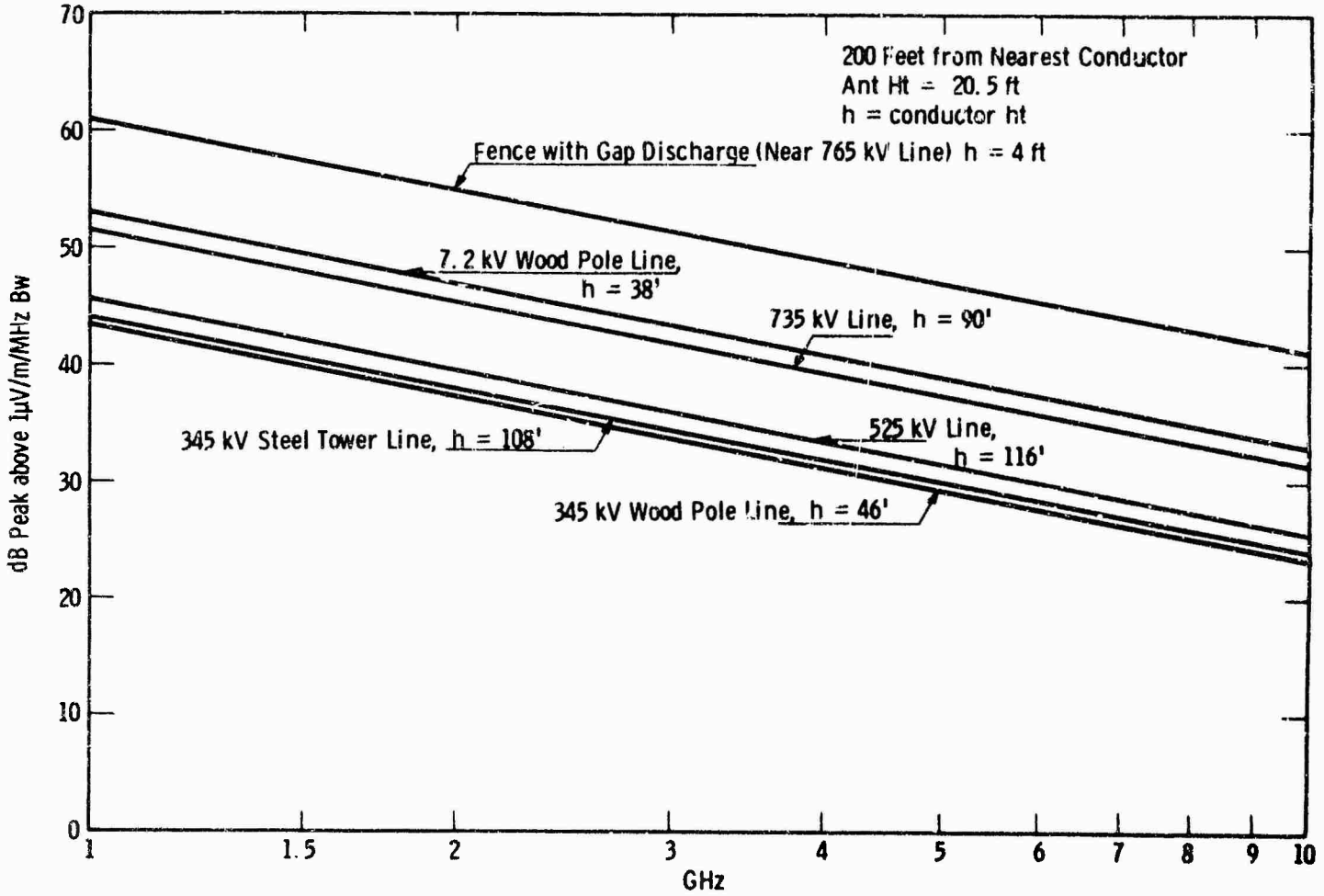


Fig. 60 — Measured radio noise in the 1-10 Ghz range

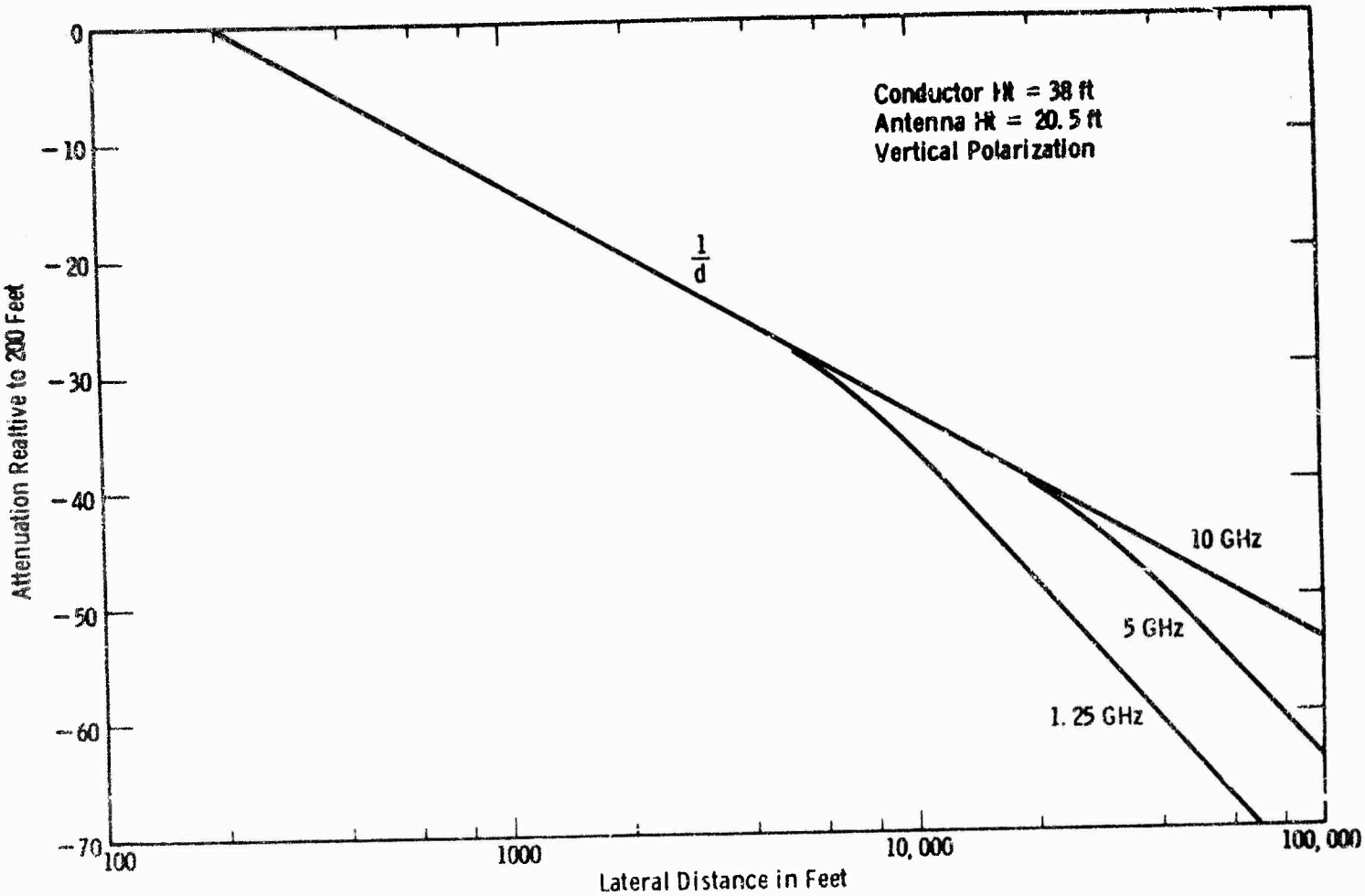


Fig. 61—Lateral attenuation in the 1-10 GHz range

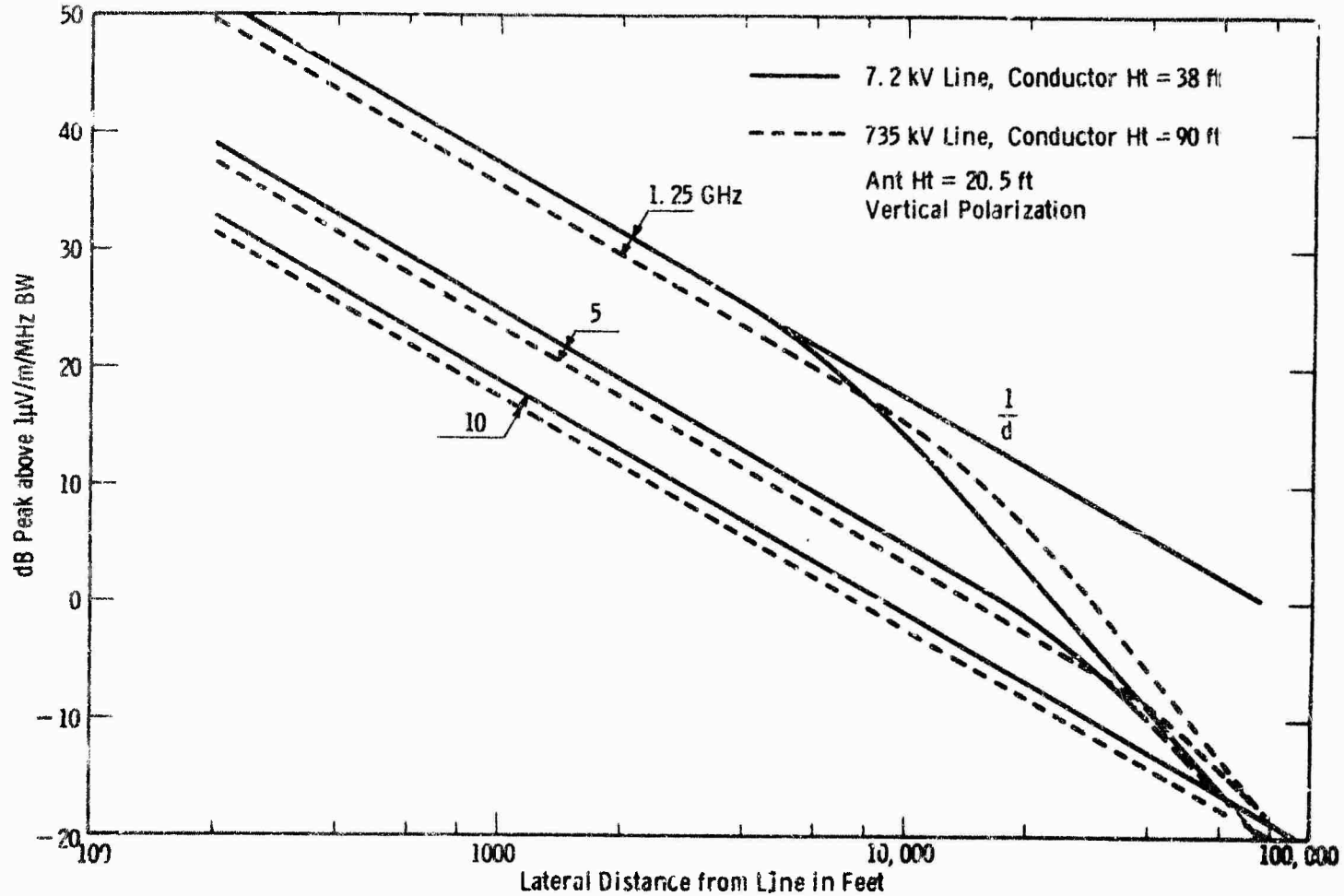


Fig. 62– Predicted power line radio noise in the 1-10 GHz range

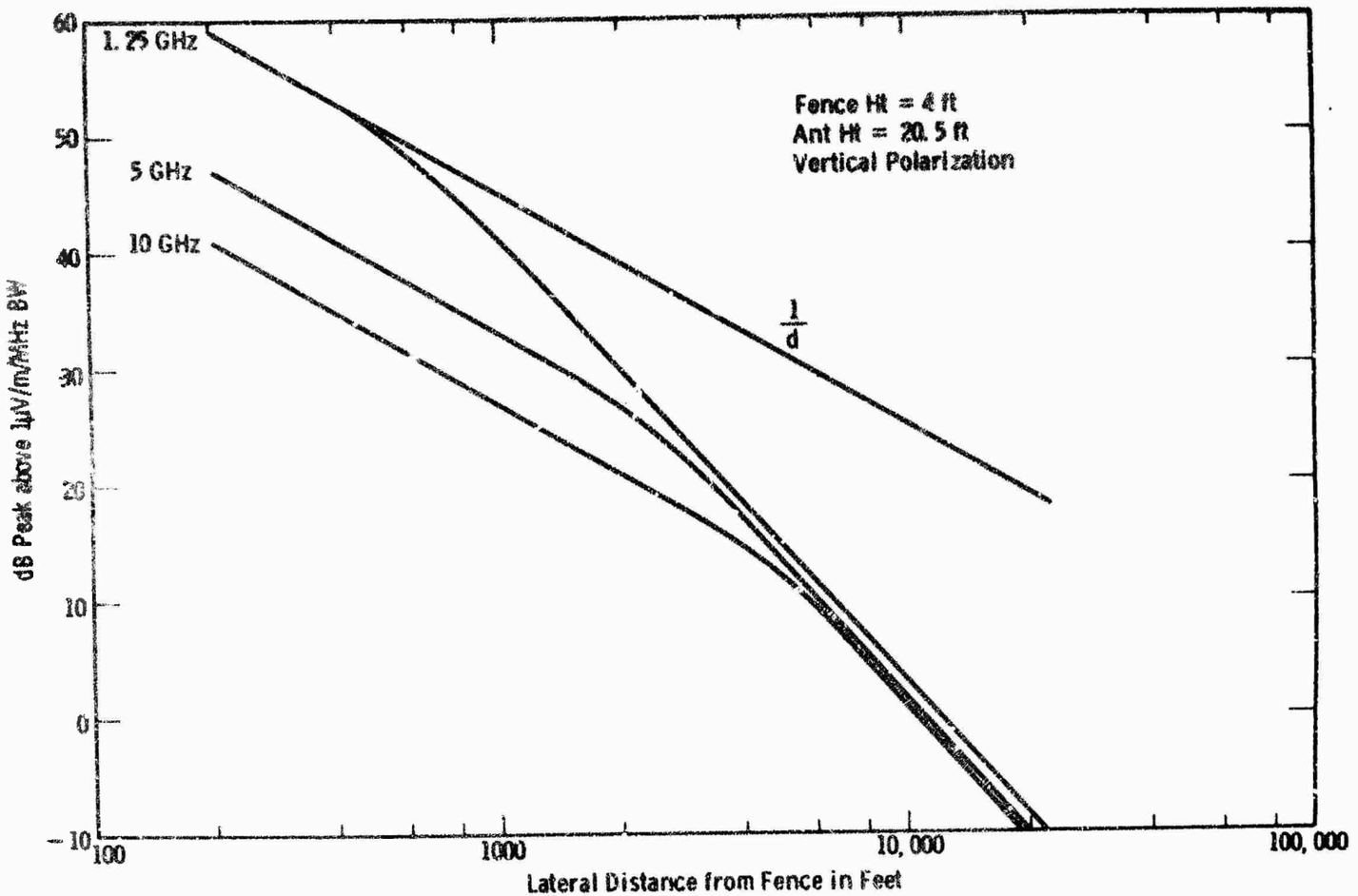


Fig. 63—Predicted radio noise form gap source on fence near 765 kV line

HIGH VOLTAGE POWER LINE SITING CRITERIA

APPENDIX I

MEASUREMENT TECHNIQUES

WESTINGHOUSE ELECTRIC CORPORATION
ELECTRIC UTILITY HEADQUARTERS DEPARTMENT
RESEARCH AND DEVELOPMENT CENTER
PITTSBURGH, PENNSYLVANIA

ROME AIR DEVELOPMENT CENTER
(RADC)
GRIFFISS AIR FORCE BASE
ROME, NEW YORK 13442

CONTRACT AF306(602)-67-C-0171

CONTENTS
APPENDIX I

		Page No.
1.	INTRODUCTION	98
2.	INSTRUMENTS AND ANTENNAS	99
	2.1 Instruments	99
	2.2 Antennas	100
3.	MEASUREMENT PROCEDURE	101
4.	THE RADIO NOISE METER/X-Y RECORDER COMBINATION	101
	4.1 Measurements on EHV Lines with Radio Noise Meter/X-Y Recorder	102
5.	THE SPECTRUM ANALYZER	103
	5.1 Pulse Spectra	103
	5.2 Calibration and Operation of HP Spectrum Analyzer	103
	5.2.1 CW Calibration of HP Spectrum Analyzer	103
	5.2.2 Impulse Calibration of HP Spectrum Analyzer	104
	5.2.3 Correction of Measurements from HP Spectrum Analyzer to dB Pk μV/m/MHz Bandwidth	104
	5.2.4 Operation of the HP Spectrum Analyzer	104
	5.3 Measurement on EHV Lines with Spectrum Analyzers	105
	5.3.1 Frequency Spectra from 345-kV VCDCST-ac Line with 5/16-inch Air Gap, 10 kHz to 1 GHz	105
	5.3.2 Frequency Spectra from 525-kV HC-ac Line with 5/16-inch Air Gap, 10 kHz to 3.5 GHz	105
	5.3.3 Frequency Spectra from 800-kV HC-dc Test Line, 80 MHz to 147 MHz	106
	5.3.4 Frequency Spectra from 500-kV HC-ac Line, 0.27 to 1.87 MHz	106
	5.3.5 Frequency Spectra from 525-kV HC- Line with and without 5/16-inch Air Gap ine De-energized, 0.3 MHz to 2 MHz	106

CONTENTS
APPENDIX I, CONT'D.

		Page No.
5.3.6	Frequency Spectra 800-kV HC-dc Test Line in Fair Weather and Rain, 0.3 to 1.96 MHz	106
5.3.7	Frequency Spectra from 765-kV HCST-ac Test Line	107
5.3.8	Harmonic Measurement near 500-kV HCST-ac Line	107
5.3.9	Radio Station Signal to Line Noise Ratios	108
6.	COMPARISON OF RADIO NOISE METER/X-Y RECORDER AND SPECTRUM ANALYZER QUANTITATIVE MEASUREMENTS	109
7.	CONCLUSIONS.	109

LIST OF FIGURES
APPENDIX I

		Page No.
Fig. 1	Radio Noise Meter/X-Y Plot and Spectrum Analyzer Comparison with Artificial Gap on 345-kV ac Line, 10 - 21 KHz	110
Fig. 2	Radio Noise Meter/X-Y Plot and Spectrum Analyzer Comparison with Artificial Gap on 345-kV ac Line, 20 - 42 KHz.	111
Fig. 3	Radio Noise Meter/X-Y Plot and Spectrum Analyzer Comparison with Artificial Gap on 345-kV ac Line, 40 - 84 KHz.	112
Fig. 4	Radio Noise Meter/X-Y Plot and Spectrum Analyzer Comparison with Artificial Gap on 345-kV ac Line, 80 - 168 KHz.	113
Fig. 5	Radio Noise Meter/X-Y Plot and Spectrum Analyzer Comparison with Artificial Gap on 345-kV ac Line, 0.15 - 3.05 MHz.	114
Fig. 6	Radio Noise Meter/X-Y Plot and Spectrum Analyzer Comparison with Artificial Gap on 345-kV ac Line, 0.29 - 0.59 MHz.	115
Fig. 7	Radio Noise Meter/X-Y Plot and Spectrum Analyzer Comparison with Artificial Gap on 345-kV ac Line, 0.56 - 1.15 MHz.	116
Fig. 8	Radio Noise Meter/X-Y Plot and Spectrum Analyzer Comparison with Artificial Gap on 345-kV ac Line, 1.1 - 2.25 MHz.	117
Fig. 9	Radio Noise Meter/X-Y Plot and Spectrum Analyzer Comparison with Artificial Gap on 345-kV ac Line, 2.1 - 4.3 MHz.	118
Fig. 10	Radio Noise Meter/X-Y Plot and Spectrum Analyzer Comparison with Artificial Gap on 345-kV ac Line, 4.1 - 8.4 MHz.	119
Fig. 11	Radio Noise Meter/X-Y Plot and Spectrum Analyzer Comparison with Artificial Gap on 345-kV ac Line, 8.0 - 16.5 MHz.	120
Fig. 12	Radio Noise Meter/X-Y Plot and Spectrum Analyzer Comparison with Artificial Gap on 345-kV ac Line, 15.5 - 32 MHz.	121

LIST OF FIGURES
APPENDIX I, CONT'D.

		Page No.
Fig. 13	Radio Noise Meter/X-Y Plot and Spectrum Analyzer Comparison with Artificial Gap on 345-kV ac Line, 20 - 33 MHz.	122
Fig. 14	Radio Noise Meter/X-Y Plot and Spectrum Analyzer Comparison with Artificial Gap on 345-kV ac Line, 33 - 54 MHz.	123
Fig. 15	Radio Noise Meter/X-Y Plot and Spectrum Analyzer Comparison with Artificial Gap on 345-kV ac Line, 54 - 88 MHz.	124
Fig. 16	Radio Noise Meter/X-Y Plot and Spectrum Analyzer Comparison with Artificial Gap on 345-kV ac Line, 88 - 145 MHz.	125
Fig. 17	Radio Noise Meter/X-Y Plot and Spectrum Analyzer Comparison with Artificial Gap on 345-kV ac Line, 145 - 240 MHz.	126
Fig. 18	Radio Noise Meter/X-Y Plot and Spectrum Analyzer Comparison with Artificial Gap on 345-kV ac Line, 240 - 400 MHz.	127
Fig. 19	Radio Noise Meter/X-Y Plot and Spectrum Analyzer Comparison with Artificial Gap on 345-kV ac Line, 375 - 610 MHz.	128
Fig. 20	Radio Noise Meter/X-Y Plot and Spectrum Analyzer Comparison with Artificial Gap on 345-kV ac Line, 610 - 1000 MHz.	129
Fig. 21	Radio Noise Meter/X-Y Plot and Spectrum Analyzer Comparisons with Artificial Gap on 345-kV ac Line, 0.01 MHz - 1 GHz.	130
Fig. 22	Radio Noise Meter/X-Y Plot and Spectrum Analyzer Comparisons for Different Lateral Distances from 525-kV ac Line with Artificial Gap, 4.1 - 8.4 MHz.	131
Fig. 23	Radio Noise Meter/X-Y Plot and Spectrum Analyzer Comparison 50 feet from 525-kV ac Line, 1.1 - 2.25 MHz.	132
Fig. 24	Radio Noise Meter/X-Y Plot and Spectrum Analyzer Comparisons 73 feet from Positive Conductor of 800-kV dc Test Line, 1.1 - 2.25 MHz.	133

LIST OF FIGURES
APPENDIX I, CONT'D.

		Page No.
Fig. 25a	Typical Theoretical Spectra of Repeated Rectangular Pulse.	134
Fig. 25b	Typical Spectrum Analyzer Display of Repeated Rectangular Pulse.	134
Fig. 26	CW Response of H.P. 851A/8551A Spectrum Analyzer for Frequencies and Control Settings Tabulated - Sweep Rate.	135
Fig. 27	345-kV ac Frequency Spectra 108 feet from Bottom Conductor with Artificial Gap on and Rain at Same Time (10 kHz to 2 MHz); at Tower.	136
Fig. 28	345-kV ac Frequency Spectra 108 feet from Bottom Conductor with Artificial Gap on and Rain at Same Time (2 MHz to 54 MHz); at Tower.	137
Fig. 29	345-kV ac Frequency Spectra 108 feet from Bottom Conductor with Artificial Gap on and Rain at Same Time (54 MHz to 1 GHz); at Tower.	138
Fig. 30	345-kV ac Frequency Spectra (0.3 to 9.6 MHz) with Artificial Gap (accompanied by Rain Some of the Time); at Tower.	139
Fig. 31	525-kV ac Frequency Spectra 110 feet from Outside Conductor with Artificial Gap (10 kHz to 2.25 MHz); at Tower.	140
Fig. 32	525-kV ac Frequency Spectra 110 feet from Outside Conductor with Artificial Gap (2.1 to 80 MHz); at Tower.	141
Fig. 33	525-kV ac Frequency Spectra 110 feet from Outside Conductor with Artificial Gap (100 MHz to 3.5 GHz); at Tower.	142
Fig. 34	800-kV dc Frequency Spectra (80 to 147 MHz) 69 feet from + conductor; at Tower, in Rain and Fair Weather.	143
Fig. 35	800-kV dc Frequency Spectra (80 to 147 MHz) 69 feet from + Conductor; at Tower in Rain and Fair Weather.	144
Fig. 36	500-kV ac Frequency Spectra (0.27 to 1.87 MHz) in Fair Weather and Heavy Rain at Tower.	145

LIST OF FIGURES
APPENDIX I, CONT'D.

		Page No.
Fig. 37	525-kV ac Frequency Spectra (0.3 to 2 MHz) with and without Artificial Gap and De-energized; at Tower.	146
Fig. 38	800-kV dc Frequency Spectra (0.3 to 1.96 MHz) in Fair Weather and Rain; at Tower.	147
Fig. 39	Frequency Spectra 59 feet from Outside Phase of Line "C" at Mid-span, Apple Grove 765-kV ac Test Line.	148
Fig. 40	Harmonic Spectra with Radio Noise Meter and Spectrum Analyzer 400 feet from 500-kV ac Line.	149

APPENDIX I

MEASUREMENT TECHNIQUES

1. INTRODUCTION

In the previous contract on High Voltage Power Line Siting Criteria (RADC-TR-66-606 March 1967) manual measurements of radio noise were made at discrete frequencies. This technique has deficiencies in that it is very time consuming to measure the variations of radio noise throughout certain frequency ranges and short duration changes in radio noise level cannot be observed simultaneously over a wide frequency range.

This present contract requires radio noise measurements on power lines from 60 Hz to 10 GHz. In order to reduce time and improve the quality of measurements, spectrum analyzers and X-Y recording techniques with radio noise meters were investigated for the measurement of power line radio noise. Comparisons were made with the usual manual readings taken at the same time from radio noise meters and these were used as the standard measurement. Conductor corona in the rain and fair weather and gap type sources were measured. In addition laboratory measurements of corona, gap sources and pulse generators were performed with the spectrum analyzer. Measurements were correlated between the spectrum analyzer and X-Y recorder/radio noise meter methods over the frequency range 10 kHz to 1 GHz. Some measurements were tried from 1 GHz to 10 GHz with the spectrum analyzer and TWT pre-amplifiers but due to overload problems these were not considered reliable. Power line harmonics were recorded with one spectrum analyzer unit in the range of 60 Hz to 650 Hz. Straightforward use of an X-Y recorder with a radio noise meter is a step forward over manual readings from a speed of measurement and resolution viewpoint. Line transients, lightning, etc., are not too troublesome since an X-Y plot of any particular frequency band can be quickly repeated. Only quasi-peak readings could be taken but these are easily corrected to peak. Susceptibility to overload and spurious responses can be a drawback to the use of spectrum analyzers if they have wide open inputs, also drift on the frequency axis can be encountered and picture taking of low noise values in the presence of high CW signals requires approximation. The use of a tuned input is desirable; however, with electronic tuning spurious response may still be a problem. Therefore, it is suggested that passive band-pass filters be used, each filter for at least one octave pass-band. Repeated checking of the frequency axis with a signal generator overcomes the drift problems. In the case of the analyzer used for measuring power line harmonics overload from the high intensity 60 Hz field has to be avoided.

Very good agreement was found between the semi-automatic and manual methods of measurement. Data can, for instance, be recorded quickly by the spectrum analyzer over a wide frequency range compared to many hours that would be required for manual measurements. Better resolution and more accurate information can be obtained especially when short duration weather changes occur which change the radio noise level.

2. INSTRUMENTS AND ANTENNAS

2.1 Instruments

New instrumentation (compared to RADC TR-66-606 March 1967) consists of spectrum analyzers and the use of an X-Y recorder with the radio noise meters. In most cases the radio noise meters cover the same frequency range as the spectrum analyzers. The instruments used are listed below.

Frequency Range	Name	Manufacturer
60 - 15,000 Hz (60 Hz to 1 MHz capability)	Spectrum Analyzer Plug in Unit 1 L5 with storage oscilloscope 549	Tektronix
60 - 15,000 Hz	NM40 Field Intensity Meter	Stoddart Electro Systems
10 kHz - 250 kHz	NM12T Field Intensity Meter	Stoddart Electro Systems
150 kHz - 25 MHz	NM20B Field Intensity Meter	Stoddart Electro Systems
150 kHz - 32 MHz	NM22A Field Intensity Meter	Stoddart Electro Systems
20 MHz - 400 MHz	NM30A Field Intensity Meter	Stoddart Electro Systems
375 MHz - 1000 MHz	NM52A Field Intensity Meter	Stoddart Electro Systems
10 kHz - 1000 MHz	X-Y Recorder	Moseley
10 MHz - 10 GHz (Capability to 40 GHz)	Spectrum Analyzer 851A/8551A	Hewlett Packard
10 kHz - 10 MHz	Up-Converter K15-8551B	Hewlett-Packard
10 kHz - 100 MHz (1 kHz to 150 Hz capability)	Broadband Pre-Amplifier 461A	Hewlett-Packard
30 MHz - 300 MHz	AP-501R Low Noise Tunable Pre-Amplifier	Electro-International Inc.
300 MHz to 1000 MHz	AP-502R Low Noise Pre-Amplifier	Electro-International Inc.

Frequency Range	Name	Manufacturer
20 Hz - 1000 MHz	Spectrum Analyzer consisting of interference analyzers, Models EMC25 and EMC10 and Display Module SPD-125	Fairchild Electrometrics Corp.
1 GHz - 2 GHz	Travelling Wave Tube Pre-Amplifier WJ268	Watkins-Johnson Co.
2 GHz - 4 GHz	Travelling Wave Tube Pre-Amplifier WJ269	Watkins-Johnson Co.
4 GHz - 8 GHz	Travelling Wave Tube Pre-Amplifier WJ271	Watkins-Johnson Co.
8 GHz - 12 GHz	Travelling Wave Tube Pre-Amplifier WJ276	Watkins-Johnson Co.
85 kHz - 40 MHz	Signal Generator Model 22D	Ferris
2 MHz - 400 MHz	Signal Generator Model 80	Measurement Corp.
300 MHz - 1 GHz	Signal Generator Model 84 TV	Measurement Corp.
10 kHz - 1 GHz	1G - 11S Impulse Generator	Empire Devices Inc.

2.2 Antennas

The antennas used were as follows:

Frequency Range	Name	Manufacturer
60 Hz - 15,000 Hz	Electric Probe	Stoddart Electro Systems
10 kHz - 250 kHz	2 Meter Vertical Rod (with Antenna Coupler for NM12T)	Stoddart Electro Systems
150 kHz - 32 MHz	1 Meter Vertical Rod (with Antenna Coupler for NM22A)	Stoddart Electro Systems
20 MHz - 88 MHz	Dipole Tuned to 60 MHz	Stoddart Electro Systems

Frequency Range	Name	Manufacturer
88 MHz - 350 MHz	BCA-902 Bi-Conical	Electro International Inc.
375 MHz - 1000 MHz	BCA-901 Bi-Triangle	Electro International Inc.
1 GHz - 2 GHz	Microwave Horn Antenna "L" Band	Polarad
2 GHz - 4 GHz	Microwave Horn Antenna "S" Band	Polarad
4 GHz - 7 GHz	Microwave Parabolic Antenna "M" Band	Polarad
7 GHz - 10 GHz	Microwave Parabolic Antenna "X" Band	Polarad

3. MEASUREMENT PROCEDURE

The following is a brief description of the general measurement procedure. Details, calibrations etc. will be found under other headings in this appendix.

To check the accuracy of the automatic instruments, manual measurements with the NM20C were compared with the X-Y recorder plots from the NM22A and the spectrum analyzer pictures from the Hewlett Packard spectrum analyzer. There was good agreement in all these data. Starting with the NM12T on band (1) an X-Y record would be run of line noise together with meter ambient and calibration curves. Then the antenna system would be switched to the spectrum analyzer (HP 851A/8551A) operating with its up converter (K15-8551B) and a picture taken of the CRT display of line noise. The analyzer would be arranged to be as near as possible the same bandwidth and frequency range as the NM12T on band (1). All control settings of the analyzer were recorded and the frequency axis and sine wave response checked. Checks were continually made for analyzer overload and spurious responses and records made identifying the X-Y record with the spectrum analyzer picture. This procedure was followed from 10 kHz to 1 GHz except that the up converter was not used beyond 10 MHz. X-Y records were made to 1 GHz. Above 1 GHz some spectrum analyzer pictures were taken for comparison with the manual results from the Polarad microwave receivers but they were not considered reliable due to overloading of the spectrum analyzer.

4. THE RADIO NOISE METER/X-Y RECORDER COMBINATION

It is a simple matter to speed up the usual manual readings taken with the Stoddart radio noise meters by the addition of an X-Y recorder.

The procedure for each frequency band is to ensure that the recorded vertical axis is linear in decibels and run meter calibration and ambient curves with the frequency axis spread the width of the recorder paper. It is best to use the meter calibration value for the low frequency end of each band throughout that band so that for any particular frequency the calibration is known and recorded and corrections can be made if necessary. The meters with X-Y recorder output connections have quite constant gain-frequency characteristics. With manual tuning about one minute is required to obtain an accurate recording of noise. Faster recording can result in lost information, such as not obtaining the actual maximum values. Listening with headphones enables radio stations etc. to be identified and marked on the recorder paper. Only field intensity and quasi-peak values of noise can be plotted readily but peak values may be marked on the paper at desired frequencies by stopping the run and measuring the peak value manually. Care may be necessary to prevent inaccuracies due to physical contact with the instrumentation.

4.1 Measurements on EHV Lines with Radio Noise Meter/X-Y Recorder

The spectra recorded from 10 kHz to 1 GHz, 50 feet from a 345-kV ac line with artificial gap are shown in Figs. 1 to 20. They are further illustrated in Fig. 21 but this time corrected to dB peak above 1 μV/m/Mhz bandwidth. The low frequencies 10 kHz to 2 MHz were recorded in heavy to light rain while the remaining spectra were taken when the rain had ended. Figures 9, 10, and 11 show clearly a dominant feature of these spectra of quite sharp peaks evenly spaced at approximately 378 kHz intervals. This apparent resonant frequency gives a half wavelength of 1300 feet which may be due to the distance between towers (about 600 feet). Details such as this resonance are easily spotted using X-Y recorder techniques but are harder to notice taking manual readings. Figure 22 shows a very similar resonance recorded at different distances laterally from a 525-kV ac line with artificial gap. The frequency is 417 kHz and half wavelength, 1175 feet. The distance between towers being 1462 feet. This is a good example of the complex spectra encountered. The attenuation with distance (d) from Fig. 22 can be seen to be on an average proportional to 1/d, i.e. from 200 feet to 400 feet the average level of the spectrum falls by 6 dB.

In Fig. 23, spectra 1 to 2.25 MHz from a 525-kV ac line some peak readings are marked. These are 4 to 5 dB higher than the quasi-peak values of noise and about 1 dB higher for the AM station measurements. These peak to quasi-peak differences are typical of those over a wide frequency range. Figure 24 was recorded near an 800-kV, dc test line and the peak values shown are about 12 dB higher than the quasi-peak, which could be due to a lower pulse repetition rate from the corona compared to ac corona. The higher the pulse repetition rate the closer the quasi-peak value approaches the peak. Also on Fig. 24 a resonance may be observed of approximately an interval of 39 kHz and a full wavelength of 4.78 miles which agrees well with the actual length of the test line of 4.9 miles.

All the figures mentioned also have superimposed upon them a spectrum analyzer picture taken at the same time as the X-Y plot. These pictures and comparisons are discussed later.

5. THE SPECTRUM ANALYZER

5.1 Pulse Spectra

Fourier analysis of a periodic rectangular pulse yields a spectrum of $\frac{\sin \pi x}{x}$ where x = T/Tr and T = the pulse width and Tr the pulse repetition rate, see Fig. 25a. The first zero in the frequency spectrum occurs at a frequency $f = \frac{1}{T}$ e.g. a 1 μsec wide pulse will exhibit a first zero at 1 MHz; the harmonics would be at intervals of $fr = \frac{1}{Tr}$, e.g. a pulse repeated 60 times a second would have a spectrum with 60 Hz between the harmonics. In Fig. 25b it is seen that the spectral lines each below as well as above the baseline which corresponds to the harmonics in the pulse being 180° out of phase with the fundamental. The spectrum analyzer can detect amplitude only and not phase therefore all the spectral lines will be displayed above the baseline as in Fig. 25b. If we amplitude modulate an RF carrier with a pulse waveform we get essentially the same $\frac{\sin \pi x}{x}$ spectrum.

When considering spark gaps on power lines generating exponential pulses with two time constants one must bear in mind that these gaps fire several times each half cycle of the ac voltage. Thus we have the situation of bursts of pulses at a repetition rate of 120 pulses per second for single phase. However, it is likely that one pulse out of each burst has a larger magnitude than the rest and the spectrum measured is from the largest repeated pulse although in the GHz region some of the smaller pulses may dominate if they have smaller widths than the large pulse.

Laboratory measurements were made prior to field measurements to become familiar with the operation of the spectrum analyzer and confirm the theoretical spectra from pulses. A rectangular pulse will give a spectrum falling off at 6 dB per octave with increasing frequency while a triangular pulse would fall 12 dB per octave. This was confirmed in the measurements.

5.2 Calibration and Operation of HP Spectrum Analyzer

In order to convert the radio noise measurements to dB Pk above 1 μV/m/MHz bandwidth, both CW and impulse calibrations of the spectrum analyzer were required.

5.2.1 CW Calibration of HP Spectrum Analyzer

With the frequencies and spectrum analyzer control settings used, a convenient CW input level to read on the CRT display was 50 μVrms (37 dB Pk). This level was used for calibrations from 10 kHz to 1 GHz and up to 25 MHz a calibrated thermocouple and microammeter was used for measuring the signal generator output. At higher frequencies an RF voltmeter was employed. In this way calibration of the spectrum analyzer in dB Pk μVCW was achieved, e.g. measuring from the CRT baseline; if a 37 dB Pk μV CW signal reads 40 dB, then 3 dB would be subtracted from the reading; etc.

Sweep rate is an important consideration for calibration purposes. If the local oscillator sweeps through at a high rate the IF amplifier will not have time to reach its full amplitude before the input is gone; e.g. a change in sweep rate from 3 msec per cm to 30 msec per cm can result in a change in displayed signal of 10 dB. See Fig. 26.

5.2.2 Impulse Calibration of HP Spectrum Analyzer

Impulse bandwidth could not be measured using conventional impulse calibrators because of analyzer front end overload. Filters tried in front of the analyzer would not prevent overload. Hewlett-Packard suggested producing an impulse signal of accurately known spectral intensity by using a CW signal generator and a PIN modulator (HP series 8730) built into an HP 8403 Modulator. With this apparatus, J. Scherer of RADC measured the following impulse bandwidths for a HP 8551A spectrum analyzer:

3 dB Bandwidth	Impulse Bandwidth
3 kHz	6.7 kHz
10 kHz	19.66 kHz
100 kHz	166.34 kHz
1 MHz	1.59 MHz (Extrapolated)

The MHz bandwidth correction is easily obtained from the above values e.g. for 6.7 kHz impulse bandwidth the correction is 43.5 dB.

5.2.3 Correction of Measurements from HP Spectrum Analyzer to dB Pk μV/m/MHz Bandwidth

The correction of the radio noise values displayed on the spectrum analyzer to dB Pk μV/m/MHz bandwidth is easily carried out once the CW and impulse calibration are known. First, a correction is found from Fig. 26 for CW response at the frequency control settings, and sweep rate used. Then the impulse bandwidth correction is added and lastly the antenna correction factor. If additional broadband pre-amplifiers are used, then their gain when used in conjunction with the spectrum analyzer would be subtracted.

5.2.4 Operation of the HP Spectrum Analyzer

In order to avoid damage to the input attenuator of the spectrum analyzer converter unit, care was taken to measure the rms value of input voltage with a sensitive HP voltmeter. The input power across the 50 ohm input must be kept below 1/4 watt. The attenuator and gain controls on the converter and analyzer were adjusted so that a 10 dB change in converter attenuator setting, for example, would give a 10 dB change in displayed spectrum. This ensured the input amplifier was not overdriven. Frequency accuracy was checked by feeding in a signal from a standard signal generator. Adjustment of the converter and analyzer tuning controls was required until an accuracy of about 2% to 4% was achieved up to a frequency of 100 MHz, with the VHF oscillator in the converter set at 184 MHz. Measurements were made

using the same antennas and couplers and octave bands as the radio noise meters with X-Y plots. On each band the center frequency on the analyzer display would be ch ed with a signal generator.

It should be emphasized that care must be exercised throughout the spectrum analyzer measurements to ensure that measured signals or noise are from the source and not spurious responses due to analyzer overload. This may be checked by observing the displayed spectra when the input attenuator is increased by 10 dB. If the whole display reduces by 10 dB then measurements are from the source; if some displayed signals do not change in amplitude then these are spurious responses generated internally within the analyzer. The settings of input attenuation, gain controls, sweep rate, IF bandwidth, spectrum width, film exposure time, etc. were recorded for each frequency band over which measurements were made. Typical analyzer settings, antennas, etc. used throughout the frequency spectrum are listed in the table on Fig. 26. Initially the graticule of the analyzer CRT was superimposed upon the pictures taken by means of a flashlight which resulted in a bright area that can be seen on some of the pictures. Later an ultraviolet light was used to illuminate the graticule and much better pictures resulted.

5.3 Measurements on EHV Lines with Spectrum Analyzers

5.3.1 Frequency Spectra from 345-kV VCDCST-ac Line with 5/16-inch Air Gap, 10 kHz to 1 GHz

Figures 27 to 29 cover twenty pictures taken 50 feet laterally from the bottom conductor of the above line. They are of approximately the same octave bands as the radio noise meters. All the pictures in Fig. 27 were taken with heavy to light rain falling. For the rest of the pictures no rain occurred. Picture 55 on Fig. 28 illustrates the 378 kHz resonance noticed in the X-Y records. Picture 62, Fig. 2& shows stations beneath the air gap noise, taken by reducing the CRT brightness so that the stations just appeared then taking a picture of these with many sweeps; increasing the brightness to show the noise; clipping the stations and re-exposing the film. Picture 68, Fig. 29 illustrates the difficulty of picture taking when station amplitudes are similar to noise amplitudes because the CW signal gives such a bright display on the CRT compared to the radio noise. Figure 30 shows the spectrum for 0.3 to 9.6 MHz for comparison of radio noise magnitudes with other lines; such as shown in Figs. 36, 37 and 38.

5.3.2 Frequency Spectra from 525-kV HC-ac Line with 5/16-inch Air Gap, 10 kHz to 3.5 GHz

Figures 31 to 33 cover twenty pictures taken 50 feet laterally from the outside conductor of the above line. Most of the bands measured are of a similar frequency range of those from the 345-kV line. Pictures 289, 294 and 299B on Fig. 22 show the 417 kHz resonance noticed in the X-Y records. Picture 269, Fig. 32 shows some large spikes at 2.3 MHz intervals which gives a half wavelength of 214 feet which may be a function of the tower and guy configuration. These spikes appeared on X-Y records as well. Pictures

280 and 281, Fig. 33 cover the frequency range 2.5 to 3.5 GHz and were taken with (280) and without (281) the appropriate TWT pre-amplifier. Only about 10 dB gain resulted with the pre-amplifier used instead of 24 dB, the capability of the amplifier.

5.3.3 Frequency Spectra from 800-kV HC-dc Test Line, 80 MHz to 147 MHz

Figures 34 and 35 illustrate 35 pictures taken 50 feet laterally from the positive conductor at tower of the above line during intermittent rain. The first picture is with no input to the analyzer and just displays the internal noise. Subsequent pictures of line or insulator noise were taken at five minute intervals. This interesting sequence of pictures indicates generally very low noise values during periods of rain; increasing in value after the rain has stopped, especially when sunny and windy; then reducing to zero value. At these high frequencies this noise is thought to be from the line insulators (glass) on the tower drying after rain. Lending weight to this argument is the possible resonant effect seen in some pictures, picture 140 for example. This gives a frequency of 6.7 MHz and half wavelengths of 73.5 feet which is very comparable with the conductor height at the tower of 70 feet. Results of this nature would be impossible to obtain manually and difficult with radio noise meter X-Y recorder techniques. The advantage of the analyzer is its wide spectral coverage on one picture and of one being able to see the spectra before taking the picture. The antenna was covered with polyethylene to prevent precipitation static.

5.3.4 Frequency Spectra from 500-kV HC-ac Line, 0.27 to 1.87 MHz

Figure 36 shows mainly the spectra 50 feet laterally from the outside phase of the above line in fair weather and heavy rain; clearly indicating about a 24 dB increase in corona noise level in the rain.

5.3.5 Frequency Spectra from 525-kV HC-ac Line with and without 5/16-inch Air Gap and Line De-energized, 0.3 MHz to 2 MHz

Figure 37 illustrates the above spectra taken 50 feet laterally from the outside conductor. No increase in noise level is noticed with the air gap on the line. This indicates that the fair weather corona noise from this line is equal to, or greater than, the gap noise in this frequency range. This was confirmed by manual measurements.

5.3.6 Frequency Spectra 800-kV HC-dc Test Line in Fair Weather and Rain, 0.3 to 1.96 MHz

Figure 38 shows some interesting spectra. The noise from fair weather corona is higher than that in the rain which is characteristic of dc lines and different from ac lines. In fair weather at these frequencies the peak readings are about 12 dB higher than quasi-peak while in rain the difference is usually about 5 dB (observed from manual readings). Thus in rain it is likely that

many corona pulses of low amplitude exist while in fair weather fewer pulses of higher amplitude is the case.

Near EHV dc lines precipitation static can be a problem. Raindrops passing near the energized conductor acquire a charge and discharge upon hitting the antenna. This is not observed near ac lines. To prevent raindrops hitting the antenna, the antenna was covered with about a 4-inch diameter polyethylene tube. In Fig. 38 the spectrum due to precipitation static can be clearly seen but also the corona noise level shows up well on the same picture. This is another virtue of the spectrum analyzer use where pulses of different repetition rates and different amplitudes may be displayed together.

Similar to the X-Y records the full wave resonant frequency (approximately 39 kHz) of this 4.9 mile long dc test line is seen. If the noise level for a long dc transmission line is to be derived from this short test line it is likely that the geometric mean of the resonant peaks should be taken; similar to the case of the 765-kV ac Apple Grove[1] test line.

5.3.7 Frequency Spectra from 765-kV HCST-ac Test Line

The spectra from the above line is shown in Fig. 39, clearly indicating the full wave resonant frequency (approximately 400 kHz) of this short test line. A multiple of this "natural" frequency is observed at 1.83 MHz. These peak values agree well with manual quasi-peak radio noise meter readings taken in the past[1] except for the absence of a sharp spike at the resonance frequency.

An opportunity arose to record a portion of the same spectra measured with the Hewlett Packard spectrum analyzer with a Fairchild spectrum analyzer. Similar bandwidths, sweep rate etc. were used and the same antenna system. A tracing of the Fairchild spectrum analyzer picture is displayed on Fig. 39. The picture is small but details are sharp and clear. The spectra seen on both analyzers are quite similar from a shape and signal to noise viewpoint. The Fairchild instrument consists of interference Analyzer Model EMC25 and spectrum display Module, Model SPD125. It covers the frequency band 14 kHz to 1000 MHz; can be used manually as a battery operated radio noise meter or combined with an X-Y recorder to read peak values or used as a spectrum analyzer with built-in pre-selection over 15 octave frequency ranges. It has features such as a remote control of antenna coupler bands and "bright up" and expansion of any region of displayed spectra which may be of specific interest. It was not possible to get a detailed evaluation of this instrument.

5.3.8 Harmonic Measurement near 500-kV HCST-ac Line

A few harmonic measurements were made with the Tektronix plug-in spectrum analyzer unit 1L5 in conjunction with a Tektronix 549 storage oscilloscope. The site at which readings were made was 400 feet from the

above line. Initially a Stoddart NM40A radio noise meter with electric probe was used to measure the harmonic values seen on Fig. 40, high readings for the even harmonics are observed and these are discussed in Sec. 5.8 of the main report. Next, the Tektronix spectrum analyzer was used with the electric probe. Different sensitivities were used, see Fig. 40, and it is seen that with high sensitivity 0.01 V/cm, false readings occur (compare with NM40A readings) due to the high value 60 Hz field overloading the analyzer. With lower sensitivity 0.05 V/cm the spectrum analyzer display is similar to the NM40A readings, but then some harmonics barely show above the internal noise level of the instrument. The difference between the 60 Hz and 120 Hz measurement is seen in the picture with 0.2 V/cm sensitivity, Fig. 40. This spectrum analyzer unit would be ideal for harmonic measurement if the 60 Hz field is reduced or filtered out.

5.3.9 Radio Station Signal to Line Noise Ratios

Peak radio station signal to line noise ratios compare well, i.e. Fig. 23 in the 1 to 2 MHz region near a 525-kV ac line using both radio noise meter X-Y plots and the Hewlett-Packard spectrum analyzer; S/N ratios of 15 to 20 dB result; with the radio noise meter measuring a few dB less than the analyzer which is to be expected from an impulse bandwidth consideration i.e., Stoddart NM22A, 10.24 kHz impulse bandwidth and the Hewlett-Packard 8551A spectrum analyzer 6.7 kHz (when the 3 dB, 3 kHz bandwidth is used). In the case of the 800-kV dc line, Fig. 24, the radio noise meter indicates a S/N ratio of about 23 dB while the spectrum analyzer gives around 40 dB. The apparent large difference being possibly due to the few large pulses per second from dc line corona, (evident usually in fair weather but on this occasion also in rain), which were measured manually with the radio noise meter but not on the spectrum analyzer probably because of too rapid picture taking; about 1 second exposure.

6. COMPARISON OF RADIO NOISE METER/X-Y RECORDER AND SPECTRUM ANALYZER QUANTITATIVE MEASUREMENTS

The X-Y recorder plots, taken 50 feet from the 345-kV VC-DC line with the artificial gap on the lower phase, corrected to dB Pk. above 1 μV/m/MHz bandwidth are shown on Fig. 21. Values are in the range expected from previous measurements i.e., Fig. 71 RADC TR 66-606 March 1967, measurements at 200 feet. Similarly corrected results from the Hewlett-Packard spectrum analyzer are also illustrated in Fig. 21. These are within 6 to 10 dB of the X-Y plots throughout the spectrum measured (0.01 MHz to 1 GHz) and in the 2 to 10 MHz region the peaks and valleys in the spectrum compare closely. Most of the time the spectrum analyzer corrected readings are higher than those of the radio noise meter which may be possibly due to an error in impulse bandwidth (impulse bandwidth values were taken from another identical model spectrum analyzer) or the analyzer reading a higher peak value than the radio noise meter. Also there may be errors in the 400 MHz to 1 GHz region since the 1 MHz bandwidth was used on the analyzer and this is not recommended in the log mode since the response of the log shaping network is not fast enough. However, with such good agreement

above line. Initially a Stoddart NM40A radio noise meter with electric probe was used to measure the harmonic values seen on Fig. 40, high readings for the even harmonics are observed and these are discussed in Sec. 5.8 of the main report. Next, the Tektronix spectrum analyzer was used with the electric probe. Different sensitivities were used, see Fig. 40, and it is seen that with high sensitivity 0.01 V/cm, false readings occur (compare with NM40A readings) due to the high value 60 Hz field overloading the analyzer. With lower sensitivity 0.05 V/cm the spectrum analyzer display is similar to the NM40A readings, but then some harmonics barely show above the internal noise level of the instrument. The difference between the 60 Hz and 120 Hz measurement is seen in the picture with 0.2 V/cm sensitivity, Fig. 40. This spectrum analyzer unit would be ideal for harmonic measurement if the 60 Hz field is reduced or filtered out.

5.3.9 Radio Station Signal to Line Noise Ratios

Peak radio station signal to line noise ratios compare well, i.e. Fig. 23 in the 1 to 2 MHz region near a 525-kV ac line using both radio noise meter X-Y plots and the Hewlett-Packard spectrum analyzer; S/N ratios of 15 to 20 dB result; with the radio noise meter measuring a few dB less than the analyzer which is to be expected from an impulse bandwidth consideration i.e., Stoddart NM22A, 10.24 kHz impulse bandwidth and the Hewlett-Packard 8551A spectrum analyzer 6.7 kHz (when the 3 dB, 3 kHz bandwidth is used). In the case of the 800-kV dc line, Fig. 24, the radio noise meter indicates a S/N ratio of about 23 dB while the spectrum analyzer gives around 40 dB. The apparent large difference being possibly due to the few large pulses per second from dc line corona, (evident usually in fair weather but on this occasion also in rain), which were measured manually with the radio noise meter but not on the spectrum analyzer probably because of too rapid picture taking; about 1 second exposure.

6. COMPARISON OF RADIO NOISE METER/X-Y RECORDER AND SPECTRUM ANALYZER QUANTITATIVE MEASUREMENTS

The X-Y recorder plots, taken 50 feet from the 345-kV VC-DC line with the artificial gap on the lower phase, corrected to dB Pk. above 1 μV/m/MHz bandwidth are shown on Fig. 21. Values are in the range expected from previous measurements i.e., Fig. 71 RADC TR 66-606 March 1967, measurements at 200 feet. Similarly corrected results from the Hewlett-Packard spectrum analyzer are also illustrated in Fig. 21. These are within 6 to 10 dB of the X-Y plots throughout the spectrum measured (0.01 MHz to 1 GHz) and in the 2 to 10 MHz region the peaks and valleys in the spectrum compare closely. Most of the time the spectrum analyzer corrected readings are higher than those of the radio noise meter which may be possibly due to an error in impulse bandwidth (impulse bandwidth values were taken from another identical model spectrum analyzer) or the analyzer reading a higher peak value than the radio noise meter. Also there may be errors in the 400 MHz to 1 GHz region since the 1 MHz bandwidth was used on the analyzer and this is not recommended in the log mode since the response of the log shaping network is not fast enough. However, with such good agreement

between the corrected radio noise meter and spectrum analyzer values throughout the spectrum it would appear that quantitative measurements of radio noise may be made with the spectrum analyzer as long as calibrations are accurately made, appropriate correction factors used and overload conditions avoided.

7. CONCLUSIONS

7.1 Field strength measurements can be made in the frequency range 60 Hz to 1 GHz from high voltage power lines with both the radio noise meter/X-Y recorder combinations and with the spectrum analyzers. With selective input and linear pre-amplifications this instrumentation will be adequate up to 10 GHz.

7.2 The X-Y plots give better resolution in practice than the Hewlett-Packard spectrum analyzer when displaying relatively large frequency ranges, and more positive identification of radio and TV stations etc. with the use of headphones. The Hewlett-Packard analyzer with preselection to avoid overload has the advantages of displaying simultaneously the different magnitude of different repetition rate pulses; of synchronizing with the 60 Hz field from the three-phase power line and indicating the interference value from each phase on a single display. Also the revealing of stations or other sources buried beneath noise and the recording of short duration changes in interference level.

7.3 The best results, when using the HP analyzer with the converter, start at about 60 kHz.

7.4 In the power line harmonic region measurements can be conveniently made with the Tektronix plug-in unit 1L5 and storage oscilloscope 549. For best results, a means of attenuation of the high value 60 Hz field would be required.

7.5 Ideally, to obtain quick, accurate, good resolution measurements of radio interference from power lines a combination of manual, X-Y plots, and spectrum analyzer techniques is required. The spectrum analyzer chiefly for speed and resolution; X-Y techniques for resolution and station identification; and manual radio noise meter measurements for checks at particular frequencies.

REFERENCES

1. "Apple Grove 750-kV Project - 515-kV Radio Influence and Corona Loss Investigations," E. R. Taylor, W. E. Pakala, and N. Kolcio, IEEE Transactions Paper 31 TP 65-150 presented at IEEE Winter Power Meeting, January 1965.

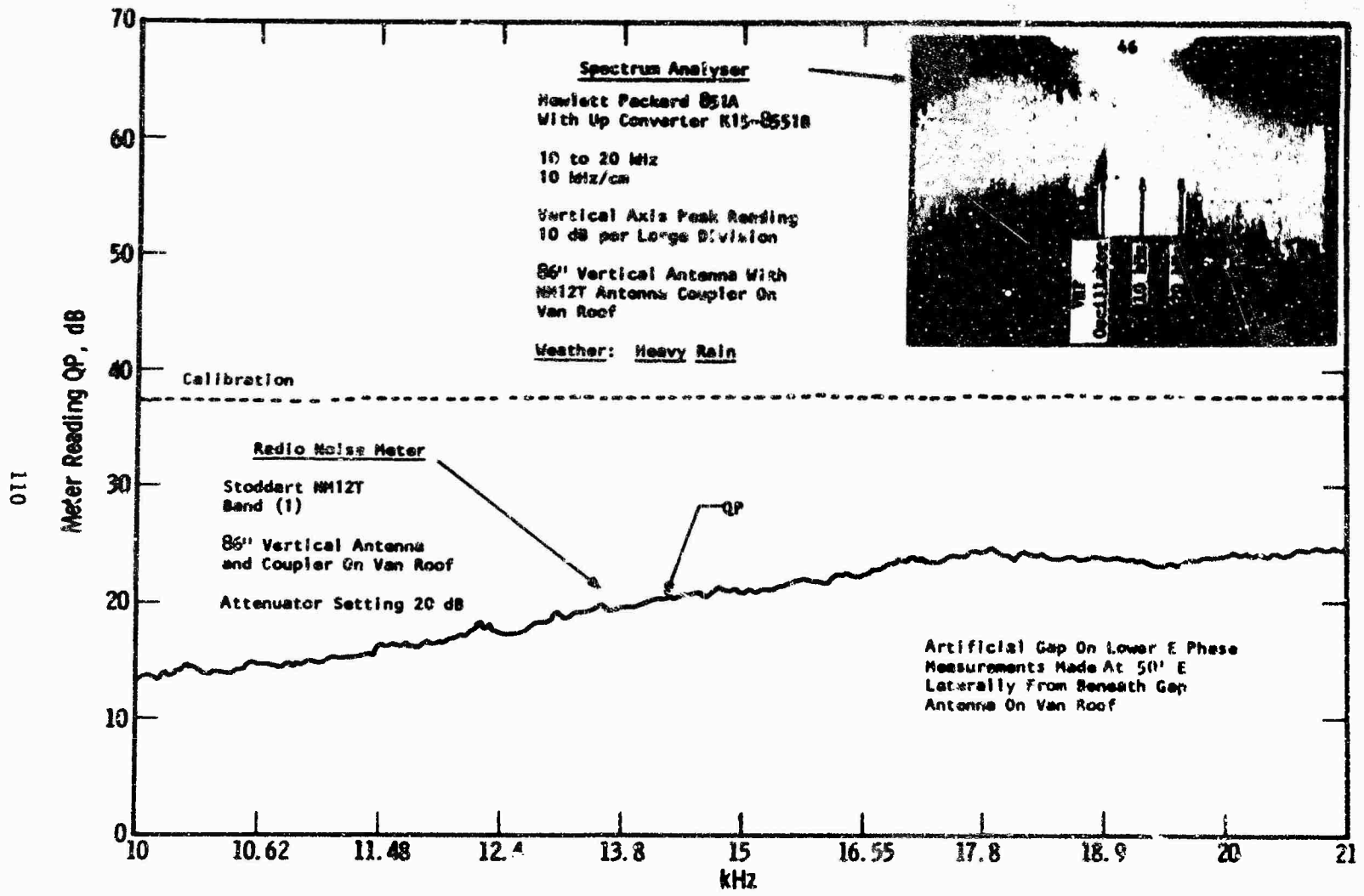


Fig. 1 —Radio noise meter/X-Y plot and spectrum analyser comparison with artificial gap on 345 kV AC line

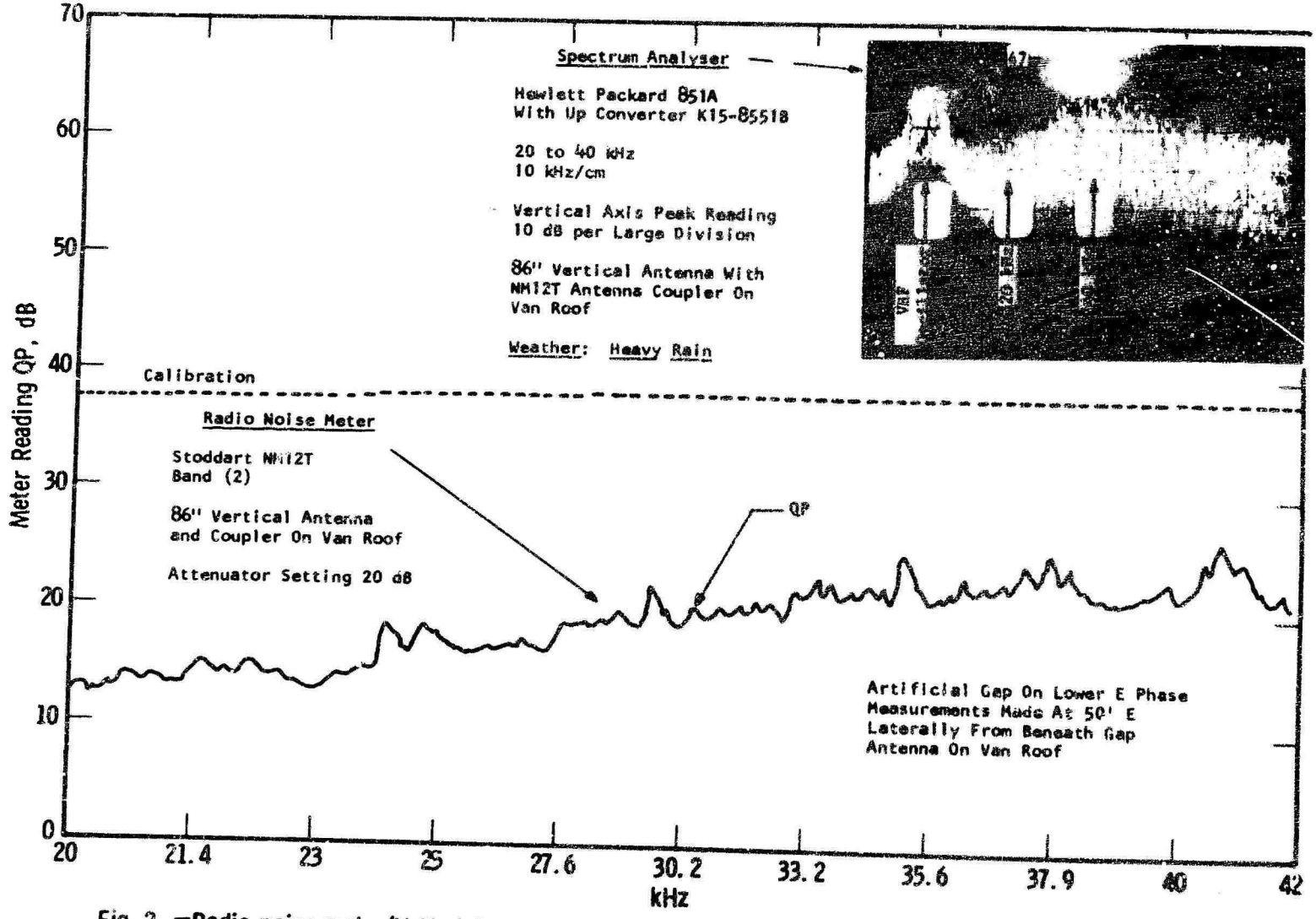


Fig. 2 —Radio noise meter/X-Y plot and spectrum analyser comparison with artificial gap on 345 kV AC line

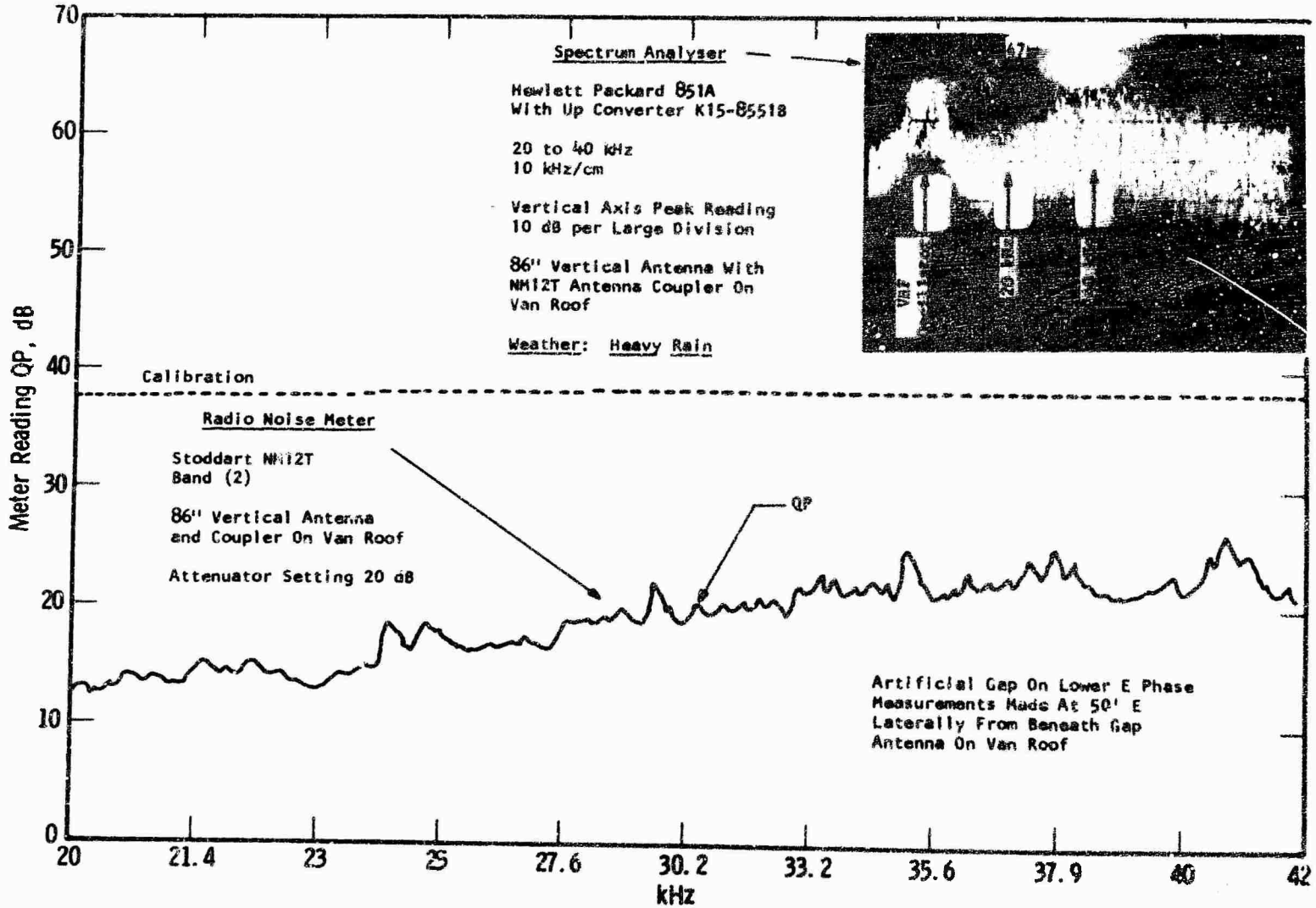


Fig. 2 —Radio noise meter/X-Y plot and spectrum analyser comparison with artificial gap on 345 kV AC line

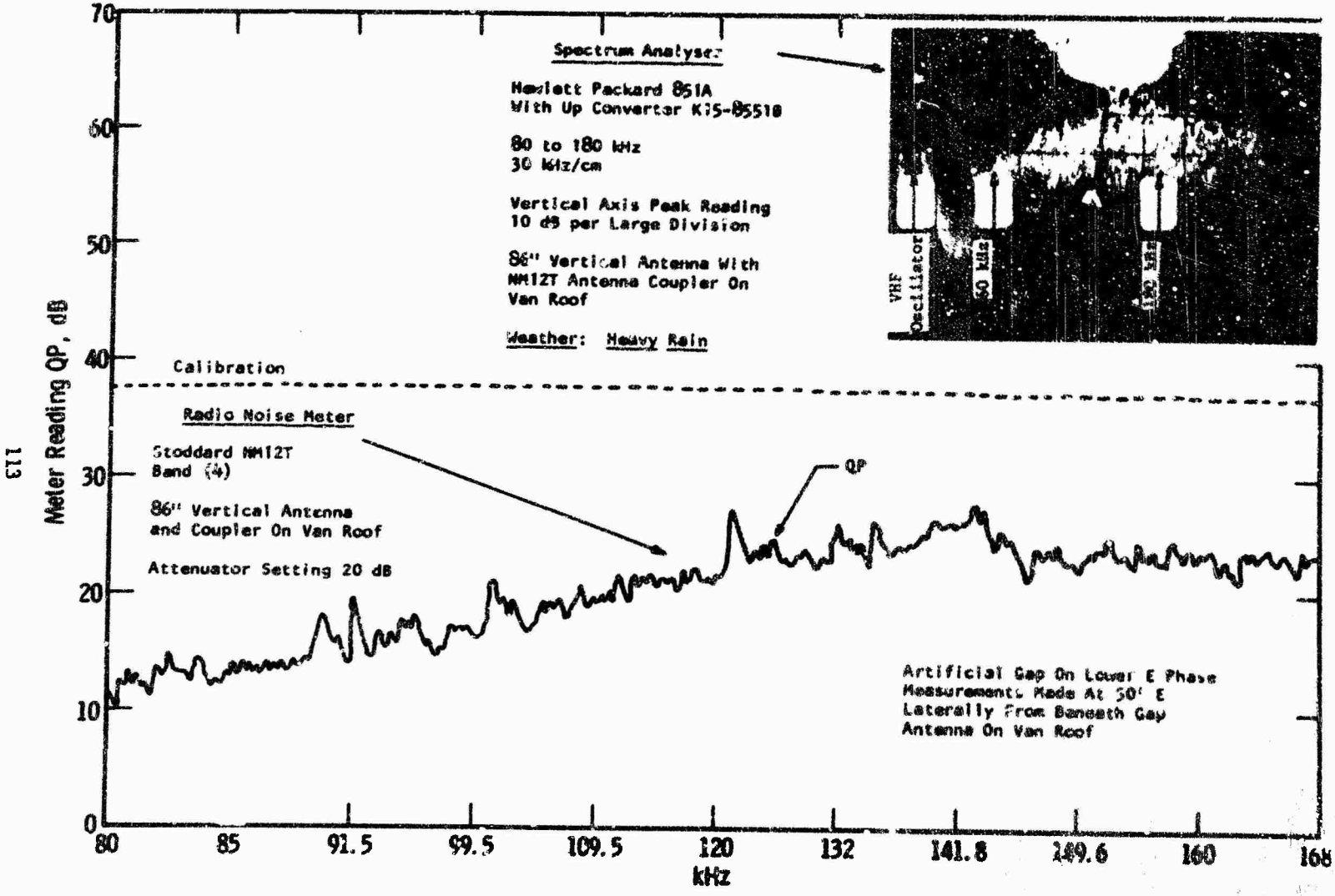


Fig. 1 —Radio noise meter/X-Y plot and spectrum analyser comparison with artificial gap on 345 kV AC line

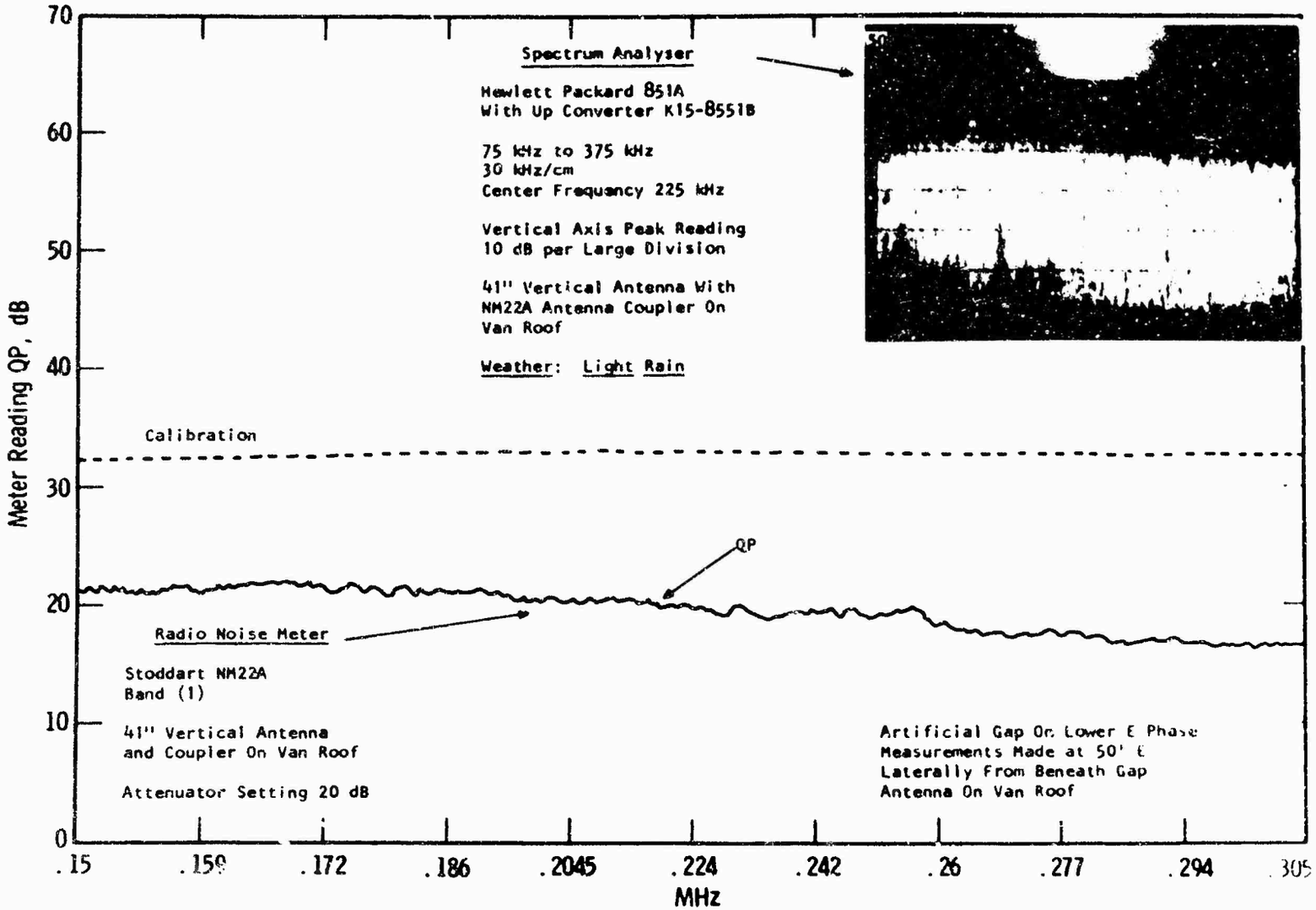


Fig. 5 —Radio noise meter/X-Y plot and spectrum analyser comparison with artificial gap on 345 kV AC line

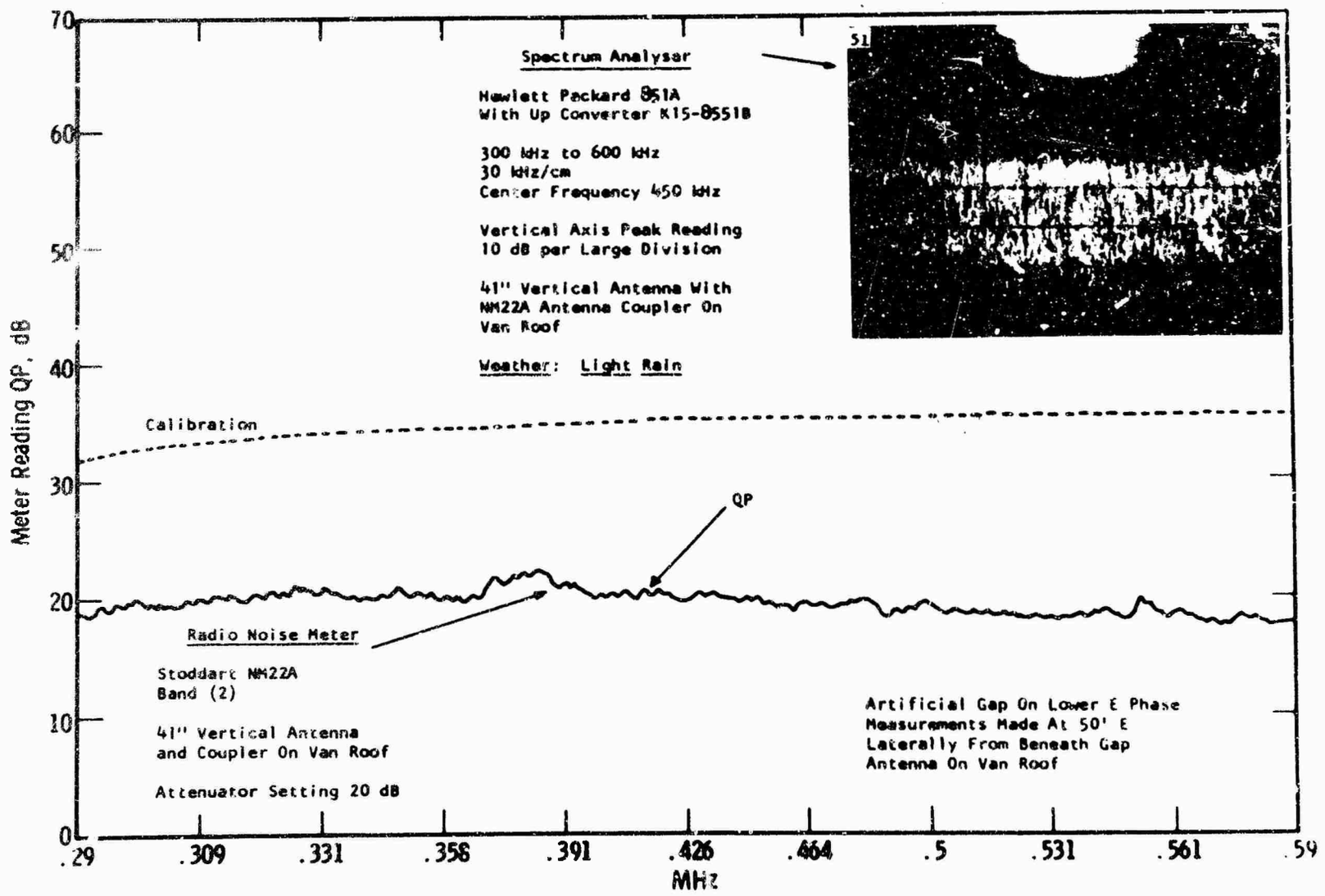


Fig. 6 —Radio noise meter/X-Y plot and spectrum analyser comparison with artificial gap on 345 kV AC line

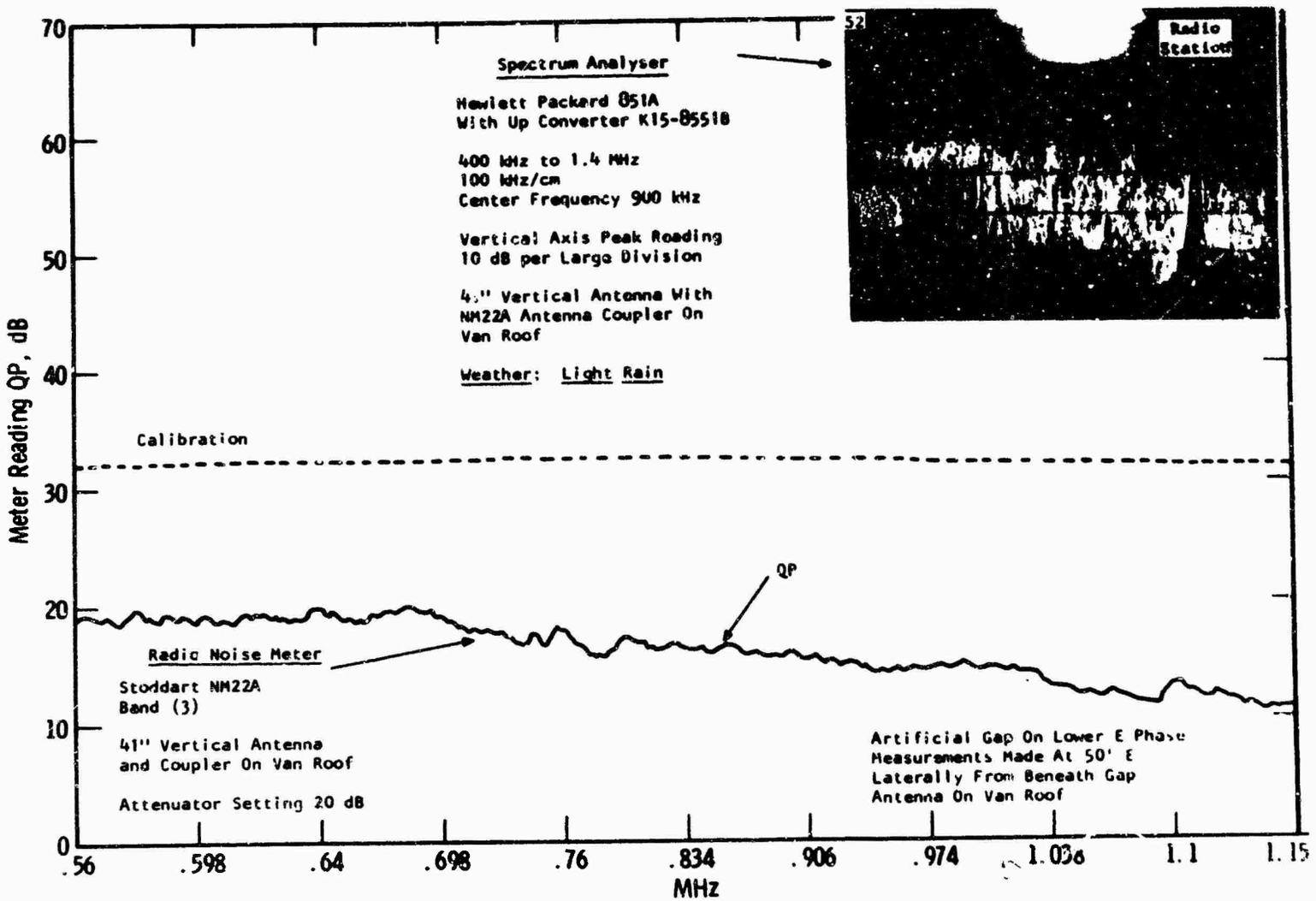


Fig. 7 —Radio noise meter/X-Y plot and spectrum analyser comparison with artificial gap on 345 kV AC line

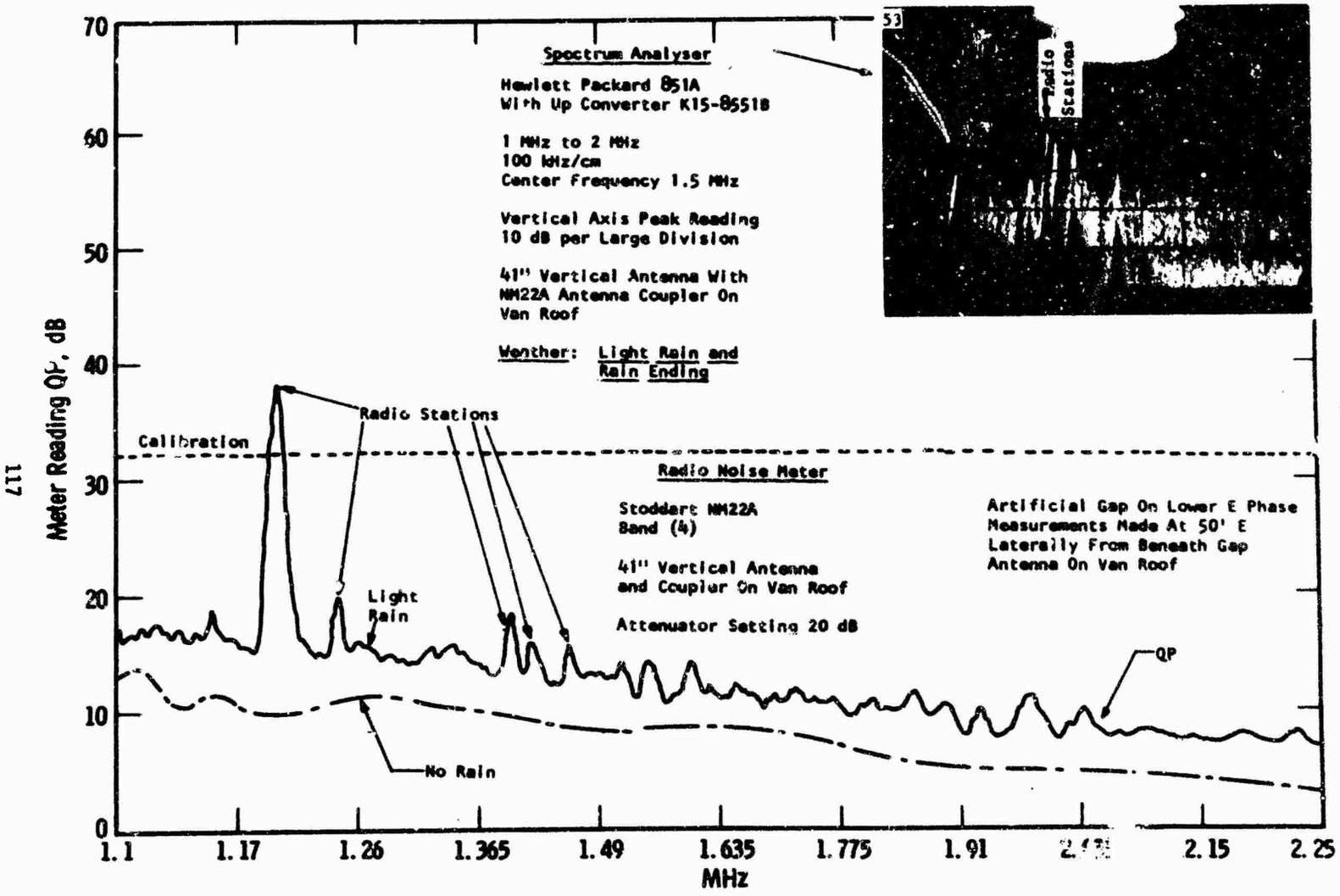


Fig. 8 —Radio noise meter/X-Y plot and spectrum analyser comparison with artificial gap on 345 kV AC line

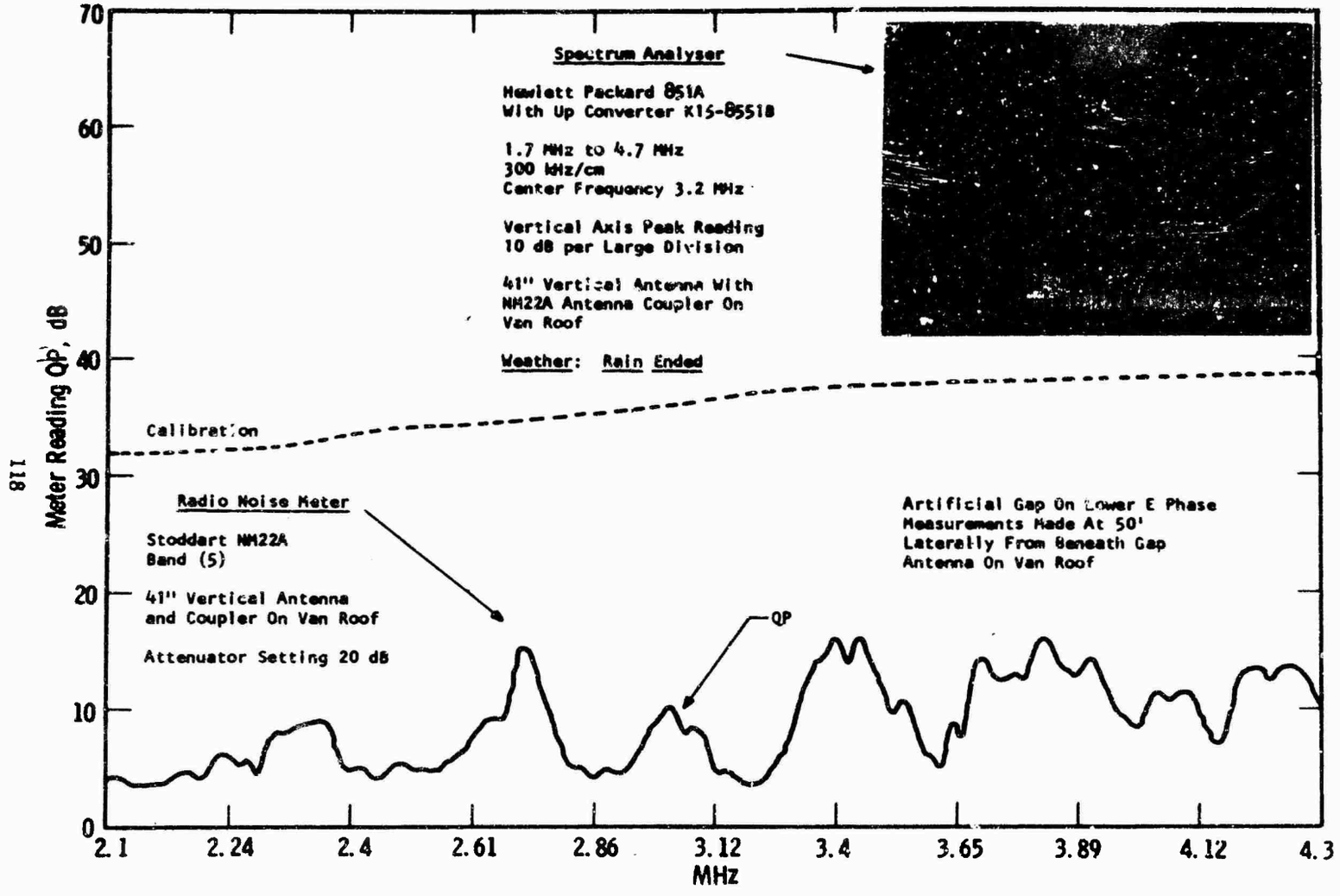


Fig. 9 —Radio noise meter/X-Y plot and spectrum analyser comparison with artificial gap on 345 kV AC line

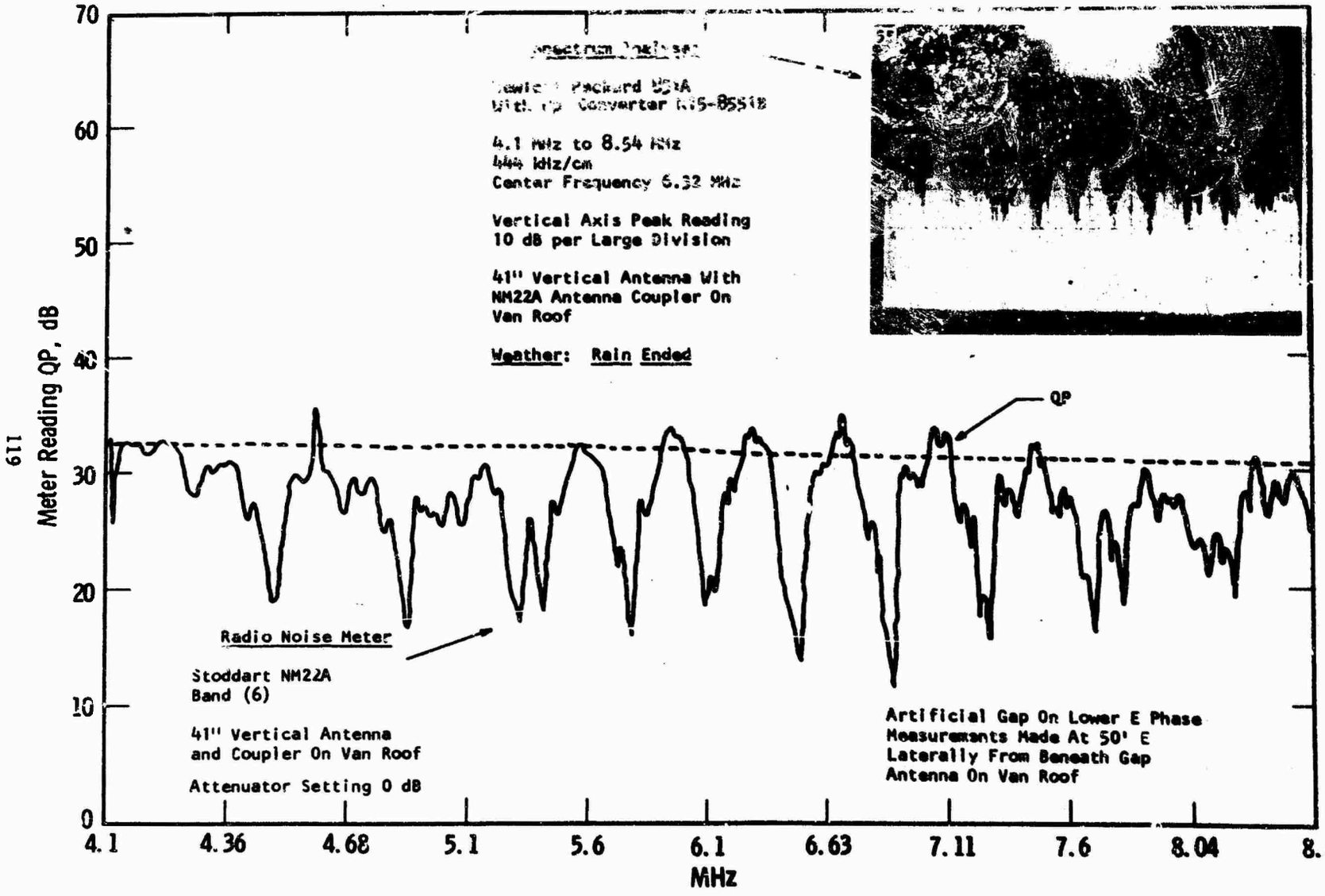


Fig. 10—Radio noise meter/X-Y plot and spectrum analyser comparison with artificial gap on 345 kV AC line

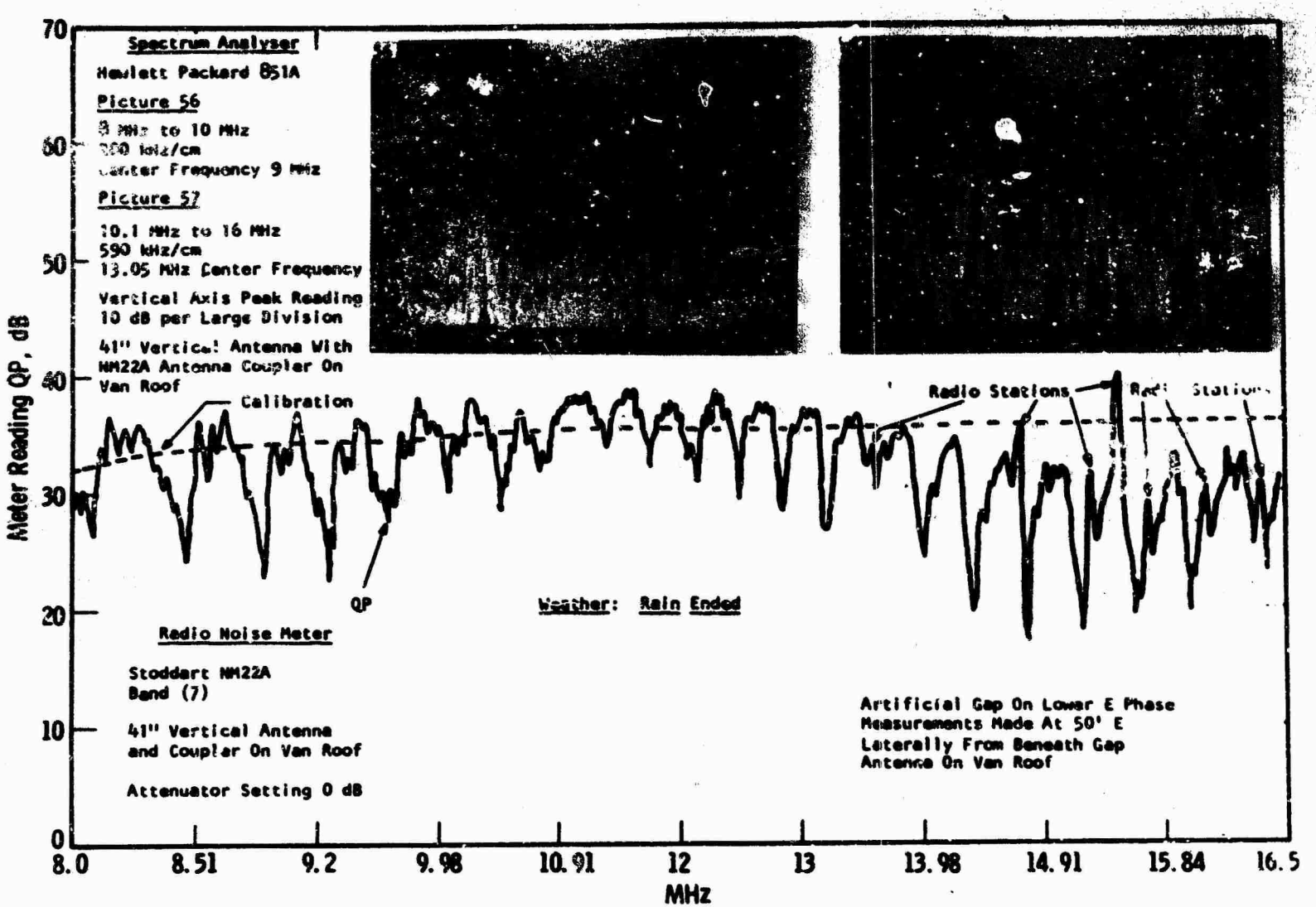


Fig. 11 —Radio noise meter/X-Y plot and spectrum analyser comparison with artificial gap on 345 kV AC line

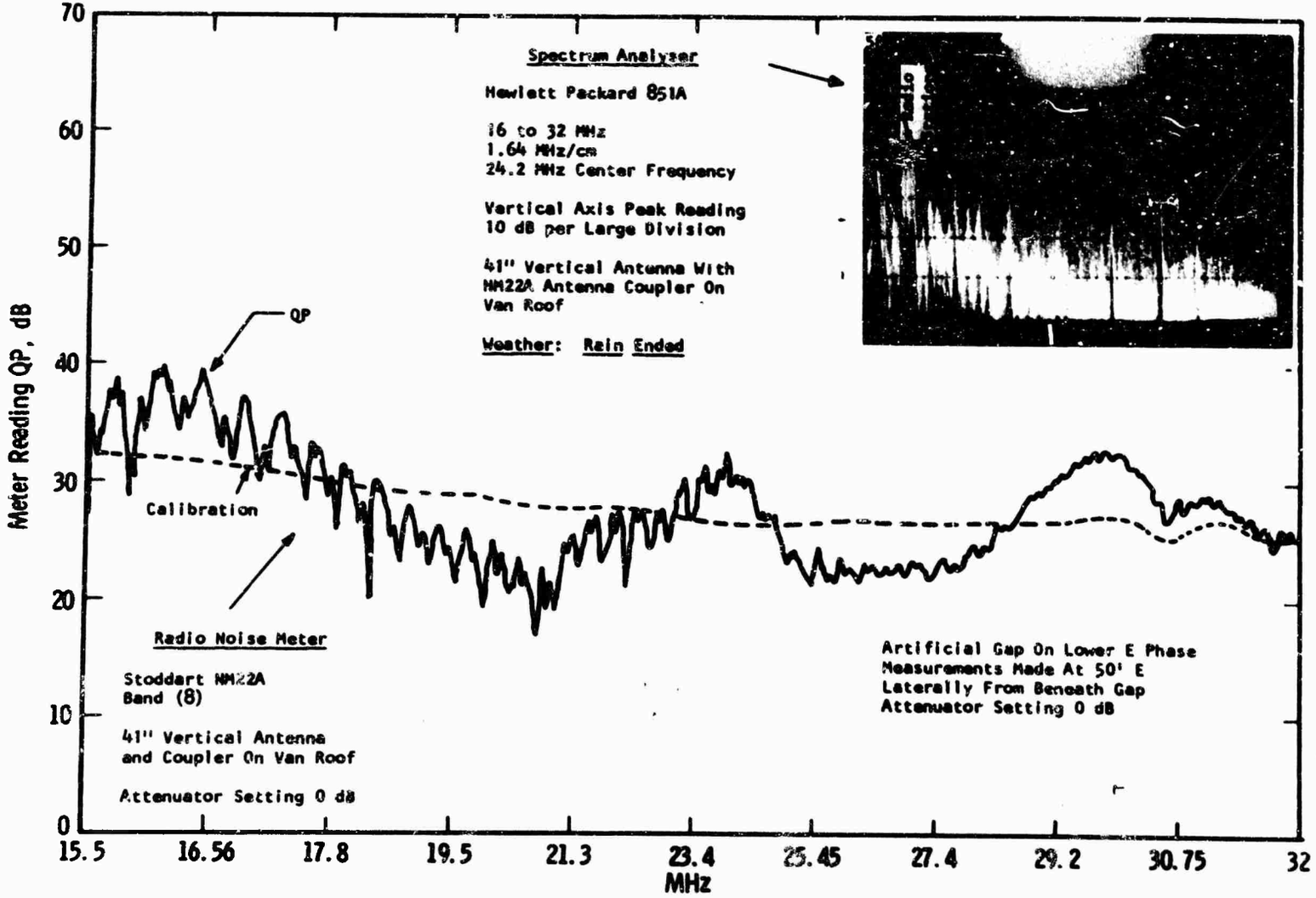


Fig. 12—Radio noise meter/X-Y plot and spectrum analyser comparison with artificial gap on 345 kV AC line

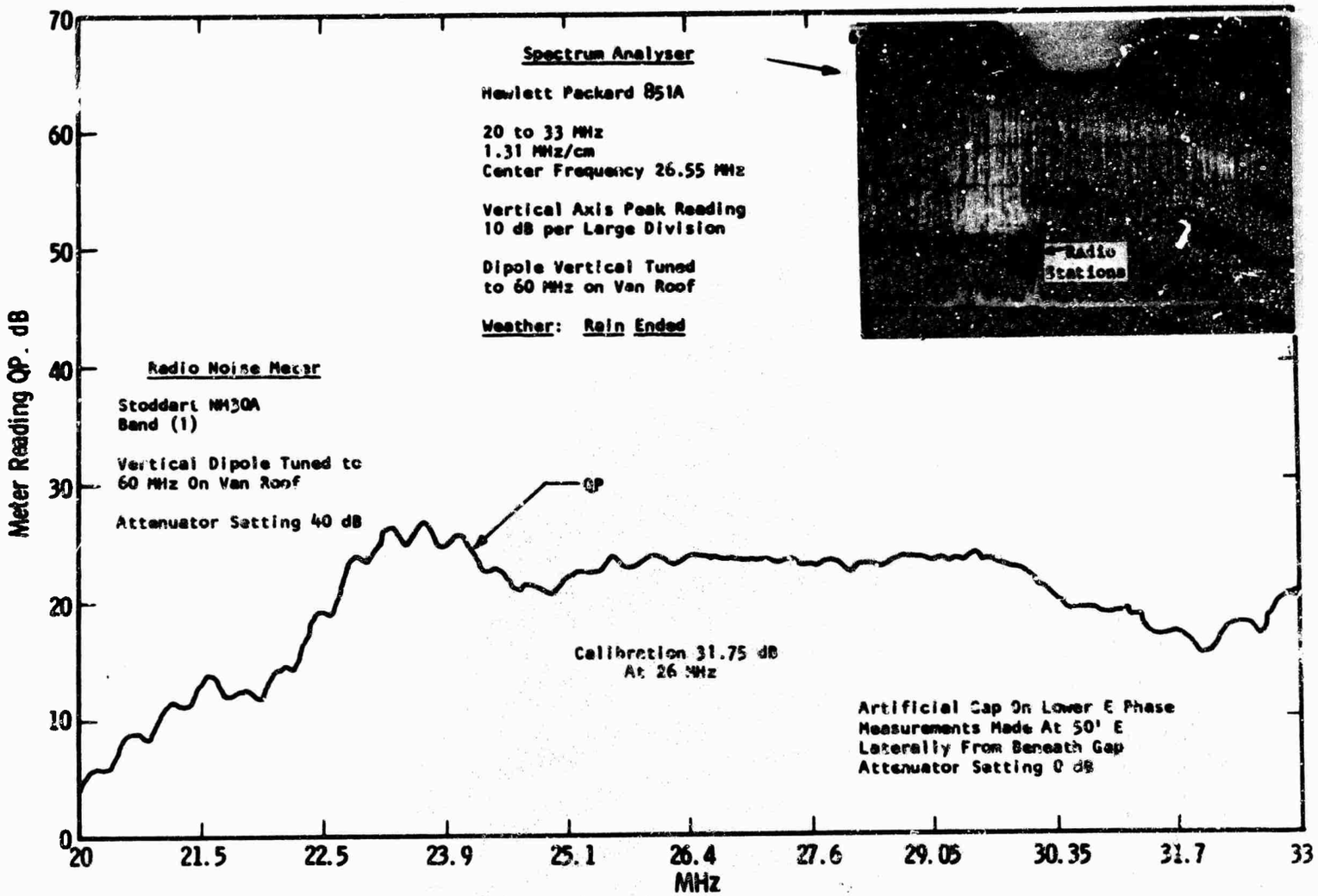


Fig. 13 – Radio noise meter/X-Y plot and spectrum analyser comparison with artificial gap on 345 kV AC line

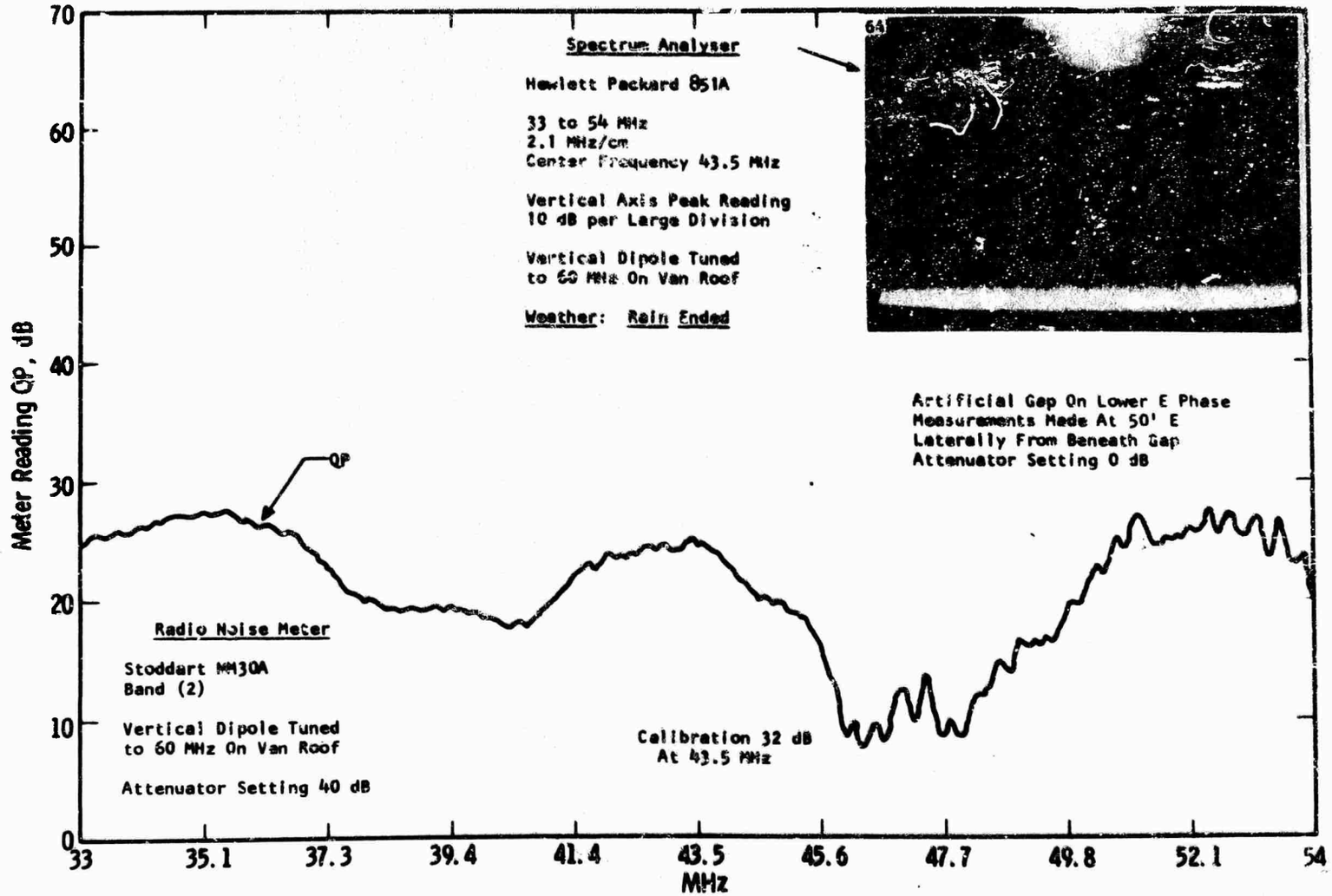


Fig. 14 —Radio noise meter/X-Y plot and spectrum analyser comparison with artificial gap on 345 kV AC line

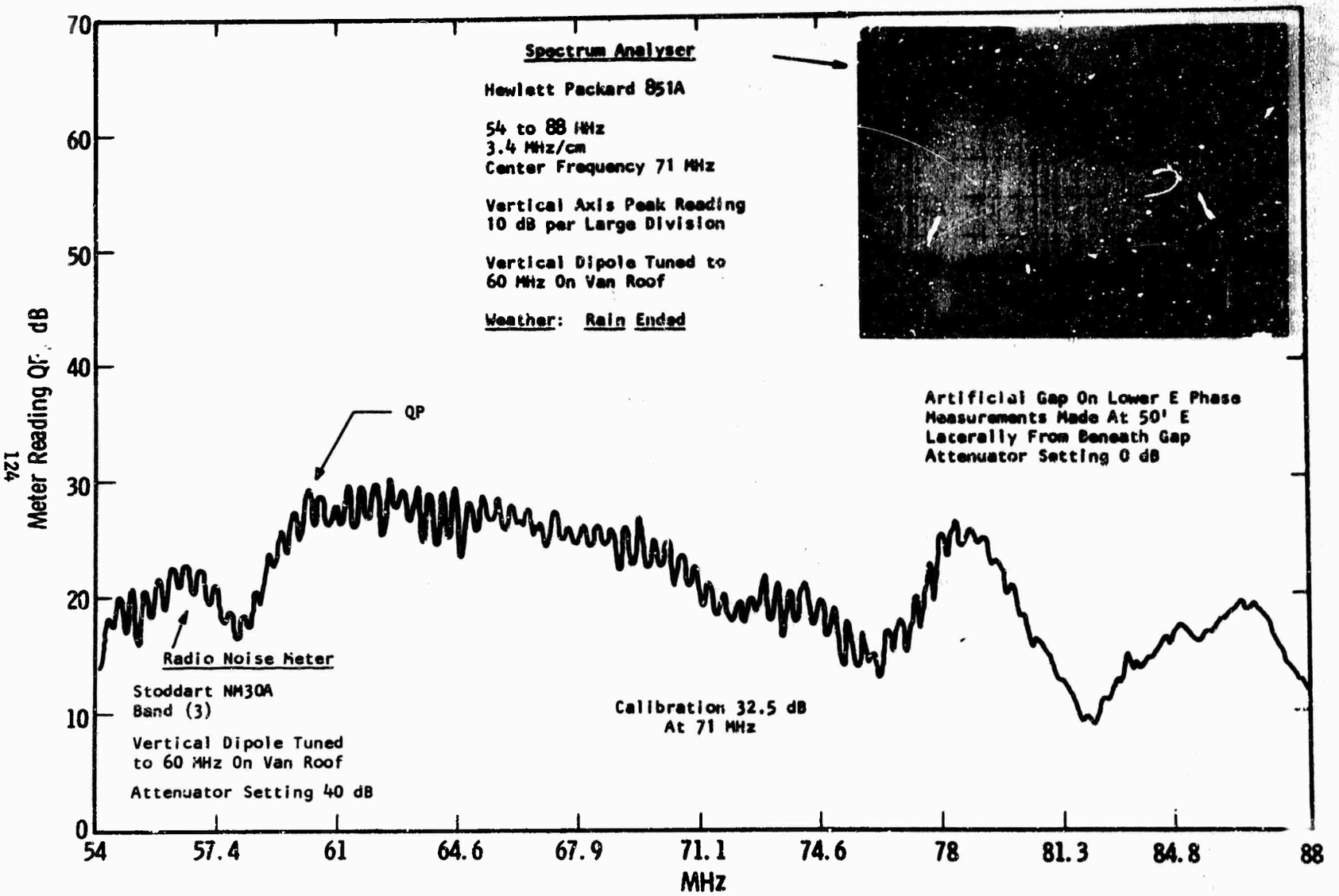


Fig. 15 —Radio noise meter/X-Y plot and spectrum analyser comparison with artificial gap on 345 kV AC line

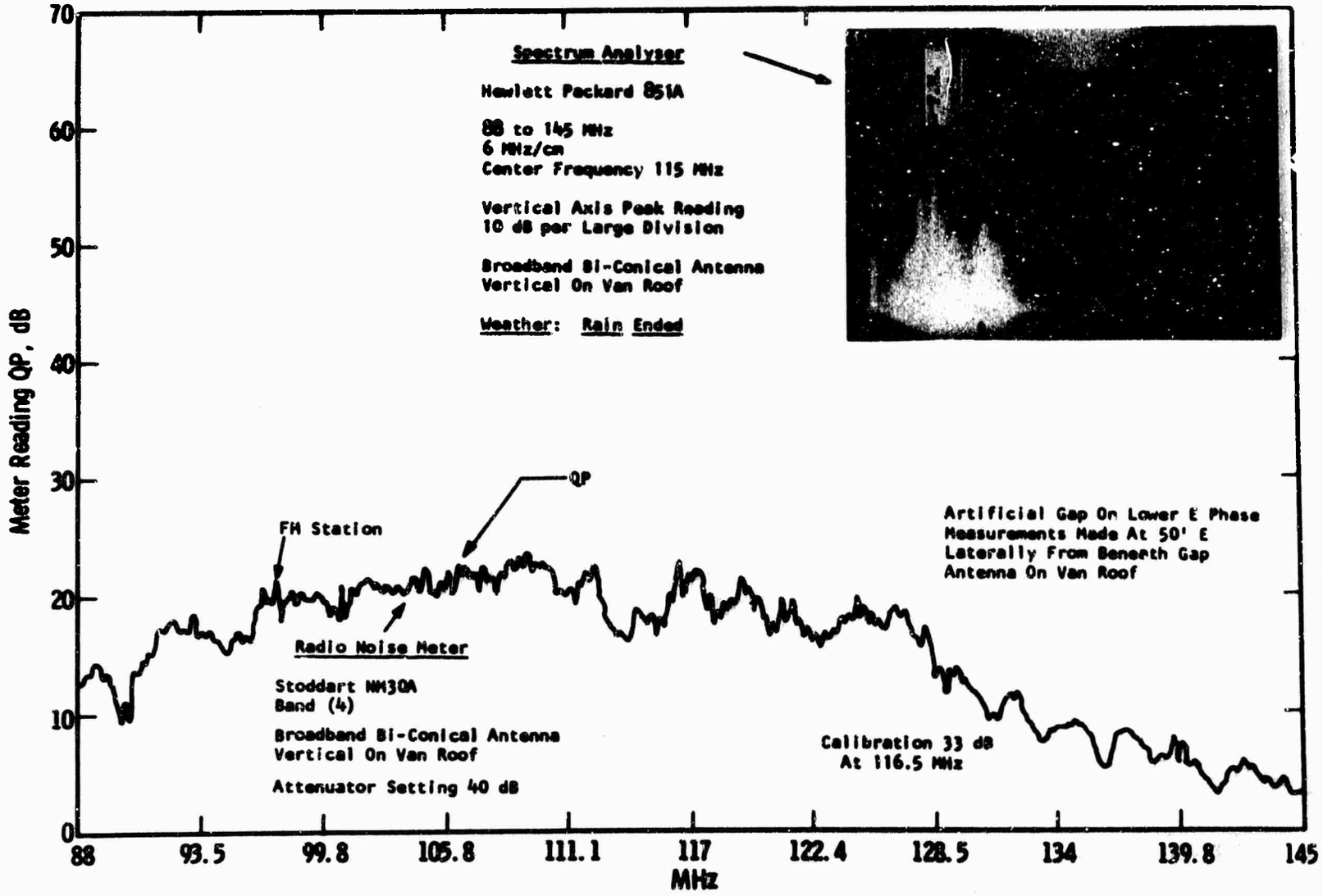


Fig. 16 —Radio noise meter/X-Y plot and spectrum analyser comparison with artificialgap on 345 kV AC line

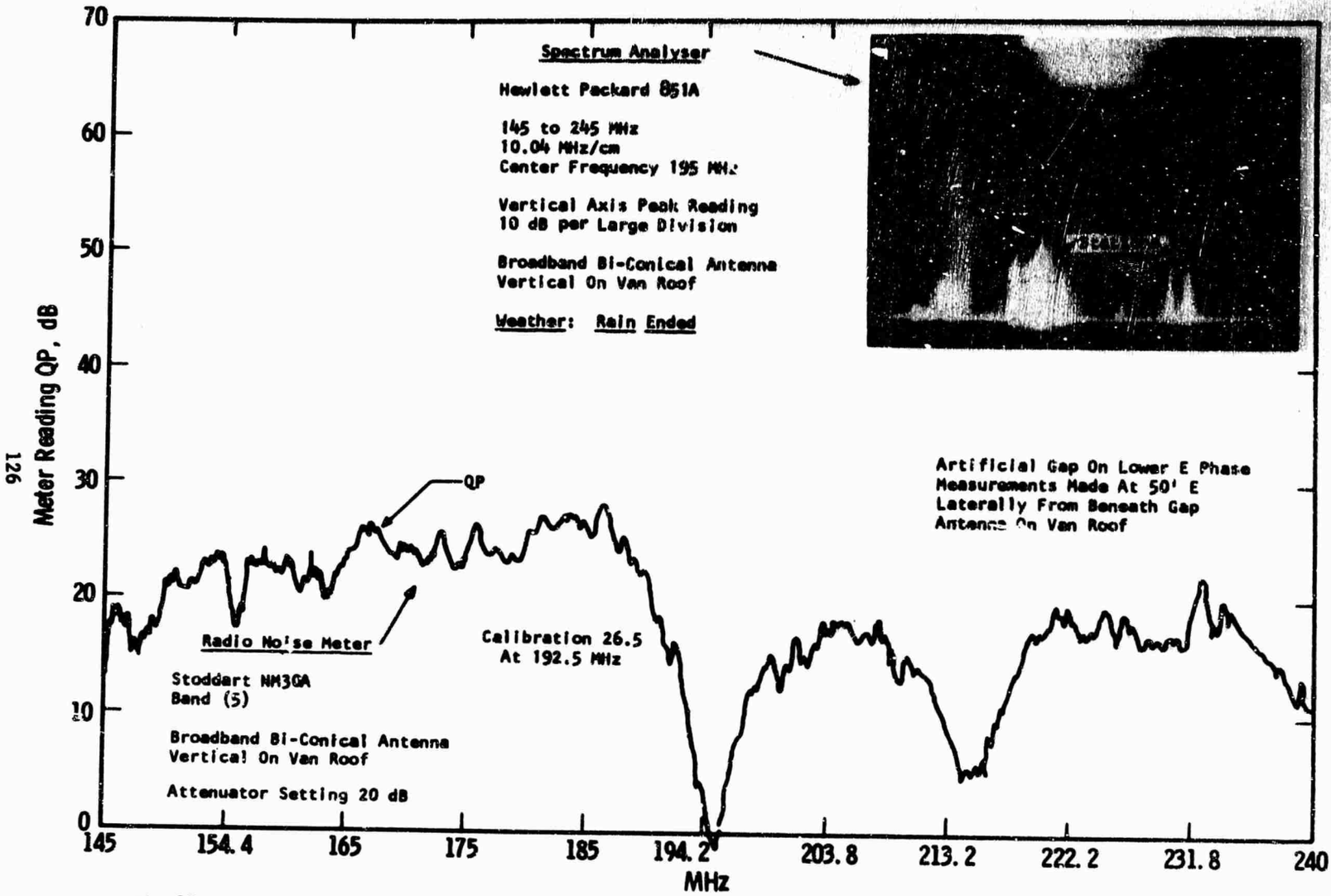


Fig. 17 --Radio noise meter/X-Y plot and spectrum analyser comparison with artificial gap on 345 kV AC line

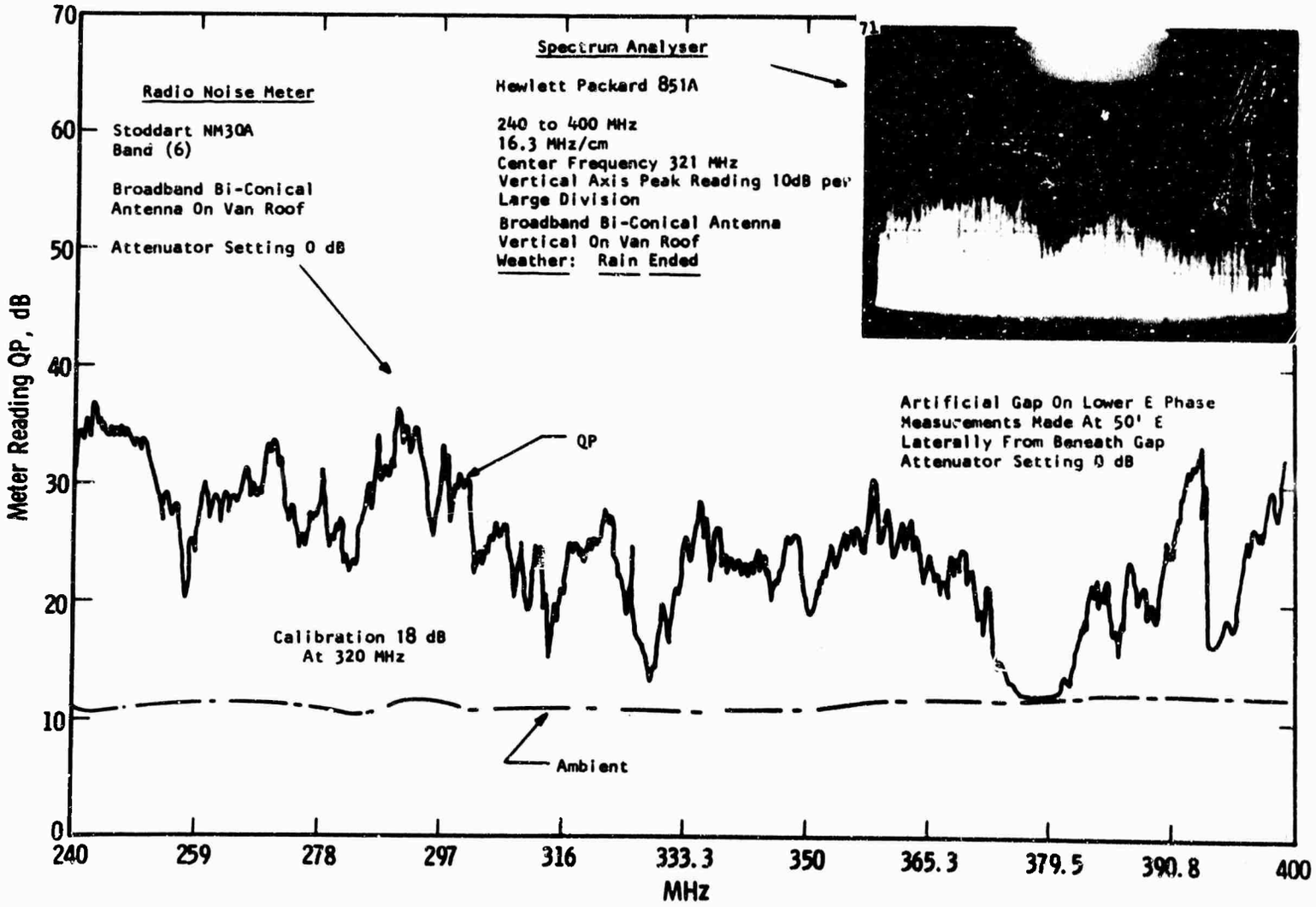


Fig. 18 --Radio noise meter/X-Y plot and spectrum analyser comparison with artificial gap on 345 kV AC line

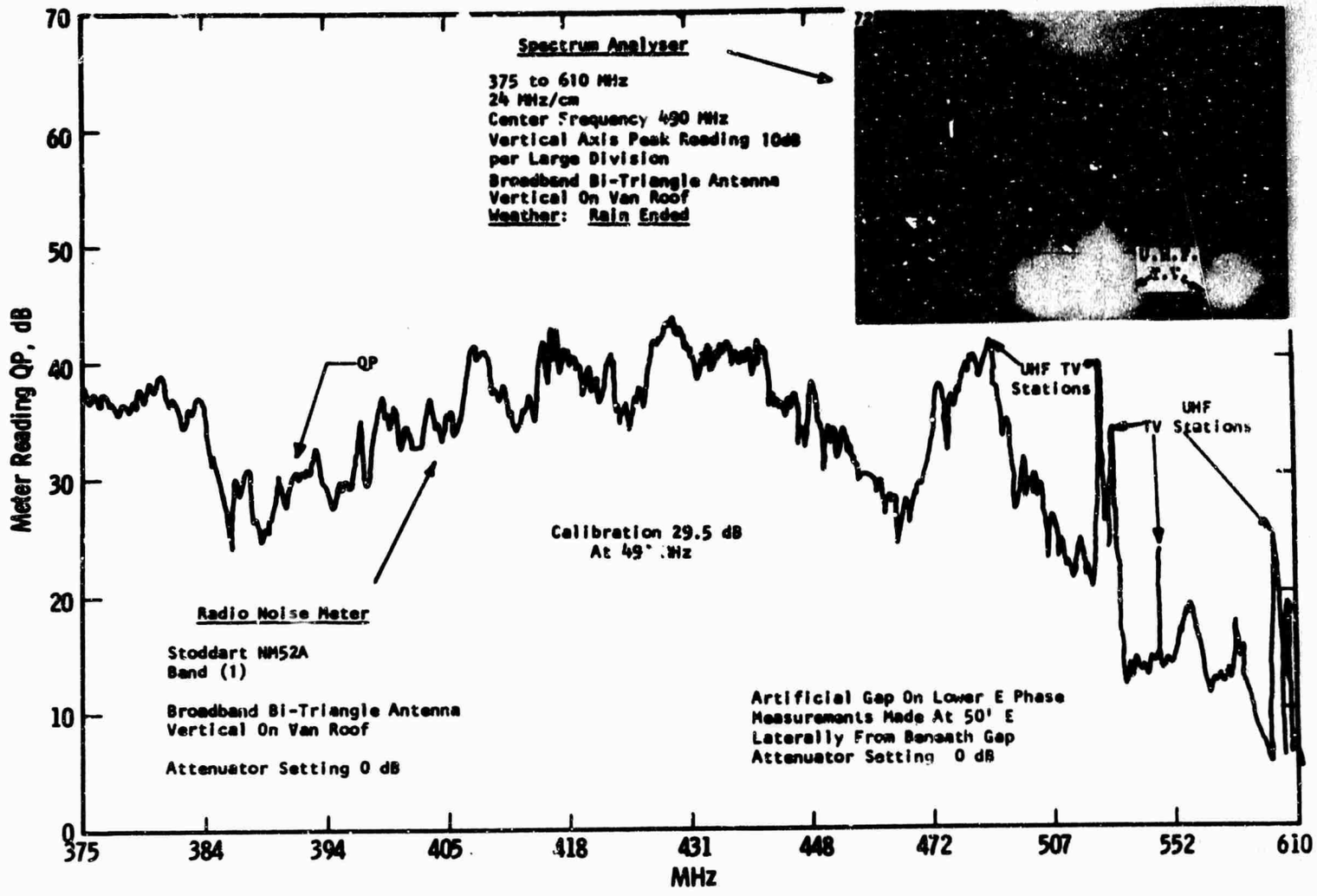


Fig. 19 —Radio noise meter/X-Y plot and spectrum analyser comparison with artificial gap on 345 kV AC line

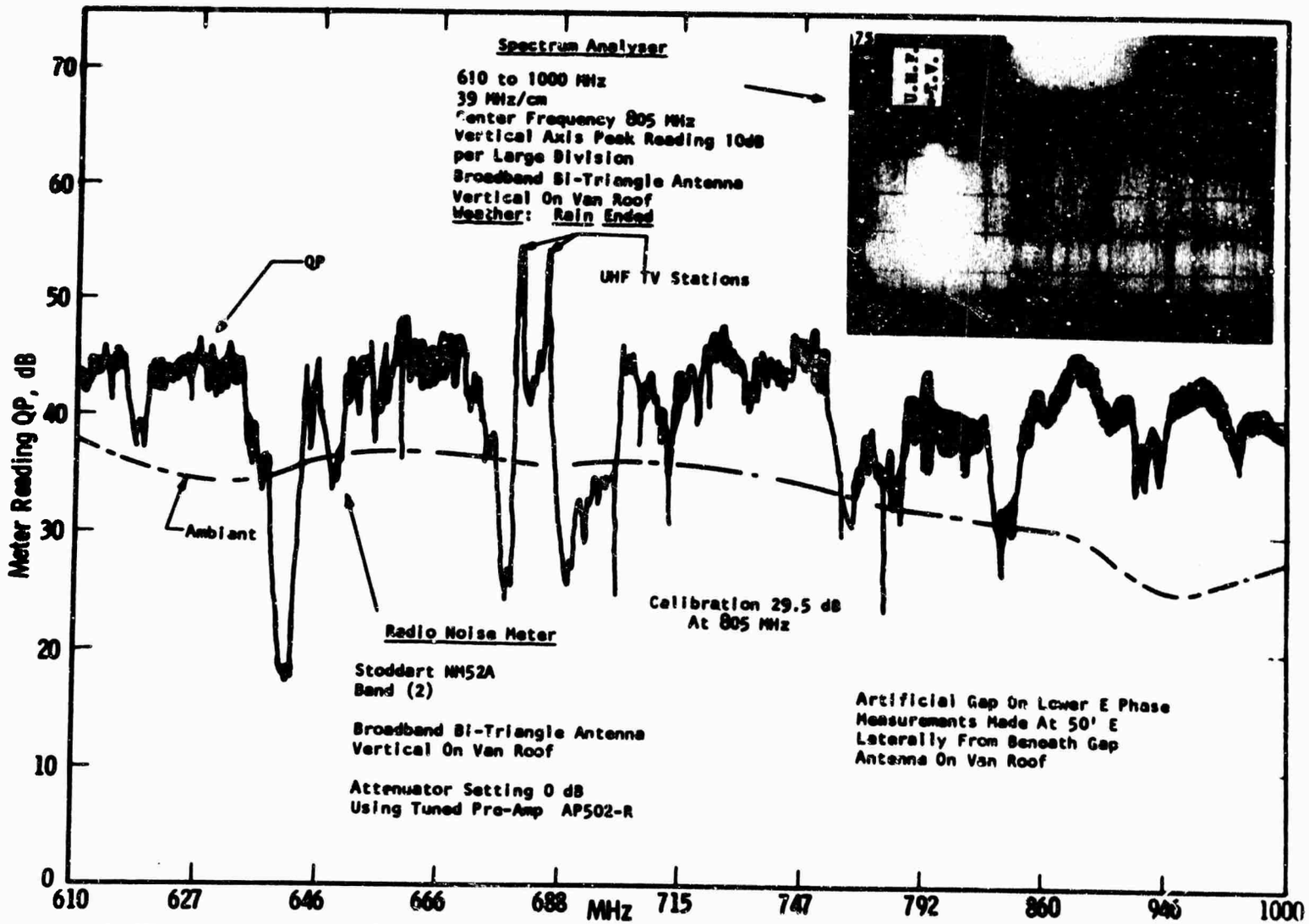


Fig. 20—Radio noise meter/X-Y plot spectrum analyser comparison with artificial gap on 345 kV AC line

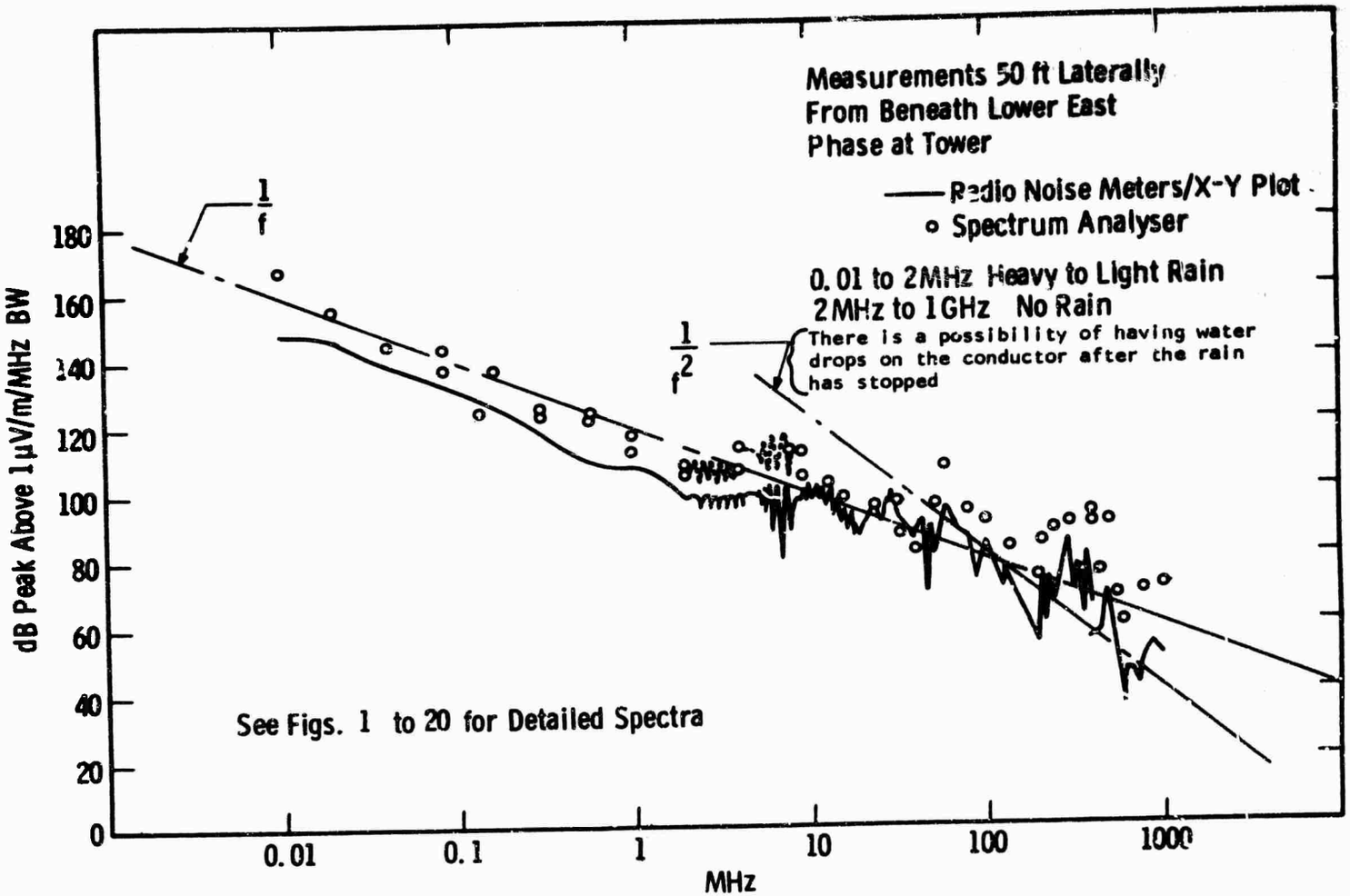


Fig. 21—Radio noise meter/X-Y plot and spectrum analyser comparison with artificial gap on 345 kV VCDC line

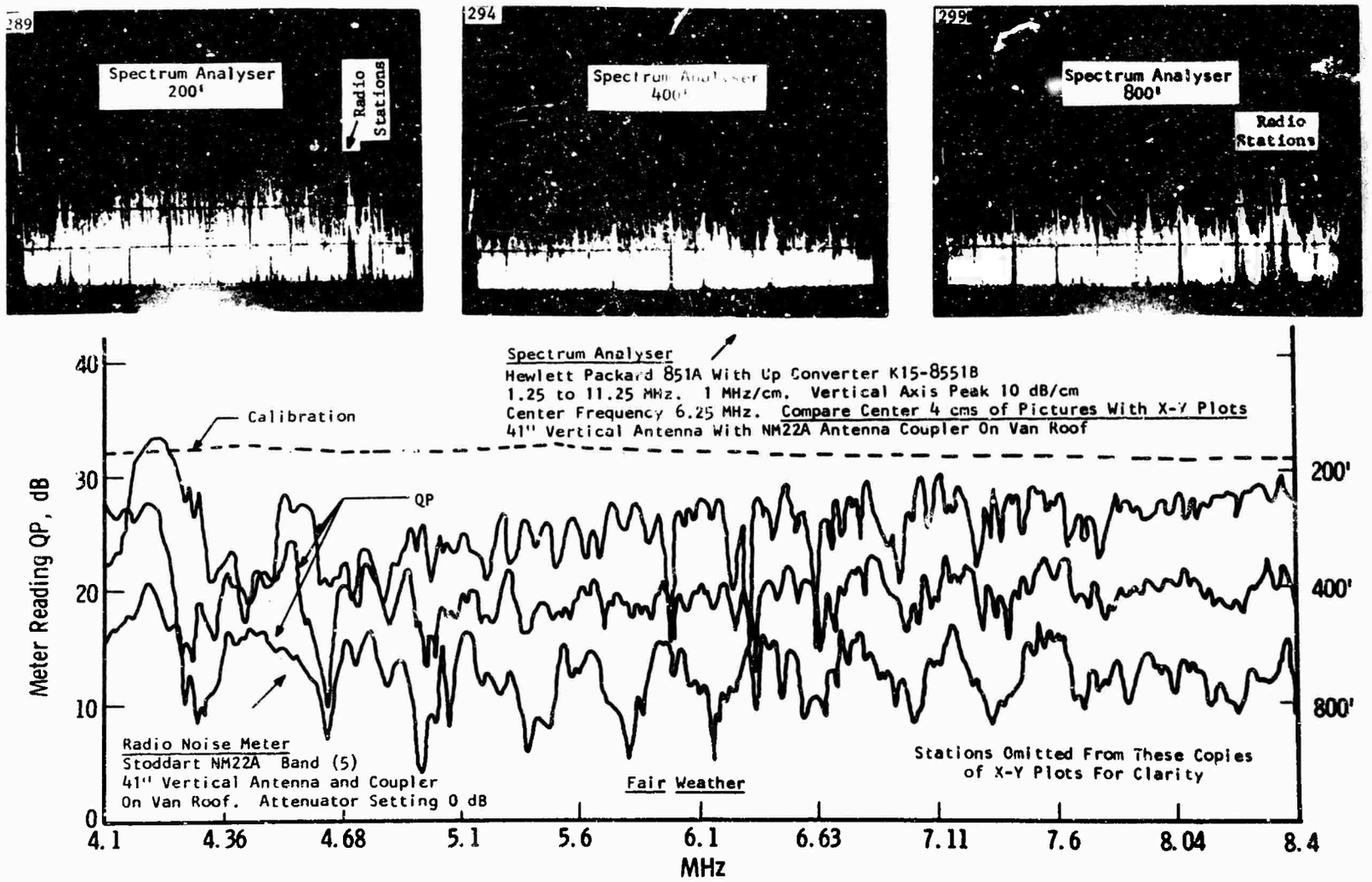


Fig. 22—Radio noise meter/X-Y plot and spectrum analyser comparison for different lateral distances from 525 kV AC line with artificial gap

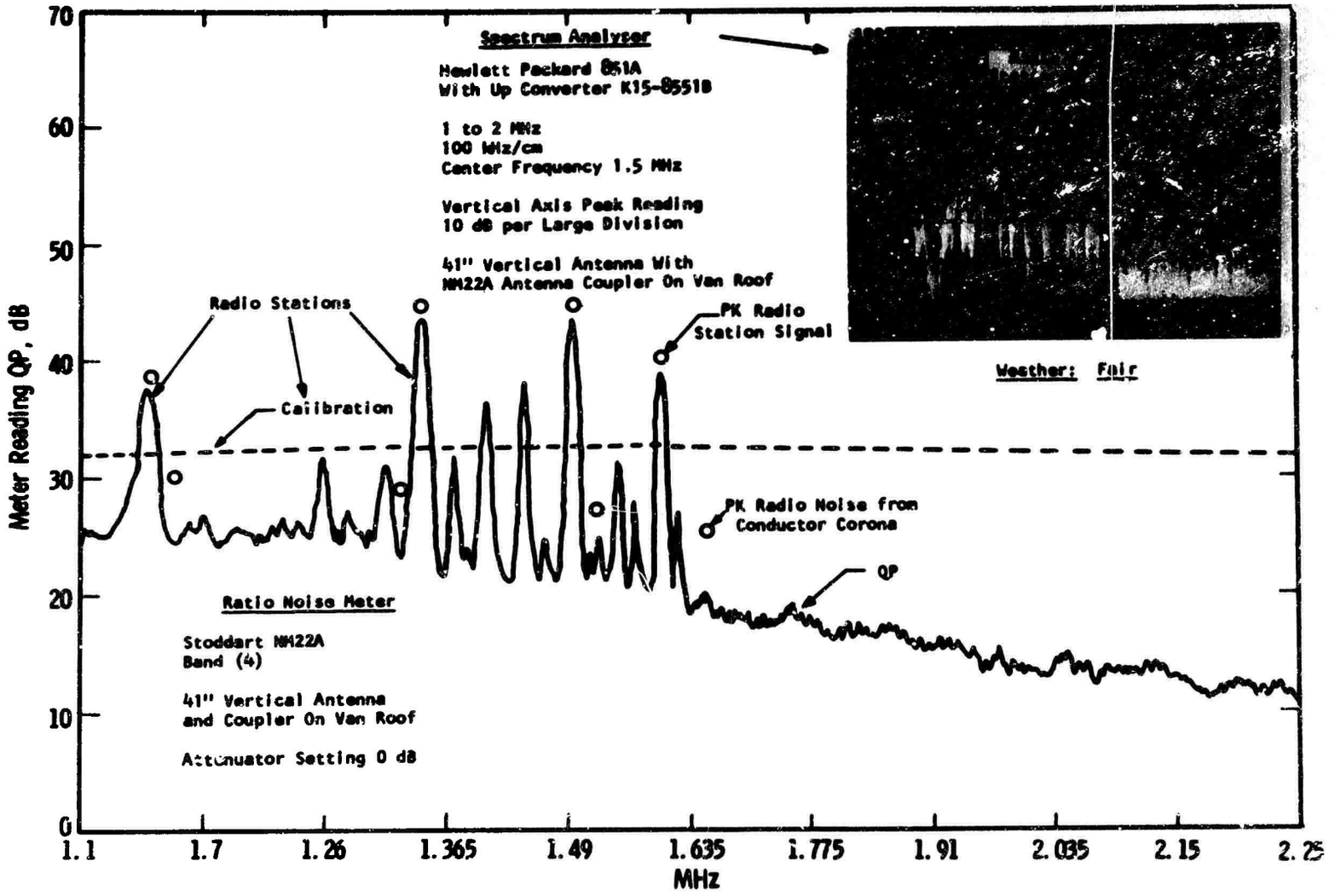


Fig. 23—Radio noise meter/X-Y plot and spectrum analyser comparisons 50 ft from 525 kV AC line

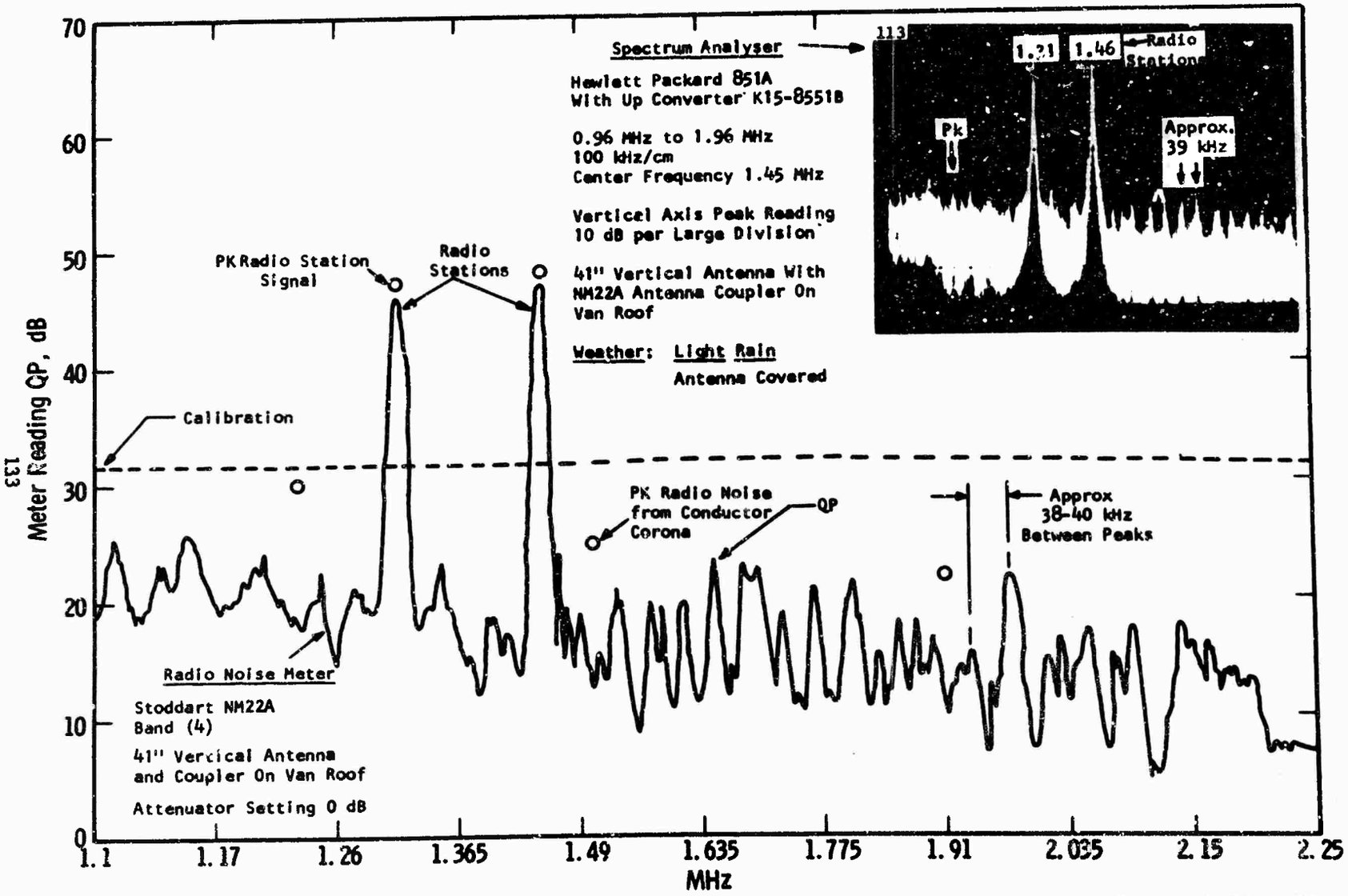
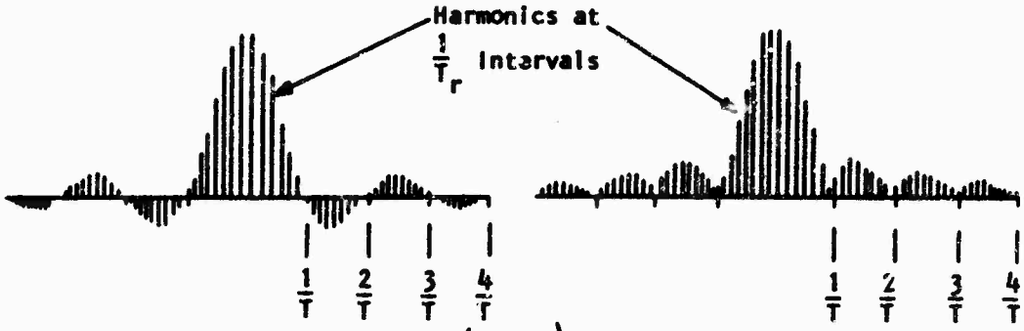


Fig. 24—Radio noise meter/X-Y plot and spectrum analyser comparisons 73' from positive conductor of 800 kV DC test line



(a) Typical theoretical spectra $\left(\frac{\sin \pi X}{\pi X}\right)$ of repeated rectangular pulse (T = Pulse Width)

(b) Typical spectrum analyser display of repeated rectangular pulse

Fig. 25

c.w.f.	c.w. Pk i/p	Converter i/p Attenuator	Analyser i/p Attenuator	461A Pre-Amp	I.F. Bandwidth	I.F. Gain	Spectrum Width	Sweep Rate
100 kHz	37 dB	10 dB	0 dB	40 dB	3 kHz	50 dB	10 kHz/cm	3 msec to 1 sec/cm
225 kHz	"	"	"	"	"	"	30 kHz/cm	"
450 kHz	"	"	"	"	"	"	"	"
900 kHz	"	"	"	"	"	"	100 kHz/cm	"
1.5 MHz	"	"	"	"	"	"	"	"
3.25 MHz	"	"	"	"	"	"	300 kHz/cm	"
6.25 MHz	"	10 dB	"	"	"	"	1 MHz/cm	"
15 MHz	"	-	"	"	"	60 dB	"	"
[illegible] MHz	"	-	"	"	3 kHz	"	3 MHz/cm	"
35 MHz	"	-	"	"	100 kHz	"	"	"
65 MHz	"	-	"	40 dB	"	"	"	"
130 MHz	"	-	"	-	"	"	10 MHz/cm	"
250 MHz	"	-	"	-	100 kHz	"	30 MHz/cm	"
550 MHz	"	-	"	-	1 MHz	60 dB	"	"
850 MHz	"	-	"	-	1 MHz	70 dB	"	"

Table of H. P. 851A/8551A spectrum analyser control settings for C. W. inputs of various frequencies

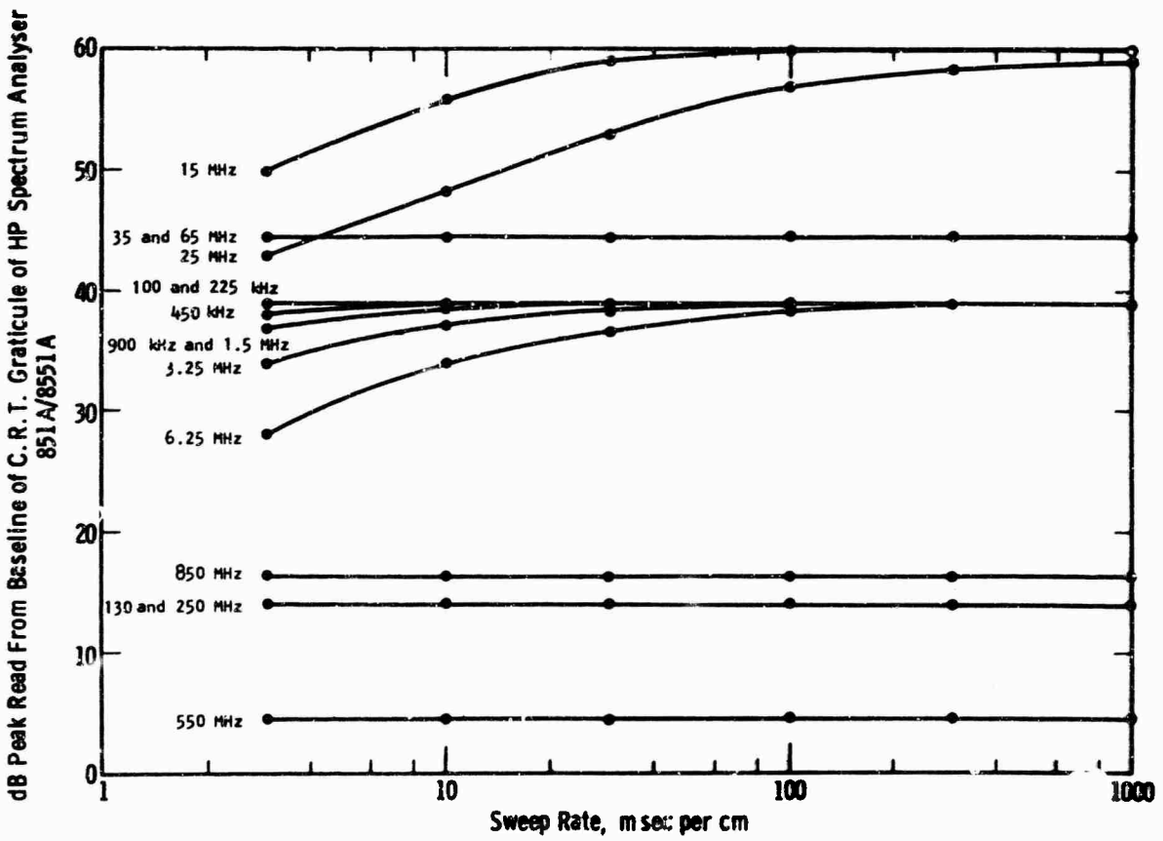


Fig. 26—C. W. response of H. P. 851A/8551A spectrum analyser for frequencies and control settings tabulated/sweep rate

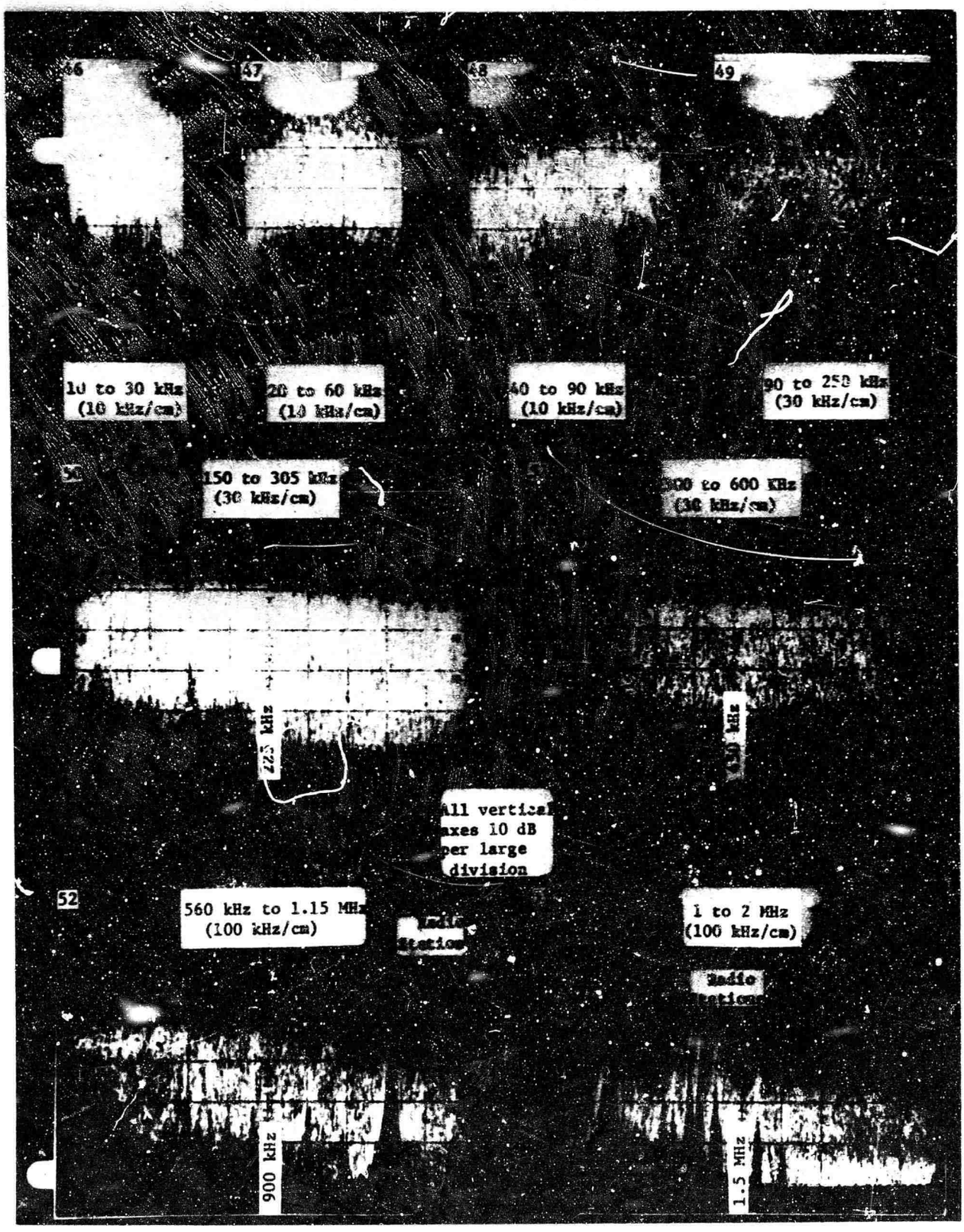


Fig. 27 345 kV AC Frequency Spectra 108 ft. from bottom conductor with artificial gap on and rain at same time (10 kHz to 2 MHz); at tower.

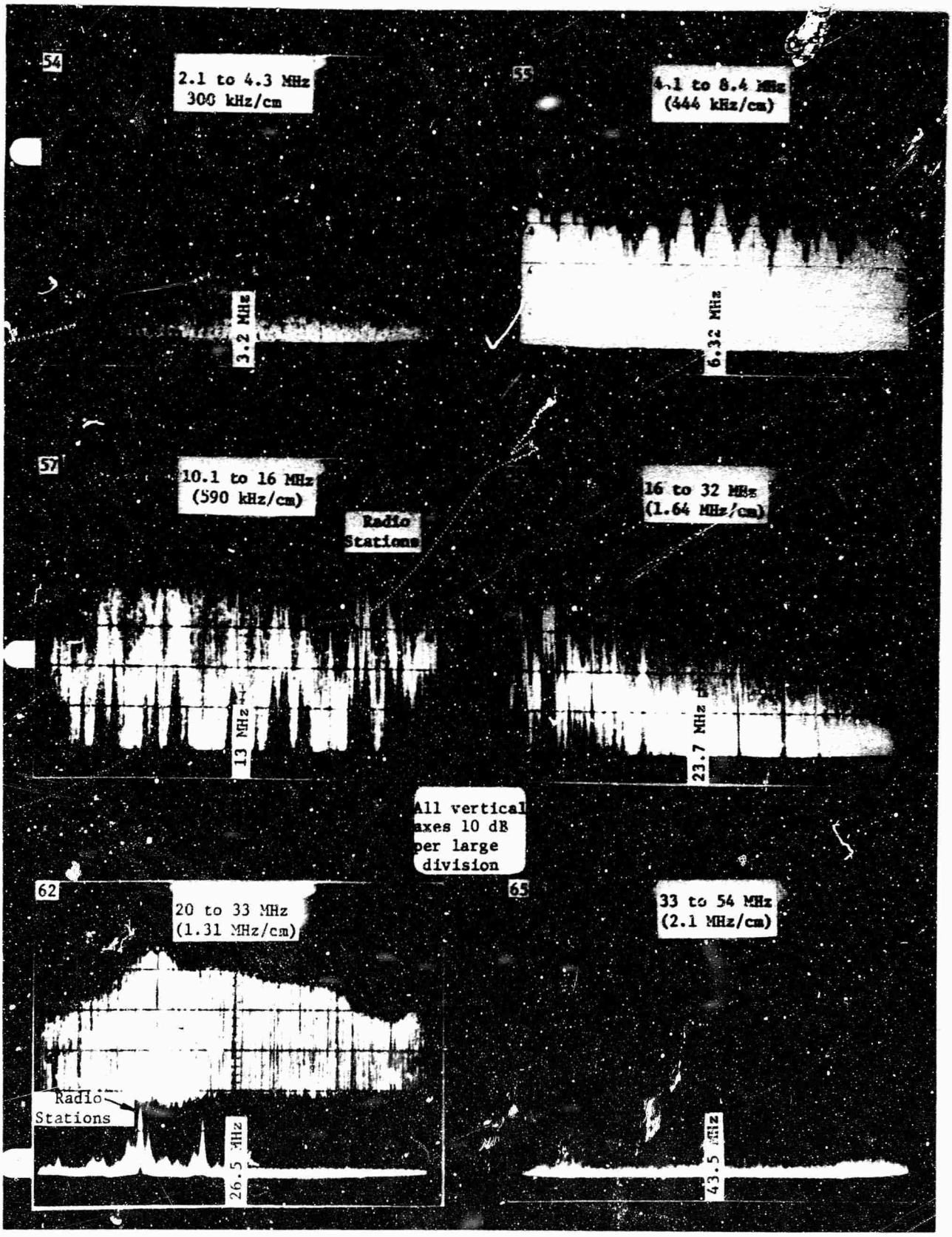


Fig. 28 345 kV AC Frequency Spectra 108 ft. from bottom conductor with artificial gap (2 MHz to 54 MHz); at tower.

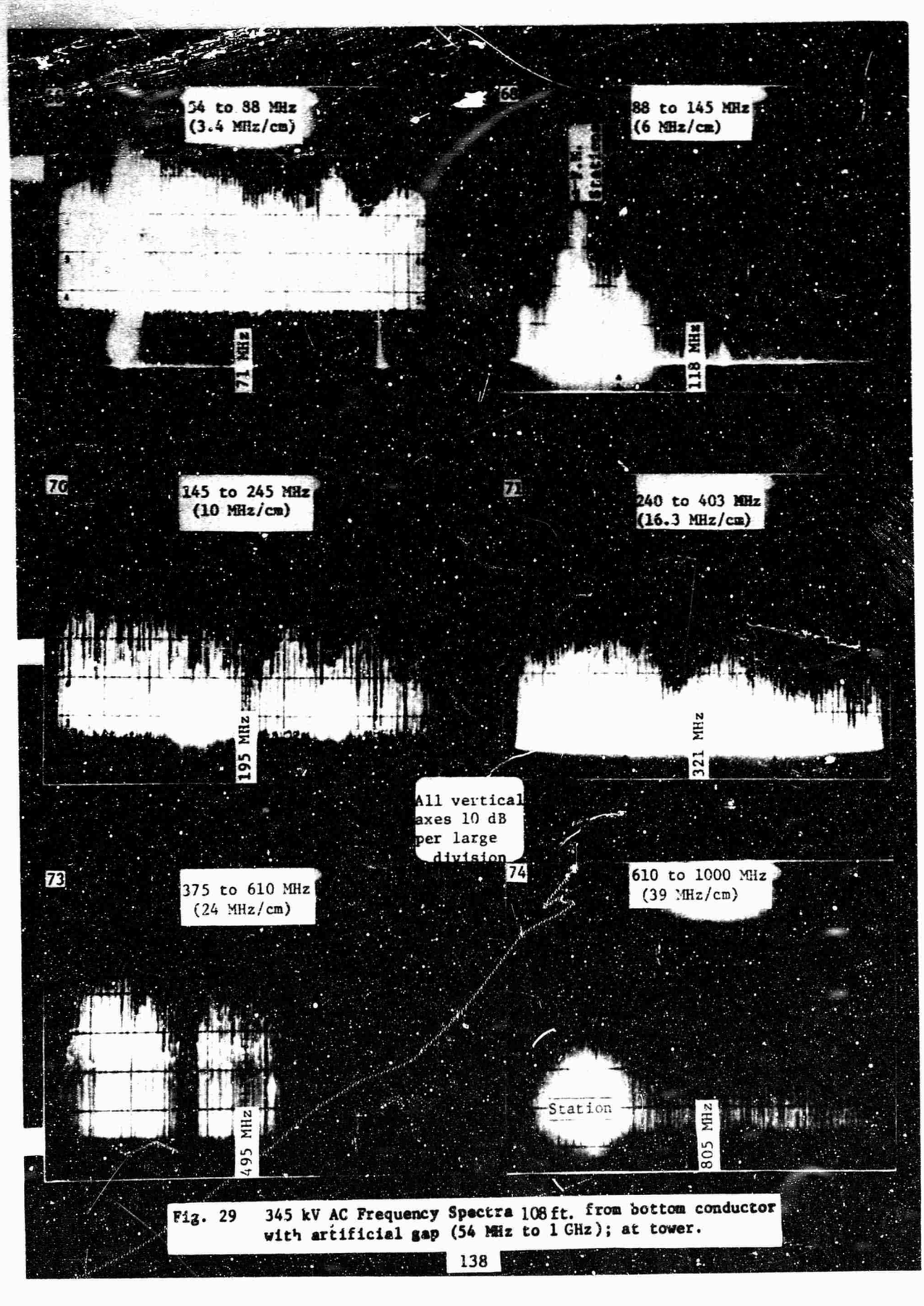


Fig. 29 345 kV AC Frequency Spectra 108 ft. from bottom conductor with artificial gap (54 MHz to 1 GHz); at tower.

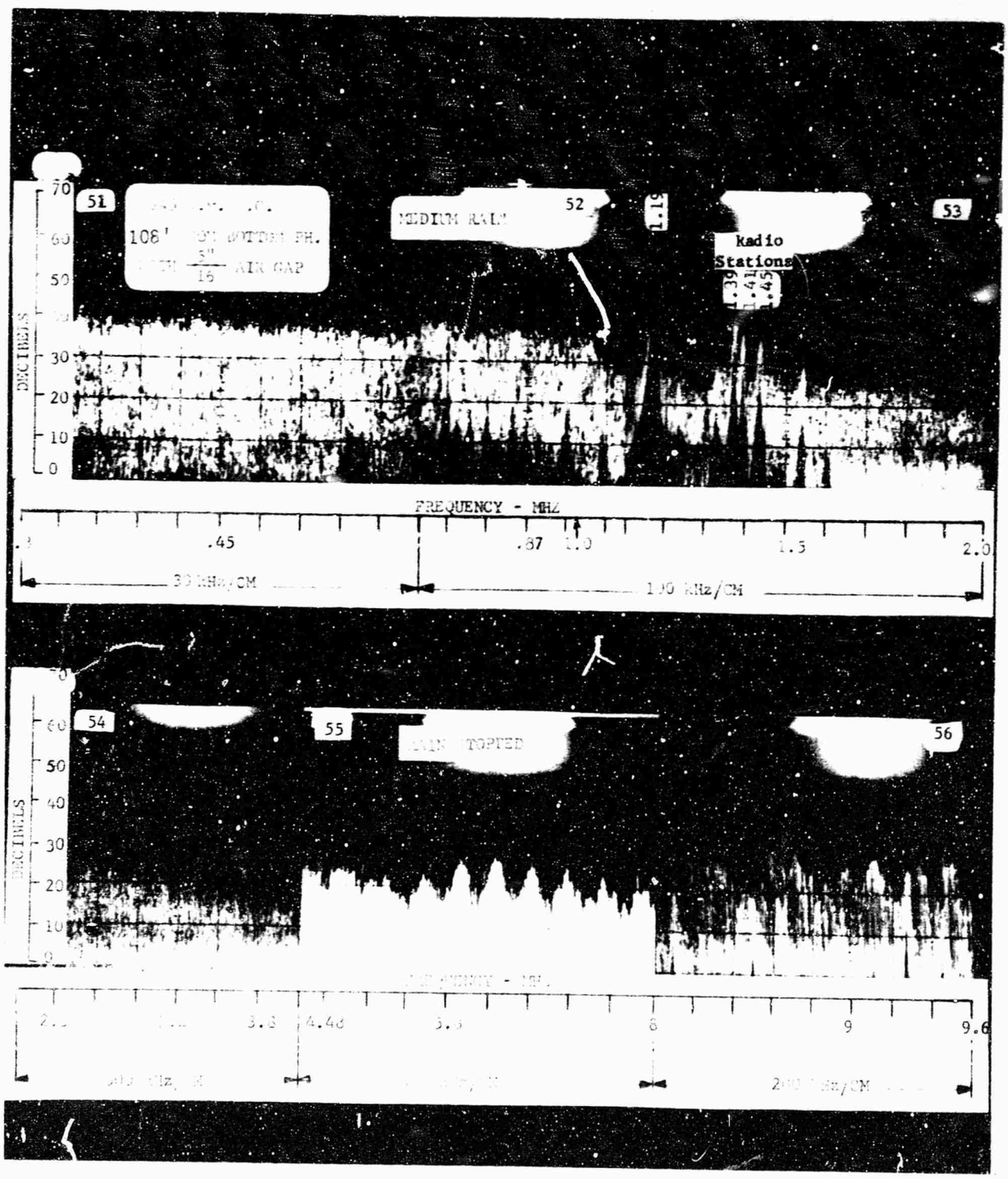


Fig. 30 345 kV AC Frequency Spectra (0.3 to 9.6 MHz) with artificial gap (accompanied by rain some of the time); at tower.

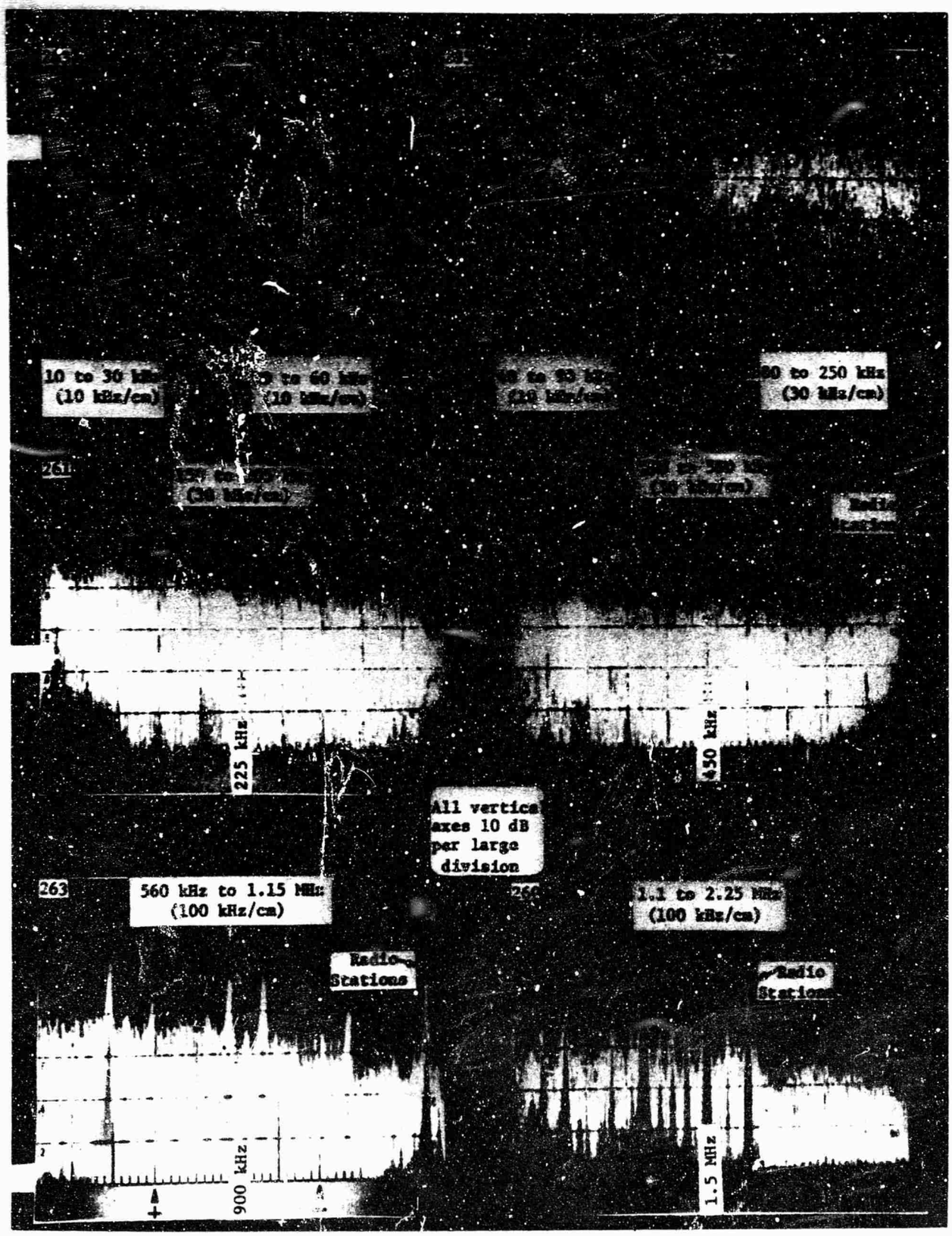


Fig. 31 525 kV AC Frequency Spectra 110 ft. from outside conductor with artificial gap (10 kHz to 2.25 MHz); at tower.

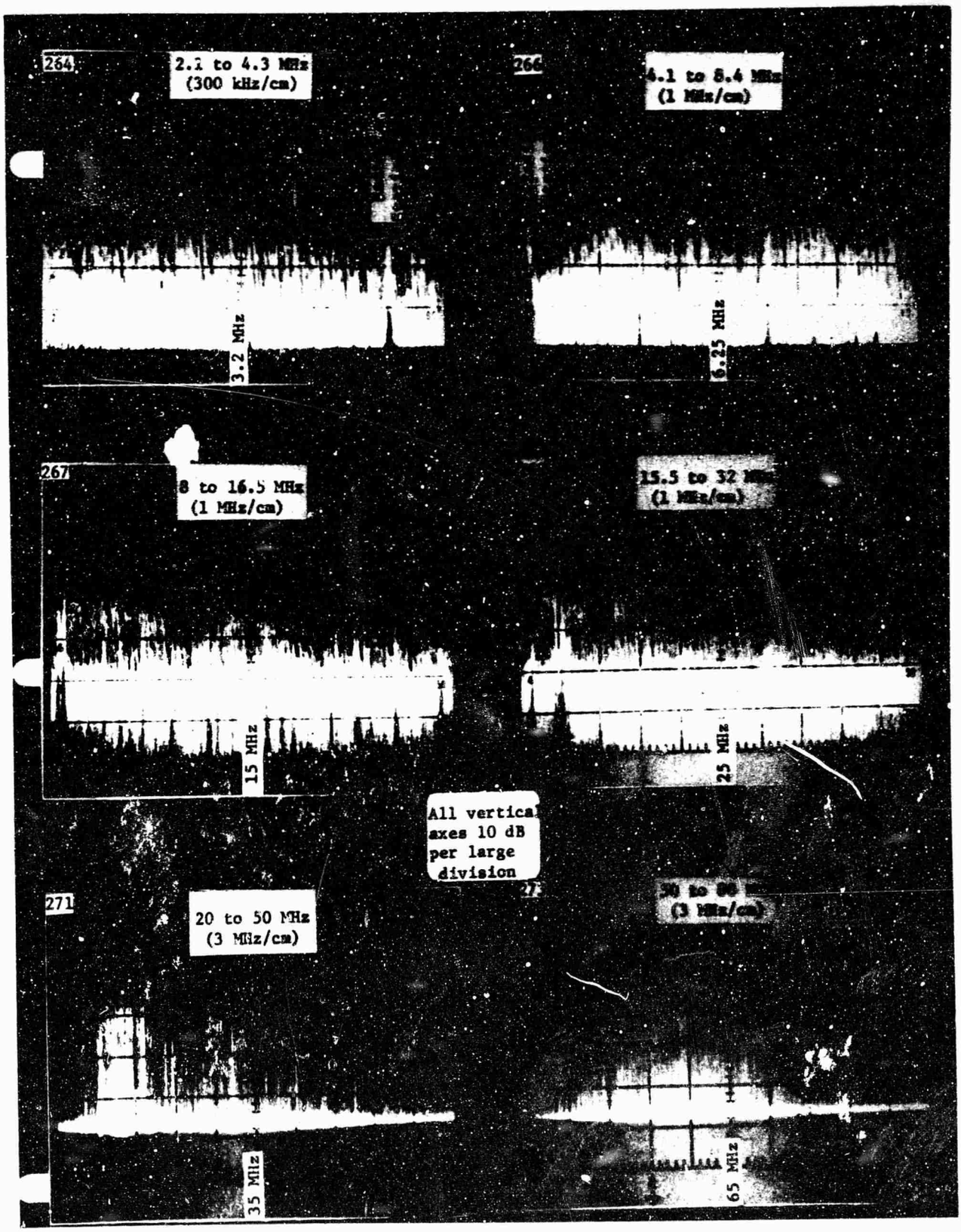


Fig. 32 525 kV AC Frequency Spectra 110 ft. from outside conductor with artificial gap (2.1 to 80 MHz): at tower.

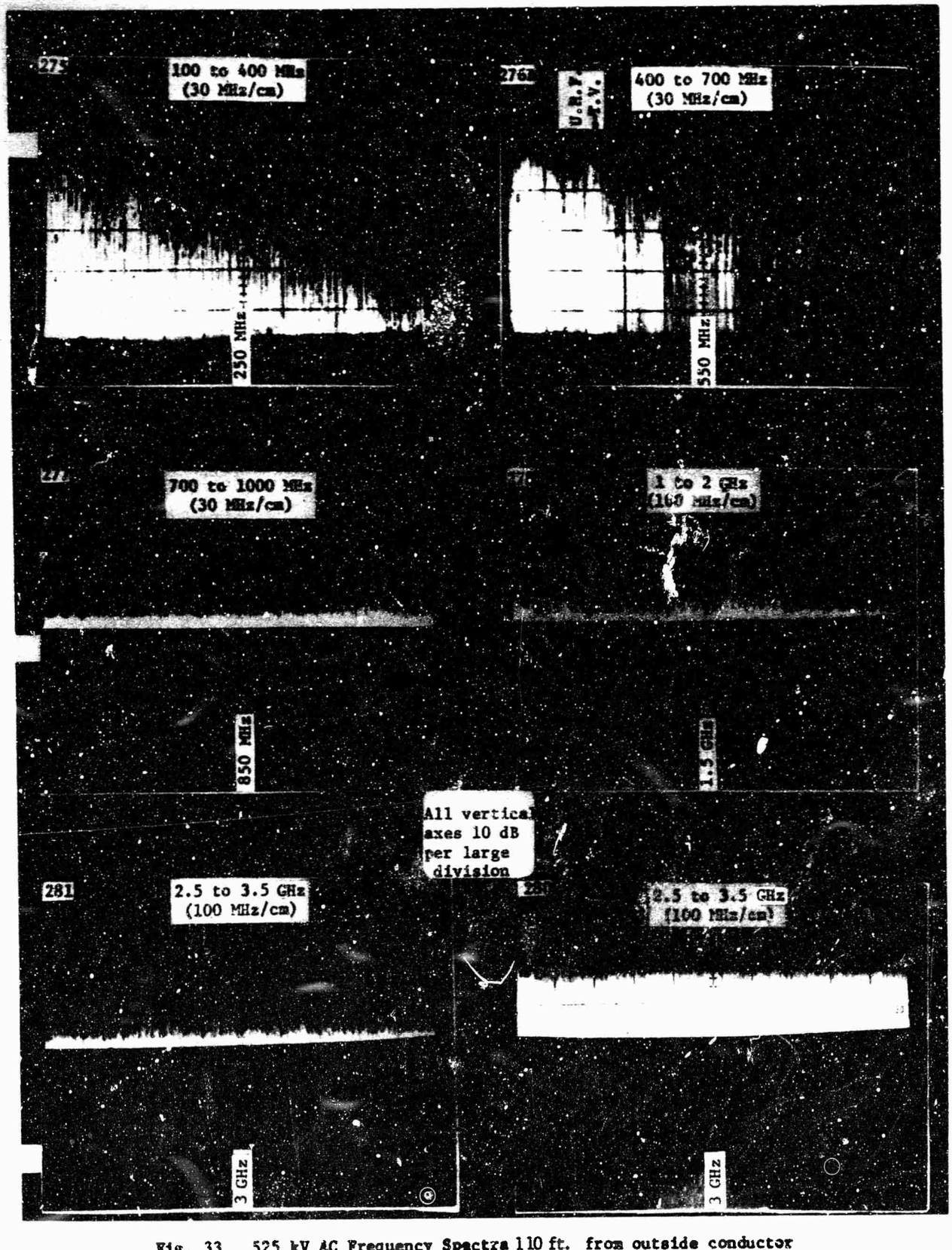


Fig. 33 525 kV AC Frequency Spectra 110 ft. from outside conductor with artificial gap (100 MHz to 3.5 GHz); at tower.

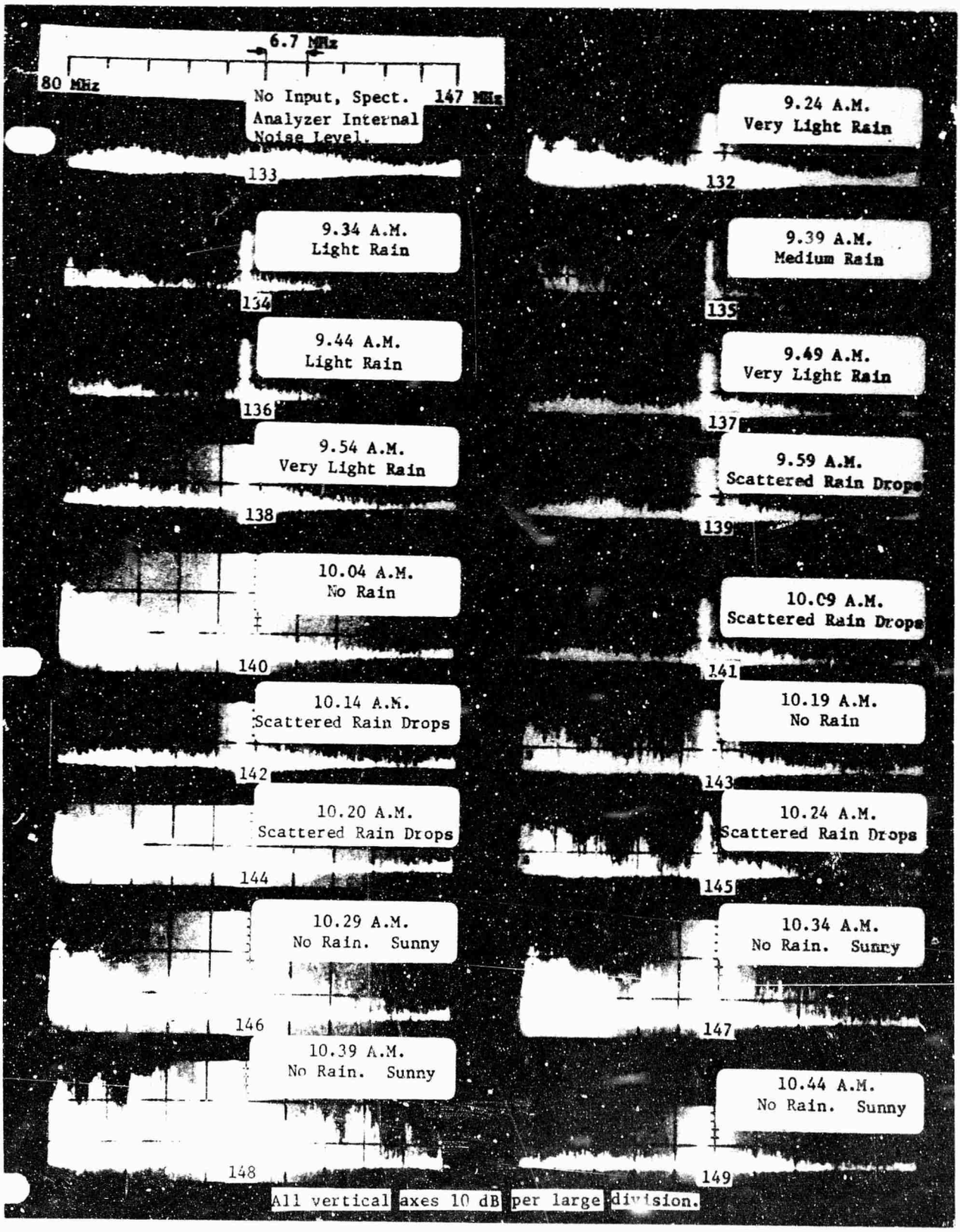


Fig.34 800 kV DC Frequency Spectra (80 to 147 MHz) 69 ft. from + conductor; at tower, in rain and fair weather.

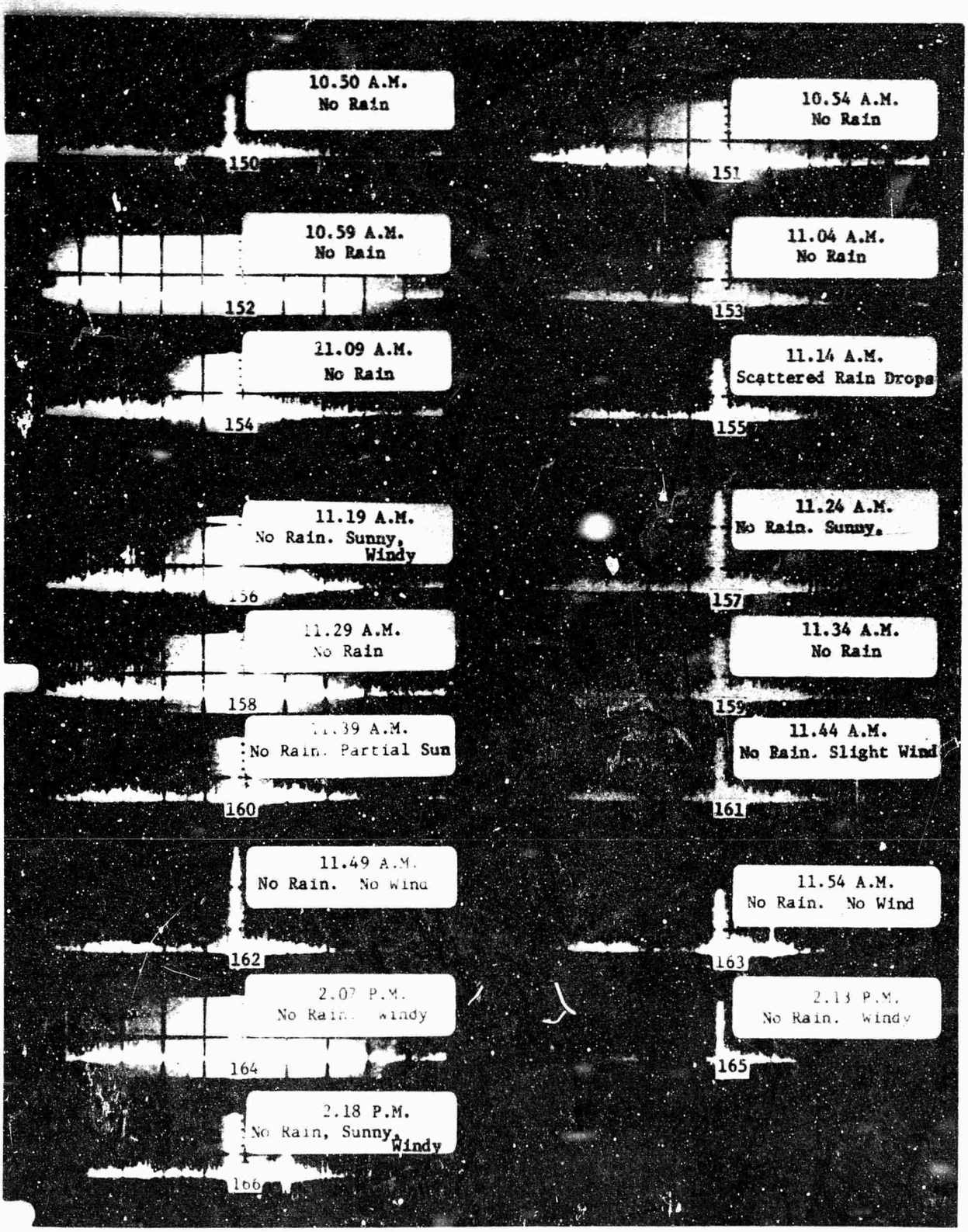


Fig.35 800 kV DC Frequency Spectra (80 to 147 MHz) 69 ft. from + conductor; at tower, in rain and fair weather.

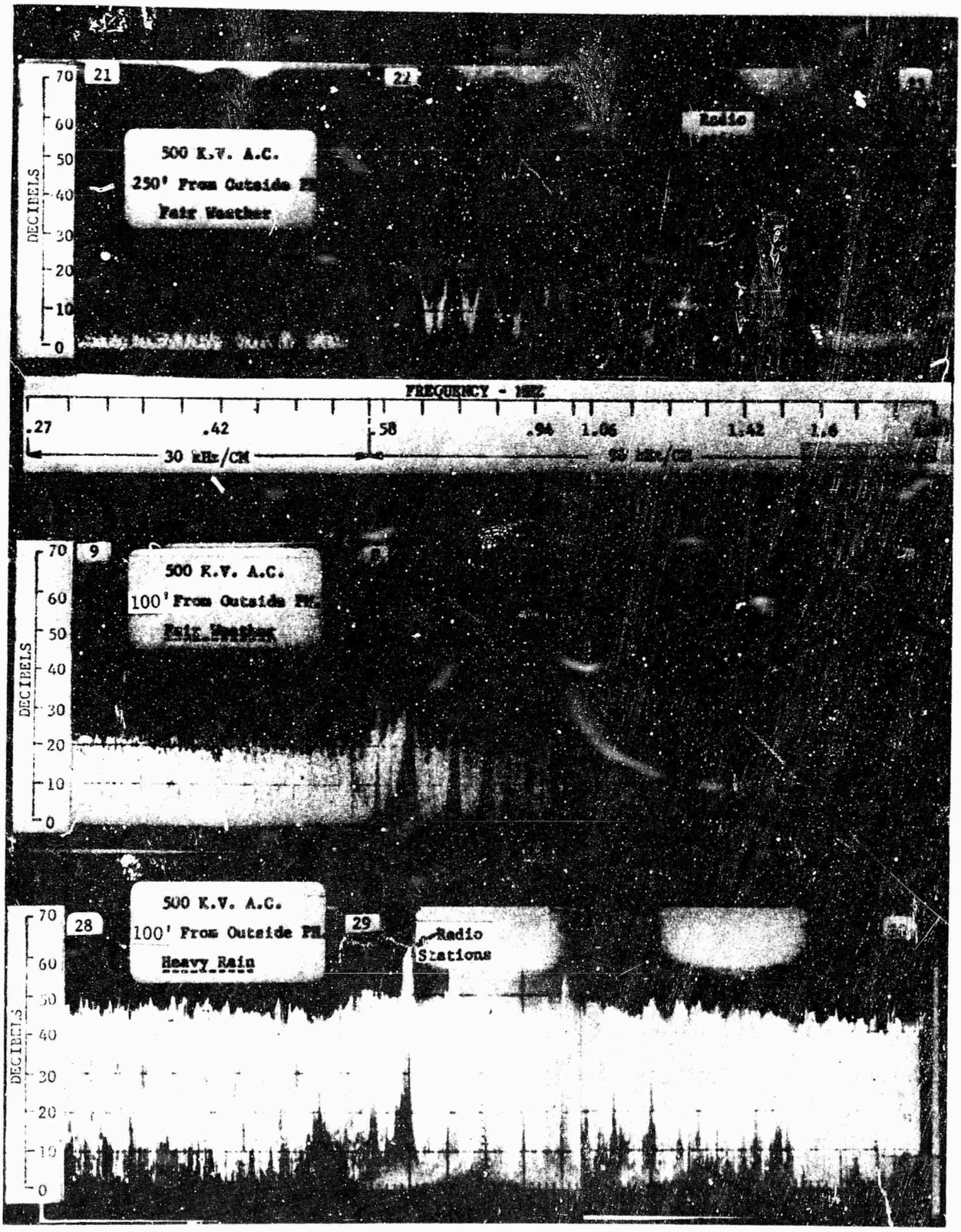


Fig. 36 500 kV AC Frequency Spectra (0.27 to 1.87 MHz) in fair weather and heavy rain; at tower.

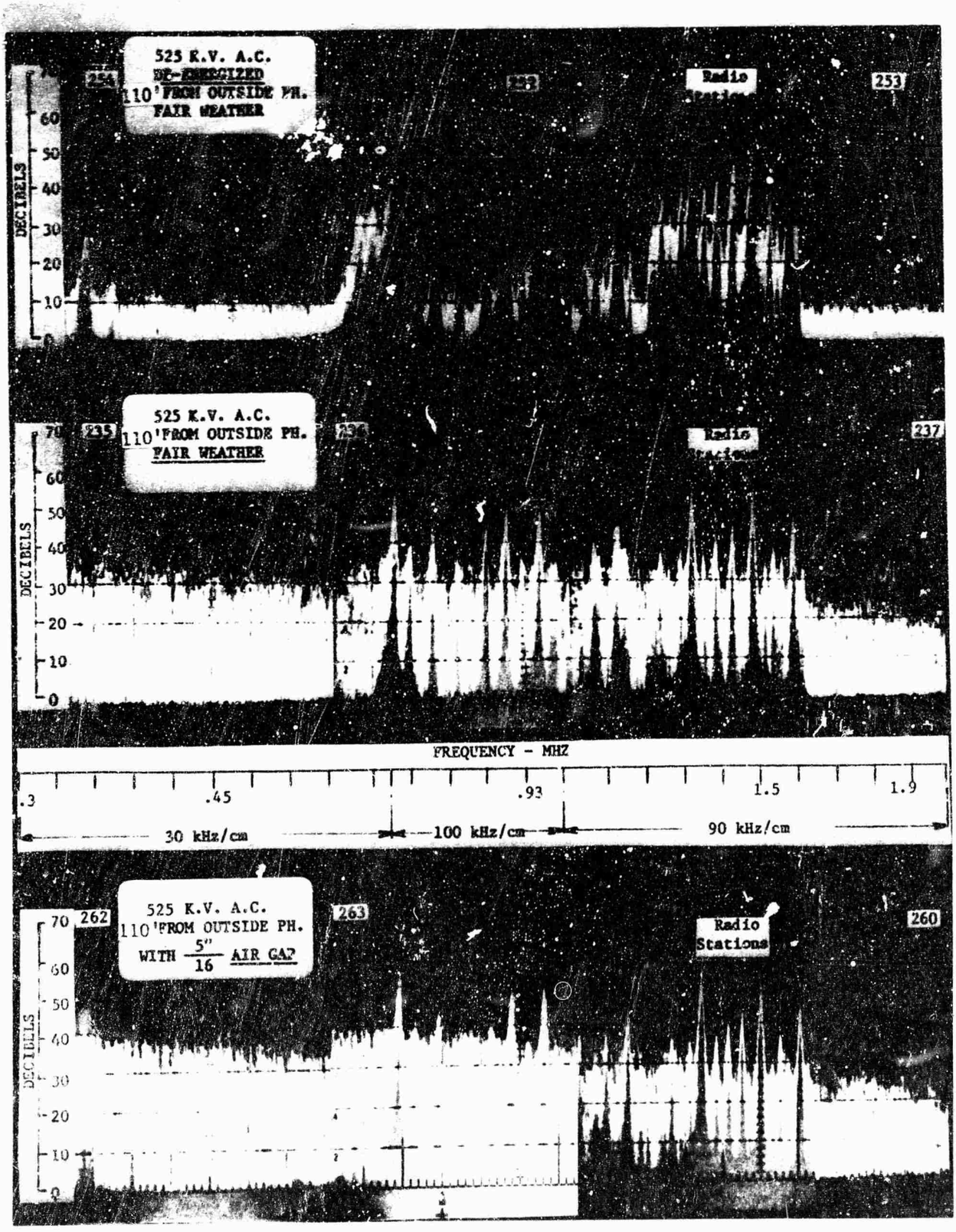


Fig.37 525 kV AC Frequency Spectra (0.3 to 2 MHz) with and without artificial gap and de-energized; at tower.

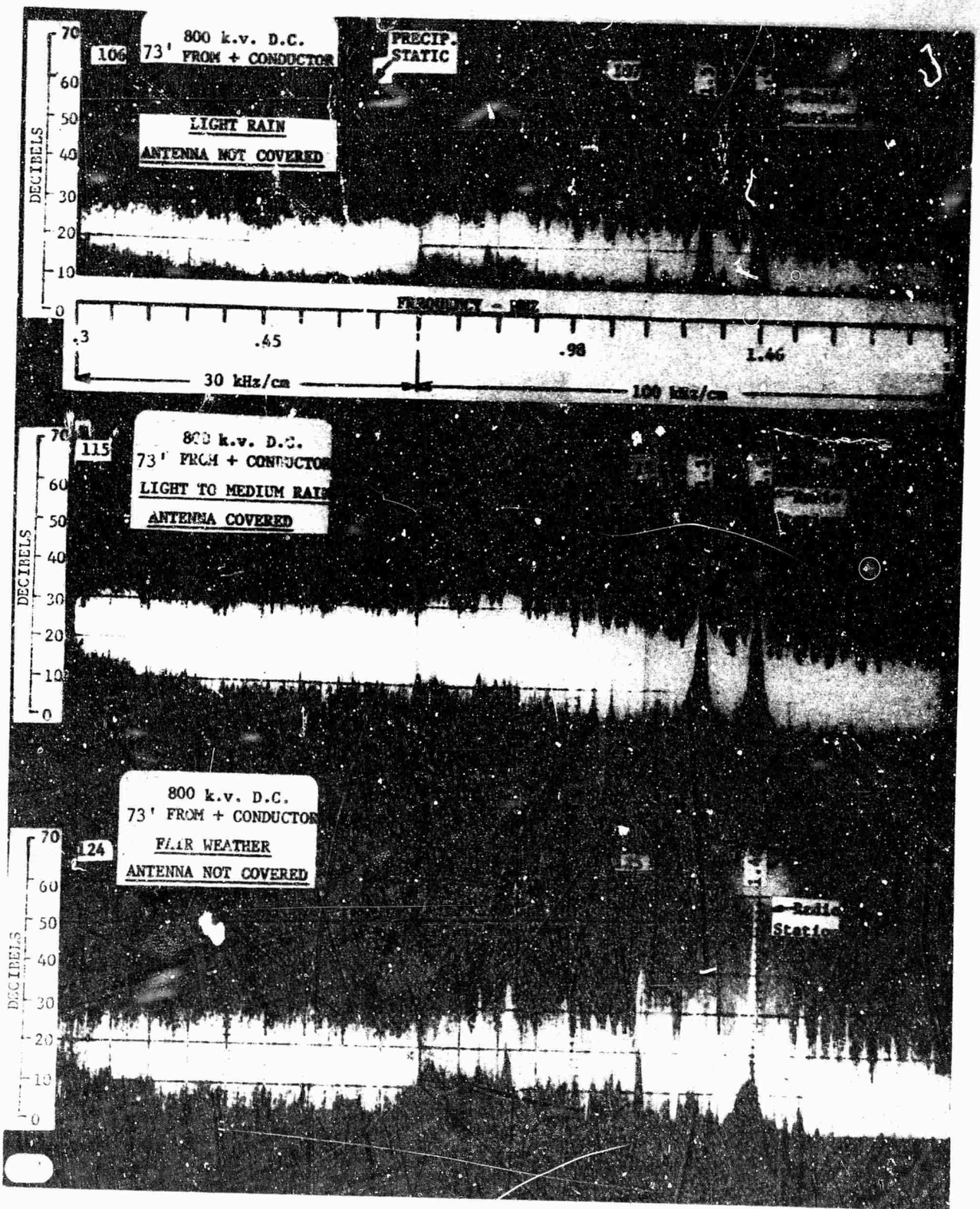


Fig. 38 ± 800 kV DC Frequency Spectra (0.3 to 1.96 MHz) in fair weather and rain; at tower.

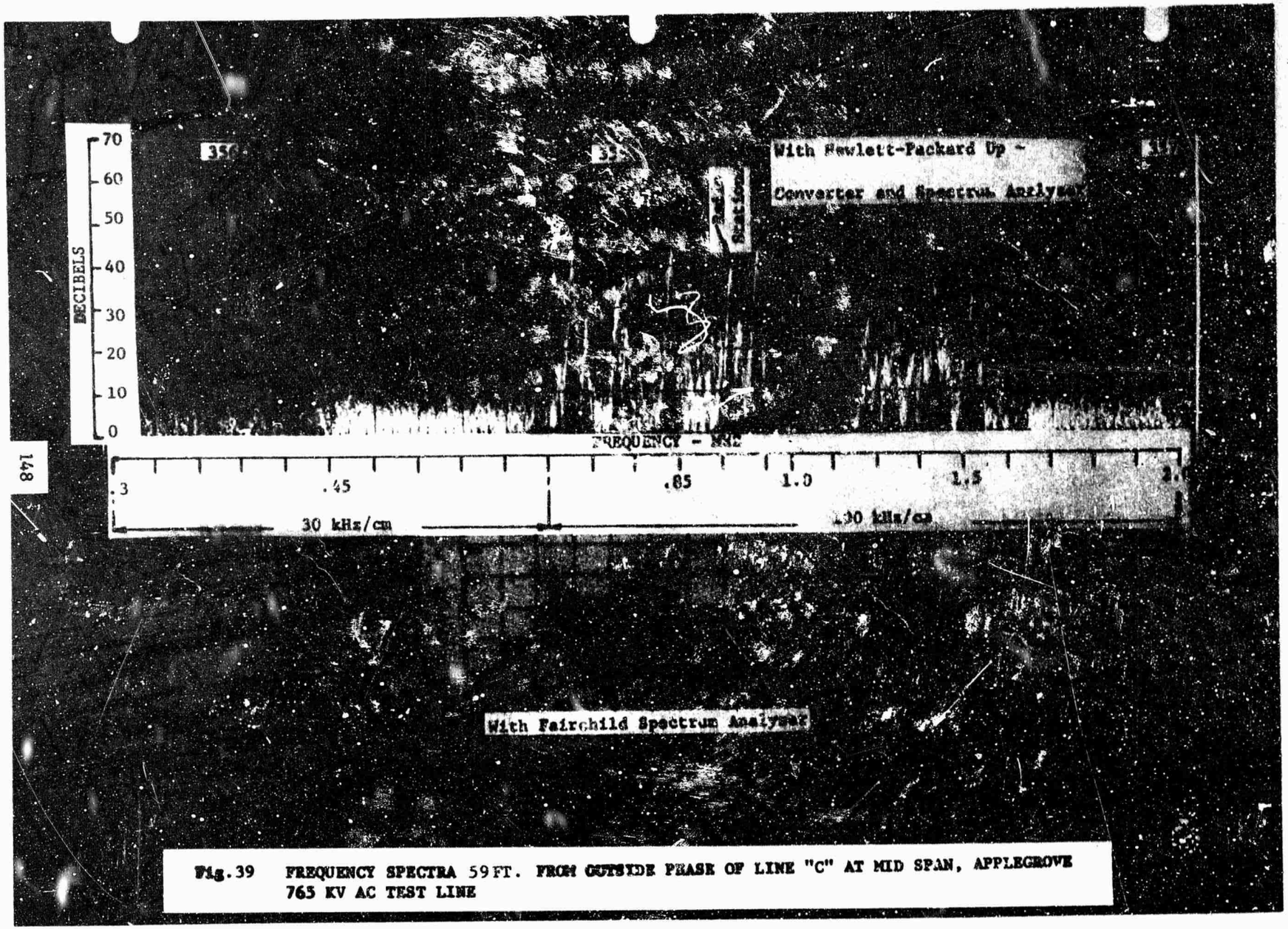


Fig. 39 FREQUENCY SPECTRA 59 FT. FROM OUTSIDE PHASE OF LINE "C" AT MID SPAN, APPLEGROVE 765 KV AC TEST LINE

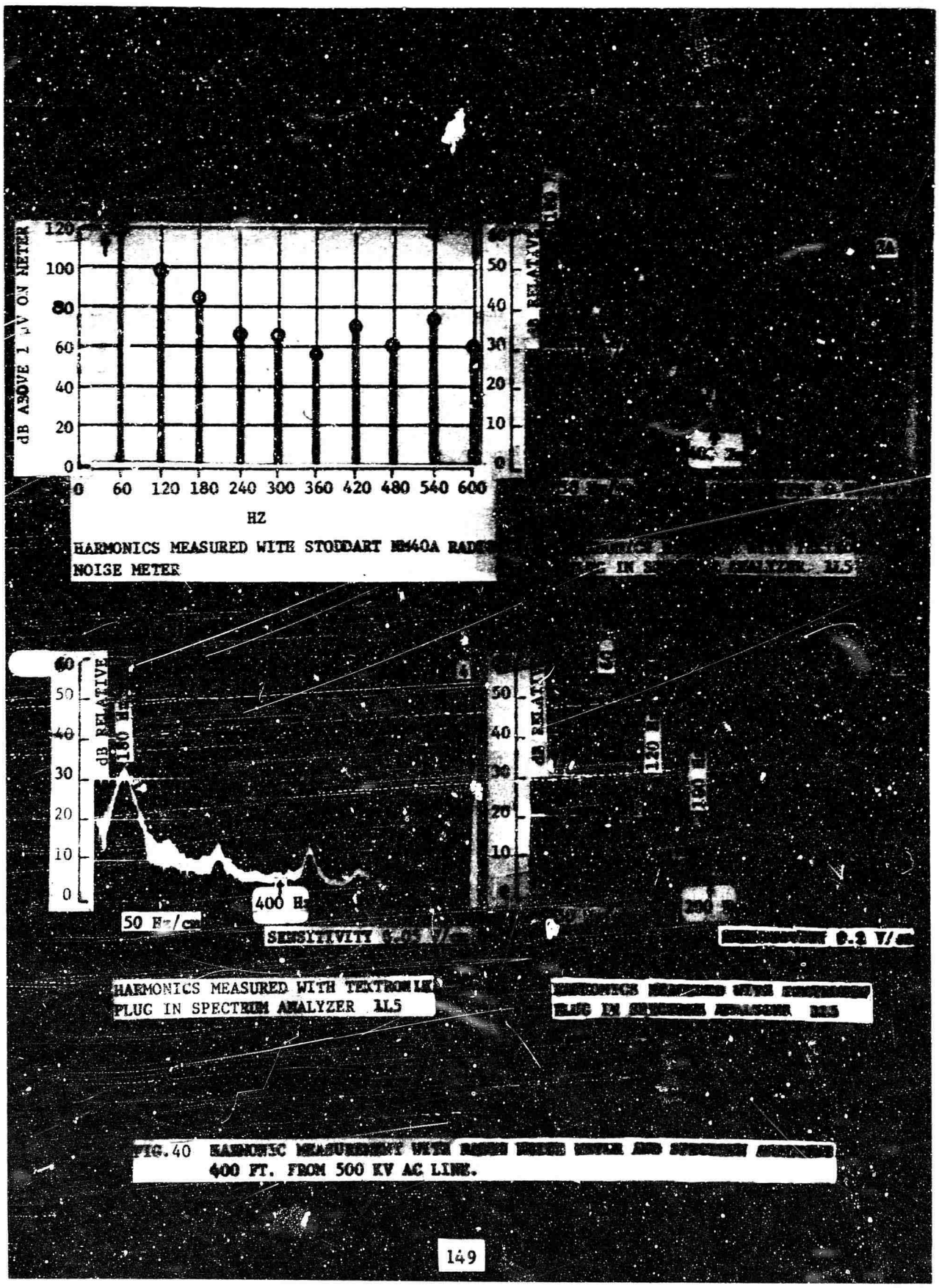


FIG. 40 HARMONIC MEASUREMENT WITH [illegible] AND SPECTRUM ANALYZER 400 FT. FROM 500 KV AC LINE.

HIGH VOLTAGE POWER LINE SITING CRITERIA

APPENDIX II

APPLICATION OF ANTENNA THEORY TO RADIATION OF TRANSMISSION LINES (1.25 - 10.0 GHz)

WESTINGHOUSE ELECTRIC CORPORATION
ELECTRIC UTILITY HEADQUARTERS DEPARTMENT
RESEARCH AND DEVELOPMENT CENTER
PITTSBURGH, PENNSYLVANIA

ROME AIR DEVELOPMENT CENTER
(RADC)
GRIFFISS AIR FORCE BASE
ROME, NEW YORK 13442

CONTRACT AF30602-67-C-0171

CONTENTS
APPENDIX II

	Page No.
List of Figures	152
1. Introduction	153
2. Limitations of Norton's General Equation for a Plane Earth	153
3. Norton's Equation for a Spherical Earth (within the Line of Sight)	154
4. Effect of Terrain and Ground Conditions	155
5. Development Description of Computer Program	156
5.1 Equation Used	156
5.2 Development of Computer Equations for the Reflection Factor R'	158
5.3 Equations for Components of Wave	160
1) Direct Wave	160
2) Ground Reflection	160
5.4 Total Field Factor	161
6. Description of Computer Programs for Field Strengths at a Distance of Several Wavelengths	162
6.1 Program Using Norton's Equation for Spherical Earth (Within Line of Sight) - Distance Variation	162
7. Description of Computer Calculated Attenuation Curves (200 to 100,000 Feet, Plane-Earth)	163
8. Description of Computer-Calculated Attenuation Curves (200 to 100,000 Feet, Spherical Earth, Within Line of Sight)	163
9. Description of Computer Calculated Attenuation Curves (50 to 200 Feet)	164
References	164
FORTRAN Statements for Radiation Propagation Calculations Norton Equation Spherical Earth Distance Variation within Line of Sight)	165

LIST OF FIGURES

APPENDIX II. CONT'D.

		Page No.
Fig. 1	Illustration of Quantities Used in Propagation Equations for Spherical Earth	170
Fig. 2	Illustration of Relation Between Quantities Specifying Ground Conditions.	171
Fig. 3	Attenuation of Field with Distance from Line - Vertical or Horizontal Dipole at 1.25 GHz.	172
Fig. 4	Attenuation of Field with Distance from Line - Vertical or Horizontal Dipole at 2.5 GHz	173
Fig. 5	Attenuation of Field with Distance from Line - Vertical or Horizontal Dipole at 3.75 GHz.	174
Fig. 6	Attenuation of Field with Distance from Line - Vertical or Horizontal Dipole at 5.0 GHz.	175
Fig. 7	Attenuation of Field with Distance from Line - Vertical or Horizontal Dipole at 7.5 GHz.	176
Fig. 8	Attenuation of Field with Distance from Line - Vertical or Horizontal Dipole at 10.0 GHz.	177
Fig. 9	Comparison of Plane and Spherical Earth Calculation for Horizontal and Vertical Field, Transmitting and Receiving Antennas are 90 Feet High (Within Line of Sight).	178
Fig. 10	Comparison of Plane and Spherical Earth Calculation for Horizontal and Vertical Field, Transmitting and Receiving Antennas are 90 and 15 Feet High Respectively (Within Line of Sight).	179
Fig. 11	Comparison of Plane and Spherical Earth Calculation for Horizontal and Vertical Field, Transmitting and Receiving Antennas are 35 and 90 Feet High Respectively (Within Line of Sight).	180
Fig. 12	Attenuation of Horizontal Field with Distance (Calculated Using $\cos^3\psi_1$ and $\cos^3\psi_2$).	181
Fig. 13	Attenuation of Field with Distance for 90 and 15 Feet Transmitting and Receiving Antenna Heights Respectively (50 - 200 Feet).	182
Fig. 14	Attenuation of Field from Fence in the 1 - 10 GHz Range.	183

APPENDIX II

APPLICATION OF ANTENNA THEORY TO RADIATION FROM TRANSMISSION LINES (1.25 - 10.0 GHz)

1. Introduction

This appendix is an extension of Appendix IV Volume I of previous technical report No. RADC-TR-66-606, High Voltage Power Line Siting Criteria, March 1967. The previous mentioned report used computer programs based on Norton's General Equation* for a plane-earth to develop lateral attenuation profiles for the frequency range from approximately 0.015 to 1000 MHz and the distance range of 200 to 100,000 feet. Depending on frequency and the combination of conductor and antenna height, at some point in distance the calculated attenuation changed from the trend of inverse distance to the inverse-distance-squared relationship. Measured data showed comparable results.

In this report the same computer programs were used to calculate lateral profiles for the 1.25 to 10.0 GHz range. Also, a new computer program was written based on Norton's equation[1] for a spherical earth within the line of sight since the transmitting and receiving antennas used in this study are classified by Norton as high antennas, and the curvature of the earth affects the calculated field intensity both at points within and beyond the line of sight. The lateral range of 50 to 100 feet from the source was also calculated and studied since field data had been obtained at 50 feet.

2. Limitations of Norton's General Equation for a Plane-Earth

Considering the earth a flat plane, the field intensity of a small dipole antenna at distances of several wavelengths is calculated by the following:

$$\frac{E}{E_o} = \frac{1}{d}\left[\cos^3\psi_1\, e^{j\frac{2\pi r_1}{\lambda}} + R\cos^3\psi_2\, e^{j\frac{2\pi r_2}{\lambda}} + (1-R)\,F\cos^2\psi_2\, e^{j\frac{2\pi r_2}{\lambda}}\right] \quad (1)$$

(See Appendix IV, Technical Report No. RADC-TR-66-606, on computer equation development for explanation of this equation.)

The above equation (hereafter referred to as Norton"s general equation) does not allow for diffraction loss due to earth curvature and the field strength calculated from it will therefore be increasingly higher or more conservative - at particularly long distances. Gerks[2] and Norton[1] give a rough rule for the distance limit of accuracy for this equation as $50/(f_{MHz})^{1/3}$ miles, hence for 10.0 GHz, a distance limit of 2.3 miles.

---

* References are given at the end of this appendix.

When the receiving antenna is high ($h > 2000/f_{MHz}^{2/3}$ ft.) the curvature of the earth will modify the approximations that are normally made in calculating field intensity both at areas within and beyond the line of sight. Norton states that at sufficiently large antenna heights beyond the line of sight the field intensity increases exponentially with the height rather than linearly as occurs with medium antenna heights. ($h < 2000/f_{MHz}^{2/3}$ ft., which for 1000 MHz is only 20 feet, while for 10 GHz it is 4.3 feet.)

Within the line of sight, the curvature of the earth can still have several effects on the propagation of radio waves for high transmitting or receiving antennas. The reflection coefficient of the ground-reflected wave is different for the curved surface of the earth than for a plane surface. Also, since the ground-reflected wave is reflected against the curved surface of the earth, its energy is diverged more than would be indicated by the inverse-distance law discussed previously. This energy divergence can be taken into account by applying a divergence factor D. This factor has the effect of reducing the ground-reflected component of the space wave, the effect on the reflection coefficient being small for moderate distances. The overall result is, therefore, a smaller oscillation of the field intensity about the free-space value, but with maximum and minimum occurring at essentially the same distances as those if the divergence factor is not included.

3. Norton's Equation for a Spherical Earth (within the Line of Sight)

When antennas are high (1) must be modified as follows to calculate the ground wave at points within the line of sight.

$$\frac{E}{E_o} = \frac{1}{d}\left[\cos^3\psi_1' \; e^{j2\pi r_1'/\lambda} + DR' \cos^3\psi_2' \; e^{j2\pi r_2'/\lambda} + (1 - R')\, F \cos^2\psi_2' \cos^2\psi_2' \; e^{j2\pi r_2'/\lambda}\right] \qquad (2)$$

where

$$\tan\psi_2' > (\lambda/2\pi ka)^{1/3}$$

(See section on computer equetion development for explanation of this equation.)

The angles ψ_1' and ψ_2' which are the angles between the direct ray and a plane and the ground-reflected rey and a plane respectively are functions of the heights of the antenna to the plane which are smaller than the actual antenna heights.

As Norton[1] points out, equation (2) needs to be used in place of (1) only for high antennas. It is also restricted to points within the line of sight which are the ones of interest.

The line of sight distance can be calculated as:

$$dLs = \sqrt{2Rh_1} + \sqrt{2Rh_2}$$

where R is the effective radius of the earth, and h_1 and h_2 are the heights of the two antennas. The refractive index of the air decreases with the height above earth, which has the effect of refracting radio waves downward towards the earth. This effect is included in the field calculation by using an earth radius larger than the actual, experimental evidence[1] indicating an effective radius about 4/3 the actual, or about 5280 miles.

4. Effect of Terrain and Ground Conditions

Where propagation is over a rough surface, multipath reflections occur, especially at the higher frequencies, and the resultant field pattern is no longer than that determined by the combination of the direct wave with one reflected wave. For rough terrain, movement of the receiving antenna causes large variations at higher frequencies in the magnitude and phase of ground reflections. For high receiving antennas, such as in airplanes, the field pattern over mountainous terrain can show a complete absence of any interaction with the ground reflection.

A reflecting surface may be considered flat if surface irregularities are of such magnitude as not to cause path differences larger than some small fraction of the wavelength, and Day and Trolese[3] give the following limit definition:

$$\frac{H \cos \theta}{\lambda} < 1$$

where H is the height of the surface irregularities, λ the wavelength, and θ the angle of incidence.

For the highest frequency covered by this study (10 GHz) if cos θ is taken very nearly equal to 1.0 this definition would limit the height of the surface irregularities to something very much less than 0.1 foot.

For a more detailed discussion of these effects, see Appendix IV, Technical Report No. RADC-TR-66-606.

5. Development Description of Computer Program

5.1 Equation Used

The basic equation used is Norton's equation (28)[1] for a spherical earth

$$\frac{E}{E_o} = \frac{1}{d}\left[\underbrace{\text{Cos}^3\psi_1' \; e^{j2\pi r_1'/\lambda}}_{\text{direct wave}} + \underbrace{DR' \; \text{Cos}^3\psi_2' \; e^{j2\pi r_2'/\lambda}}_{\text{ground-reflected wave}}\right.$$

$$\left. + \underbrace{(1 - R')\, F\, \text{Cos}^2\psi_2' \; e^{j2\pi r_2'/\lambda}}_{\text{Surface Wave}}\right]$$

Space Wave

Norton says this equation is limited to distances within the line of sight such that

$$\tan\psi_2' > (\lambda/2\pi ka)^{1/2}$$

The quantities d, d_1, d_2, r_1', r_2', h_1, h_2, h_1', h_2', ψ_1', and ψ_2' are as indicated in Fig. 1; and ka are the wave length of the frequency of interest and the effective radius of the earth respectively. R' is the spherical-wave reflection coefficient of the ground, and D is the divergence factor.

From Fig. 1, it can be shown that

$$r_1' = \frac{d}{\text{Cos}\psi_1'} \qquad r_2' = \frac{d}{\text{Cos}\psi_2'}$$

$$\frac{2\pi r_{1,2}'}{\lambda} = \frac{2\pi(f_{MHz})}{984.2344}$$

$$r_{1,2}' = 0.0063838(f_{MHz})r_{1,2}' = \underline{\text{ANG11,22*}}$$

---

* Underlined quantities are symbols used in Computer Program

$$h_1' = h_1 - \frac{d_1^2}{2ka} \quad , \quad h_2' = h_2 - \frac{d_2^2}{2ka}$$

$$\tan\psi_2' = \frac{h_1' + h_2'}{d} = \frac{h_1'}{d} = \frac{h_2'}{d}$$

$$\tan\psi_1' = \frac{h_1' - h_2'}{d}$$

Solving these equations for d_1 in terms of known quantities d, h_1, h_2 and ka results in the following cubic equation

$$d_1^3 - 1.5\, d\, d_1^2 + 0.5 \left[d^2 - 2ka\,(h_1 + h_2) \right] d_1 + ka\, h_1 d = 0$$

This has the form

$$y^3 + P_1 y^2 + P_2 y + P_3 = 0$$

By substituting for y the value, $Z - \frac{P_1}{3}$. [4]

Then $Z^3 + aZ + b = 0$

$a = 1/3\,(3\,P_2 - P_1^2)$ and

$b = 1/27\,(2\,P_1^3 - 9P_1P_2 + 27P_3)$

The real root of interest

$$Z = -\sqrt{-\frac{a}{3}} \cos\frac{\Phi}{3}$$

where

$$\cos\Phi = -b/2 \pm \sqrt{-\frac{a^3}{27}}$$

Basic parameters not a function of distance used by Norton are:

$$X = \frac{17.9731 \times 10^{15} \sigma_{emu}}{f_{MHz}}$$

$$\text{Cos } b'' = \frac{X}{\sqrt{\epsilon^2 + X^2}} = \frac{1}{\sqrt{1 + \frac{\epsilon^2}{X^2}}}$$

as indicated by Fig. 2, where σ is the ground conductivity expressed in millimho-meters/meter square and ϵ is the dielectric constant of the ground referred to air as unity.

A basic parameter which is a function, additionally, of distance is given by Norton (see Fig. 2):

1) $$\text{Cos } b' = \frac{X}{\sqrt{(\epsilon - \text{Cos}^2 \psi_2')^2 + X^2}}$$

5.2 Development of Computer Equations for the Reflection Factor R'

From Norton,[1] the reflection factor for a spherical earth is given as:

$$R' = \frac{\text{Sin}\psi_2' \left[\frac{X \cos b'}{\text{Cos}^2 b''}\right]^{1/2} e^{j(\pi/4 - b/2)} - 1}{\text{Sin}\psi_2' \left[\frac{X \cos b'}{\text{Cos}^2 b''}\right]^{1/2} e^{j(\pi/4 - b/2)} + 1} \quad \text{(Vertical Polarization)}$$

$$R' = \frac{\text{Sin}\psi_2' \left[\frac{\text{Cos } b'}{X}\right]^{1/2} e^{-j(\pi/4 - b'/2)} - 1}{\text{Sin}\psi_2' \left[\frac{\text{Cos } b'}{X}\right]^{1/2} e^{-j(\pi/4 - b'/2)} + 1} \quad \text{(Horizontal Polarization)}$$

also

$$-j(\pi/4 - b'/2) = j(\pi/4 - b/2)$$

Use Computer Program Symbols

$\underline{TANPH2}$ = $\tan\psi_2'$

$\underline{HD}$ $\quad$ SIN(ATAN)TANPH2))

THETA = $(\pi/4 - b_{/2}) = 0.785398 - \frac{BW}{2}$

For vertical polarization

$$R' = \frac{(HD)\ (XB)\ [\text{COS (THETA)} + j\text{SIN (THETA)}]\ -1}{(HD)\ (XB)\ [\text{COS (THETA)} - j\text{SIN (THETA)}]\ +1}$$

$$\underline{Q} = (HD)\ (XB)$$

$$R' = \frac{\left[\begin{array}{l}(Q\ \text{COS (THETA)} - 1)\ (Q\ \text{COS (THETA} + 1) + Q^2\text{SIN}^2\ \text{(THETA)} \\ +j\ (Q\ \text{SIN (THETA)} \qquad (Q\ \text{COS (THETA} + 1) - (Q\ \text{COS (THETA)} - 1)\end{array}\right]}{(Q\ \text{COS (THETA)} + 1)^2 + Q^2\ \text{SIN}^2\ \text{(THETA)}}$$

$$R' = \frac{Q^2\ \text{COS}^2\ \text{(THETA)} - 1 + Q^2\ \text{SIN}^2\ \text{(THETA)} + j\ 2Q\ \text{SIN (THETA)}}{Q^2\ \text{COS}^2\ \text{(THETA)} + 2Q\ \text{COS (THETA)} + 1 + Q^2\ \text{SIN}^2\ \text{(THETA)}}$$

$$= \frac{(Q^2 - 1) + j2Q\ \text{SIN (THETA)}}{(Q^2 + 1) + 2Q\ \text{COS (THETA)}}$$

The real part of the numerator is then

$\underline{RR} = (Q^2 - 1) = \underline{QS} - 1$,

the imaginary part

$\underline{RI} = 2Q\ \text{SIN (THETA)}$

and the denominator

$\underline{RDEN} = (Q^2 + 1) + 2Q\ \text{COS (THETA)}$

$= QS + 1 + 2Q\ \text{COS (THETA)}$

for horizontal polarization

$\underline{HD} = \text{SIN}\psi_2'$

$\underline{XB} = \left[\frac{\text{Cos } b'}{X}\right]^{1/2}$

$\underline{Q}$ = (HD) (XH)

$\underline{BB}$ = $b = 2b' = b' = 2\ \cos^{-1}(\cos b'') - \cos^{-1}(\cos b')$

$\underline{BPCOS}$ = $\cos b'$

$\underline{BPPCOS}$ = $\cos b''$

$\underline{X}$ = X

$\underline{TANPH1}$ = $\tan\psi_1'$

$\underline{TANPH2}$ = $\tan\psi_2'$

$\underline{HD}$ = $\sin(\tan^{-1}(TANPH2))$

$\underline{HC}$ = h_1 , $\underline{HA}$ = h_2

$\underline{HCC}$ = h_1' , $\underline{HAA}$ = h_2'

$\underline{R22}$ = r_2' , $\underline{R11}$ = r_1'

5.3 Equations for Components of Wave

1) Direct Wave

$$\cos^3\psi_1' \; e^{j2\pi r_1'/\lambda} = \cos^3\psi_1' \left(\cos\frac{2\pi r_1'}{\lambda} + j\sin\frac{2\pi r_1'}{\lambda}\right)$$

$$DWCR = \left(\frac{D}{R11}\right)^3 \cos\frac{2\pi r_1'}{\lambda} = \underline{DWK} \times \cos(ANG11)$$

$$DWCI = \left(\frac{D}{R11}\right)^3 \sin\frac{2\pi r_1'}{\lambda} = \underline{DWK} \times \sin(ANG11)$$

2) Ground Reflection

$$R' \cos^3\psi_2' \; e^{j2\pi r_2'/\lambda}$$

$$= \frac{RR + iRI}{RDEN} \cos^3\psi_2' \left(\cos\frac{2\pi r_2'}{\lambda} + j\sin\frac{2\pi r_2'}{\lambda}\right)$$

$\cos\psi_2'$ = COS (ATAN (TANPS2))

= $\underline{COPH2}$

$\cos^2\psi_2'$ = $\underline{SCOPH2}$

$\underline{2\pi r_2'}$ = ANG22

GRK = (COPH2) (SCOPH2)

Real part of ground reflectad wave = GRCR

= GRK (RR COS (ANG22) - RI SIN (ANG22)/RDEN

Imaginary part of component

= GRCI

= GRK (RR Sin (ANG22) + RI Cos (ANG22)/RDEN

Include Divergence

Then GRCR = DIVF (GRCR)

and GRCI = DIVF (GRCI)

The program has also been written with the option of letting

DWK = COPH2 = SCOPH2 = 1.0

The surface wave attenuation factor (F) is the same as used in Norton's General Equation for a Plane-Earth. The surface wave component is also the same except for the use of Cos Ψ_2, R', and ANG22 as developed in this section (See Appendix IV, Technical Report No. RADC-TR-66-606, High Voltage Power Line Siting Criteria).

5.4 Total Field Factor

The total field at some distance then becomes the vectorial sum of the real and imaginary parts of the three components:

Sum of real parts = R = DWCR + GRCR + SWR

Sum of imaginary parts = U = DWCI + GRCI + SWI

The magnitude of the total field factor is then

FIELD = $T^2 + U^2$

Or, calculated in decibels is

FIELD = 10 $\log_{10} T^2 + U^2$)

The ratio of the field intensity at a given distance is that of free space at a unit distance, or $\frac{E}{E_o}$, for each polarization is

$$\text{FIELD} = \text{FIELD} - 20.0 \log_{10} D$$

This value is printed out for horizontal and vertical dipole along with D, DI, HCC, HAA, DIVF, TANPH2 and COPH2.

6. Description of Computer Programs for Field Strengths at a Distance of Several Wavelengths

The computer programs used in the previous report were slightly modified for use on the Control Data Corporation 6600. These programs assumed the noise source to be an elevated transmitter and only a single phase conductor of the power line and its image are considered. The equation utilized were for the electric field.

6.1 Program Using Norton's Equation for Spherical Earth (Within Line of Sight) - Distance Variation

This program calculates the vertical and horizontal fields within the line of sight over a spherical earth. The noise source is considered a vertical electric doublet and a vertical magnetic doublet for the vertical and horizontal field calculations respectively which includes the cube of the cosine of the angle (cosine ψ_1, and cosine ψ_2 in the earlier description). The program also will calculate the fields with the cosines equal to one.

The following input cards with their respective format must be specified for each case.

1. Title card (any title of 71 characters or less; first space a blank).

2. Card specifying:

   a. Conductor height in feet.

   b. The receiving antenna height above ground.

   c. Frequency in MHz.

   d. The dielectric constant, and

   e. The ground conductivity in milli-mhos per meter or millimhometers per square meter.

The Fortran format for this card is as follows: 2F5.1, F9.3, 2F7.1.

3. Card specifying:

   a. The starting distance (do not start with zero) in feet.

b. The ending distance in feet.

c. The distance increment in feet.

d. A "Flag" character.

This card has a format of 3F8.1, I6.

If the character 1 is inputted for item (d), the program will set the cosines equal to one. If item (d) is left blank, the program will use the cosines cubed.

7. Description of Computer Calculated Attenuation Curves (200 to 100,000 Feet, Plane-Earth)

Figures 3 through 8 are calculated distance attenuation curves for frequencies from 1.25 to 10.0 GHz from 200 feet to 100,000 feet. Attenuation was calculated for vertical and horizontal antennas using Norton's general equation ($\cos^3\psi_1$ and $\cos^3\psi_2$ for direct and ground-reflected waves respectively). A ground dielectric constant of 30 and a conductivity of 20 millimhometers per meter square was assumed. See Appendix IV, Technical Report No. RADC-TR-66-606.

These curves were plotted as in the above mentioned report; therefore a trend line was drawn along the crests of the maximum points. This line which is labeled "approximate" follows this inverse distance relationship and has been used in the attenuation curves from 200 to 100,000 feet. Thus, values for any given curve may be below this "approximate" base value at 200 feet, but the method is more appropriate for establishing attenuation over the range of distance.

At these frequencies and for these distances, the difference between the calculated vertical and horizontal fields was insignificant; therefore Figures 3 through 8 are for both vertical and horizontal polarization. Depending on frequency and the combination of conductor and antenna heights, at some point in distance the calculated attenuation changes from the trend of inverse distance to the inverse-distance-squared relationship. The curves are, therefore, an aid in determining where this change takes place.

8. Description of Computer-Calculated Attenuation Curves (200 to 100,000 Feet, Spherical Earth, Within Line of Sight)

Figures 9, 10 and 11 are a comparison of calculated distance attenuation curves assuming a plane-earth and a spherical-earth for 1.25, 5.00 and 10.0 GHz. Figure 9 is for a transmitting and receiving antenna height of 90 feet; Fig. 10 is for a transmitting and receiving antenna height of 90 and 15 feet respectively, and Fig. 11 is for a transmitting and receiving antenna height of 35 and 90 feet respectively. These heights were picked as typical of what may be encountered in practice.

The curves as calculated for a spherical earth do not vary from those calculated for a plane-earth until about 4000 feet where the attenuation is faster than the inverse distance squared relationship. The curves

show that the degree of attenuation depends upon frequency and antenna height. As either frequency or antenna height is increased, the attenuation will be greater beyond the distance where the inverse distance relationship changes to some other relationship.

Norton's equation for a spherical earth, of course, assumes a perfect sphere with uniform ground constants. In practice, at these microwave frequencies, the effect of the terrain has a tremendous effect on the calculated value as was discussed in section 4 of this appendix. The theory will give average fields encountered in practice. A conservative practice would be to use the plane-earth calculation. An even more conservative practice would be to use the inverse distance relationship and this is recommended.

9. Description of Computer Calculated Attenuation Curves (50 to 200 Feet)

If the transmitting and receiving antenna are the same height above ground, the calculated crest values of field strength (Norton's equation)[1] will attenuate as the inverse distance relationship for the distance range of 50 to 200 feet. Since the $\cos^3\psi_1$ term is a function of the difference in antenna heights, the curves will tend to saturate in this range, the degree of saturation dependent upon the difference. See Fig. 12. The $\cos^3\psi_{1,2}$ terms are a result of the type of transmitting antenna that Norton uses to develop his equation, a vertical electric doublet for vertical polarization and a vertical magnetic doublet for horizontal polarization.

The field data obtained with the 5/16-inch gap attenuated as the inverse distance relationship. By setting the Cosines equal to 1.0 Norton's equation will give a similar relationship. Figure 13 shows this result for both the vertical and horizontal dipole and for $\cos^3\psi_{1,2}$ with transmitting and receiving antenna heights of 90 and 15 feet respectively.

Based on the field data obtained in this study, if measurements are made 50 feet laterally from a gap, the data should be corrected to other distances as the inverse distance relationship.

REFERENCES

1. K. A. Norton, "The Calculation of a Ground Wave Field Intensity Over a Finite Conducting Spherical Earth," Proc. IRE, Vol. 29, pp. 623-639, December, 1941.

2. T H. Gerks, "Use of a High-Speed Computer for Ground Wave Calculations " IRE Trans. on Antennas and Propagation, May, 1962, pp. 292-299.

3. J P. Day and L. G. Trolese, "Propagation of Short Radio Waves over Desert Terrain," Proc. IRE, Feb., 1950, pp. 163-175.

4. Standard Mathematical Tables, (book) 11th ed., Chemical Rubber Publishing Company, 1957, pp. 344-345.

FORTRAN Statements

For

Radiation Propagation Calculations

Norton Equation

Spherical Earth

Distance Variation

(Within Line of Sight)

```
      PROGRAM MAIN(INPUT,OUTPUT,TAPE5=INPUT,TAPE6=OUTPUT)
32000 FORMAT (1H1                                                    )NEW PAGE
32100 WRITE (6,32000)
31000 FORMAT (93H0 RADIO HIGH - FREQUENCY PROPAGATION CALCULATIONS
     1(SPHERICAL EARTH WITHIN LINE OF SIGHT))
      WRITE(6,31000)
30000 FORMAT (72H                                                    BLANK
     1               )                                               TITLE
      READ (5,30000)
      WRITE(6,30000)
10000 FORMAT (2F5.1,F9.3,2F7.1)
      READ (5,10000)HC,HA,FREQ,DIELC,COND                            INPUT
10001 FORMAT (15H CONDUCTOR HT.  ,F5.1,14H  ANTENNA HT. ,F5.1, 8H  FREQ.
     1,F9.3,4H MHZ  )                                               WRITE
      WRITE(6,10001)HC,HA,FREQ                                       INPUT
10002 FORMAT (20H DIELECTRIC CONSTANT,F7.1,18HEARTH CONDUCTIVITY ,F6.1)
      WRITE(6,10002)DIELC,COND                                       INPUT
10003 FORMAT (3F8.1,I6)
      READ (5,10003)SD,ED,DI,L
10007 FORMAT(72H                                                   (COSI
     1NES SET TO ONE) )
      IF (L) 210,210,402
402   WRITE (6,10007)
10004 FORMAT(91H0        D       D1       ANT HT  COND HT DIFF  TANPH2   CO
     1PH2      VERT/DIST.       HORIZ/DIST.)
10008 FORMAT(91H       (FT)     (FT)      HAA(FT) HCC(FT)
     1              (DB)              (DB) )
  210 WRITE (6,10004)
      WRITE (6,10008)
      X=17.9731*COND/FREQ
      BPPCOS=1.0/SQRT(1.0+((DIELC/X)*(DIELC/X)))
      D=SD
      NI=INT((ED-SD)/DI)+1.
      DO 500 M=1,NI
      P1=-1.5D
      P2=0.5*(D*D-(2.0*5280.0*5280.0)*(HC+HA))
      P3=5280.0*5280.0*HC*D
      A=(3.0*P2-P1*P1)/3.0
      B=(2.0*P1*P1*P1-9.0*P1*P2+27.0*P3)/27.0
      PHICOS=(-B/2.0)/SQRT((A**3)/(-27.0))
      Z=-2.0*SQRT(A/(-3.0))*COS(ACOS(PHICOS/3.0))
      D1=Z-(P1/3.0)
      HCC=HC-(D1*D1)/(2.0*5280.0*5280.0)
      TANPH2=HCC/D1
      ANGLIM=(.186/(FREQ*6.2831*5280.0))**.3333
      IF(TANPH2-ANGLIM)32100,32100,1
```

```
     1 CONTINUE
       D2=D-D1
       HAA=HA-(D2**2)/(2.0*5280.0*5280.0)
       TANPH1=(HCC-HAA)/D
       COPH1=COS(ATAN(TANPH1))
       COPH2=COS(ATAN(TANPH2))
       R11=D/COPH1
       R22=D/COPH2
       ANG11=0.0063938*FREQ*R11
       ANG22=0.0063938*FREQ*R22
       PK=0.5*ANG22
       DIVF=1.0/SQRT(1.0+((2.0*D1*D2)/(5280.0*5280.0*TANPH2*D)))
       HD=SIN(ATAN(TANPH2))
       SCOPH2=(COPH2)*(COPH2)
       IF (L) 301,301,302
  302  COPH1=1.0
       COPH2=1.0
       SCOPH2=1.0
  301  BPCOS=1.0/ SQRT(1.0+((DIELC-SCOPH2)/X)**2)
       DWK=COPH1**3
       GRK=SCOPH2*COPH2
       SWK=SCOPH2
       DWCR=DWK*COS(ANG11)
       DWCI=DWK*SIN(ANG11)
C      GROUND-REFLECTED WAVE COMP. CALC.-VERTICAL POLARIZED
  600  XH=SQRT(X*HPCOS/(BPCOS*BPPCOS))
       BN=2.0*ACOS(HPPCOS)-ACOS(BPCOS)
       J=1
       GO TO 200
C      GROUND-REFLECTED WAVE COMP. CALC.-HORIZONTAL POLARIZED
  201  XH=SQRT(BPCOS/X)
       BN=3.14159-ACOS(BPCOS)
  200  THETA=0.785398-0.5*BN
       Q=HD*XH
       QS=Q**2
       PN=PK/(XH*XH)
       RDEN=QS+2.0*Q*COS(THETA)+1.0                                    REFLECT
       RR=QS-1.0                                                        FACTOR
       RI=2.0*Q*SIN(THETA)
       GRCR=GRK*(RR*COS(ANG22)-RI*SIN(ANG22))/RDEN
       GRCI=GRK*(RR*SIN(ANG22)+RI*COS(ANG22))/RDEN
       GRCR=DIVF*GRCR
       GRCI=DIVF*GRCI
       IF (L) 601,601,300
  300  SWR=0.
       SWI=0.
       GO TO 602
```

```
C       SURFACE-WAVE COMPONENT
  A01   RRM=1.0-(RR/RDEN)
        RIM=(RI/RDEN)
        RRMS=RRM*RRM
        RIMS=RIM*RIM
        PBDEN=(RRMS+RIMS)**2
        PBRN =(RRMS-RIMS)*COS(BN)-2.0*RIM*RRM*SIN(BN)
        PBIN =2.0*RIM*RRM*COS(BN)+(RRMS-RIMS)*SIN(BN)
        BC=ATAN(PBIN/PBRN)
        PC=4.0*PN*SQRT(PBRN*PBRN+PBIN*PBIN)/PBDEN
        IF (PC-10.0) 201,201,202
C       SURFACE ATTENUATION FACTOR                                  PCEQTEN
  201   HR=0.0
        HI=0.0
        C=1.0
        SN=1.0
        COM=1.0
        DO 2011 I=1,35
        E=I
        C=(2.0*E-1.0)
        COM=(2.0*PC)*COM/C
        SN=-SN
        HR=SN*COM*COS(E*BC)+HR                                      REALFACT
  169
 2011   HI=SN*COM*SIN(E*BC)+HI                                      IMAGFACT
        A=SQRT(3.14159*PC)/EXP(PC*COS(BC))
        B=0.5*BC-PC*SIN(BC)
        FR=1.0-A*SIN(B)+HR                                          REALATTN
        FI=A*COS(B)+HI                                              IMAGATTN
        GO TO 204                                                   PCCVTEN
  202   HR=0.0
        HI=0.0
        C=1.0
        COM=1.0
  901   DO 2021 I=1,20
        E=I
        C=(2.0*E-1.0)
        COM=C/(2.0*PC)*COM
        HR=COM*COS(E*BC)+HR
 2021   HI=COM*SIN(E*BC)+HI
 2023   FR=-HR
        FI=-HI
C       SURFACE WAVE CALC.
  204   SWK1=RRM*FR+RIM*FI
        SWK2=RRM*FI-RIM*FR
        SWR=SWK*(SWK1*COS(ANG22)-SWK2*SIN(ANG22))
        SWI=SWK*(SWK2*COS(ANG22)+SWK1*SIN(ANG22))
C       TOTAL FIELD CALC.
```

```
  602   T=D+CR+GRCR+SWR
        U=DWCI+GRCI+SWI
        FIELD=10.0*ALOG10(T*T+U*U)
        FIEDD=FIELD-20.0*ALOG10(D)
10005 FORMAT(4X,4FH.1,3F8.3,F16.4)
10006 FORMAT(1H+,76X,F16.4)
        IF (J) 206,206,205
  205 WRITE (6,10005) D,DI,HAA,HCC,DIVF,TANPH2,COPH2,FIEDD
        J=J-1
        GO TO 207
  206 WRITE (6,10006) FIEDD
  500 D=D+DI
  501 GO TO 32100
        END
```

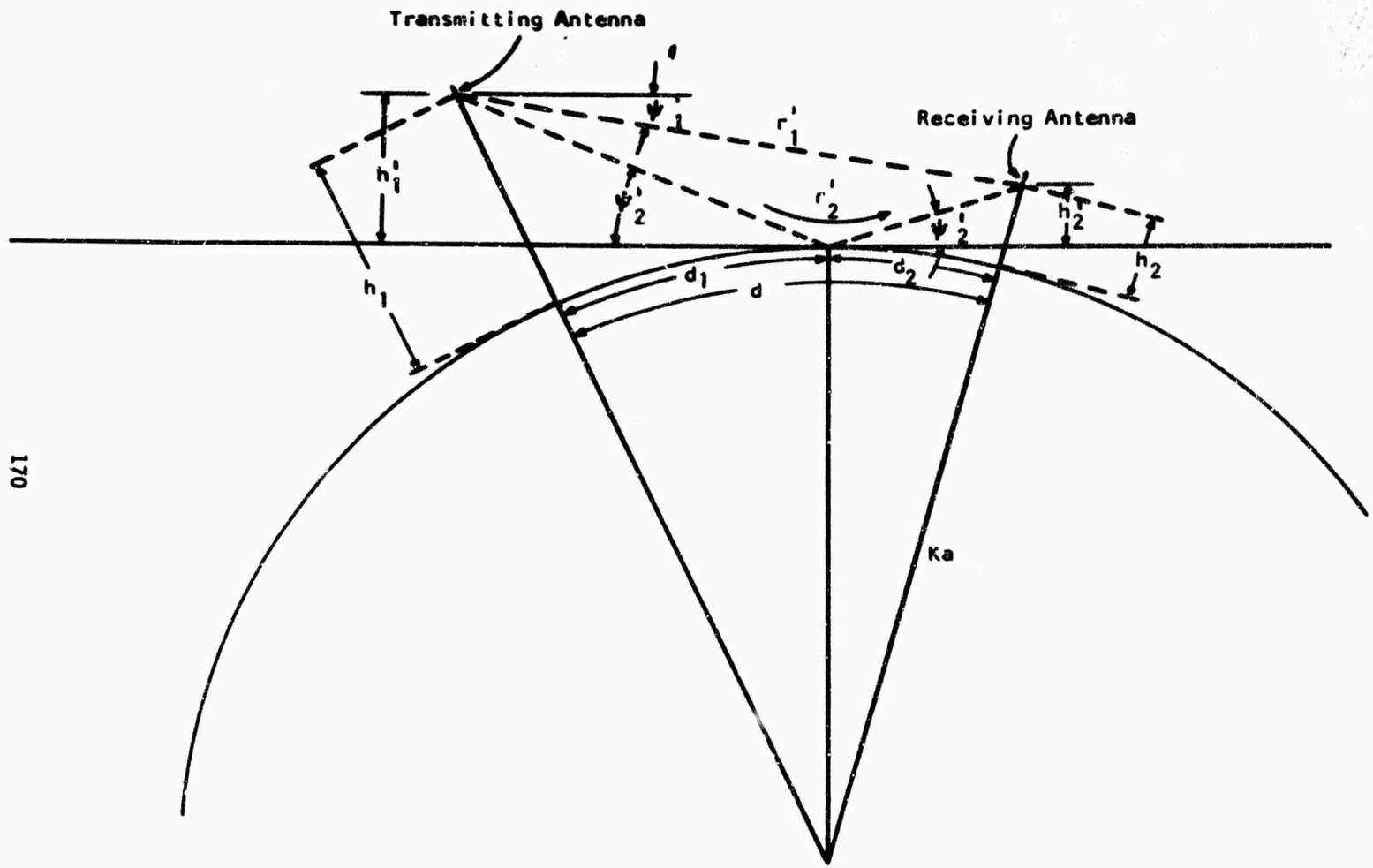


Fig. 1—Illustrations of quantities used in propagation equations for spherical earth

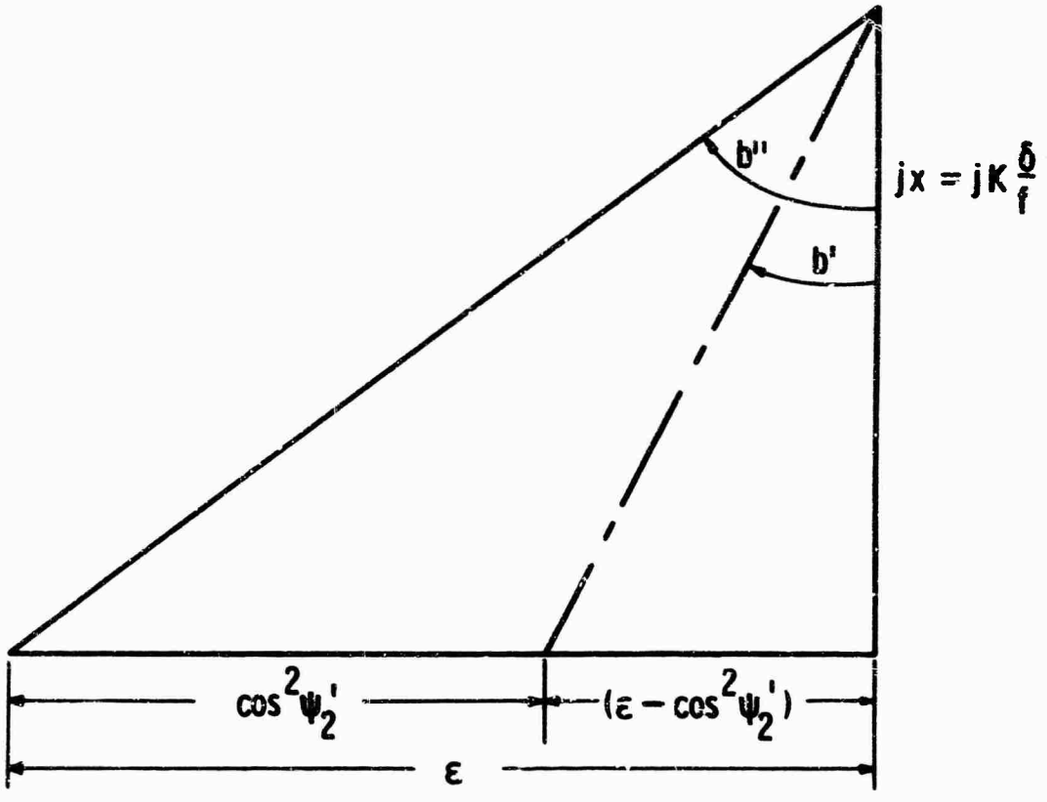


Fig. 2—Illustration of relation between quantities specifying ground conditions

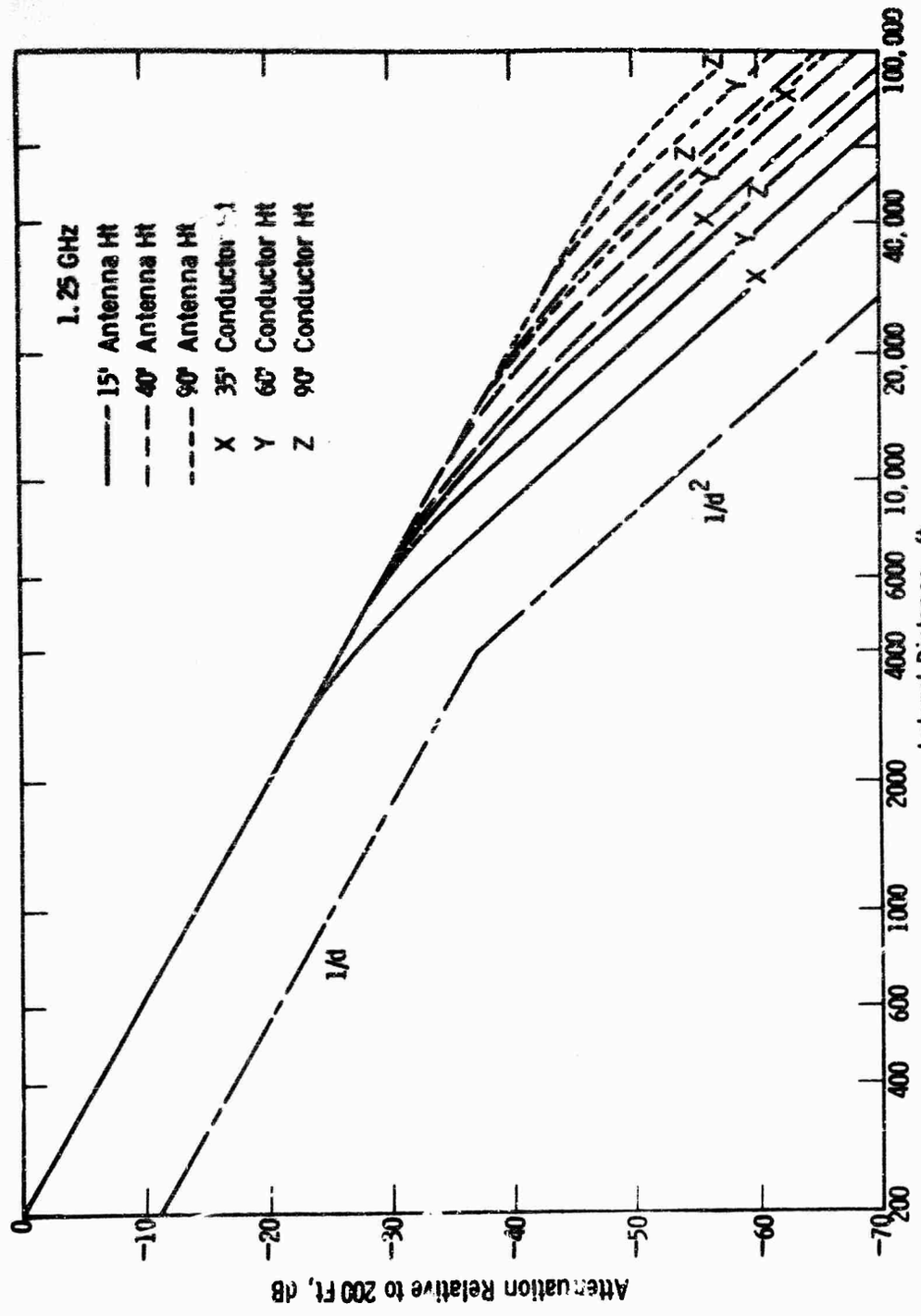


Fig. 3 --Attenuation of field with distance from line-vertical or horizontal dipole

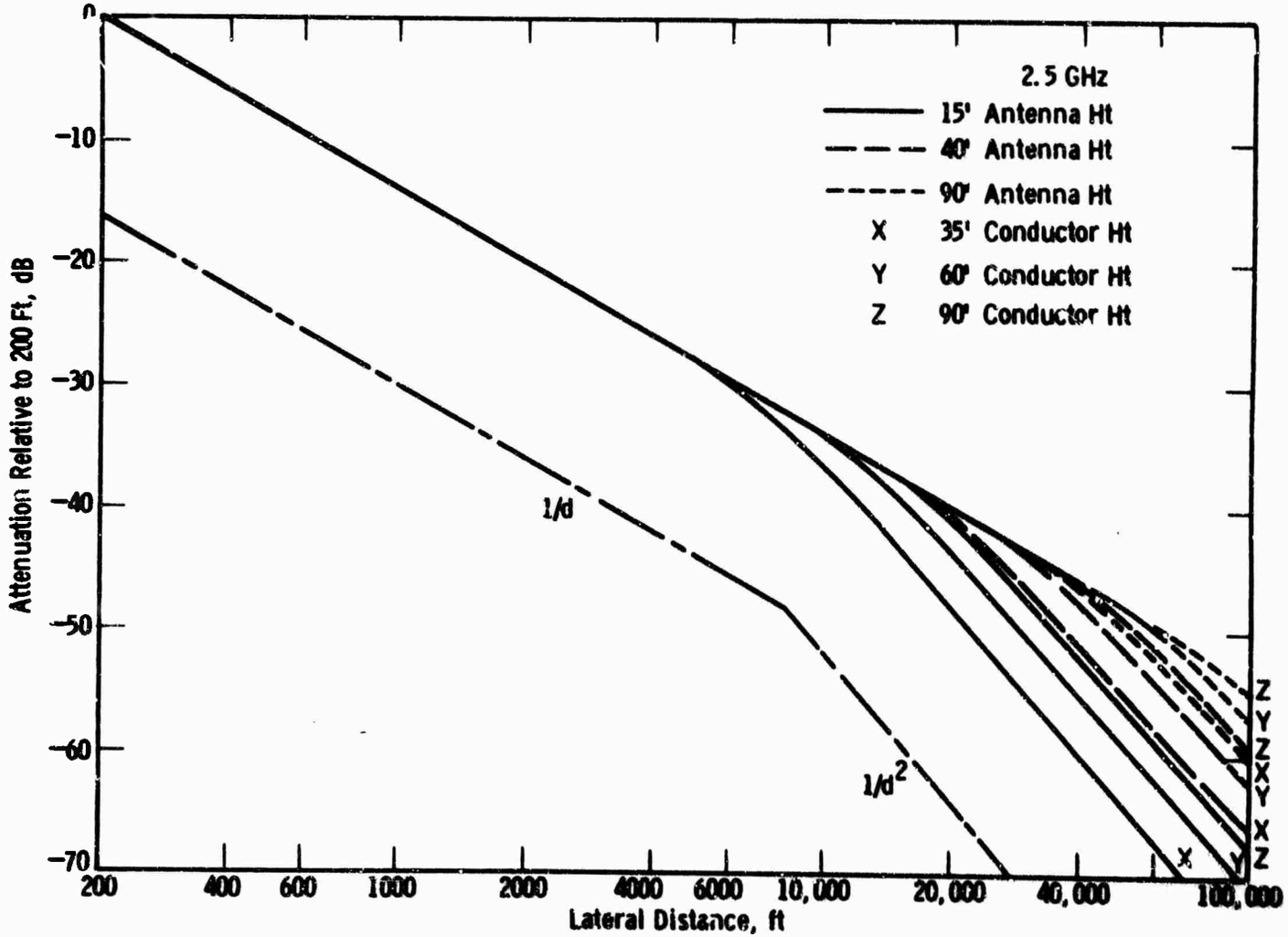


Fig. 4 —Attenuation of field with distance from line-vertical or horizontal dipole

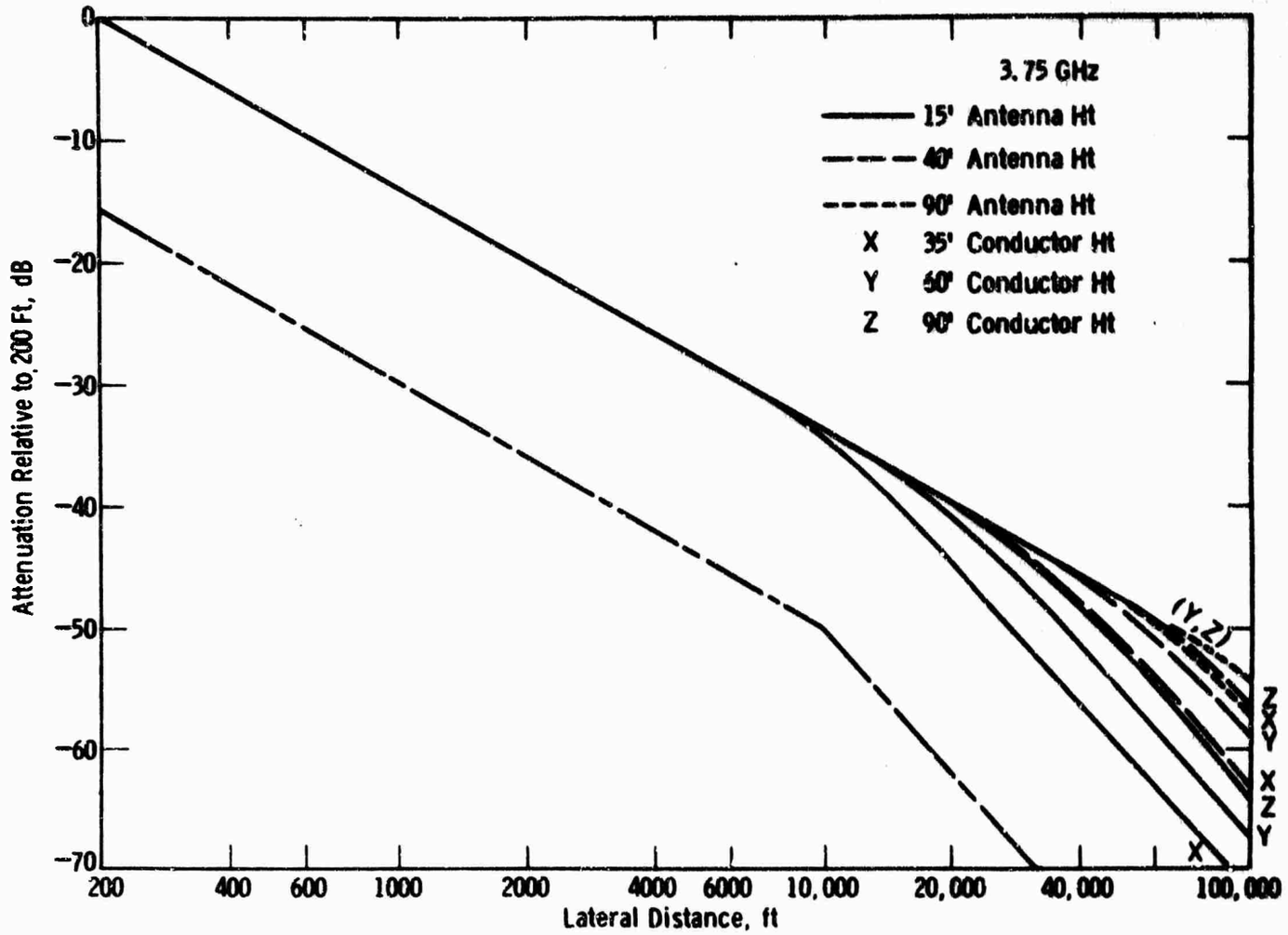


Fig. 5 —Attenuation of field with distance from line-vertical or horizontal dipole

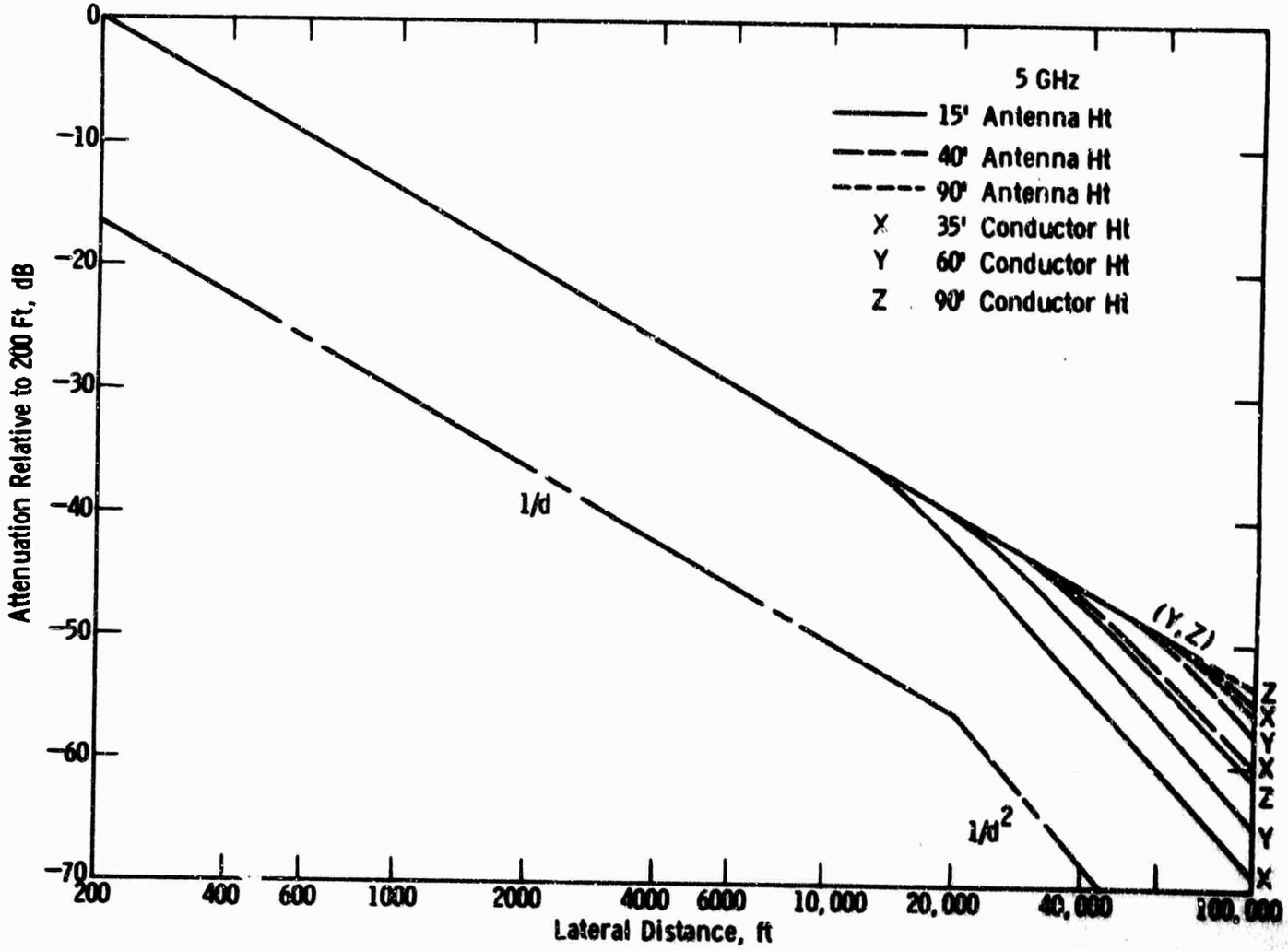


Fig. 6 —Attenuation of field with distance from line-vertical or horizontal dipole

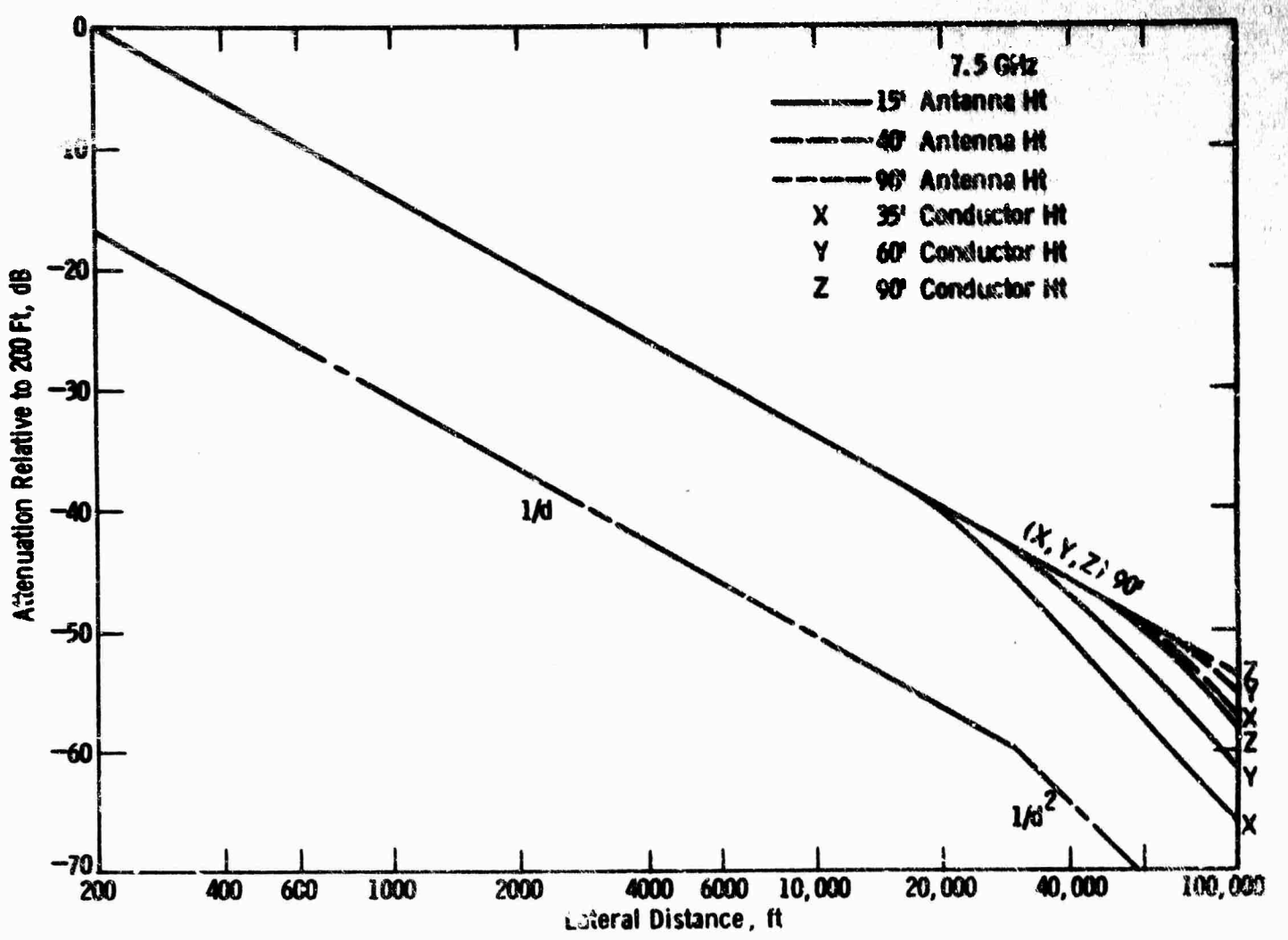


Fig. 7 —Attenuation of field with distance from line-vertical or horizontal dipole

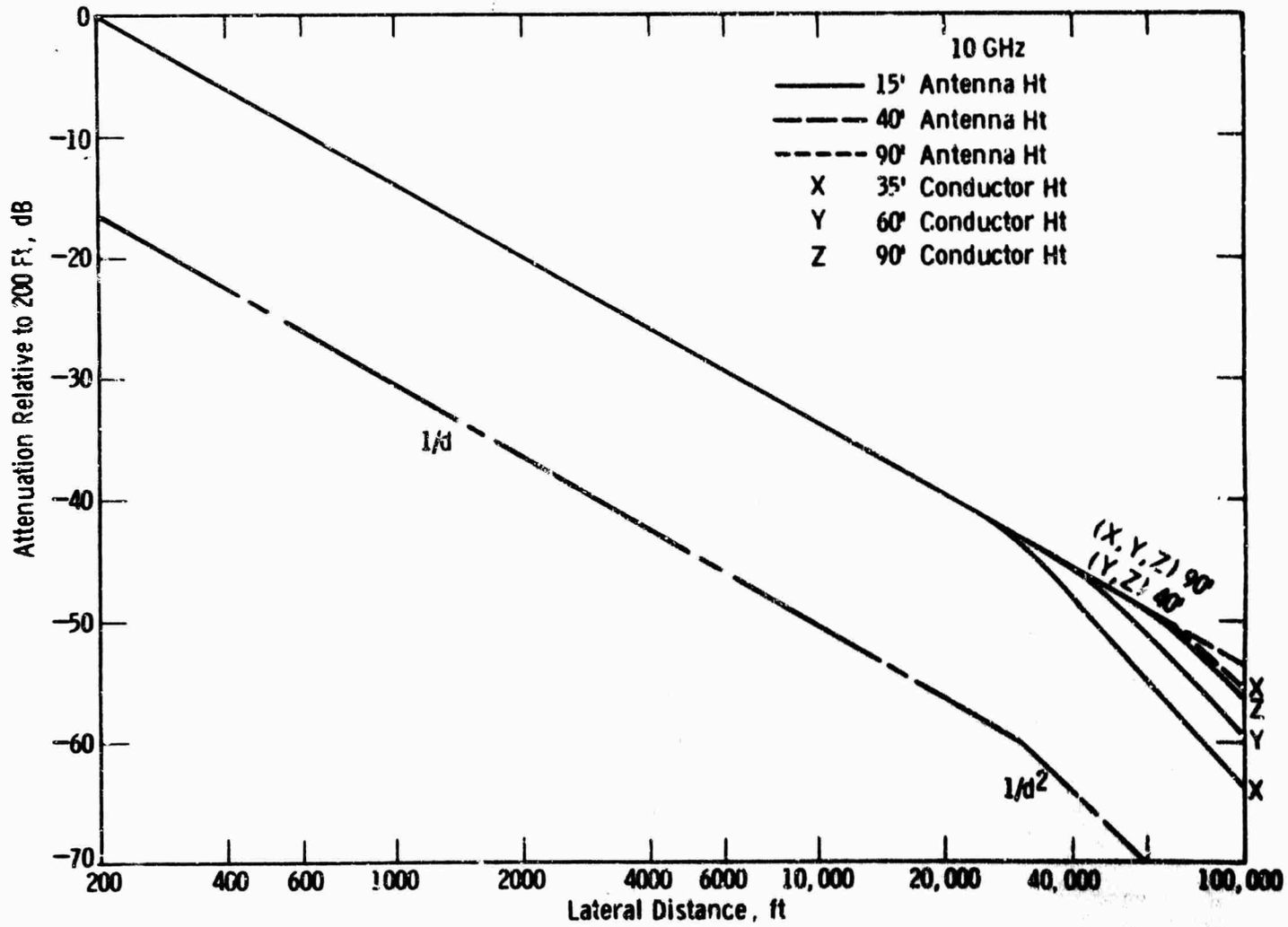


Fig. 8 —Attenuation of field with distance from line-vertical or horizontal dipole

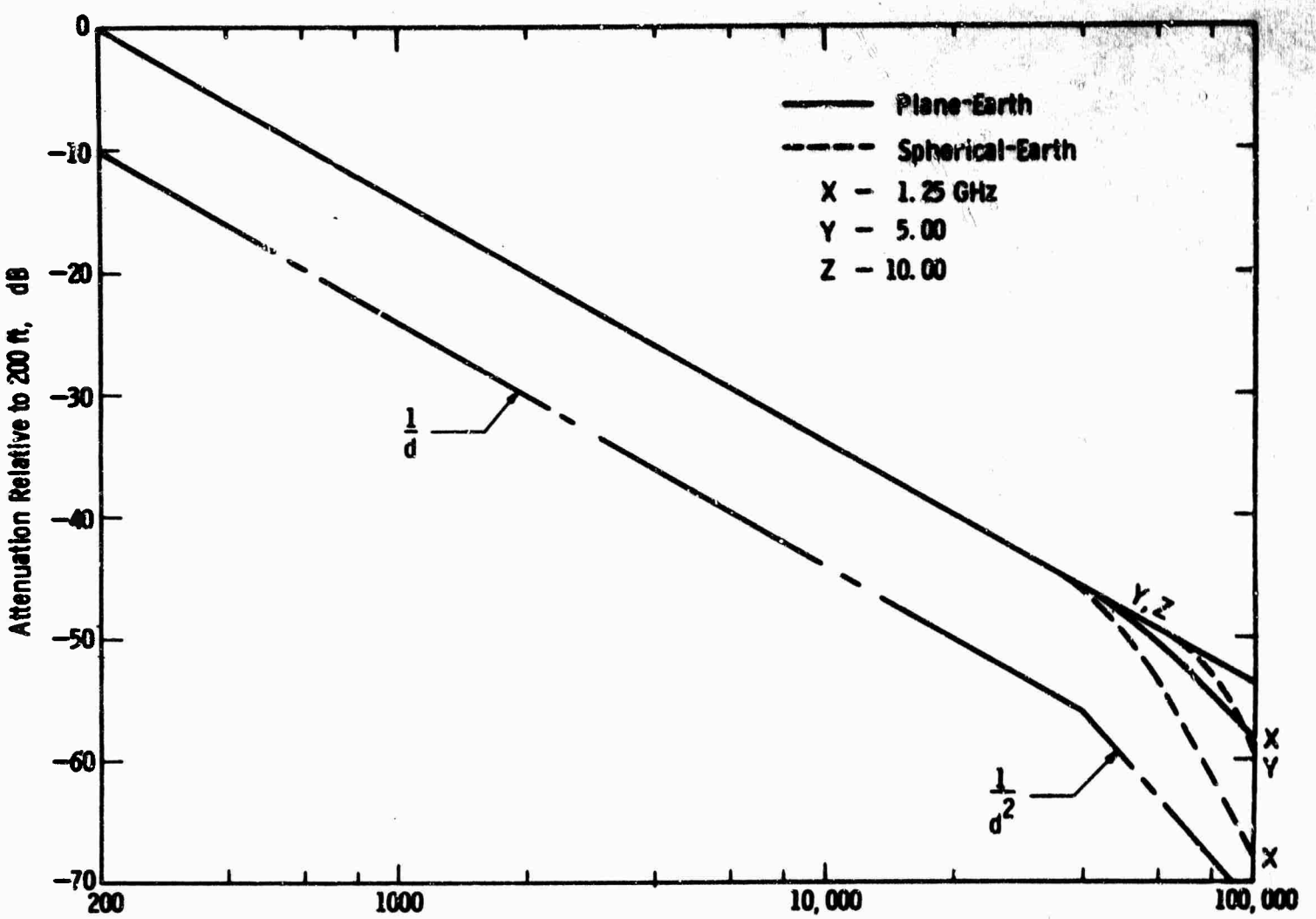


Fig. 9 —Comparison of plane and spherical earth calculation for horizontal and vertical field, transmitting and receiving antennas are 90 ft high (within line of sight)

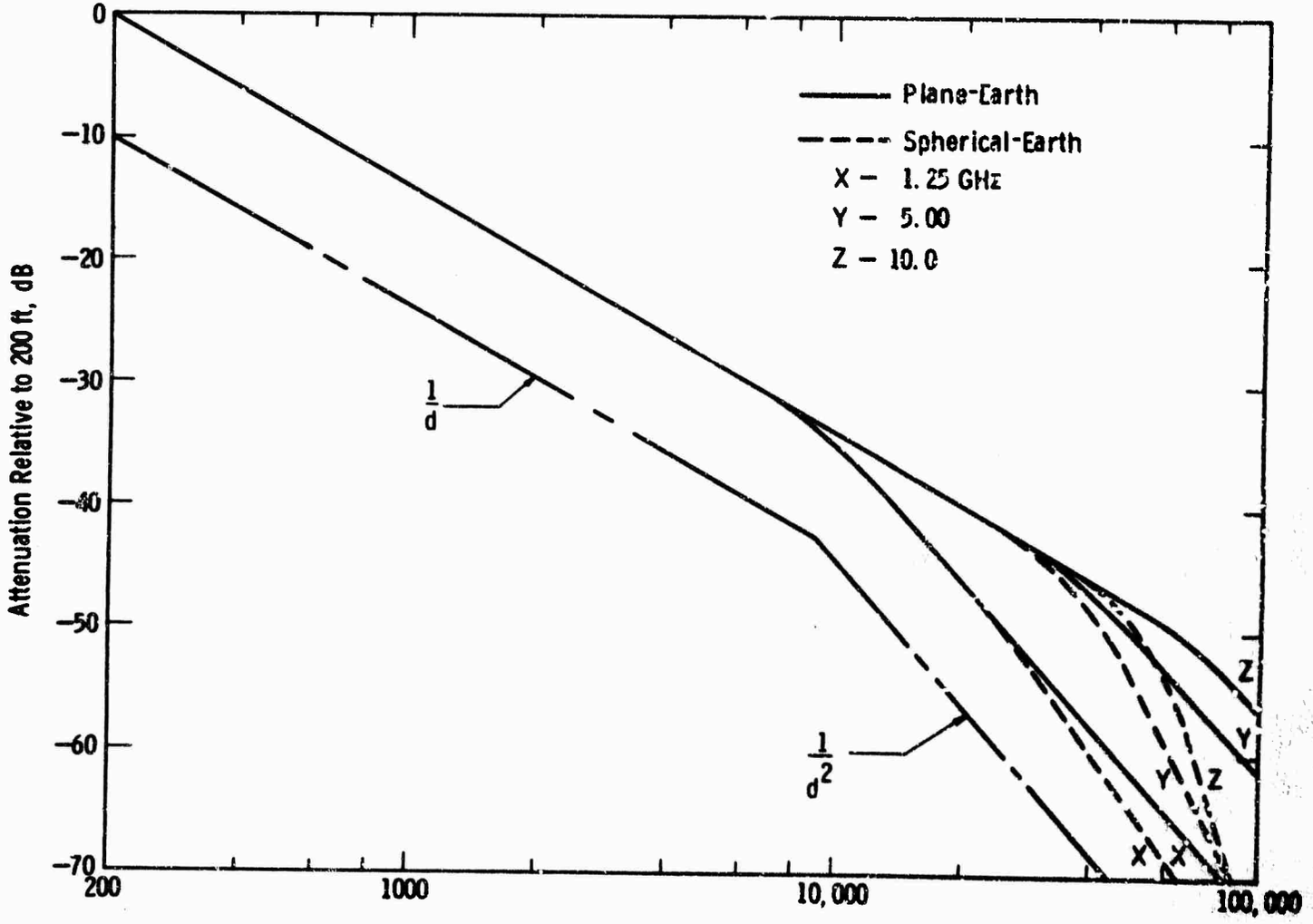


Fig. 10 – Comparison of plane and spherical earth calculation for horizontal and vertical field, transmitting and receiving antennas are 90 and 15 ft. high respectively (within Line of Sight)

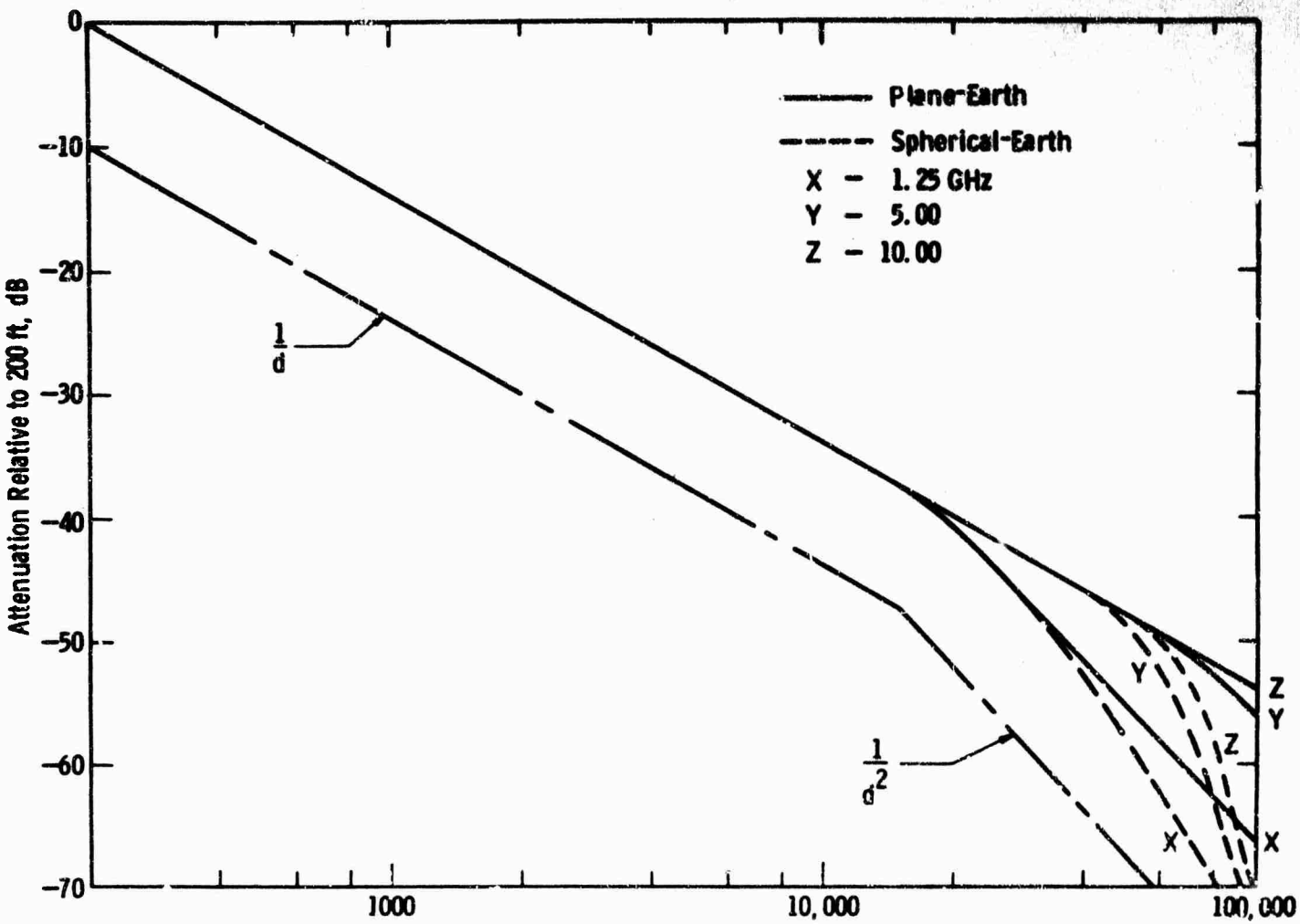


Fig. 11 —Comparison of plane and spherical earth calculation for horizontal and vertical field, transmitting and receiving antennas are 35 and 90 ft high respectively (within line of sight)

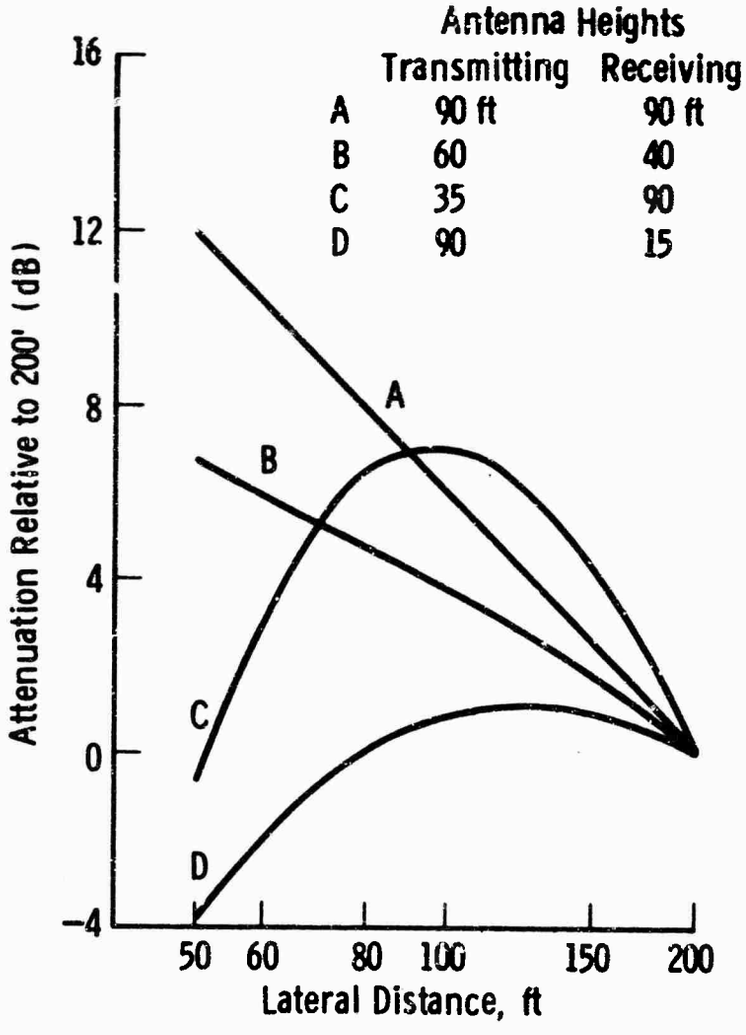


Fig. 12—Attenuation of horizontal field with distance (calculated using $\cos^3\psi_1$ and $\cos^3\psi_2$)

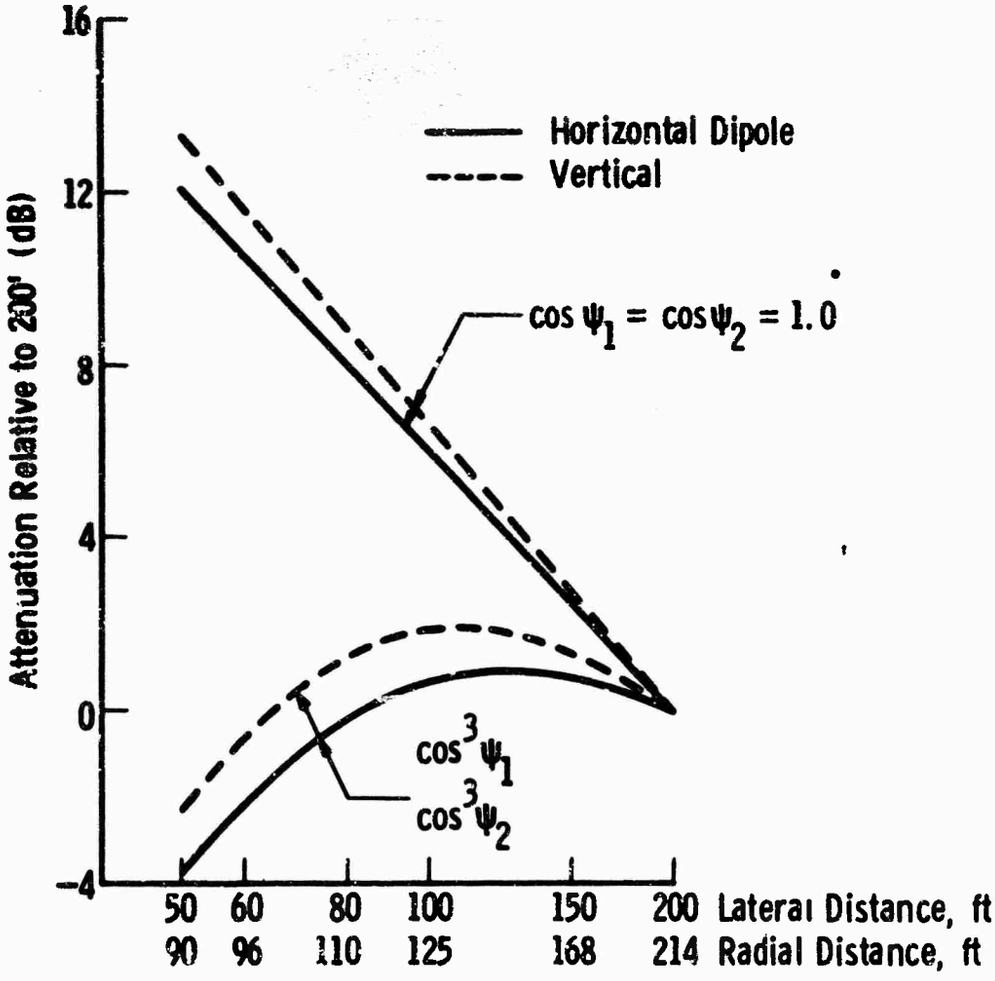


Fig. 13—Attenuation of field with distance for 90 and 15 ft transmitting and receiving antenna heights respectively

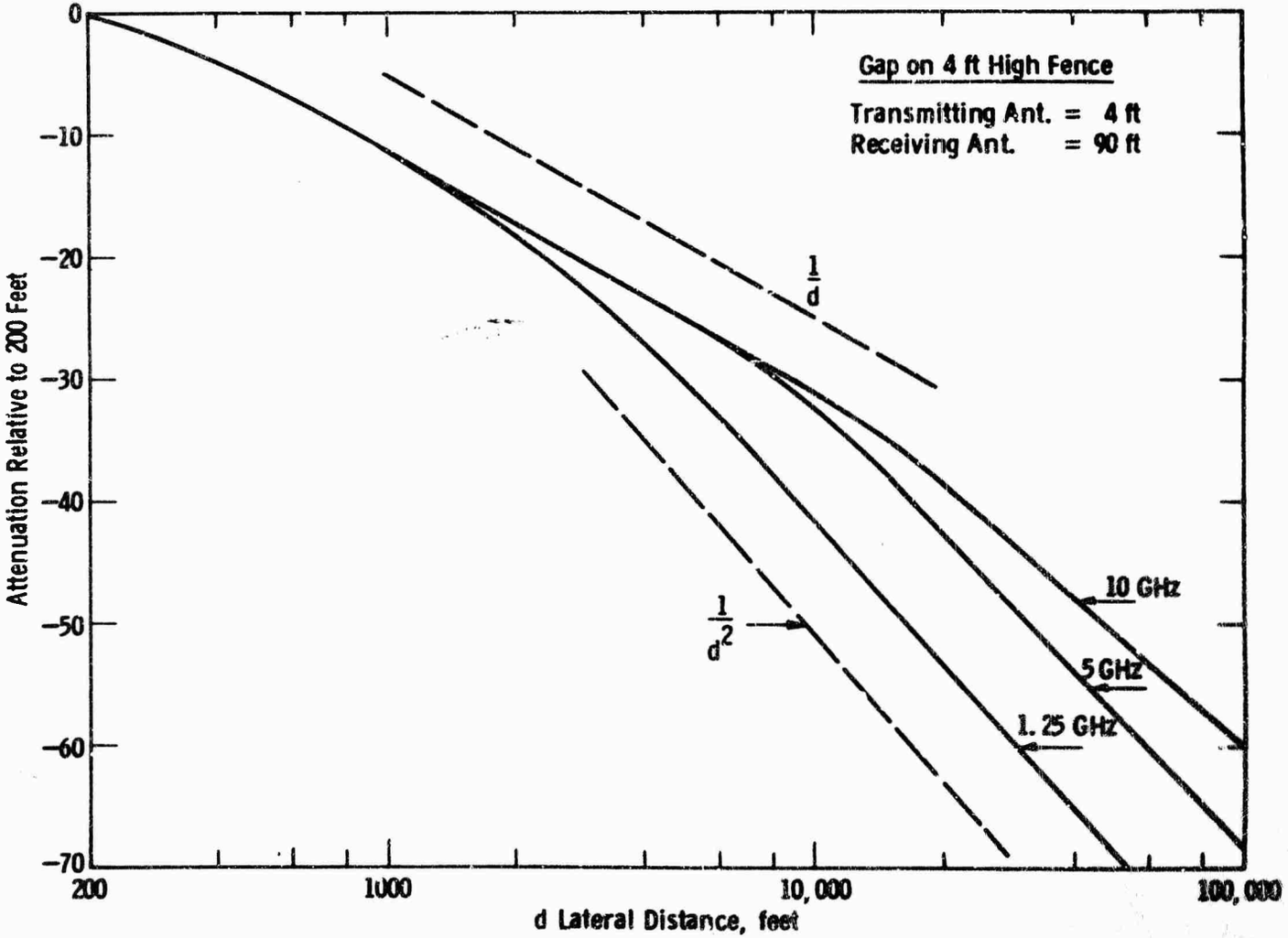


Fig. 14—Attenuation of field from fence in the 1-10 GHz range

HIGH VOLTAGE POWER LINE SITING CRITERIA

APPENDIX III

BIBLIOGRAPHY

WESTINGHOUSE ELECTRIC CORPORATION
ELECTRIC UTILITY HEADQUARTERS DEPARTMENT
RESEARCH AND DEVELOPMENT CENTER
PITTSBURGH, PENNSYLVANIA

ROME AIR DEVELOPMENT CENTER
(RADC)
GRIFFISS AIR FORCE BASE
ROME, NEW YORK 13442

CONTRACT AF30602-67-C-0171

APPENDIX III

BIBLIOGRAPHY

This follows on from the previous contract on High Voltage Power Line Siting Criteria where EMI measurements were made in the frequency range of 60 Hz to 1 GHz from ac high voltage power lines to 345 kV. The new contract calls for interference studies to a frequency of 10 GHz on ac lines to 735 kV and an 800-kV dc line.

The literature is divided into two sections as follows:

I. Microwave Measuring Instruments and Techniques

II. High Voltage ac and dc Power Lines - Radio Noise and Associated Data,

Note: Many papers covering measurements related to dc lines may be found on the previous contract Bibliography.

RADC-TR-66-606, March 1967.

I. Microwave Measuring Instruments and Techniques

1. **Standing Wave Reduction in an RFI Laboratory**

   Cory, W. E.

   IEEE Transactions on Electromagnetic Compatibility. Vol. EMC7 No. 1, March 1965.

   The properties of RF absorber materials are discussed and measurement techniques in relation to absorber quality reviewed. A general purpose RFI Laboratory is described within which standard RFI measuring equipment covering the 1 to 10 GHz range is used. The receiver generator and calibrated antenna used are listed with manufacturer's name.
   A straightforward technique for evaluating the performance of absorber material is described and in the laboratory used as effective background reflectivity of about 4% from 1 to 10 GHz was measured.

2. A New 10 GHz to 40 GHz RFI Measuring Instrument

   Currans, J. K.

   IEEE Transactions on Electromagnetic Compatibility. Vol. EMC7 No. 2, June 1965.

   In view of the increasing use of the X band (8.2 - 12.4 GHz) and Ku band (12.4 - 18 GHz0 etc.,for communications and radar the range of the Stoddart NM62A (1 to 10 GHz) RFI measuring instrument has been increased. This is achieved by use of the NMC-1040 Microwave Frequency Converter enabling RFI measurements to be made from 10 to 40 GHz. A description of the converter is given.
   Three tuning modes are available: Manual, Autoscan and Sweep. X-Y records of frequency spectra may be made with manual or automatic drive of the X axis and the sweep mode may be used in conjunction with an oscilloscope to obtain a panoramic display of a frequency spectrum.

3. A DC Triggered High-Speed High-Power Microwave Spark Gap Switch

   Farber, H.

   IEEE Transactions on Microwave Theory & Techniques. Vol. M77/13 No. 1, January 1965.

   A Method of switching pulsed RF power up to 60 kW peak in the 5 GHz range is described.

This is achieved by means of a spark gap switch triggered by dc pulse of 10-15 kV amplitude with a rise time in the order of 5 η s.
Physical dimensions are small as it consists essentially of a 5/32" diameter trigger sphere between two 3/8 inch diameter hemispheres within a section of waveguide.
May be adaptable as microwave reference source on HV Power Lines triggered by line volts as instrument check.

4. Radio Telescopes — IEEE Transactions on Military Electronics July/October 1964.

Findlay, J. W.

Describes various types of Radio Telescopes that have been built and tested.
States general frequency range from 20 MHz to 10 GHz. Table given lists the available power fluxes of some typical radio sources.
With good radiometers it is possible to detect with reasonable certainty powers of 10^{-23} w/cps.

5. Microwave Engineering — Ronald Press Co. New York 1966.

Ishii, T. Koryu

6. Predicting the Antenna's Role in RFI — Electronic Industries May 1960

Jacobs, E.

Discusses antenna characteristics such as gain, impedance and radiation pattern.
The near and far field regions of operation are mentioned and it is noted that the near field region requires more study with the trend toward larger antenna sizes. It is important to consider that due possibly to small dimensional changes antennas of the same type may have different minor lobe patterns.

7. The Determination of the Usable Field-Strength of Frequencies above 470 MHz over Irregular Terrain — Nachrichtentechnik (Germany) Vol. 15, No. 5, 161-6 (May 1965)

Kühn, V. (not abstracted)

A brief description of UHF field strength investigations in the East German Republic

is presented, undertaken at 43 sites at mostly two spot frequencies (480 and 780 MHz), supported by maps, height profiles and field strength plots. The results indicate that the measured field strengths in mountainous terrain departed as much as by 30 dB from the Stockholm CCIR curves. At 780 MHz on average, they were down by 10 dB in the mountains and 3-4 dB in the hills. It was also found that the CCIR method of testing by the scaled-down 3-16 Fm method yields too pessimistic results, and more realistic tests at full aerial heights are to be preferred.

8. Investigation of Spectrum Signature Instrumentation.

Metcalfe, R. E.

IEEE Transactions on Electromagnetic Compatibility. Vol. EMC7 June 1965

Calibration and comparison of the power measured by various RIFI meters and spectrum analyzers. Experimental data verifies the derived theoretical relationship between the pulse power input to a receiver of finite bandwidth and a substituted CW signal. The RIFI meters were the Polorad Model FIM-2; Empire Model NF-112 and Stoddart Models NM-62A and AN/URM-42 and the Spectrum Analyzers, the Polorad Models AN/UPM-84 and TSA-F; Lavoie Model LA-18A and Hewlett-Packard Model 851A/8551A. Measurements were made of various width pulses and the actual spectrum obtained on the Hewlett-Packard Spectrum Analyzer for a one-microsecond pulse is shown. Results indicate that data from different bandwidth Spectrum Analyzers may be correlated. Measurements using three different RIFI meters by each of ten different operations are tabulated. It is concluded that present calibration techniques in the EMC field are inadequate and extreme care be taken when specifying instrument parameters. Also there is need for the power per unit bandwidth equations in MIL-STD-449B to be reconsidered.

9. Technique of Microwave Measurements

Montgomery, C. G.

MIT Radiation Lab Series. McGraw-Hill Book Co., 1947.

10. Airborne Radar Signal Density Measurements

IEEE Transactions on Radio Frequency Interference, June 1963

Myers, H. A.

A study was undertaken to develop a reliable method for predicting the environmental interference conditions due to ambient radar energy in a particular area.
The predictions made for radar dense areas of USA were verified by actual measurements. These measurements were made in a series of flights over the areas in question using a receiver of -70 dBm resistivity and 20 MHz bandwidth. Graphs of pulses per second frequency (L and S bands) are presented.

11. Principles of Radar

Reintjes and Coate

MIT Radar School Staff
Third Edition
McGraw-Hill Book Co., 1952.

12. The Future of EMC Instrumentation

IEEE Transactions on Electromagnetic Compatibility, Vol. EMC7, No. 1, March 1965.

Sproul, R. W.

Present EMC Instrumentation is reviewed in particular with reference to frequency domain and time domain measurements.
Instrument performance and characteristics are discussed.
Future needs are outlined especially the use of time domain analysis of interference in view of the increasing use of digital communications.

13. Analytical Prediction of Electromagnetic Environments

IRE Transactions on Communications Systems, June 1961.

In view of the present development rate it is expected in the near future that radar pulses in excess of 10 MW peak power and receiver sensitivities in the order of -110 dBm will exist which will further increase interference problems.

This paper discusses programmes in USA and UK concerning Electromagnetic Compatibility and prediction of electromagnetic environments, etc.
In all cases mathematical models are developed for solution by digital computer.
Gives example of histogram relating the number of receivers jammed by mutual interference to the probability of this occurring in a desire signal complex.

14. A Handbook on Methods and Procedures for Automating RFI/EMI Measurements

White, D. R. J.

White Electromagnetics, Inc., Rockville, Maryland. Library of Congress Catalog Card No. 66.26617.

15. New Electromagnetic Compatibility Instrumentation and Measurement Requirements and Techniques

White, D. R. J.

IEEE Transactions on Electromagnetic Compatibility, Vol. EMC7 No. 2, June 1965.

Discusses measurement accuracy and misleading definitions. Probable instrumentation errors are listed. New RIFI instrument needs are discussed together with the various responses of X-Y recorders.
Antenna pattern measurements using the sun as a signal generator and the conduct of electromagnetic site surveys are reviewed.

II. High Voltage ac and dc Power Lines - Radio Noise and Associated Data

1. Corona-Loss Characteristics of EHV Transmission Lines Based on Project EHV Research

   Anderson, J.G., Baretsky, Jr., M., McCarthy, D.D.

   Since 1960 the corona-loss characteristics of a variety of extra-high-voltage (EHV) transmission-line configurations have been under study at Project EHV (1), (2). This paper presents results from the analysis of corona losses measured under all weather conditions experienced during 2-1/2 years of observation of single or bundled conductors at 500 or 700 kV. In addition, corona characteristics are presented for switching-surge transients and severe steady-state overvoltages. The purpose of this paper is: (1) to summarize some of the statistical aspects of fair- and foul-weather corona-loss observations for the configurations studied, and (2) in terms of electrical and meteorological parameters, to describe an equation for corona loss on EHV lines that is in a form directly applicable by transmission engineers to EHV line design.

   Paper 31 TP 65-700, IEEE Transactions on Power Apparatus and Systems, Vol. PAS-85, No. 12, December 1966, pp. 1196-1212

2. Progress Report on BPA HV DC Test Line Radio Noise and Corona Loss

   Bailey, Burt M.

   Power transmission of high-voltage direct current (HV dc) by overhead lines presents a new concept with which the industry has had little experience. Radio noise and corona loss values were recorded on a full-scale test line and statistically analyzed in relation to prevailing weather conditions. Comparison was made to radio noise readings taken on a nearby ac line. Results cover the analysis of approximately six months' data.

   Paper 31 TP 66-403, IEEE Transactions on Power Apparatus and Systems, Vol. PAS-86, No. 10, October 1967, pp. 1141-45.

3. Alternating Current Corona in Foul Weather II - Below Freezing Point

Boulet, L., Cahill, L., Jakubszyk, B. J.

Paper 31 TP 65-80?, IEEE Transactions on Power Apparatus and Systems, Vol. PAS-85, No. 6, June 1966.

The mechanisms of ac corona caused by the presence of ice particles is shown. Two kinds of precipitation are distinguished: the snow-like and hail-like forms. Conditions of snowcover formation on transmission-line conductors are analyzed. This cover may result in the highest corona energy losses, caused mainly by steady pulseless corona in the positive and Trichel impulses in the negative, half-cycle. No streamers are reported from the snowcover by conductor voltage gradients of less than 20 kV rms/cm. Streamer discharges and high radio interference are caused by impinging snowflakes and liquid or frozen waterdrops on the conductor surface. The results of laboratory tests confirmed field investigations on the Hydro-Quebec 315-kV transmission system.

4. Effect of Station Radio Noise Sources on Transmission Line Noise Levels - Experimental Results

Davey, Jack, Deloney, H. L., LaForest, J. J.

Paper 31 TP 66-490, IEEE Transactions on Power Apparatus and Systems, Vol. PAS-86, No. 8, August 1967, pp. 1007-11.

Known sources (gaps) of radio noise (RI) generation were applied to a transmission line close to a station and the resultant transmission line RI levels were monitored. Measurements are in good agreement with calculated values. Measurements of station impedance were made. RI gaps were found to be stable and operated as constant current generators over a wide range of load impedance.

5. BPA's 1100-kV Direct Current Test Project: II Radio Interference and Corona Loss

IEEE Transactions on Power Apparatus and Systems, Vol. PAS-86, No. 3, March 1967

Gehrig, E. J.

Radio interference and corona loss was investigated over a one year period from bipolar (±550 kV) and monopolar dc test lines of 1.3 to 4.2 miles in length. Influence of line construction, conductors, frequency and weather were studied. Radio influence found to be similar to ac lines except for precipitation and wind effects. Also dc radio influence exerted less disturbance to radio receivers than ac for the same signal to noise ratio.

6. Modes of Corona Discharges in Air

Paper 31 C 44-A, IEEE Transactions on Power Apparatus and Systems, Vol. PAS-87, No. 5, May 1968, pp. 1207-15.

Giao, Trinh N., Jordan, Jan B.

Corona discharges in air exist under several distinctive forms, either pulsative or stable. The properties of different corona modes are analyzed as they appear in a cylindrical distorted field. Differences between dc and ac excitations are emphasized. Corona discharges may produce energy loss without detectable radio noise or high noise at low energy loss, depending upon their form of appearance. The different withstands of asymmetric gaps under different polarities also find their explanation in corona mechanism.

7. Right-of-Way and Conductor Selection for the Allegheny Power System 500-kV Transmission System

Paper 31 TP 65-812, IEEE Transactions on Power Apparatus and Systems, Vol. PAS-85, No. 6, June 1966, pp. 624-32.

Guyker, W. C., O'Neil, J. E., Hileman, A. R.

The Allegheny Power System 500-kV transmission system has been designed before commercial 500-kV lines have had any service experience. To achieve an optimum design, studies

were performed in all areas. This paper presents the results of the study of right-of-way width and conductor size. The line was designed to be compatible with existing Type B (54 dB) radio station signal levels and the minimum conductor size and right-of-way width (200 feet) were selected based on comparative data from operating and test facility lines. An economic evaluation of a number of satisfactory conductor systems (2-, 3-, and 4-conductor bundles) was made resulting in the selection of a 2-conductor bundle of 1.681-inch ACSR condctors for this system.

8. Tennessee Valley Authority's Radio Interference Experiences on 500-kV Transmission Lines

   Hartley, James W., Smith, Robert T., Dobson, Herbert I.

   This paper describes a two-year investigation of radio interference (RI) levels in the vicinity of 400 miles of operating 500-kV transmission lines. Discussions are given of instruments, antennas, and types of surveys; the design and development of RI monitoring stations; and comparisons of the relative merits of various supplementary items. Results from RI profiles, RIV measurements, and monitor station recordings are analyzed and presented along with brief discussions of signal-to-noise ratios and evaluation of TVA's transmission line design and construction techniques.

   Paper 31 TP 67-455, IEEE Transactions on Power Apparatus and Systems, Vol. PAS-87, No. 4, April 1968, pp. 903-11

9. Insulation Requirements, Corona Losses, and Corona Radio Interference for High Voltage dc Lines

   Hylten-Cavallius, N.

   Discusses at length the problems of insulator pollution and gives

   Paper 63-998, IEEE Transactions on Power Apparatus and Systems, Vol. 83, May 1964, pp.500-08

details of tests over a two year period on both ac and dc. Desirable features for good dc insulators are outlined. Radio interference on dc lines is due to corona pulses on the line, partial discharges on insulators and by pulses occurring at the ignition of the valves, being transmitted via the switchyard to the line. Mentions Radio Interference measurements in the extreme high frequency range; 30 MHz to 1.5 GHz. Measurements carried out on a 30 m long test line at 250 kV dc with positive polarity corresponding to 2.9 cm/kV on the insulators. Instrument used was a radio telescope at a distance of 100 to 200 m and no significant radiation was recorded from the line in foul or fair weather. During bad weather the insulator chains radiated about 10^{-15} watts/Hz period of the receivers bandwidth in the whole frequency range.

10. Corona Losses, Radio Interference and Insulator Requirements for HV dc Lines. Studies Regarding Insulator Interference for Frequencies between 30 and 1500 MHz.

CIGRE Paper No. 407, 1964

Hylten-Cavallius, N.

Describes measurements of radio interference and corona losses carried out simultaneously on HV dc lines. Monopolar to 1000 kV and bipolar to ±350 kV. Details are given on insulator choice and long term pollution tests.
Results are tabulated regarding radio interference measurements from line insulators for frequencies between 30 MHz and 1.5 GHz. These measurements were carried out on a short unloaded test line by Orsala Space Observatory; a division of the Research Lab of Electrophysics, Chalmers' Tecnical University, Gothenburg, Sweden. A radio telescope was used and the insulators found to radiate on an

average 10^{-15} w/Hz. Silicon treatment of insulators was found to reduce radiation by about 10 dB. It is concluded that since in high sensitivity radio astronomy work the flux density of radio frequency interference should not exceed 10^{-26} w/Hz/m^2. Then insulator radiation makes power lines a potential source of disturbance for radio astronomy observations and space communications at distances closer than 100 km.

11. Correlation of Various RI Meters and Reading Comparison of RI Meter Operators on a 735-kV Line

Paper 31 C 44-B, IEEE Transactions on Power Apparatus and Systems, Vol. PAS-87, No. 5, May 1968, pp. 1249-1259.

This paper describes the results of a study, sponsored by Working Group No. 1 of the RI Subcommittee, on Hydro-Quebec's 735-kV line. Various RI measuring techniques were used in obtaining frequency-spectrum and lateral profiles. Radio noise measuring locations were studied and compared with measuring practices for determining statistical RI levels of operating EHV lines. Comparison between different RI meters has indicated that in the broadcast band the Stoddart NM20B reads 1 to3 dB higher than the Siemens. An RI measuring test among 14 meter operators indicated the "human" error to be plus or minus 2 dB. Nighttime visual corona was observed and discussed.

12. A Laboratory Study of the Effects by Wind on dc Corona

IEEE Transactions on Power Apparatus and Systems, Vol. PAS-86, March 1967, No. 3.

Khalifa, M. M.

The corona vs wind characteristics of dc lines having in one case discrete metal projections from smooth conductors and in the other, stranded conductors were studied using two laboratory models. The model with projections had wind speeds up to 15 mph across it from blowers whilst the other model was used in conjunction with a 15 foot wind tunnel and wind speed up to 50 mph.

13. Study of Overhead Ground Wires for dc Transmission Lines

Khalifa, Mohamed M.

Paper 31 C 44-D, IEEE Transactions on Power Apparatus and Systems, Vol. PAS-87, No. 7, July 1968, pp. 1648-56.

The influence of overhead ground wires on the corona losses, RI, and telephone interference of dc lines was studied. Corona losses and RI were measured on a full-scale bipolar test line. Corona losses were measured on laboratory models of monopolar, homopolar, and bipolar lines. Telephone interference levels were calculated. Experimental and calculated results are presented.

14. Radio Interference from the First 735-kV Line of Hydro-Quebec

Lacroix, Real and Charbonneau, Hulbert

Paper 31 TP 67-435, IEEE Transactions on Power Apparatus and Systems, Vol. PAS-87, No. 4, April 1968, pp. 932-39.

Results of radio interference (RI) level measurements on the first 735-kV line of Hydro-Quebec are presented. The cumulative relative frequency of RI levels for the period from October 1, 1963 to July 17, 1966, is studied. An approximation of this curve by three uniformly distributed meteorological conditions and the distribution curve of absolute humidity are presented. An ensuing equation for the evaluation of RI levels in terms of temperature and relative humidity is included. The rate of change of RI levels with the maximum surface gradient on the conductors is reported. Frequency spectra and lateral profiles measured at mid-span are shown. The evaluation of RI levels using a published method is also illustrated.

15. Radio-Noise Levels of EHV Transmission Lines Based on Project EHV Research

LaForest, J.J., Baretsky, Jr., M. and MacCarthy, D. D.

Paper 31 TP 65-706, IEEE Transactions on Power Apparatus and Systems, Vol. PAS-85, No. 12, December 1966, pp. 1213-20

The results of three years of experiments and theoretical research on transmission-line radio noise at Project EHV are presented. Computer

programs were developed to process the data on a statistical basis, and as output provide both histograms and regression analyses for four test configurations operated at the 600- and 700-kV levels. Fair weather radio-noise levels were found to be significantly affected by relative humidity, relative air density, and absolute value of wind velocity, and these relationships are discussed. Wet-weather effects are presented and discussed. Both fair-weather and wet-weather experimental results are incorporated in a theoretical analysis of transmission-line radio noise resulting in a procedure which enables the transmission-line designer to predict in advance of construction, average fair-weather and wet-weather radio noise profiles for EHV transmission lines.

16. Seasonal Variation of Fair-Weather Radio Noise

LaForest, James J.

Paper 31 TP 67-436, IEEE Transactions on Power Apparatus and Systems, Vol. PAS-87, No. 4, April 1968, pp. 928-31.

One year of fair-weather radio noise (RI) data from an EHV line was analyzed. Two types of variation were found: long-term over several months and short-term over several days. Summer RI readings were higher than winter readings by 12 dB and lasted longer. Based on these results, a procedure for predicting average monthly RI levels is outlined. Short-term variations of fair-weather RI levels were analyzed statistically using the washing effect of rain on the conductor surface as an explanation of the RI variation. Results yielded a favorable inference for the statistical model.

17. Propagation Data for Interference Analysis

Read, Dr. H. R., et al.

The information contained in Volume I on Propagation Data for Interference Analysis presents methods useful in the computation of propagation characteristics for persons involved in interference analysis and prediction. The data include theoretical equations, worked-out examples, and representative curves showing typical information for most all modes of propagation encountered.
The second volume on Propagation Data for Interference Analysis is entirely supplemental to Volume I. Working curves only, with a few examples showing their usage, are presented in order to enhance the value of Volume I by supplying the Radio Frequency Interference Engineer with data whereby he can make quick estimates to aid in the analysis of interference.

Jansky & Bailey
A Division of Atlantic Research Corporation, Washington 7, D. C.
Alexandria, Va.

Volumes I and II, January 1962.

18. A Method to Detect the Deionization Margin Angle and to Prevent the Commutation Failure of an Inverter for dc Transmission

Machida, T.

Describes a method of continuously monitoring the extinction angle of valves used as inverters for dc transmission so that with the aid of a comparison circuit the extinction angle may be continuously controlled and maintained between critical desired limits.
The deviation of extinction margin angle is around 15.5 percent without control and 1.1 percent with control.

IEEE Transactions on Power Apparatus and Systems, Vol. PAS-86, No. 3, March 1967.

19. **Investigation of Corona on Overhead Transmission Line Conductors at High Voltage dc**

National Research Council of Canada, June 1961

Morris, R. M.

Corona loss investigations were made on a 370 foot outdoor test line of 1.108 inches diameter and then on a two conductor bundle spaced 18 inches. Voltages up to 500 kV were used. Two types of tests were carried out: one, recording corona loss current while varying the voltage in increment with the weather conditions constant; two, recording loss current with constant voltage for long periods under variable weather conditions. Preliminary results indicate that in wet weather losses are considerably higher than in dry weather.

20. **Corona and RI Caused by Particles On or Near EHV Conductors: I - Fair Weather**

Paper 31 TP 66-310, IEEE Transactions on Power Apparatus and Systems, Vol. PAS-86, No. 11, November 1967, pp. 1375-83.

Newell, Hobart H., Liao, Tseng-Wu, and Warburton, Frank W.

This study was made to identify, photograph, and establish the radio noise importance of the fair-weather coronas occurring on an ac high-voltage transmission line conductor. Excursions of fair-weather interference to over ten times the base value of the line noise are attributed to corona plumes from vegetable particles and insects attached to the conductor. Vegetable particles and insects are dielectrics whose plumes occur on the positive half-cycle of potential. Radio noise from these plumes overrides other corona noises associated with the dielectric particles, the noise from weathered metal protrusions on the conductor strands, and the nor-

mal noise from insulators, accessories, and hardware. The conductor surface gradient, the total conductor surface area, and the rate of gradient decay outward from the surface are important to both particle attachment and severity of plume formation.

21. Corona and RI Caused by Particles On or Near EHV Conductors: II - Foul Weather

Paper 31 C 44-C, IEEE Transactions on Power Apparatus and Systems, Vol. PAS-87, No. 4, April 1968, pp. 911-27.

Newell, Hobert H., Liao, Tseng-Wu, and Warburton, Frank W.

This study was made to identify and photograph the foul-weather coronas occurring on a high-voltage transmission-line conductor and to establish their radio-noise importance. On the most tested 230-kV line, snow impingement plumes caused radio interference (RI) to 90 times, and water drop spray plumes to 75 times, that of the base fair-weather noise level. Foul-weather RI caused by snow, rain, fog, ice, and condensate associated with the conductor overrode RI generated on insulators, accessories, hardware, and weathered conductor protrusions. H_2O particles in different forms were present in the conductor environment for one-fifth the yearly time. The conductor surface gradient, the rate of decay outward from the conductor, the total conductor surface area, H_2O particle size and formation, and air velocity over the conductor are important to both particle attachment to the conductor and to the severity and form of corona. This corona occurs as plumes, impingement plumes, spray plumes, glows, and microsparks. Confirming laboratory tests were made at 230 and 345 kV. Confirming observations were made on 345- and 500-kV lines. Corona losses were caused by impingement plumes during snowstorms and principally by spray plumes in rain.

22. **A Method for Analysis of Radio Noise on High-Voltage Transmission Lines**

Paper 31 TP 66-407, IEEE Transactions on Power Apparatus and Systems, Vol. PAS-87 No. 2, February 1968, pp. 334-45

Pakala, W. E., and Taylor, Edgar R.

A technique is described for approximating the effect of various factors on the radio noise level, due to conductor corona, on EHV transmission lines. The technique is essentially one of comparison. Relations are given in the Appendix for calculating the conductor gradients and results are presented in curve form. The application is intended only for comparison of radio noise generated by conductor corona on ac lines, with conductors ranging only from 0.3 to 1.3 inches radius (1.5 to 3.3 cm) and for the frequency range from about 0.2 to 1.6 MHz. If an existing line has been evaluated statistically the technique can be used to approximate the radio noise level of another line. A relation is also given for obtaining curves of 3-phase voltage to conductor radius for the same radio noise generation. Because of possible conductor surface differences and environmental differences, which cannot be too accurately evaluated, care is necessary in any final estimation of the average radio noise level.

23. **Radio Noise Measurements on High Voltage Lines from 2.4 to 345 kV**

1968 IEEE EMC Symposium Record, Seattle, Washington, July 23-24-25, 1968; IEEE 68 C12-EMC, pp. 96-107.

Pakala, W. E., Taylor, Jr., E. R. and Harrold, R. T.

This paper is based on radio noise measurements made near overhead power lines operating at voltages from 2.4 kV to 345 kV inclusive. Some of the measurements made are discussed and analyzed and used in a radio noise prediction technique for determining the location of communication and electronic sites with respect to high voltage overhead power lines.

This paper is necessarily only a summary of the work which has been reported and detailed test results, calculations, appendices, and complete bibliography have been omitted.

24. RI Problems in HV-Line Design

Paris, Luigi and Sforzini, Mario

Paper 31 TP 67-406, IEEE Transactions on Power Apparatus and Systems, Vol. PAS-87, No. 4, April 1968, pp. 940-946.

Criteria for the selection of line conductors and insulators are presented which may be helpful to the HV line designer when choosing among different line solutions. Methods are given for the predetermination of RI from both conductors and insulator strings, then criteria are exposed for the definition of "limit" values for RI levels; these criteria are for the designer's reference.

25. Generation of Abnormal Harmonics in High-Voltage ac-dc Power Systems

Paper 31 TP 67-495, IEEE Transactions on Power Apparatus and Systems, Vol. PAS-87, No. 3, March 1968, pp. 873-83.

The possibility of abnormal harmonic generation in an ac system feeding a converter load is examined from the standpoint of automatic control systems used in modern HVDC transmission systems. It is shown that with certain types of automatic controls, the firing angles of converter valves may sustain some errors, which in turn could generate abnormal harmonic currents in the three-phase ac system feeding the converter. A criterion for predetermining the type and extent of abnormal harmonic generation is defined, and numerical examples given. Methods of reducing abnormal harmonic generation are discussed, and some experimental data supporting the theoretical calculations are also included.

26. **BPA's 1100-kV dc Test Project: I Measurements and Instrumentation**

IEEE Transactions on Power Apparatus and Systems, Vol. PAS-86, March 1967, No. 3.

Poland, M. G.

Describes instrumentation and measuring techniques for the automatic long term recording of data, such as radio influence, corona loss, insulator leakage surge currents, etc. from a five-mile long ±500 kV dc test line. Mainly solid state equipment is used and information such as radio influence current which is measured by a clamp on transformer is telemetered to the recording station. RIV is recorded at the same time from a 345-kV ac line four miles away as a check between ac and dc lines under the same weather conditions. 167 KHz and 834 KHz are the frequencies at which RIV is recorded.

27. Investigation of Corona on Overhead Transmission Line Conductors at High Voltage dc

National Research Council of Canada, March 1962

Rakoshdas, B.

Experimental investigations were made of the radio interference characteristics of two 370 foot long test lines, one a single 1.108 inch diameter conductor, the other a two conductor bundle spaced 18 inches. The experiments were made in fair weather with voltages up to 500 kV dc. Radio interference frequency spectra were recorded under the line center and lateral profiles and measurement of antenna patterns made. Frequencies measured extended to 10 MHz. The performance of a long line of similar combination is estimated from the standing wave pattern of the frequency spectrum and lateral profile of the test line. Pictures of a Spectrum Analyzer display of

corona radio noise and radio stations up to a frequency of 9 MHz, and radio stations alone are given.

28. Pulses and Radio Influence Voltage of Direct Voltage Corona

National Research Council, Ottawa, Canada, March 1963

Rakoshdas, B.

Describes experiments carried out to determine the pulse and RIV characteristics of smooth and stranded conductors with respect to polarity and conductor diameter at high voltage dc. Mainly the measurements were made in the laboratory using a cylinder-coaxial wire electrode arrangement and wire diameters less than 1/4". Other measurements were made outdoors with conductor diameters up to 3/8". It was found that on negative polarity the pulses causing RIV were smaller in amplitude but sharp with a high repetition rate. On positive polarity, the pulses are larger in amplitude, of longer duration and their repetition rate is lower. The positive corona pulse is described as a double exponential with a 50 nanosecond rise time whilst the negative pulse has a linear front of 20 nanosecond rise. The frequency spectrum of positive pulses drops very rapidly beyond 1 MHz whilst the spectrum from negative pulses remains flat to 3 MHz. The RIV from positive pulses is dominant at low frequencies due to the large pulse amplitude. Covers theoretically by means of Fourier analysis the spectrum from these different pulse shapes.

29. Unusual Current Harmonics Arising from High-Voltage DC Transmission

Paper 31 TP 67-500, IEEE Transactions on Power Apparatus and Systems, Vol. PAS-87, No. 3, March 1968, pp. 883-93.

Reeve, John and Krishnayya, P. C. S.

Unbalance in the operation of high voltage dc converters gives rise to unusual or uncharacteristic harmonics

in the ac waveform not expected from the existing theory relating to balanced operation. Analysis of the effect of unbalances in the alternating voltages and the valve firing angles is provided together with selected characteristics illustrating the variations in the harmonics with unbalance as determined by a comprehensive digital computer program. Six-pulse and 12-pulse operation is considered.

30. 500-kV Line Design: II - Corona and RIV Characteristics of Insulator-Hardware Assemblies

Paper 31 TP 66-352, IEEE Transactions on Power Apparatus and Systems, Vol. PAS-86, No. 9, September 1967, pp. 1091-97.

Saruyama, Yukio; Yasui, Mitsuru, and Nagasaki, Shoji.

This paper describes the corona noise characteristics of insulator-hardware assemblies in the Boso Power Transmission Line of Tokyo Electric Power Company which is the first 800-kV transmission line in Japan. The results of corona noise measurement made on a V-string insulator assembly and a strain insulator assembly are reported. Data on the corona noise level of insulator-hardware obtained from a test line were converted into noise level values for an actual transmission line for comparison with the conductor corona noise levels. The design of the insulator hardware was decided accordingly.

31. Comparative Radio Noise Levels of Transmission Lines, Automotive Traffic, and Stabilized Arc Welders

IEEE Transactions on Electromagnetic Compatibility, Vol. EMC-9 No. 2, September 1967, pp. 73-77.

Skomal, Edward N.

Radio interference data that have been measured throughout the frequency range of 30 Hz to 1 GHz on power transmission lines, automotive

traffic, and RF stabilized arc welders by many investigators have been assembled, converted to a common system of units, and collectively plotted. The resulting composite presentations permit an assessment of the relative interference levels produced by the three types of radio noise sources. It is concluded that below 25 MHz, lower voltage transmission, lines and RF stabilized arc welders are the major incidental radio noise sources when the observer is within 100 feet of the source. Above 40 MHz, automotive traffic and lower voltage transmission lines are the major radio noise sources with neither appearing to be consistently the greater when an observer is within 50 feet or less of the source.

32. Communication Circuits on 500-kV Lines

Swingle, T. M., and Dobson, H. L.

Paper 31 TP 66-53, IEEE Transactions on Power Apparatus and Systems, Vol. PAS-85, No. 10, October 1966, pp. 1059-64.

The characteristics of 500-kV transmission lines from a communication viewpoint are discussed based on tests and observations of the Tennessee Valley Authority's first 500-kV line to be placed in service. Dead-line carrier frequency tests included attenuation on the insulated shield wires and phase-coupled powerline carrier arrangements. Model component attenuation, relative velocity of propagation, and other characteristics of natural mode behaviour are covered. Experiences to date on operation of powerline carrier terminals and audio equipment are given, along with a brief resume of RI measurements.

33. Verification Tests of the VEPCO 500-kV System

Wagner, Charles L., Smith, H. Melvin, Taylor, Jr., Edgar R., and LaPrade, John H.

Paper 31 C45-B, IEEE Transactions on Power Apparatus and Systems, Vol. PAS-87, No. 4, April 1968, pp. 1032-44.

The results of the first field tests performed to verify the design of the Virginia Electric Power Company 500-kV system are presented. Initial radio influence measurements made on each line section are compared with levels calculated during the design studies. Switching-surge voltages recorded during various normal and abnormal switching conditions are given, and are shown to be well within predicted values. Descriptions are given of the measuring equipment and techniques used for the field tests and for a continual monitoring of the system.

UNCLASSIFIED

Security Classification

DOCUMENT CONTROL DATA - R & D

(Security classification of title, body of abstract and indexing annotation must be entered when the overall report is classified)

1. ORIGINATING ACTIVITY (Corporate author)
Westinghouse Electric
East Pittsburgh, PA 15112

2a. REPORT SECURITY CLASSIFICATION
Unclassified

2b. GROUP

3. REPORT TITLE
HIGH VOLTAGE POWER LINE SITING CRITERIA

4. DESCRIPTIVE NOTES (Type of report and inclusive dates)
Final

5. AUTHOR(S) (First name, middle initial, last name)
William E. Pakala
Vern L. Chartier
Ronald T. Harrold

6. REPORT DATE	7a. TOTAL NO. OF PAGES	7b. NO. OF REFS
November 1968	224	6

8a. CONTRACT OR GRANT NO.	9a. ORIGINATOR'S REPORT NUMBER(S)
F30602-67-C-0171	
b. PROJECT NO. 4540 Task No. 454002	Westinghouse Report # 68 696
d.	9b. OTHER REPORT NO(S) (Any other numbers that may be assigned this report) RADC-TR-68-316

10. DISTRIBUTION STATEMENT
This document is subject to special export controls and each transmittal to foreign governments, foreign nationals or representatives thereto may be made only with prior approval of RADC (EMCVI), GAFB, N.Y. 13440.

11. SUPPLEMENTARY NOTES	12. SPONSORING MILITARY ACTIVITY
	Rome Air Development Center (EMCVI) Griffiss Air Force Base, New York 13440

13. ABSTRACT

This Technical Report describes the work performed under Contract F30602-67-C-0171. The objective was to develop a High Voltage Power Line Siting Criteria so that communication sites can be selected which will not be seriously affected by radio interference from existing power lines, or proposed lines in the vicinity of the communication site.

Under ~~a previous Contract AF30(602)-3822,~~ a High Voltage Power Line Siting Criteria was developed and reported in ~~Technical Report No. RADC-TR-66-606, March 1967, Vols. I, II, III~~ for power lines rated 2.4 kV through 345 kV, and covering the frequency spectrum of 60 Hertz through one Gigahertz.

This Technical Report extends the Siting Criteria to power lines operating at 525 kV ac, 735 kV ac and 800 kV dc, covering the frequency range from 60 Hz to 10 GHz. Also the investigation of the radio noise and frequency spectrum of the 345-kV lines studied in the previous contract has been extended to 10 GHz.

The following information is included in this report:

1. A systematic procedure to determine the radio noise generated by 525-kV ac, 735-kV ac and 800-kV dc lines covering the frequency spectrum of 60 Hz to 10 GHz, and lines from 2.4-kV ac to 345-kV ac covering the frequency spectrum of 1 GHz to 10 GHz.

2. Description and comparison of test methods using radio noise meters both manually and with X-Y recorder and spectrum analyzer.

3. Measured data and data analysis.

(Cont'd on reverse side)

DD FORM 1 NOV 65 1473

UNCLASSIFIED

Security Classification

UNCLASSIFIED
Security Classification

14. KEY WORDS	LINK A		LINK B		LINK C	
	ROLE	WT	ROLE	WT	ROLE	WT
Electric Corona Transmission Lines Radio Frequency Interference						

Abstract continued

4. Methods to determine the propagation loss of the noise generated by power lines.

5. Literature Survey.

UNCLASSIFIED
Security Classification